ASSESSING REPRODUCTIVE TOXICITIES OF BISPHENOL A (BPA) AND ITS

ANALOGS BISPHENOL S (BPS), BISPHENOL AF (BPAF), AND

TETRABROMOBISPHENOL A (TBBPA) USING HIGH-CONTENT ANALYSIS IN *IN*

VITRO TESTICULAR CELL MODELS

by

SHENXUAN LIANG

(Under the Direction of Xiaozhong Yu)

ABSTRACT

Bisphenol A (BPA), an endocrine disruptor, was shown to be a testicular toxicant in animal models. Its structural analogs were introduced to the market as BPA alternatives. However, their reproductive toxicological data are limited. Traditional reproductive toxicity testing is expensive and time-consuming with extensive animal use. High-content analysis (HCA) has emerged as a powerful tool for chemical toxicity profiling and screening. This dissertation project aimed to use HCA assays to examine testicular toxicities of BPA and its analogs, bisphenol S (BPS), bisphenol AF (BPAF), and tetrabromobisphenol A (TBBPA) in single testicular cell type cultures and a testicular cell co-culture model.

HCA assays were developed and validated in mouse spermatogonial cell line C18-4. HCA revealed that BPAF and TBBPA exhibited higher toxicities than BPA or BPS, including reduction of cell number, alteration in nuclear morphology, perturbation of cell cycle progression and cytoskeleton, and induction of DNA damage responses. A machine learning (ML)-powered HCA pipeline was developed to determine phenotypic changes in a testicular cell co-culture

model
model utilizing mouse spermatogonial, Leydig, and Sertoli cell lines. Exposure to BPA and its analogs resulted in the loss of spatial arrangement of three-dimensional (3D) structure and M phase arrest in the co-cultures. BPAF induced multinucleated cells, which were associated with increased DNA damage responses and impaired actin cytoskeleton. Multiple HCA endpoints measured in the co-cultures also showed BPAF and TBBPA exerted higher toxicities than BPA or BPS. The HCA-based comparative toxicity profiling of BPA and its analogs in mouse spermatogonial, Leydig, and Sertoli cell lines showed cell-specific toxicities of tested chemicals. BPA and BPS exerted higher toxicities in Sertoli and Leydig cells, as compared to spermatogonial cells. BPAF exhibited distinct toxicity profiles among three types of cells at different doses. TBBPA showed low toxicity in Leydig cells.

In conclusion, BPA and its analogs affect multiple cellular and molecular events and show differential toxicities in three types of testicular cells and co-cultures, with testicular toxicities being cell-type specific. The newly developed HCA assays, together with the ML algorithm, can be used in identification, screening, and comparison of potential reproductive toxins.

INDEX WORDS: Bisphenol A, bisphenol S, bisphenol AF, tetrabromobisphenol A, high-content analysis, machine learning, spermatogonial cells, Leydig cells, Sertoli cells, testicular cell co-cultures, testicular toxicity

ASSESSING REPRODUCTIVE TOXICITIES OF BISPHENOL A (BPA) AND ITS

ANALOGS BISPHENOL S (BPS), BISPHENOL AF (BPAF), AND

TETRABROMOBISPHENOL A (TBBPA) USING HIGH-CONTENT ANALYSIS IN *IN*

VITRO TESTICULAR CELL MODELS

by

SHENXUAN LIANG

B.S., Capital Medical University, China, 2012

A Dissertation Submitted to the Graduate Faculty of The University of Georgia in Partial

Fulfillment of the Requirements for the Degree

DOCTOR OF PHILOSOPHY

ATHENS, GEORGIA

2017

ASSESSING REPRODUCTIVE TOXICITIES OF BISPHENOL A (BPA) AND ITS

ANALOGS BISPHENOL S (BPS), BISPHENOL AF (BPAF), AND

TETRABROMOBISPHENOL A (TBBPA) USING HIGH-CONTENT ANALYSIS IN *IN*

VITRO TESTICULAR CELL MODELS

by

SHENXUAN LIANG

Major Professor:	Xiaozhong Yu
Committee:	Jia-sheng Wang
	Xiaoqin Ye
	Travis Glenn

ACKNOWLEDGEMENTS

During the past four years, I have been supported by many people in my life, study, and research. This dissertation could not have been finished without your support and help.

First, I would like to express my deep gratitude to my advisor, Dr. Xiaozhong Yu. His knowledge, experience, diligence, and passion deeply impressed me and will benefit me in my career. I am grateful for his constant assistance, encouragement, and guidance, and tremendous support and opportunities that he provided throughout my doctoral study. I also want to thank my advisory committee members: Dr. Jia-sheng Wang, Dr. Xiaoqin Ye, and Dr. Travis Glenn. Thank you all for your advice and help in my study and research.

Second, I sincerely thanks Dr. Lei Yin, Xuelin Guan, Jacob Siracusa, Emily Measel and Adrianne Smith, members of Dr. Yu's lab, for their kind help in my dissertation work. My special gratitude goes to Dr. Lei Yin, who taught me a lot, and provided valuable suggestion and critical comments on my dissertation. I also want to thank Haoguang Liu, Elizabeth Bush, and many people in our Department of Environmental Health Science and College of Public Health, all the staffs in the Paul D. Coverdell Center, and all my friends in Athens and China for your help, care, and support.

Last but not least, I want to thank my mother, Aiping Chu and my father, Hong Liang. Their encouragement, support, love, and trust have been essential for my study and research.

Once again, I would like to express sincere thanks and appreciation to my advisor, committee members, friends, and parents. Without your help and support, I would not have completed my dissertation.

TABLE OF CONTENTS

LIST OF ABBREVIATIONS

AD: Androstenedione; AFC: Antral follicle count; AR: Androgen receptor; BPA: Bisphenol A; BPAF: Bisphenol AF; BPS: Bisphenol S; BrdU: 5-Bromo-2'-deoxyuridine; BTB: Blood-testis-barrier; CDC: the US Centers for Disease Control and Preventions; Ch1: Channel one; Ch2: Channel two; Ch3: Channel three; CIS: Carcinoma *in situ*; DBP: Di-(n-butyl) phthalate; DILI: Drug-induced liver injury; DME/F1: Modified eagle's medium/ nutrient mixture F-12; DMEM: Dulbecco's modified eagle medium; ECHA: the European Chemical Agency; ECM : Extracellular matrix; EC20: 20% Maximal effect concentration; EDC: Endocrine disrupting chemical; EPA: the United States Environmental Protection Agency; ER: Estrogen receptor; ES: Ectoplasmic specialization; E2: Estradiol; FBS: Fetal bovine serum; FDA: the U.S. Food, and Drug Administration; FSH: Follicle-stimulating hormone; GSH: glutathione; HCA: High-content analysis; HCS: High-content screening; HPV: High production volume; HTS: High-throughput screening; IVF: *In vitro* fertilization; LOAEL: Lowest adverse effect level; LC50: Median lethal concentration; LH: Luteinizing hormone; LC3B: Light chain 3B; LWR: Length-width ratio; MBD1: Methyl CpG binding protein 1; ML: Machine learning; MMP: Mitochondrial membrane potential; NHANES: the National Health and Nutrition Examination Survey; NR: Neutral red; NTP: the National Toxicology Program; PBS: Phosphate buffered saline; PCOS: Polycystic ovary syndrome; PF: Post fertilization; PKA: Protein kinase A; PMP: Plasma membrane permeability; PND: Postnatal day; PP: Precocious puberty; PPARs: Peroxisome proliferator–activated receptors; P4: Progesterone; REACH: the European Registration, Evaluation, Authorization, and Restriction of Chemicals; ROS: Reactive oxygen species; SHBG: Sex

hormone-binding globulin; SSCs: Spermatogonial stem cells; T: Testosterone; TBBPA: Tetrabromobisphenol A; TGCT: Testicular germ cell tumors; T3: Triiodothyronine; T4: Thyroxine; VEGF: Vascular endothelial growth factor; 3β-HSD: 3β-hydroxysteroid dehydrogenase; 3D: 3-Dimensional; 8-OHdG: 8-Hydroxy-2'-deoxyguanosine; γ-H2AX: Phospho-Histone-H2AX (Ser139)

LIST OF TABLES

LIST OF FIGURES

CHAPTER 1

INTRODUCTION AND LITERATURE REVIEW

1.1 Reproductive toxicities of bisphenol A and its analogs

1.1.1 Introduction

BPA is a high production volume (HPV) chemical commonly used in food packaging materials, dental sealants, medical devices and thermal receipts (Rochester, 2013). Exposure to BPA is ubiquitous via ingestion, inhalation, and dermal contact (Kang *et al.*, 2006; Vandenberg *et al.*, 2007). The Centers for Disease Control and Preventions (CDC) has reported measurable levels of BPA in urine samples of over 90% of the United States population (Calafat *et al.*, 2008; Lakind and Naiman, 2011). BPA has been demonstrated to be an endocrine disruptor that acts with various physiological receptors, such as estrogen receptor α/β (ER α/β), estrogen-related receptor γ, androgen receptor (AR), and thyroid hormone receptor (Dong *et al.*, 2011; Gould *et al.*, 1998; Kuiper *et al.*, 1998; Matsushima *et al.*, 2007; Okada *et al.*, 2008; Richter *et al.*, 2007; Tokarz *et al.*, 2013; Wozniak *et al.*, 2005). Although numerous studies have demonstrated that BPA is a reproductive toxicant in animal models, the risk assessment of low-dose BPA exposure[1] is continued to evaluate the safety of BPA that currently is approved for use in containers and packaging (Peretz *et al.*, 2014; Richter, *et al.*, 2007; Rochester, 2013; vom Saal *et al.*, 2007). As proposed by the National Research Council of the National Academy of Science, the hazard identification, dose-response assessment, and exposure assessment are three critical components for risk assessment and regulation development of environmental chemicals (Brewer, 2009). With the respect of low-dose BPA exposure and reproduction, Peretz, et al.

reviewed experimental and human evidence from 2007-2013 and indicated BPA impacted female reproduction and had potential adverse effects on male reproductive systems. But the conclusion was not definitive given the inconsistency among animal experimental designs and short-time exposure assessment in human studies (Peretz, et al., 2014).

Due to the concern over widespread human exposure and potential adverse reproductive effects of BPA, the use of BPA in baby bottles, sippy cups, and infant formula packaging had been abandoned (FDA., 2013; FDA., 2012). Some of BPA analogs are used as substitute chemicals for BPA to produce "BPA-free" products. Others are used as crosslinking reagents and flame retardants in the plastics industry. Although there is a general lack of production data for BPA analogs, the usage of these chemicals is expected to rise globally. Recently, the occurrences of BPA analogs in the environment, foods, consumer products, and human urine samples have been reported (Geens *et al.*, 2009; Liao *et al.*, 2012a; Liao *et al.*, 2012b; Shi *et al.*, 2013; Ye *et al.*, 2015). With the high degree of structural similarities with BPA, these analogs potentially have the similar endocrine disrupting capacity and exerted adverse effects on the reproductive system. Emerging evidence suggests that BPA analogs act with various physiological receptors (Kitamura *et al.*, 2005; Stossi *et al.*, 2014). However, as compared to BPA, little is known about the reproductive toxicities of these analogs.

Here, the current literature on BPA and its analogs and male/female reproduction were reviewed to summarize the current state of knowledge, identify the knowledge gaps, and highlight future research directions that could provide valuable information for risk assessment, specifically to human reproductive health. The aims of this review included 1) update the BPA exposure and reproductive health outcomes in human and laboratory animals, as well as *in vitro* studies to examine possible molecular mechanisms that mediate reproductive effects during

2014-2017; 2) compile and analyze the current state of knowledge on the environmental occurrences, human biomonitoring, endocrine disrupting capacity, and reproductive toxicities of BPA analogs. This review is structured into 6 topics, (1) BPA and female reproductive health; (2) BPA and male reproductive health; (3) BPS and reproductive health; (4) BPAF and reproductive health; (5) TBBPA and reproductive health; and (6) conclusion and research needs. Thus, this review is a compilation of the recent literature, and it focuses on the effects of BPA and its analogs on male and female reproductive system. The information and conclusions in this review could potentially direct future studies and be useful in risk assessment and regulation formation of BPA and its analogs.

[1] Through the review, the term "low dose" was defined as a BPA treatment dose of $\leqslant 50$ mg/ kg/ day (Rochester and Bolden, 2015; vom Saal, *et al.*, 2007). It is the lowest adverse effect level (LOAEL) used by the Environmental Protection Agency (EPA) (EPA, 1993). The term "high dose" refers using concentrations > 50 mg/ kg/ day.

1.1.2 Search strategy

A literature search was performed to identify journal articles related to BPA, BPS, BPAF, and TBBPA and reproduction. The research included all articles published between 2014 and 2017 for BPA and all years to 2017 for BPA analogs. An electronic search was performed using PubMed (http,//www.ncbi.nlm.nih.gov/pubmed). Search terms included the following,

Bisphenol A, bisphenol S, 4,4'-Sulfonyldiphenol, bisphenol AF, hexafluorobisphenol A, tetrabromobisphenol A, 2,2',6,6'-Tetrabromo-4,4'-isopropylidenediphenol, oocyte, ovary, uterus, testes, sperm, Leydig cell, Sertoli cell, steroidogenesis, estradiol, testosterone, follicle-stimulating hormone, luteinizing hormone, thyroid, or pregnenolone.

1.1.3 BPA and female reproductive health

1.1.3.1 Oocyte production and quality

Recent experimental studies report that BPA exposure affects oocyte quality, fertilization, and maturation (overview in Table 1.1), which is consistent with previous findings (Peretz, *et al.*, 2014). Low-dose BPA (50 μg/kg) was given orally to adult C57BL/6J mice and significantly decreased the percentage of fertilized oocytes without ovulation changes (Moore-Ambriz *et al.*, 2015). In *in vitro* studies, BPA treatment has been reported to decrease meiosis progression and increase spindle abnormalities, including abnormal spindle morphology and chromosome alignment at doses of 15 and 30 ng/ml (Ferris *et al.*, 2015). Further, bovine oocytes exposed to BPA showed significant increases in DNA damage and apoptosis at a dose of 130 nM, while the gene expression in blastocysts was not altered after oocyte fertilization. (Ferris *et al.*, 2016). Wang et al. reported that porcine oocytes exposed to BPA at a dose of 250 μM showed a decrease in maturation rate, increases in reactive oxygen species (ROS), abnormal cytoskeleton and apoptosis/autophagy rate, and alteration of epigenetic pattern (Wang *et al.*, 2016d). Similarly, Nakano et al. reported BPA treatment (2 μg/ml) decreased maturation rate and induced cell cycle delay and spindle abnormalities in ICR mouse oocyte (Nakano *et al.*, 2016).

1.1.3.2 Steroidogenesis

Several epidemiological studies have investigated the association between BPA exposure and hormone production in women (overview in Table 1.2). In Korean girls with precocious puberty (PP), urinary BPA levels were associated with high levels of testosterone (T), estradiol (E2), progesterone (P4), and alteration of steroid metabolism among individuals with high BPA levels, while BPA levels were not associated with the onset of precocious puberty (Lee *et al.*, 2014). Akin et al. reported that BPA levels were associated with high levels of serum T in

polycystic ovary syndrome (PCOS) patients in Turkey (Akin *et al.*, 2015). Miao et al. found that urinary BPA concentrations were positively associated with higher prolactin, E2 and P4 levels in Chinese female workers with occupational BPA exposure (Miao *et al.*, 2015). Further, in the National Health and Nutrition Examination Survey (NHANES) 2011-2012, BPA exposure levels were associated with higher total T levels in female adolescents (Scinicariello and Buser, 2016). However, a prospective cohort study by Minguez-Alarcon et al. showed that BPA concentrations were not associated with peak E2 levels in women with at least one *in vitro* fertilization (IVF) cycle (Minguez-Alarcon *et al.*, 2015). Zhou et al. also reported that no associations between BPA levels and serum FSH levels were observed in infertile women with PCOS (Zhou *et al.*, 2016). Overall, multiple epidemiological studies indicated the urinary or serum BPA levels were associated with alterations of hormone levels in the female. However given that most studies were conducted in women with impaired reproductive functions and used single spot urine sample to estimate BPA exposure level, it is important to examine the association between long-term BPA exposure and hormone levels in the general population.

Recent experimental studies have examined the effects of BPA exposure on female steroidogenesis using rodent models (overview in Table 1.3). In one study of Wistar rats, low-dose BPA neonatal exposure via intraperitoneal injection decreased serum P4 levels without changes of E2 levels (Li *et al.*, 2014). Conversely, prenatal and neonatal BPA treatment increased serum P4 levels coupled with high mRNA expression of 3β-hydroxysteroid dehydrogenase(3β-HSD) in the Wistar rats with (Santamaria *et al.*, 2016). Further, low-dose BPA exposure via drinking water increased serum luteinizing hormone (LH), E2 levels and follicle number, while no changes in serum follicle-stimulating hormone (FSH) level were observed in Wistar rats (Gamez *et al.*, 2015). In other strains, Delclos, et al. reported SD rats

with prenatal and neonatal oral exposure to BPA showed increases in E2 and prolactin levels, and a decrease in P4 levels only at the highest dose group (300000 μg/kg) (Delclos *et al.*, 2014). Sadowski et al. reported Long-Evans rats exposed to low-dose BPA during the prenatal and neonatal period showed a decrease in FSH levels but no changes in other hormone levels and maze behavior were observed (Sadowski *et al.*, 2014). Low-dose BPA (50 μg/kg) given orally to adult C57BL/6J mice during 3 estrous cycles did not alter the serum E2, FSH, and LH levels (Moore-Ambriz*, et al.*, 2015). Only one *in vitro* study reported that BPA exposure (2 or 20 mg/ml) decreased P4 synthesis and the protein expression levels of steroidogenesis enzymes (3b-HSD, CYP11A1, and CYP19A1) in human granulosa cells (Mansur *et al.*, 2016). Collectively, current data indicate that BPA adversely affects the female steroidogenesis but its effects vary by animal species, strains, exposure routes and exposure windows.

1.1.3.3 Ovary and uterus

The limited studies investigated the effects of BPA on women's ovaries (overview in Table 1.2). One case-control study of 112 women between 13 and 19 years of age suggested that urinary BPA levels were associated with higher risk of PCOS (Akin*, et al.*, 2015). Further, in 268 infertile women diagnosed with PCOS, urinary BPA levels were associated with a significant decrease in antral follicle counts (AFCs) (Zhou*, et al.*, 2016). In 62 cashiers with PCOS, the serum levels of BPA and LH/FSH ratio were significantly increased, while TSH levels decreased, as compared to healthy women with the similar job (Vahedi *et al.*, 2016). However, in a case-control study of 52 women, no association was found between urinary BPA concentration and risk in PCOS (Vagi *et al.*, 2014). Given the limited study numbers, the association between BPA exposure and PCOS symptoms needs further studies to validate current

findings. Additional studies in animal models are needed to fully understand whether BPA exposure is associated with high risk in PCOS and underlying mechanism.

In rodents (overview in Table 1.4.1), prenatal and postnatal exposure to low-dose BPA resulted in decreases in ovarian weight, follicle numbers, and primordial follicle recruitment, with an increase in the number of corpora lutea, and a delay in vaginal opening in Wistar rats (Li, *et al.*, 2014; Patisaul *et al.*, 2014; Santamaria, *et al.*, 2016). Also, high-dose BPA exposure (300000 μg/kg) in SD rats lead to an increase in cystic follicles and decreases in corpora lutea and antral follicles (Delclos, *et al.*, 2014). Zhou et al. reported that BPA exposure decreased germ cell nest breakdown and altered the expression of key genes involved in apoptosis and anti-oxidation in CD-1 mice ovary *in vitro*, while the effects varied by ovary collection times and exposure doses (Zhou *et al.*, 2015). Further, BPA has been reported to reduce small primary, large primary and secondary follicle numbers and increase DNA manage markers (γ-H2AX, ATM) and DNA repair genes in F344 rats ovary *in vitro*, suggesting DNA damage could be one of the potential mechanisms of BPA ovarian toxicity (Ganesan and Keating, 2016). The transgenerational effects of BPA on ovary were observed in the F3 generation in a non-monotonic dose-dependent manner (Berger *et al.*, 2016).

Three studies have reported the impacts of BPA exposure on uterine morphology in women (overview in Table 1.2). In a case-control study from women with endometriosis, Upson et al. found that urinary BPA levels were associated with non-ovarian pelvic endometriosis, but not in relation to ovarian endometriosis (Upson *et al.*, 2014). Conversely, Minguez-Alarcon et al. reported no association between urinary BPA level and endometrial wall thickness in 256 women undergoing IVF, while younger women (<37 years old) had thick endometrium and older women (≥37 years old) had thinner endometrium with increasing urinary BPA concentrations.

(Minguez-Alarcon, *et al.*, 2015). In addition, in 68 patients with endometriosis, urinary BPA levels were significantly higher as compared with BPA levels in the control group (Simonelli *et al.*, 2017). Given the limited number of studies and lack of BPA exposure data during endometriosis development, future studies are needed to elucidate the association between chronic BPA exposure and uterine morphology alteration in general population.

Multiple experimental studies have reported the effects of BPA exposure on uterine in rodent models (overview in Table 1.4.2). In two studies of CD-1 mice, low-dose BPA exposure increased gland nest density, periglandular collagen accumulation, and improper endometrial epithelial and stromal functions (Kendziorski and Belcher, 2015; Li *et al.*, 2016b). Calhoun et al. reported postnatal exposure to BPA via food consumption (400 μg/kg) altered three genes (HOXA13, WNT4, and WNT5A) involved in reproductive organ development in rhesus macaque uterus, while fatal uteri did not show notable changes in uterus histology, proliferation, and expression of hormone receptors. (Calhoun *et al.*, 2014). In one study of Wistar rats, prenatal and postnatal exposure to low-dose BPA resulted in decreases in glandular proliferation and α-actin expression at postnatal day (PND) 90 and increases in the abnormal luminal and glandular epithelium at PND360 (Vigezzi *et al.*, 2015). In addition, low-dose BPA exposure in SD rats uterine *ex vivo* decreased the force of uterine contraction (Salleh *et al.*, 2015). Kim et al. reported that short-time exposure to high-dose BPA led to a rapid and transient increase in early growth response 1 gene via ER-ERK1/2 pathway in ICR mice (Kim *et al.*, 2014). However, no dose-dependent changes in global genomic DNA methylation in uterus were observed in SD rats orally given low-dose of BPA, which could result from BPA contamination in negative controls during housing and dosing (Camacho *et al.*, 2015). In *in vitro* studies, BPA (2.28 ng/ml) upregulated genes involved in cell differentiation and proliferation and downregulated genes in

mitosis and adhesion in uterine smooth muscle cells (Kang *et al.*, 2014). Importantly, in human endometrial endothelial cell and uterine leiomyoma, BPA exposure increased the protein expression of vascular endothelial growth factor (VEGF) at micromolar level (Helmestam *et al.*, 2014; Shen *et al.*, 2014). Further, Wang et al. reported BPA exposure increased growth rate and colony-forming efficiency via CoX-2 in endometrial carcinoma cells line (Wang *et al.*, 2015b). Collectively, these studies provide compelling evidence to suggest that BPA adversely affects the uterine both *in vivo* and *in vitro*, whereas the assessment endpoints are varied across all studies.

1.1.4 BPA male reproductive toxicities

1.1.4.1 Sperm production and quality

Human studies on BPA exposure and sperm quality are still limited in current studies (overview in Table 1.2). In a prospective cohort study of male partners undergoing IVF treatments, the log-transformed urinary BPA concentrations were associated with lower log-transformed sperm count, concentration, and motility (Knez *et al.*, 2014). Further, a study of young men from Denmark general population reported that men in the highest quartile of urinary BPA levels also had significantly lower sperm progressive motility, as compared to men in the lowest quartile (Lassen *et al.*, 2014). However, in a study of couples trying to become pregnant, urinary BPA levels were associated with lower sperm DNA fragmentation, which could be explained by low BPA levels detected in the study population as compared with NHANES data and sperm analysis on the next day of sample collection (Goldstone *et al.*, 2015). Given the limited information and the discrepancy among results, additional studies using sensitive and reliable approach to monitor continuous BPA exposure and cost-effective semen analysis are

needed to examine the association between BPA exposure and sperm quality in men from the general population.

In multiple animal studies on BPA exposure and male reproduction (overview in Table 1.5), the prenatal and postnatal exposure to low-dose BPA adversely affected sperm production and quality. However, the variations in exposure windows, duration, species or strains and endpoints made it difficult to develop consensus statements on effects of low-dose BPA exposure on the male spermatogenesis. Despite the variability in study design, several findings are commonly observed, including a decrease in sperm number, induction of sperm apoptosis and oxidative stress, and alteration of seminiferous tubules morphology. Both prenatal and postnatal exposure to low-dose BPA decreased sperm number in mice and rats (Gurmeet *et al.*, 2014; Hass *et al.*, 2016; Kalb *et al.*, 2016; LI *et al.*, 2015; Rahman *et al.*, 2016; Vilela *et al.*, 2014; Wang *et al.*, 2016b; Wisniewski *et al.*, 2015).

Further, induction of testicular oxidative stress or apoptosis was observed in mice and rats exposed to low-dose BPA during the prenatal or postnatal period (Kalb*, et al.*, 2016; Quan *et al.*, 2016a; Quan *et al.*, 2016b; Wang*, et al.*, 2016b; Wang *et al.*, 2014; Yin *et al.*, 2016). In addition, low-dose BPA exposure delayed meiosis, induced the accumulation of chromosomal abnormalities, meiotic DNA double-strand breaks (DSBs) in the late meiotic stage (Liu *et al.*, 2014a). Further, few studies indicated that low-dose BPA exposure potentially altered the epigenetic pattern in testes, including an increase in methylation of Igf2 and a decrease in protein lysine acetylation levels in rats (Chen *et al.*, 2017; Vrooman *et al.*, 2015). Whereas in multiple mouse strains, exposure to BPA did not affect the chromosome pairing and synapsis (Mao *et al.*, 2015; Vrooman*, et al.*, 2015). Overall, the strength of current evidence for risk assessment regarding low-dose BPA exposure is still limited. The relevance of doses in the experimental

studies to human exposure is still unclear because the internal (urinary or serum) BPA levels in tested animals were not examined, which made extrapolation of these findings to human difficult.

Several *in vitro* studies further investigated modes of action of BPA testicular toxicity (overview in Table 1.5). In two studies using mice spermatocyte GC-2 cell line, BPA exposure induced germ cell apoptosis via Ca^{2+}/CaM/CaMKII signaling pathway and PERK/EIF2α/chop pathway at a dose of 20 μM (Qian *et al.*, 2015; Yin*, et al.*, 2016). An increase in tyrosine phosphorylation via protein kinase A (PKA) was observed in the primary spermatozoa isolated form mice and rats (Rahman *et al.*, 2015; Wan *et al.*, 2016). Further BPA exposure (50 μM) induced early DNA damage responses and perturbed cytoskeleton in spermatogonial cell line C18-4 (Liang *et al.*, 2017). A study of human spermatozoa found BPA exposure (300 μM) decreased mitochondrial membrane potential, and increased apoptosis, and DNA oxidative damage marker (8-hydroxy-2'-deoxyguanosine) (Barbonetti *et al.*, 2016). In addition, another study found short-time BPA exposure increased velocity straight linear, homogeneity of progressive movement velocity and intracellular free Ca^{2+} concentrations in human spermatozoa at a dose of 1mM (Kotwicka *et al.*, 2016). Collectively, these data suggest that BPA exposure may impact the male germ cells through perturbation of Ca^{2+} homeostasis and cytoskeleton structure, and induction of apoptosis and DNA damage. The doses that induced adverse effects on *in vitro* germ cells are restively high, as compared to serum BPA levels measured in general population. But considering workers with extensive occupational exposure to BPA, these study still provide meaning information for mechanisms of BPA testicular toxicities and its occupational hazards (Heinala et al., 2017; Hines et al., 2017).

1.1.4.2 Sertoli and Leydig cells

Sertoli and Leydig cells play critical roles in maintaining the normal functions of spermatogenesis. The functions of the Sertoli cells include the formation of blood-testis barrier, secretion proteins, and growth factors to nurture germ cells and regulation of apoptosis and mitosis of germ cells (Haywood *et al.*, 2003; Lui *et al.*, 2003). Leydig cells synthesize and secrete T to support spermiogenesis (Payne, 1990).

Multiple *in vitro* studies have examined the effects of BPA on Sertoli cells (overview in Table 1.6). In three studies using Sertoli cell line TM4, nanomolar BPA increased proliferation via promoting energy metabolism, GPR 30 and ER α/β, while micromolar BPA decreased cellular proliferation via inducing oxidative stress, activating CaM-CaMKII-ERK and mitochondrial apoptotic pathways (Boudalia *et al.*, 2014; Ge *et al.*, 2014; Qian *et al.*, 2014). In studies using primary rat Sertoli cells, BPA (~50 μM) induced cellular apoptosis via ROS, mitochondrial dysfunction, and activated HNKs/p38 MAPK, NF-kB, and Pten/Akt pathways (Qi *et al.*, 2014; Wang *et al.*, 2016a; Wang *et al.*, 2015a). Importantly, in human primary Sertoli cells, BPA exposure significantly decreased the cell viability, expression levels of occludin, ZO-1, β-catenin, and AR at a dose of 20 μM without changes in F-actin expression or localization (de Freitas *et al.*, 2016). In another study, BPA treatment perturbed actin filaments starting at 0.4 μM and induced improper localization of actin regulatory proteins Arp3 and Eps8 at a dose of 200 μM (Xiao *et al.*, 2014).

In vivo study showed high-dose BPA exposure decreased Leydig cell number and StAR protein level in adult rat testes whereas low-dose BPA-induced Leydig cell proliferation with increases in protein expressions of proliferating cell nuclear antigen, MAPK, AR, and ER α/β,

and increased secretion of the anti-Mullerian hormone in the adult rat testes (Nakamura *et al.*, 2010; Nanjappa *et al.*, 2012). In *in vitro* studies, BPA exposure decreased T biosynthesis and E2 levels, mRNA expression of aromatase and the steroidogenic enzyme 17α-hydroxylase/17–20 lyases in rat primary Leydig cells (Akingbemi *et al.*, 2004). In Leydig cell line TM3, micromolar BPA decreased cellular proliferation and increased cell migration and invasion (Chen *et al.*, 2016c). Given the current *in vitro* studies, BPA exposure affected the proliferation and steroidogenesis of rodent Sertoli and Leydig cells. Further, the experimental studies indicated that BPA exposure decreased hormone levels in male animals, suggested the direct effects of BPA on Leydig cells (Peretz*, et al.*, 2014).

1.1.4.3 Steroidogenesis

Five epidemiology studies examined the association between urinary BPA levels and hormone levels in men (overview in Table 1.2). In a study of young men from Denmark general population reported that men with BPA levels above the lowest quartile had higher levels of T, LH, and E2, as compared with men in the lowest quartile (Lassen*, et al.*, 2014). In two cross-sectional studies in male workers with occupational BPA exposure, urinary BPA concentrations were associated with higher sex hormone-binding globulin (SHBG) and lower androstenedione (AD) levels (Liu *et al.*, 2015b; Zhuang *et al.*, 2015). In male children and adolescents from NHANES 2011-2012, BPA levels were associated with lower total T levels (Scinicariello and Buser, 2016). While in a retrospective cohort study, parental (3rd trimester) or childhood BPA exposure was not associated with hormone levels in boys ages 8-14 (Ferguson *et al.*, 2014). These data indicate that BPA exposure can perturb hormone levels in men. However, some studies' strength was limited by the specific study population, single spot urine sample, and lack

of co-exposure assessment. Future studies in the general population are critical to determine whether BPA exposure affects male steroidogenesis.

In experimental studies, prenatal and postnatal exposure to low-dose BPA was reported to alter the hormone levels in mice and rats, but the data were not consistent (overview in Table 1.7). Gamez et al. reported low-dose BPA exposure led to increases in serum LH and FSH levels in young Wistar rats (Gamez *et al.*, 2014). Conversely, in one study using adult Wistar rats, Wisniewski, et al. found the BPA exposure decreased serum T, LH, and FSH levels and increased E2 level (Wisniewski*, et al.*, 2015). In two studies using SD rats, one reported decreases in serum T and E2 levels with postnatal low-dose BPA exposure (Gurmeet*, et al.*, 2014). BPA exposure significantly increased serum thyroxine (T4) levels at the highest BPA dose group (300000 μg/kg) without changes in serum triiodothyronine (T3) and FSH levels (Delclos*, et al.*, 2014). BPA exposure also decreased serum T levels in Swiss albino and C57BL/6 mice, but the toxic doses varied between 0.5μg/kg to 100 mg/kg (Chouhan *et al.*, 2015; Zang *et al.*, 2016). In addition, Sadowski et al. reported Long-Evans rats exposed to low-dose BPA showed decreased FSH levels at weaning (Sadowski*, et al.*, 2014). In an *in vitro* study, BPA exposure reduced basal T secretion in the rat (10000 nM), mouse (1000 nM) and human (10 nM) fetal testis explants. (Eladak *et al.*, 2015). These data suggest BPA exposure impaired the male steroidogenesis in rodents but the effects varied by species, strains, exposure window, and duration.

1.1.5 BPA analogs and reproductive health

Due to the limited number of studies examining the effects of BPA analogs on male and female reproductive system, literature search was expanded and studies using the zebrafish model were included. As a vertebrate, zebrafish has conserved pharmacological targets and

nervous system structures, which is comparable to mammals. It has been widely used as a model to identify targets as well as modes of the action of endocrine disrupting chemicals (EDCs) (Tokarz, *et al.*, 2013).

<u>*1.1.5.1 BPS and reproductive health*</u>

BPS is structurally similar to BPA and now used in a variety of common consumer products as a BPA alternative. BPS has been detected in food, indoor dust, personal care products, sediment and paper products, such as cashier's receipts and currency (Liao and Kannan, 2013; Liao and Kannan, 2014; Liao, *et al.*, 2012b; Liao *et al.*, 2012c). Exposure to BPS usually occurs through ingestion, inhalation and dermal contact. The metabolic and biological fate of BPS have not been fully examined. *In vitro* study indicated that glucuronidation was the major metabolic pathway for BPS (Skledar *et al.*, 2016). BPS was detected in 81% of human urine samples in the United States and seven Asian countries, with the mean concentration of 0.654 ng/ml, which was comparable to BPA (Liao, *et al.*, 2012a). As a potential EDC, BPS has been examined in the National Toxicology Program (NTP) Tox21 High Throughput Screening (HTS) Program and classified as an estrogen agonist with weak affinity for the ER. In addition, Rochester and Bolden reviewed the endocrine activities of BPS and reported the average estrogenic potency of BPS compared with BPA was 0.32 ± 0.28, which indicated the potency of BPS was similar to the potency of BPA (Rochester and Bolden, 2015).

However, only a few *in vivo* studies have examined the effects of BPS exposure on female and male reproductive systems (overview in Table 1.8). Yamasaki et al. reported that in the immature rat uterotrophic assay, BPS exposure significantly increased absolute and relative uterine wet weight and blotted weight at doses of 20 and 500 mg/kg (Yamasaki *et al.*, 2004). Further, in two studies using zebrafish, BPS exposure was reported to increase plasma E2 levels

15

and hatching time (Ji *et al.*, 2013; Naderi *et al.*, 2014). In addition, BPS exposure decreased egg production (Ji*, et al.*, 2013). In male zebrafish, BPS exposure increased plasma E2 levels and decreased T levels (Ji*, et al.*, 2013; Naderi*, et al.*, 2014). Last, BPS exposure induced the testicular ROS and lipid peroxidation, altered seminiferous epithelium morphology, and decreased antioxidant enzymes activity and plasma T levels in the highest dose group (50 µg/kg) in SD adult rats (Ullah *et al.*, 2016). Thus, the data from different species provide compelling evidence that BPS exposure altered hormone homeostasis in both male and female animals. Further *in vivo* studies are needed to validate the current findings, and to examine the effects of BPS exposure on multiple rodent strains.

In *in vitro* studies, Eladak et al. reported that BPS exposure decreased basal T secretion in mouse fetal testis explants (100 nM) and human fetal testis explants (1000 nM) (Eladak*, et al.*, 2015). BPS treatment significantly increased P4 levels and expression of 5aRed1gene at a dose of 10 µM in Leydig cell line MA-10 (Roelofs *et al.*, 2015). Chen et al. reported that *Caenorhabditis. elegans* exposed to BPS showed an increase in germline apoptosis and activation of DNA damage checkpoint kinase CHK-1. Further BPS showed distinct alterations of gene expression at whole transcriptome level, as compared with BPA(Chen *et al.*, 2016b). BPS exposure also decreased cell viability and increased early DNA damage response and abnormal cytoskeleton structure at a dose of 50 µM in mouse spermatogonial cell line C18-4 (Liang*, et al.*, 2017).

1.1.5.2 BPAF and reproductive health

BPAF is used widely as a crosslinking agent and a monomer in the plastics industry. Limited information is available on the occurrence of BPAF in consumer products and human urine or blood samples. BPAF has been found in various food items in the United States with a

lower detection rate (6% - 30%), as compared to BPA (Liao and Kannan, 2013). *In vivo*, BPAF was metabolized mainly through glucuronidation and excreted through feces and urine in SD rats (Li *et al.*, 2013; Yang *et al.*, 2012). In human, BPAF was detected in urine samples at concentrations ranging from below detection level to 3.93 μg/L in China and Saudi Arabia (Asimakopoulos *et al.*, 2016; Yang *et al.*, 2014). However, BPAF exhibit estrogenic potencies greater than that of BPA (Kitamura*, et al.*, 2005; Stossi*, et al.*, 2014). Furthermore, BPAF exhibited three times stronger receptor binding activity for ER β than for ER α (Matsushima *et al.*, 2010).

Few studies have examined the effects of BPAF exposure on steroidogenesis *in vivo* (overview in Table 1.9). In two studies of zebrafish, exposure to BPAF led to an increase in E2 levels in the female fish (Shi *et al.*, 2015; Yang *et al.*, 2016). In addition, BPAF exposure induced retardation of oocyte development (Yang*, et al.*, 2016). Further, an *in vitro* study indicated the BPAF exposure delayed the mice oocytes maturation and induced cell cycle arrest by activation of the spindle assembly checkpoint (Nakano *et al.*, 2015).

Similarly, two studies of zebrafish showed that BPAF exposure decreased T levels in male fish and altered the testicular morphology (Shi*, et al.*, 2015; Yang*, et al.*, 2016). In contrast, no decreases in T production were observed in SD rat dams prenatally exposed to BPAF even at a dose of 750 mg/kg (Furr *et al.*, 2014). Further, Li et al. reported BPAF could be transferred via cord blood and lactation, finally accumulated in the offspring testes. Offsprings exposed to BPAF both prenatally and postnatally showed a significant increase in testicular T levels and alterations in genes involved in cell differentiation and meiosis(Li *et al.*, 2016a). Feng et al. reported that BPAF exposure decreased serum T levels and T biosynthesis (200 mg/kg), and increased serum LH (50 mg/kg) and FSH (10 mg/kg) levels in adult male SD rats (Feng *et al.*,

2012). In oocytes, *in vitro* exposure to BPAF inhibited oocyte maturation at concentrations of 50 and 100 µg/ml and induced spindle abnormalities (Nakano*, et al.*, 2016). In spermatogonial cells, BPAF exposure altered nuclear morphology starting at 1 µM, perturbed cell cycle progression, and induced cytoskeleton perturbation and multinucleated cells starting at 10 µM, and increased DNA damage response at a dose of 25 µM (Liang*, et al.*, 2017). Given the discrepant results, the effects of BPAF on steroidogenesis are unclear and likely differ depending on different exposure window. Further studies should be conducted to examine the effects of BPAF exposure on hormone levels and multiple reproductive outcomes in multiple experimental strains, species, and exposure windows.

1.1.5.3 TBBPA and reproductive health

TBBPA is mainly used as a reactive flame retardant in plastics, paper, textiles and circuit boards. In general population, exposure to TBBPA is mainly through dermal contact, inhalation, and ingestion of fish and shellfish (Driffield *et al.*, 2008). TBBPA is absorbed from the gastrointestinal tract, biotransformed to glucuronides and sulfates, and excreted through feces in animal models (Lai *et al.*, 2015). TBBPA exposure levels in the general population have been examined in several studies. The serum TBBPA levels were below the level of detection (0.03 ng/L) in pregnant women in Canada but detectable in 5 % of the Inuit adults with concentrations up to 480 ng/L (Dallaire *et al.*, 2009). In the United States population, TBBPA was found in approximately 35% of human breast milk samples at concentrations between 50-350 pg/kg/day (Carignan *et al.*, 2012). However, the current data demonstrated that TBBPA did not interact with ER α/β or AR in a panel of *in vitro* bioassays (Molina-Molina *et al.*, 2013).

Several studies have examined the effects of TBBPA exposure on the female reproductive system (overview in Table 1.10). Van der Ven, et al. reported that paternal and

18

maternal exposure to TBBPA leads to a decrease in circulating T4 levels without uterus change in adult female Wistar rats. In addition, the concentrations of TBBPA metabolites in plasma increased with increasing exposure levels (Van der Ven *et al.*, 2008). Similarly, in female SD rats exposed to TBBPA, significant decreases in serum T4 levels in F0 and F1 generations were observed at a dose of 1000 mg/kg (ECB., 2012). A study of B6C3F1/N mice exposed to TBBPA for 2 years (500 mg/kg) showed increases in uterine epithelial tumors including adenomas, adenocarcinomas, and malignant mixed Mullerian tumors (Dunnick *et al.*, 2015). In zebrafish, TBBPA exposure decreased egg production (0.047 μM) and increased premature egg (1.5 μM) (Kuiper *et al.*, 2007). In contrast, no changes in the ovary or uterine weight were observed in ICR mice exposed to 1.0% TBBPA in the diet (Tada *et al.*, 2006).

In the studies of male rodents, maternal and paternal exposure to TBBPA decreased circulating T4 levels and testis weight and increased the circulating T3 levels in Wistar rats (Van der Ven*, et al.*, 2008). TBBPA exposure (300 mg/kg) showed increases in testis weight and DNA oxidative damage biomarker 8-hydroxy-2'-deoxyguanosine (8-OHdG) in Wistar rats. However, the reported changes were small and lack of dose-response (Van der Ven*, et al.*, 2008). Conversely, Cope, et al. only observed a decrease in T4 levels in SD rats exposed to TBBPA at a dose of 1000 mg/kg. No changes in sperm motility, concentration, abnormal sperm percentage were observed in multiple generations (Cope *et al.*, 2015). In addition, TBBPA exposure decreased serum T4 and T3 levels at a dose of 1000 mg/kg without changing reproductive organ weight and sperm quality in SD rats (ECB., 2012).

In mice, Zatecka, et al. reported that CD1 mice exposed to TBBPA (35 μg/kg) showed decreases in testis weight, seminal vesicles weight and gene expression of AR. Further, TBBPA exposure (35 μg/kg) increased apoptotic cells and apoptotic genes expressions in seminiferous

tubules. However, no changes in sperm parameters were observed (Zatecka *et al.*, 2013). In C57BL/6J mice exposed to the same level of TBBPA, Zatecka, et al. found TBBPA decreased protamine 1/protamine 2 and increased total protamine/DNA ratio in sperms and number of apoptotic spermatozoa (Zatecka *et al.*, 2014). In two *in vitro* studies, TBBPA exposure was reported to increase T secretion in Leydig cell line MA-10 (Dankers *et al.*, 2013; Roelofs*, et al.*, 2015). Ogunbayo et al. reported that TBBPA induced Sertoli cell death by disrupting Ca^{2+} signaling and affecting Ca^{2+} transport proteins (Ogunbayo *et al.*, 2008). In addition, TBBPA exposure (25 uM) increased DNA damage response and perturbed cytoskeleton structure in mouse spermatogonial cell line C18-4 (Liang*, et al.*, 2017). Taken together, current studies indicate that effects of TBBPA on reproduction varied in limited studies and even at high doses, TBBPA did not exert clear adverse reproductive effects in animals. The alterations in T3 or T4 levels did not accompany histological changes in the thyroid gland or other reproductive organs. Whereas *in vitro* studies, TBBPA exposure impacted testicular cells at relatively low doses, which suggests the potential metabolic deactivation in animals.

1.1.6 Discussion and conclusions

  This review performed a literature search of epidemiological and experimental studies, which examined the reproductive toxicities of BPA and BPA analogs. Recent epidemiological studies indicate that BPA exposure potentially is associated with alterations in hormone levels, impairment of ovary and uterine functions, and reduction of sperm quality. However, the strong association between BPA exposure and human adverse reproductive outcome is still difficult to determine. The single spot urine sample is employed by most of the studies, while due to the rapid metabolism and excretion of BPA (half-life ≈ 6 h) in human, the urine sample may not accurately reflect long-term BPA exposure (Dekant and Voelkel, 2008). Additionally, the

majority of studies focused on couples receiving treatment for infertility or workers with occupational exposure, which makes it difficult to generalize the observed adverse effects to the general fertile population. In many studies, BPA concentrations have been adjusted by confounding factors, such as age, sex, body mass index, social status, smoking history, and other parameters, while the co-exposure to other EDCs may also contribute to the observed adverse reproductive outcomes. Finally, most of the human studies are cross-sectional, which limited the determination of causality. Future epidemiological studies need to employ advanced exposure assessment to monitor the long-term BPA exposure in the individual.

For experimental studies, current data have suggested that low-dose BPA exposure adversely affects oocyte quality and maturation, decreases sperm production and quality, and disrupts ovary function and uterine morphology in animal models. Further BPA exposure is associated with changes in circulating hormone levels both in animal models and human. The underlying mechanism of BPA effects may include oxidative stress and DNA damage. However, definitive conclusions regarding the reproductive toxicity of low-dose BPA exposure is difficult to draw due to the differences in experimental designs and lack of positive controls. However, adverse reproductive outcomes were repeatedly observed in low-dose BPA exposure despite differences in experimental species, strains, exposure window or duration. For the BPA and risk assessment, the FDA and the European Registration, Evaluation, Authorization, and Restriction of Chemicals (REACH) program continue to review the currently available information on BPA to identify any potential health risks from all relevant uses of BPA.

For BPA analogs, emerging evidence has suggested exposure to these chemicals can adversely affect reproductive functions, including oocyte and sperm quality, steroidogenesis, and ovary and testis functions in animal models. It is worth noting that our previous study using

mouse spermatogonial cells combined with high-content analysis (HCA) revealed BPAF exhibited unique testicular toxicities at lower doses (20% maximal effect concentration EC20≈ 10 μM), as compared to BPA (Liang*, et al.*, 2017). Further, the latest *in vivo* study showed consistent data that BPAF exposure uniquely impaired pregnancies and sexual development in rats, as compared to BPA at similar doses (Sutherland. *et al.*, 2017). In addition, BPS uniquely reduced reproductive life span and induced distinct transcriptome changes in *C. elegans* (Chen*, et al.*, 2016b). Given the similarities in their estrogenic potencies with BPA, current data indicate that BPA analogs, especially for BPAF, may disrupt reproductive functions in an ER-independent manner. Currently, the NTP is carrying rodent toxicology studies of BPS and BPAF, and toxicokinetic studies of BPS following oral and intravenous exposure. Still, these are insufficient *in vivo* toxicological data and epidemiological data to characterize the reproductive health effects of BPA analogs in human. Future studies on BPA analogs should assess their absorption, distribution, metabolism, and excretion, validate the current findings on *in vivo* reproductive toxicities, elucidate *in vitro* mechanisms of action, and monitor human exposure levels. These multifaceted data will potentially allow for comparing information across BPA analogs and a better risk assessment of bisphenols in general.

Given current data and potential opportunities, research studies are needed in the future.

- Environmental studies are needed to better elucidate the environmental occurrence of BPA analogs and determine sources and pathways of human exposure.
- Epidemiological studies should be conducted in general population with precise measurement of chronic exposure level. Co-exposure should be considered.

- *In vivo* studies are needed to better elucidate the metabolic pathways of BPA analogs and target the internal doses and exposure time relevant to human BPA exposure with appropriate selection of the positive control.

- *In vitro* studies are needed to elucidate the unique mechanisms and modes of actions of BPA analogs in reproductive systems.

Table 1.1. BPA and oocyte outcomes in experimental studies.

Animal	Strain	Exposure route	Time of exposure	Doses	Age at collection	Summary	Reference
Mouse	C57B L/6J	Oral doses	3 estrous cycle	50 μg/kg	After the 3 estrous cycles	Young (PND 28-32) female rats were exposed to BPA at a dose of 50 μg/kg during the first estrous cycle. In *in vivo* and *in vitro* fertilization assay, BPA exposure significantly decreased the percentage of fertilized oocytes. No changes of ovulation were observed	(Moore-Ambriz, *et al.*, 2015)
Bovine		*In vitro* oocyte	24 h	15 and 30 ng/ml		In bovine oocytes, BPA treatment decreased meiosis progression and increased spindle abnormalities, including abnormal spindle morphology and chromosome alignment at a dose of 30 ng/ml.	(Ferris, *et al.*, 2015)
Porcine		*In vitro* oocyte		250 μM		BPA treatment increased ROS, abnormal cytoskeleton, apoptosis/autophagy rate, and altered epigenetic pattern in porcine oocyte	(Wang, *et al.*, 2016d)
Bovine		*In vitro* cumulus oocyte complexes	8 days	65 and 130 nM		Bovine oocytes exposed to BPA were fertilized in embryo culture and showed significant induction of DNA damage and apoptosis at a dose of 130 nM, while gene expression in blastocysts was not altered.	(Ferris, *et al.*, 2016)
Mouse	ICR	*In vitro* oocyte	6, 9, 12, 15 and 18 h	2, 20, 50 and 100 μg/ml		BPA exposure inhibited oocyte maturation at doses of 50 and 100 μg/ml and delayed cell cycle at a dose of 2 μg/ml. Further BPA treatment caused spindle abnormalities and activated the spindle assembly checkpoint at a dose of 50 μg/ml	(Nakano, *et al.*, 2016)

Table 1.2. BPA and human reproductive outcomes.

Study design	Study population	Sample size	Measurement time	BPA concentrations	Summary	Reference
Retrospective cohort	Boys ages 8–14 (ELEMENT) [a]	118	At the time of hormone measurement	NA	In 118 boys during the peripubertal period, parental (3rd trimester) or childhood BPA exposure was not associated with hormone levels, adrenarche or puberty.	(Ferguson, et al., 2014)
Prospective cohort	Male partners undergoing IVF treatments (Slovenia)	149	Same day as follicle aspiration	Geometric mean 1.55 ng/mL	In 149 couples undergoing IVF, the log-transformed urinary BPA concentration were associated with lower log-transformed sperm count (b = 0.241, 95% CI 0.470 to 0.012), log-transformed sperm concentration (b=0.219, 95% CI 0.436 to 0.003), and sperm vitality (b= 2.660, 95% CI 4.991 to 0.329) in male partners, while the embryo development parameters were not associated with BPA exposure.	(Knez, et al., 2014)
Cross-sectional	Young men from general population (Denmark)	308	Same day as blood sample collection	Median 3.25 ng/mL	In 308 young men from Denmark general population, men with BPA concentrations above the lowest quartile had higher serum T, LH, E2, and free T levels, as compared with the lowest quartile ($p \leq 0.02$). Men in the highest quartile of BPA concentrations had lower sperm progressive motility, as compared with men in the lowest quartile (–6.7 %, 95% CI, –11.76, –1.63).	(Lassen, et al., 2014)
Case-control	Girls with central precocious puberty (Korea)	40 Peripheral PP/42 Central PP/32 Controls	Same day as blood sample collection	8.7 ± 7.6 µg/g creatinine (peripheral-PP), 8.0 ± 9.9 µg/g (central-PP), 6.6 ± 7.3 µg/g (control)	In 82 PP patients, BPA levels were slightly higher compared with 32 age-matched healthy girls but not associated with the onset of PP. Altered steroid metabolism was associated with urinary BPA levels. Levels of T, E2, and P4 were significantly increased in individuals with higher BPA level.	(Lee, et al., 2014)

Case-control	Women with confirmed endometriosis (WREN)[c]	143 Cases/287 Controls	After disease diagnosis	Median 1.32 ng/mL(cases), 1.24 ng/mL (control)	In 143 endometriosis cases and 287 population-based controls, total urinary BPA concentrations were positively associated with non-ovarian pelvic endometriosis (second versus lowest quartile, OR 3.0; 95% CI, 1.2, 7.3; third versus lowest quartile, OR 3.0; 95% CI, 1.1, 7.6), but not associated with ovarian endometriosis.	(Upson, et al., 2014)
Case-control	Female PCOS patients from an urban academic medical center in Los Angeles	52 Cases/50 Controls	Same day as blood sample collection	Geometric mean 1.6 µg/L (PCOS case), 2.1 µg/L (control)	In 52 patients diagnosed with PCOS, the urinary BPA concentrations were not associated with increased risk of PCOS.	(Vagi, et al., 2014)
Case-control	Female PCOS patients from a Paediatric Endocrinology Outpatient Clinic (Turkey)	112 Cases/61 Controls	During the early follicular phase	Geometric mean 1.61 ng/mL (PCOS case), 0.8 ng/mL (control)	Among 112 girls with PCOS and 61 controls between 13 and 19 years of age, serum BPA levels markedly increased in PCOS cases. BPA levels were significantly correlated with total T (r = 0.52), free T (r = 0.44) (p < 0.05).	(Akin, et al., 2015)
Prospective cohort	Male partners of couples trying to become pregnant (LIFE)	418	Two days before semen collection	Geometric mean 0.55 ng/mL	In 418 male from Michigan and Texas, 2005–2009, BPA levels were negatively associated with DNA fragmentation in adjusted linear regression (˘ = −0.0544, p = 0.035). No associations between BPA exposure and other sperm parameters were observed.	(Goldstone, et al., 2015)
Cross-sectional	Male workers with occupational exposure (China)	592	Pre and post-shift	Median 685.9 µg/g creatinine (exposed), 4.2 µg/g creatinine (unexposed)	Among 592 male workers, urinary BPA levels were associated with increased prolactin (p<0.001), E2 (p < 0.001), sex SHBG level (p = 0.001), and a reduced androstenedione (p < 0.001) and free androgen index level (p = 0.021).	(Liu, et al., 2015b)

Cross-sectional	Female workers with occupational exposure (China)	356	Pre and post-shift	Geometric mean 22 µg/g creatinine (exposed), 0.4 µg/g creatinine (unexposed)	In 106 exposed and 250 unexposed female workers, urinary BPA levels were positively associated with higher PRL and PROG levels ($p<0.05$). The BPA levels were positively associated with E2 levels among exposed workers ($p = 0.05$) and negatively associated with FSH levels among the unexposed group ($p<0.005$).	(Miao, et al., 2015)
Prospective cohort	Female completed at least one IVF cycle (Massachusetts General Hospital Fertility Center)	256	Same day of oocyte retrieval	Geometric mean 1.87 ng/mL	In 256 women undergoing IVF, urinary BPA concentrations were not associated with endometrial wall thickness, peak E2 levels. Younger women (<37 years old) had thicker endometrial thickness across increasing quartiles of urinary BPA concentrations, while older women (≥37 years old) had thinner endometrial thickness across increasing quartiles of urinary BPA concentrations.	(Minguez-Alarcon, et al., 2015)
Cross-sectional	Male workers with occupational exposure (China)	559	Pre-shift	Median 18.75 ng/mL (exposed) 3.37 ng/mL (unexposed)	In 281 exposed and 278 unexposed male workers, serum BPA levels were increased after occupational exposure. The serum BPA levels were associated with lower serum AD level (0.18 ng/mL; 95 % CI -0.22 to -0.13) and higher serum SHBG level (2.79 nmol/L; 95 % CI 2.11–3.46).104	(Zhuang, et al., 2015)
Cross-sectional	Male and female children (6-11 years) and adolescents (12-19 years) from general population (NHANES	588	NA	Geometric mean 1.40-1.94 ng/mL	In 558 child and adolescent participants, urinary BPA concentrations were associated with significantly lower total T levels in male adolescents, and significantly higher total T levels in female adolescents ($p=0.01$).	(Scinicariello and Buser, 2016)

	2011-2012)					
Case-control	Female PCOS patients who worked as marketing sellers (Iran)	62 Cases/62 Controls	NA	0.48 ng/mL (PCOS case), 0.16 ng/mL (control)	In 62 marketing cashiers with PCOS and 62 healthy women with a similar job, serum BPA levels, LH-FSH ratio were significantly increased, while TSH levels were significantly decreased in PCOS cases.	(Vahedi, et al., 2016)
Cross-sectional	Infertile women with PCOS (China)	268	NA	Median 2.35 ng/mL	In 268 infertile women diagnosed with PCOS, urinary BPA levels were associated with a significant decrease in AFC (β = −0.34, 95% CI = −0.60, −0.08; p = 0.01). But no association between BPA level and FSH level was observed.	(Zhou, et al., 2016)
Case-control	Female endometriosis patients	68 Cases/60 Controls	During the consultation	Mean 5.31 ng/mL(cases), 1.64 ng/mL (control)	In 68 patients with endometriosis, urinary BPA levels were significantly higher, as compared with BPA levels in control group.	(Simonelli, et al., 2017)

Table 1.3. BPA and female steroidogenesis in experimental studies.

Animal	Strain	Exposure route	Time of exposure	Doses	Age at collection	Summary	Reference
Rat	SD	Oral gavage	Gestational Day (GD) 6-PND 90	2.5–300000 μg/kg	PND 80	SD female rats were exposed to BPA orally from GD 6 through PND 90. The chronic BPA exposure resulted in increases in serum E2 and prolactin levels only at 100000 and 300000 μg/kg groups. P4 levels were significantly decreased at 300,000 μg groups.	(Delclos, *et al.*, 2014)
Rat	Wistar	Intraperitoneal injection	PND 28-PND 35	10, 40 and 160 mg/kg	PND 35	Pre-puberty female Wistar rats were exposed to BPA for one week. BPA exposure decreased P4 levels at 40 and 160 mg BPA/kg BW/day, while serum E2 levels were not altered.	(Li, *et al.*, 2014)
Rat	Long-Evans	Oral gavage	GD 0-PND 9	4, 40 and 400 μg/kg	PND 23	Long–Evans rats received oral administration of BPA at doses of 4, 40, and 400 μg/kg throughout pregnancy and the pups received direct oral administration of BPA between PND 1–9. Rats in both genders had decreased levels of FSH at weaning at doses of 4 and 400 μg/kg. But no changes in other hormone levels and maze behavior were observed.	(Sadowski, *et al.*, 2014)
Rat	Wistar	Drinking water	GD 0-PND 21	3 μg/kg	PND 30	Wistar mated rats were treated with BPA in their drinking water (estimated 3 μg/kg) until their offspring were weaned on the 21 days of birth. Serum LH and E2 levels were significantly increased in the treatment group with increased follicle number, while no changes in serum FSH levels were observed.	(Gamez, *et al.*, 2015)
Mouse	C57BL/6J	Oral dose	3 estrous cycle	50 μg/kg	After the 3 estrous cycles	Young (PND 28-32) female rats were exposed to BPA at a dose of 50 μg/kg during the first estrous cycle. In *in vivo* and *in vitro* fertilization assay, BPA exposure significantly decreased the percentage of fertilized oocytes. No changes of ovulation and hormone levels were observed	(Moore-Ambriz, *et al.*, 2015)

Rat	Wistar	Drinking water	GD 9-PND 21	0.5 and 50 µg/kg	PND 90	In adult female rat offsprings with gestational and lactational exposure, serum P4 levels were significantly increased in BPA 0.5 and 50 µg/kg groups coupled with high mRNA expression of 3b-HSD.	(Santamaria, *et al.*, 2016)
Human		*In vitro* granulosa cells	48 h	0.2, 0.02, 2.0, 20 mg/ml		Treatment of human granulosa cells with BPA for 48 h resulted in significant lower P4 biosynthesis at doses of 2 or 20 mg/ml and lowered E2 levels at a dose of 20 mg/ml. These two concentrations significantly reduced the mRNA and protein levels of 3b-HSD, CYP11A1, and CYP19A1 without affecting StAR and 17b-hydroxysteroid dehydrogenase mRNA expression.	(Mansur, *et al.*, 2016)

Table 1.4.1. BPA and ovary outcomes in experimental studies.

Animal	Strain	Exposure route	Time of exposure	Doses	Age at collection	Summary	Reference
Rat	SD	Oral gavage	GD 6-PND 90	2.5–300000 µg/kg	PND 21	SD rats exposed to BPA orally from GD 6 through PND 90. Adverse effects of BPA exposure on the ovary, including increased cystic follicles, depleted corpora lutea, and antral follicles at two doses (100000 and 300000 µg/kg).	(Delclos, et al., 2014)
Rat	Wistar	Intraperitoneal injection	PND 28-PND 35	10, 40 and 160 mg/kg	PND 35	Pre-puberty female Wistar rats were exposed to BPA for one week. BPA exposure significantly decreased rat ovarian weights and follicle numbers at doses of 40 and 160 mg/kg. In addition, the mRNA and protein levels of the germline alpha and oocyte-specific histone H1 variant were decreased at 160 mg/kg and 10-160 mg/kg, respectively.	(Li, et al., 2014)
Rat	Wistar	Dietary exposure and drinking water	GD 6-PND 40	0.18-0.44 mg/kg	PND 120	Wistar rats exposed to BPA during GD 6-PND 40 showed delayed vaginal opening. But no changes in corpora lutea and cystic follicles were observed.	(Patisaul, et al., 2014)
Mouse	FVB	Oral dose	GD 11-PND 0	0.5, 20, and 50 µg/kg	PND 4 and 21 (F1-F3)	To examine the transgenerational effects of BPA on the ovary, FVB mice exposed to BPA in utero and ovaries of F1-3 generations were collected at PND 4 and PND 21 to examine expression levels of multiple genes in apoptosis, antioxidant, igf family, hormone receptor, and steroidogenesis. Overall, more significant changes in gene expressions were observed at PND 21. The transgenerational effects of BPA were observed in the F3 generation in a non-monotonic dose-dependent manner.	(Berger, et al., 2016)
Rat	Wistar	Drinking water	GD 9-PND 21	0.5 and 50	PND 90	In adult female rat offsprings with maternal exposure to low doses of BPA during	(Santamaria, et al., 2016)

31

				μg/kg		gestation and breastfeeding. Ovaries from both BPA-treated groups showed decreased weight, primordial follicle recruitment and a greater number of corpora lutea.	
Rat	Wistar	Drinking water	GD 0-PND 21	3 μg/kg	PND 30	No changes in ovarian weight and its relative weight were observed.	(Gamez, *et al.*, 2015)
Mouse	CD-1	*In vitro* ovary	24-192 h	0.1, 1, 5, and 10 μg/mL	PND1, 2, 4 and 8	In ovaries of newborn mice, BPA exposure increased germ cells and decreased primordial follicle. Further, BPA exposure altered the expression of key genes involved in apoptosis and antioxidation, while the effects varied by ovary collection times and exposure doses.	(Zhou, *et al.*, 2015)
Rat	F344	*In vitro* ovary	48-192 h	440 μM	PND 4	In F344 rat ovaries, BPA treatment reduced small primary, large primary and secondary follicle numbers and increased DNA manage markers, γ-H2AX, ATM, and DNA repair genes.	(Ganesan and Keating, 2016)

Table 1.4.2. BPA and uterine outcomes in experimental studies.

Animal	Strain	Exposure route	Time of exposure	Doses	Age at collection	Summary	Reference
Monkey	Rhesus Macaque	Dietary exposure	GD 100-GD 165	400 μg/kg	GD 165 (F1)	The pregnant rhesus macaques were exposed orally to BPA. Fatal uteri did not show notable changes in uterus histology, proliferation, expression of hormone receptors. At GD 165, BPA exposure altered expression levels of three genes (HOXA13, WNT4, and WNT5A) involved in reproductive organ development.	(Calhoun, et al., 2014)
Mouse	ICR	Intraperitoneal injection	0.5, 1, 2, 4, 6 and 12 h	10, 20, 50, 100, 200 and 500 mg/kg	Adult	Early growth response 1 gene was rapidly and transiently induced by BPA (starting at 20 mg/kg) in stromal cells surrounding implanting blastocyst via nuclear ER-ERK1/2 pathway.	(Kim, et al., 2014)
Mouse	C57Bl/6 N and CD-1	Dietary exposure	4 weeks	0.004, 0.04, 0.4, 4, and 40 mg/kg	Adult	BPA treatment non-monotonically increased gland nest density and periglandular collagen accumulation, collagen I and III expressions, immune response, decreased matrix metalloproteinase 2 at a dose of 4 mg/kg in CD-1 group only.	(Kendziorski and Belcher, 2015)
Rat	SD	Oral gavage	GD 6-PND 90	2.5, 8, 25, 80, 260, 840, 2700, 100,000 and 300,000 μg/kg	PND 4, PND 90	In SD rats exposed BPA orally, no changes in global genomic DNA methylations in uterus were observed. Changes in DNA methylation in prostate and female mammary gland were only observed in BPA-high dose groups (100,000 and 300,000 μg/kg).	(Camacho, et al., 2015)
Rat	SD	Ex-vivo	3-5 min	1×10^{-8}-1×10^{-4} M	Adult	In ex-vivo uterus contraction assay, uterine	(Salleh, et al., 2015)

						contractile force decreased with increasing doses of BPA.	
Rat	Wistar	Drinking water	GD 9-PND 21	0.5 and 50 μg/kg	PND 90, PND 360	Wistar rats were exposed to BPA via drinking water through GD 9 to PND 21. The female offsprings showed decreases in glandular proliferation (0.5 and 50 μg/kg) and α-actin expression (50 μg/kg) at PND 90, increases in the incidence of abnormalities in the luminal (50 μg/kg) and glandular epithelium (0.5 and 50 μg/kg) at PND 360.	(Vigezzi, *et al.*, 2015)
Mouse	CD-1	Oral	PND 22-GD 9	60 and 600 μg/kg	GD 9	In CD-1 mice, BPA exposure affected puberty and estrous cyclicity, decreased embryo implantation, PGR and HAND2 expression in uterine with enhanced activation of fibroblast growth factor and MAPK signaling in the epithelium, and increased improper endometrial epithelial and stromal functions.	(Li, *et al.*, 2016b)
		In vitro uterine smooth muscle cells	48 h	2.28 ng/mL		In uterine smooth muscle cells, BPA treatment upregulated genes involved in cell differentiation, cellular metabolic processes, cell proliferation and smooth muscle contraction, and decreased the genes involved in mitosis, lipid metabolism, regulation of muscle cell differentiation and cell adhesion	(Kang, *et al.*, 2014)
Human		*In vitro* endometrial endothelial cell	24 h	0.01, 1, 100, 10000 nM		The HECC cells were co-cultured with primary endometrial stromal cells to mimic the *in vivo* situation and treated with environmentally relevant doses of BPA. BPA exposure did not alter the HEEC viability and proliferation, and	(Helmestam, *et al.*, 2014)

34

				increased tube formation and VEGF-D protein expression at a dose of 10000 nM.	
Human	*In vitro* uterine leiomyoma	24, 48 and 72 h	1, 2.5, 5, 10 and 20 μM	The BPA exposure increased the protein expression level of ERα, IGF-1, and VEGF at doses of 2.5, 5 and 10 μM in uterine leiomyomas.	(Shen, *et al.*, 2014)
Human	*In vitro* endometrial carcinoma cells line (RL95-2)	7 days	$1\times10\text{-}10\text{-}1\times10\text{-}4$ M	The BPA exposure increased gene expression of cyclooxygenase-2 and epithelial-mesenchymal transition, promote growth rate and colony-forming efficiency in a nonmonotonic manner in human endometrial carcinoma cells line.	(Qian, *et al.*, 2015)

35

Table 1.5. BPA and sperm outcomes in experimental studies.

Animal	Strain	Exposure route	Time of exposure	Doses	Age at collection	Summary	Reference
Rat	SD	Oral gavage	PND 28-70	1, 5 and 100 mg/kg	PND 70	In prepubertal SD rats, 6-week BPA oral exposure increased disruption of intercellular junction s, sloughing of germ cells, and number of immature germ cells and cellular debris. No testis weight changes were observed. Further BPA exposure decreased plasma T and E2 levels in all treatment groups.	(Gurmeet, et al., 2014)
Rat	Wistar	Oral gavage	60 days	20 µg/kg	Adult	In Wistar rats, a 60-day exposure to BPA at an environmentally relevant dose resulted in an significant increase in the proportion of stage VII seminiferous epithelium and a decrease in stage VII. Further, BPA exposure induced the expression level of γ-H2AX, ATM and SCP3, suggesting DNA damage and early meiosis inhibition.	(Liu, et al., 2015b) 80
Mouse	Vesper	Oral gavage	GD 0-PND 0	40, 80 and 200 µg/kg	PND 70	In vesper mice received utero BPA exposure, BPA treatment significantly reduced the sperm with normal morphology at a dose of 200 µg/kg, mitochondrial integrity at doses of 80 and 200 µg/kg, and in vitro sperm penetration rate starting at 40 µg/kg, Whereas no changes in DNA integrity and acrosome integrity were observed.	(Vilela, et al., 2014)
Rat	SD	Oral gavage	4 weeks	50, 100, and 200 mg/kg	Adult	In SD rat, BPA exposure increased germ cell apoptosis in testes and decreased sperm concentrations at doses of 100 and 200 mg/kg. Further, BPA exposure significantly increased protein and mRNA levels of cytochrome C, apoptosis-inducing factor, caspase-3/9, Bas, and decreased protein and gene levels of Bcl-2 in all treatment groups. Also, the abnormal	(Wang, et al., 2014)

Mouse	C57BL/6J	Intraperitoneal injection	PND 21-28	50 mg/kg	PND 56	structure of mitochondria was observed at a dose of 200 mg/kg. In C57BL/6J mice received BPA exposure, a decrease in epididymal sperm number and an increase in sperm deformity rate were observed. Abnormal seminiferous tubules with sloughing of germ cells were observed, while male fertility was not affected.	(LI, et al., 2015)
Rat	SD	Oral gavage	GD 0-PND 21	40 μg/kg	PND 56 (F1)	The paternal BPA exposure induced Igf2 DMR2 methylation and decreased mRNA expression of IGH2 in F1 rats' sperms, which potentially associated with hypermethylation of Igf2 observed in islets of F2 male offsprings.	(Mao, et al., 2015)
Mouse	Cd-1; C57BL/6J; C3H/HeJ	Oral gavage	PND 1-PND 12	20 and 500 μg/kg	PND 12/84/365	In multiple strains of mice, BPA exposure did not alter the chromosome pairing and synapsis in spermatogonial stem cells.	(Vrooman, et al., 2015)
Rat	Wistar	Oral gavage	PND 50-90	5 and 25mg/kg	PND 105	In Wistar rats exposed to BPA orally, serum T, LH, and FSH levels were decreased, and the E2 level was increased in both treatment groups. In addition, the gene expression levels of hormone receptors were increased in the hypothalamus. BPA exposure reduced sperm production, reserves and transit time in both treatment groups.	(Wisniewski, et al., 2015)
Rat	Wistar	Oral gavage	GD 7-PND 22	25, 250, 5000 and 50000 μg/kg	3 months	Prenatal and postnatal BPA exposure significantly decreased sperm count only at a dose of 25 μg/kg in Wistar rat. No changes in reproductive organ were observed.	(Hass, et al., 2016)
Mouse	Swiss Albino	Oral gavage	PND 0-PND 21	300, 900, and 3000 μg/kg	Adult	During breastfeeding period, maternal BPA exposure altered sperm parameters (sperm motility; normal morphology; membrane integrity; acrosomal integrity; DNA integrity;	(Kalb, et al., 2016)

					and mitochondrial functionality) at all treatment groups. 3000 µg/kg BPA treatment also induced testicular degeneration. In addition, the total antioxidant capacity was impaired at doses of 900 and 3000 µg/kg.	
Rat	SD	Intraperitoneal injection	20 days	2, 10, 50 mg/kg	6 months	In SD rat, BPA exposure induced oxidative stress (SOD activity, GSH-Px activity, and MDA level) at a dose of 50 mg/kg and sperm malformation rate and apoptosis in testes at all treatment groups. The mRNA expressions of genes in Akt/mTOR pathway were altered in the different treatment groups. In addition, the serum T (2, 10, 50 mg/kg), FSH (10 and 50 mg/kg), and LH (50 mg/kg) levels were decreased.	(Quan, *et al.*, 2016a)
Rat	SD	Oral gavage	GD 14-21	1, 10, 100 mg/kg	PND 21	In SD rat male offspring, utero BPA exposure induced oxidative stress (MDA level) at doses of 10 and 100 mg/kg, increased apoptosis in testes, and altered seminiferous tubules morphology at all treatment groups. The mRNA and protein expressions of genes in Akt/mTOR pathway were altered in the different treatment groups. In addition, the serum T (100 mg/kg), FSH (100 mg/kg) and LH (1, 10, 100 mg/kg) levels were decreased.	(Quan, *et al.*, 2016b)
Mouse	CD-1	Oral gavage	GD 7-14	50, 5000 and 50000 µg/kg	PND 120	Gestational exposure to BPA decreased sperm count, motility parameters, and intracellular ATP levels in a dose-dependent manner. BPA exposure reduced numbers of stage VIII seminiferous epithelial cells in testes at doses of 5000 and 50000 µg/kg and decreased PKA activity and tyrosine phosphorylation in spermatozoa at doses of 5000 and 50000 µg/kg. Further, BPA exposure altered the expression levels of multiple proteins	(Rahman, *et al.*, 2016)

38

Mouse	C57BL/6	Oral gavage	8 weeks	10, 50 and 250 µg/kg	Adult	involved in ATP production, oxidative stress response, and fertility. In C57BL/6J mice, BPA exposure decreased sperm viability at a dose of 250 µg/kg and motility at all treatment groups. Sperm-specific Ca^{2+} channel currents were reduced in at all treatment groups. And the mRNA and protein levels of CatSper subunits were reduced at doses of 50 and 250 µg/kg. Similar results were observed *in vitro* sperm treated with BPA.	(Wang, *et al.*, 2016b)
Mouse	Kunming	Oral gavage	5 weeks	3, 30 and 300 mg/kg	Adult	In Kunming mice, BPA exposure induced spermatogenic cellular apoptosis, sloughing of germ cells, and seminiferous tubules vacuolation in all treatment groups.	(Yin, *et al.*, 2016)
Rat	Wistar	Oral gavage	35 weeks	50 µg/kg	Adult	In Wistar rats received 50 µg/kg BPA exposure for 35 weeks, no apoptosis or sperm deformation was observed. While BPA exposure decreased protein lysine acetylation levels and increased the expression of histone deacetylase Sirt1, ERβ expression and its binding with caveolin-1 in testes.	(Chen, *et al.*, 2017)
Mouse		*In vitro* spermatocyte GC-2 cell line	0.5-48 h	0.02–20 µM		In mouse spermatocyte GC-2 cell line, BPA treatment decreased cell viability, release of mitochondrial cytochrome c and caspase-3 levels at doses from 0.2 to 20 µM. Further, BPA exposure impaired Ca^{2+} homeostasis and induced Ca^{2+} sensor proteins (CaM and CaMKII) expressions starting at 0.02 and 0.2 µM, respectively. The pretreatment with Ca^{2+} chelator or sensor protein inhibitor could partially attenuate BPA-induced cellular injury.	(Qian, *et al.*, 2015)
Mouse	ICR	*In vitro* spermatozoa	6 h	0.0001, 0.01, 1, and 100		BPA exposure significantly decreased sperm motility, fertilization rate, and intracellular ATP levels at a dose of 100 µM. In addition,	(Rahman, *et al.*, 2015)

				μM	BPA induced the protein kinaseA activity, tyrosine phosphorylation and fertility-related proteins (peroxiredoxin-5, glutathione peroxidase 4, glyceraldehyde-3-phosphate dehydrogenase, and succinate dehydrogenase), except β-actin in spermatozoa.	
Human		*In vitro* spermatozoa	4 and 20 h	10–800 μM	In human spermatozoa, BPA exposure decreased sperm motility, viability, and MMP, and increased apoptosis, DNA oxidative damage marker, 8-hydroxy-2'-deoxyguanosine starting at a dose of 300 μM.	(Barbonetti, *et al.*, 2016)
Human		*In vitro* spermatozoa	5-60 min	10–10, 10–8 and 10–6 M	In human spermatozoa, BPA treatment induced a transient increase of velocity straight linear and homogeneity of progressive movement velocity at 15 min after stimulation. 1h BPA exposure did not alter vitality phosphatidylserine membrane translocation for all doses. BPA treatment at a dose of 10–6 M induced a rapid, and transient increase in intracellular free Ca^{2+} concentration.	(Kotwicka, *et al.*, 2016)
Rat	SD	*In vitro* mature sperm	10-300 min	1-600 μg/ml	In rat sperm, exposure to BPA significantly decreased sperm motility in a dose and time-dependent manner. Further, capacitation-associated protein tyrosine phosphorylation was induced by BPA treatment, while the induction could be blocked by PKA inhibitor.	(Wan, *et al.*, 2016)
Mouse		*In vitro* spermatocyte GC-2 cell line	24 and 48 h	20, 40 and 80 μM	In mouse spermatocyte GC-2 cell line, BPA exposure decreased cell viability starting at 50 μM for 24 h hand 5 μM for 48 h, and induced apoptosis, endoplasmic reticulum stress, ROS, mitochondrial damage and mitochondrial apoptotic pathway starting at 20 μM for 48 h. Knocking down of the PERK/EIF2α/chop pathway partially attenuated the BPA-induced	(Yin, *et al.*, 2016)

| Mouse | *In vitro* Spermatog onial cell line C18-4 | 24, 48 and 72 h | 0.1, 1, 10, and 50 µM | cell apoptosis. The BPA exposure significantly decreased cell viability, altered nuclear morphology, increased γ-H2AX expression level, and perturbed cytoskeleton and cell cycle progression at a dose of 50 µM in spermatogonial cell line C18-4. | (Liang, *et al.*, 2017) |

Table 1.6. BPA and Sertoli/Leydig cells in experimental studies.

Animal	Strain	Exposure route	Time of exposure	Doses	Age at collection	Summary	Reference
Mouse		*In vitro* Sertoli cell line TM4	24 and 48 h	10^{-8} M and 10^{-5} M		Exposure to 10^{-5} M BPA induced oxidative stress and inhibited cell proliferation. Exposure to 10^{-8} M BPA increased intercellular ATP levels, activities of mitochondria, and proliferation of Sertoli cell line TM4.	(Boudalia, *et al.*, 2014)
Mouse		*In vitro* Sertoli cell line TM4	24 and 48 h	10^{-8} M and 10^{-3} M		Exposure to 1 and 10 nM BPA significantly induced the Sertoli cell proliferation via activating ERK1/2 through GPR30 and ER α/β.	(Ge, *et al.*, 2014)
Rat		*In vitro* primary Sertoli cell culture	24 h	30, 50, 70 and 90 μM		In primary rat Sertoli cells, BPA exposure significantly reduced cell viability and induced apoptosis starting at a dose of 50 μM. Further, BPA exposure activated JNKs/p38 MPAK and Fas/FasL signaling pathways, and induced translocation of NF-κ B at doses of 50 and 70 μM.	(Qi, *et al.*, 2014)
Mouse		*In vitro* Sertoli cell line TM4	12, 24 and 48 h	0.02, 0.2, 2.0 and 20 μM		In primary rat Sertoli cells, BPA treatment significantly reduced cell viability and induced apoptosis starting at a dose of 50 μM. Further, mitochondrial mass loss, membrane potential decrease, cytochrome c release, Bcl-2 family members down-regulation and caspases-3 up-regulation were observed in TM4 cells treated with BPA. Additionally, the expression of CaM, ERK1/2, and phosphorylation of CaMKII were significantly increased after BPA treatment. Treatments with CaM, ERK1/2 and CaMKII inhibitor attenuated BPA-induced cell damage.	(Qian, *et al.*, 2014)
Human		*In vitro* primary Sertoli cell culture	24, 48 and 72 h	0.4, 4, 40 and 300 μM		In human Sertoli cells, BPA exposure significantly decreased the cell viability, expression levels of ZO-1, N-Cadherin and β-Catenin at a dose of 200 μM. BPA treatment also increased truncation and depolymerization of	(Xiao, *et al.*, 2014)

Rat		*In vitro* primary Sertoli cell culture	24 h	30, 50, and 70 μM		actin microfilaments starting at 0.4 μM and improper localization of actin regulatory proteins Arp3 and Eps8 at a dose of 200 μM. In primary rat Sertoli cells, BPA exposure decreased cell viability and induced apoptosis at doses of 50 and 70 μM. BPA exposure caused the elevation of Pten expression and the inactivation of Akt, and then triggered the caspase3, which led to apoptosis of Sertoli cells.	
Human		*In vitro* primary Sertoli cell culture	6 and 24 h	20 μM		In human Sertoli cells, BPA exposure significantly decreased the cell viability, expression levels of occludin, ZO-1, β-catenine, and AR at a dose of 20 μM for 6 and 48 h without changes in F-actin expression or localization.	(de Freitas, *et al.*, 2016)
Rat		*In vitro* primary Sertoli cell culture		30, 50, and 70 μM		In primary rat Sertoli cells, BPA exposure induced ROS, intracellular Ca^{2+} release at doses of 50 and 70 μM and cellular apoptosis at a dose of 70 μM. Pretreatment with N-acetyl-L-cysteine attenuated the BPA-induced cellular apoptosis.	(Wang, *et al.*, 2016a)
Rat	Long-Evans	*In vitro* primary Leydig cell culture	18 h	0.01 nM		Treatment of adult Leydig cells with 0.01 nm BPA decreased T biosynthesis and E2 level, and mRNA expressions of aromatase and the steroidogenic enzyme 17α-hydroxylase/17–20 lyases.	(Akingbemi, *et al.*, 2004)
Rat	Wistar/ SD	Intraperitoneal injection	6 weeks	0, 20, 100 and 200mg/kg	Adult	BPA treatment significantly decreased Leydig cell number and StAR protein levels in the rat testes at a dose of 200 mg/kg.	(Nakamura, *et al.*, 2010)
Rat	Long-Evans	Oral gavage	GD 12-PND 21	2.5 and 25 μg/kg	Adult	BPA exposure (2.5 and 25 μg/kg) significantly promoted Leydig cell division during the prepubertal period and increased Leydig cell numbers at PND 90. In Leydig cells, BPA treatment induced the protein expressions of proliferating cell nuclear antigen, MAPK, AR, and ER, and increased secretion of the anti-Mullerian hormone. In addition, BPA suppressed	(Nanjappa, *et al.*, 2012)

43

| Mouse | *In vitro* Leydig cell line TM3 | 24, 48 and 72 h | 10−8 to 10−3 M | protein expressions of the LH receptor and the 17beta-hydroxysteroid dehydrogenase enzyme. In Leydig TM3 cells, BPA greater than 10−6 M inhibited proliferation of Leydig TM3 in a dose-dependent manner. The proteomic study revealed BPA could modulate the expression of proteins related to cell structure, motility, and cellular metabolism. Further, BPA treatment induced cell migration at a dose of 10−5 M via galectin-1 and ERK1/2. | (Chen, *et al.*, 2016c) |

Table 1.7. BPA and male steroidogenesis in experimental studies.

Animal	Strain	Exposure route	Time of exposure	Doses	Age at collection	Summary	Reference
Rat	SD	Oral gavage	GD 6-PND 90	2.5–300000 µg/kg	PND 15	In male offspring, BPA exposure significantly increased serum T4 level at the highest BPA dose group. No changes in serum T3 and FSH levels and testicular descent were observed.	(Delclos, et al., 2014)
Rat	Wistar	Drinking water	GD 6-PND 21	3 µg/kg	PND 35	In Wistar rats exposed to BPA, a decrease in testicular weight was observed, while seminal vesicles weight, relative weights of testes and seminal vesicles were not changed.	(Gamez, et al., 2014)
Rat	SD	Oral gavage	PND 28-70	1, 5 and 100 mg/kg	PND 70	In prepubertal SD rats, 6-week BPA oral exposure induced disruption of the intercellular junction, sloughing of germ cells, and number of immature germ cells and cellular debris. No testis weight changes were observed. Further BPA exposure decreased plasma T and E2 levels in all treatment groups.	(Gurmeet, et al., 2014)
Rat	Long-Evans	Oral gavage	GD 0-PND 9	4, 40 and 400 µg/kg	PND 23	Long–Evans rats received oral administration of BPA at doses of 4, 40, or 400 µg/kg throughout pregnancy, and the pups received direct oral administration of BPA between postnatal days 1–9. Rats had decreased levels of FSH at weaning at doses of 4 and 400 µg/kg but no changes in other hormone levels and maze behavior were observed.	(Sadowski, et al., 2014)
Mouse	Swiss albino	Intraperitoneal injection	60 days	0.5, 50 and 100 µg/kg	Adult	In Swiss albino mice, 60-day intraperitoneal BPA exposure significantly decreased sperm count, StAR expression, and serum T level in all treatment groups.	(Chouhan, et al., 2015)
Rat	SD	Intraperitoneal injection	20 days	2, 10, 50 mg/kg	6 months	In SD rat, BPA exposure induced oxidative stress (SOD activity, GSH-Px activity, and MDA level) at a dose of 50 mg/kg, sperm malformation rate and apoptosis in testes at all treatment groups. The mRNA expressions of	(Quan, et al., 2016a)

Rat	SD	Oral gavage	GD 14-21	1, 10, 100 mg/kg	PND 21	genes in Akt/mTOR pathway were altered in the different treatment groups. In addition, the serum T (2, 10, 50 mg/kg), FSH (10 and 50 mg/kg) and LH (50 mg/kg) levels were decreased. In SD rat male offsprings, utero BPA exposure induced oxidative stress at doses of 10 and 100 mg/kg, increased apoptosis in testes, and altered seminiferous tubules morphology in all treatment groups. The mRNA and protein expressions of Akt/mTOR pathway were altered in the different treatment groups. In addition, the serum T (100 mg/kg), FSH (100 mg/kg) and LH (1, 10, 100 mg/kg) levels were decreased.	(Quan, *et al.*, 2016b)
Rat	Wistar	Oral gavage	PND 50-90	5 and 25mg/kg	PND 105	In Wistar rats exposed to BPA orally, serum T, LH, and FSH levels were decreased, and E2 levels were increased in both treatment groups. In addition, the gene expression levels of hormone receptors were increased in the hypothalamus. BPA exposure decreased sperm production, reserves and transit time in both treatment groups.	(Wisniewski, *et al.*, 2015)
Mouse	C57BL/6	Intraperitoneal injection	21 days	10, 50 and 100 mg/kg	Adult	In C57BL/6 mice, BPA exposure significantly impaired the sexual behavior, decreased testis weight in all treatment groups, and perturbed epididymis at a dose of 100 mg/kg group. Further BPA exposure decreased serum T levels at a dose of 100 mg/kg and intratesticular T at doses of 50 and 100 mg/kg.	(Zang, *et al.*, 2016)
Human/ Mouse/ Rat		*In vitro* fetal testis explants	24-72 h	0.001-10000 nM		BPA exposure significantly reduced basal T secretion levels in rat fetal testis explants at a dose of 10000 nM, in mouse at doses of 1000 and 10000 nM, and in human starting at 10 nM.	(Eladak, *et al.*, 2015)

Table 1.8. BPS and reproductive outcomes in experimental studies.

Animal	Strain	Exposure route	Time of exposure	Doses	Age at collection	Summary	Reference
Rat	Wistar	Subcutaneous injection	3 days	20, 100 and 500 mg/kg	PND 24	BPS showed weaker estrogen receptor binding capacity as compared with E2 (0.0055%). In the immature rat uterotrophic assay, BPS treatment significantly increased absolute and relative uterine wet weight and blotted weight at doses of 20 and 500 mg/kg.	(Yamasaki, *et al.*, 2004)
Fish	Danio ratio	Water	21 days	0.5, 5, and 50 µg/L	Adult	Adult zebrafish were exposed to BPS at doses of]for 21 days. Egg production and gonad somatic index in female fish were significantly decreased starting at 0.5 µg/L. Plasma concentrations of E2 were significantly increased in both genders. In male fish, a significant decrease in T levels was observed with up-regulation of cyp19a and down-regulation of cyp17 and 17β-hsd transcripts at a dose of 50 µg/L. In F1 generation, parental BPS exposure resulted in a delay in hatching rate. Continuous BPS exposure in the F1 further increased malformation rates.	(Ji, *et al.*, 2013)
Fish	Danio ratio	Water	75 days	0.1, 1, 10 and 100 µg/L	Adult	Zebrafish embryos were exposed to various concentrations of BPS for 75 days. The plasma E2 levels were significantly increased in both genders starting at a dose of 100 µg/L. In male fish, BPS exposure decreased plasma T, T3, T4 levels and sperm count at doses of 10 and 100 µg/L. In female fish, BPS exposure decreased T3 and T4 levels at a dose of 100 µg/L, and egg production at doses of 10 and 100 µg/L	(Naderi, *et al.*, 2014)
Rat	SD	Oral gavage	28 days	1, 5, 25 and 50 µg/kg	Adult	In adult rat exposed to various concentrations of BPS, significant increases in the testicular ROS and lipid peroxidation were observed at a dose	(Ullah, *et al.*, 2016)

				50 µg/kg with reduced antioxidant enzyme activities. Further BPS treatment decreased plasma T levels and altered testicular morphology (thin seminiferous epithelium; reduction the tubular epithelium area; empty lumen) at a dose 50 µg/kg. No changes in spermatogenesis were observed.	
Human/ Mouse/Rat	*In vitro* fetal testis explants	24-72 h	10, 100, 1000 and 10000 nM	BPS exposure significantly reduced basal T secretion levels in mouse fetal testis explants starting at 100 nM, and in human explants starting at 1000 nM.	(Eladak*, et al.*, 2015)
Caenorhabditis Elegans		4 days	125, 250 and 500 µM	BPS exposure increased embryonic lethality, germline nuclear loss, and apoptosis at doses of 125, 250 and 500 µM in C. Elegans. 500 µM BPS exposure induced DNA damage and impaired homologous chromosome synapsis. Further BPS show distinct alterations of gene expression at whole transcriptome level, as compared with BPA.	(Chen*, et al.*, 2016b)
Mouse	*In vitro* Leydig cells MA-10	48 h	10 µM	BPS exposure significantly increased P4 levels and gene (5aRed1) in the MA-10 cells at a dose of 10 µM.	(Roelofs*, et al.*, 2015)
Mouse	*In vitro* Spermatogonial cell line C18-4	24, 48 and 72 h	0.1, 1, 10, and 50 µM	The BPS exposure significantly decreased cell viability, altered nuclear morphology, increased γ-H2AX expression level, and perturbed cytoskeleton and cell cycle progression at a dose of 50 µM in spermatogonial cell line C18-4.	(Liang*, et al.*, 2017)

Table 1.9. BPAF and reproductive outcomes in experimental studies.

Animal	Strain	Exposure route	Time of exposure	Doses	Age at collection	Summary	Reference
Rat	SD	Oral gavage	14 days	2, 10, 50 and 200 mg/kg	Adult	In adult rats orally to BPAF at doses from 2 to 200 mg/kg, the concentration of BPAF in testes increased in a dose-dependent manner. In addition, 14-days BPAF exposure decreased serum T levels and the expression levels of genes and proteins in T biosynthesis pathway, and increased serum LH and FSH levels in rats given a dose of 200 mg/kg.	(Feng, et al., 2012)
Rat	SD	Oral gavage	GD 14-GD 18	200, 300, 400,500 and 750 mg/kg	GD 18	The prenatal exposure to BPAF (200-750 mg/kg) did not alter T secretion in dams on GD 18.	(Furr, et al., 2014)
Fish	Danio ratio	Water	Post fertilization (PF) 4h - PF 140d	5, 25 and 125 µg/L	PF 140d	Zebra fish were exposed to BPAF at doses of 5, 25 and 125 ug/L, from 4-hour pf to 120 pf, representing the period from embryo to adult. The increases in E2 levels were observed in both genders, and a decreases in T levels was only observed in the male fishes. In offsprings, increase in malformation and decrease in survival rate were observed only at maternal exposure to BPAF at 125 ug/L.	(Shi, et al., 2015)
Rat	SD	Oral gavage	GD 3-GD 19		PND 23	Female rats were exposed to BPAF (100 mg/kg) orally during gestation or lactation. HPLC-MS/MS analysis showed that BPAF was transferred via cord blood and lactation, finally bio-accumulating in the offspring testes.	(Li, et al., 2016a)
			PND 3-PND 19	100 mg/kg	PND 23	Offsprings exposed to BPAF both prenatally and postnatally showed a significant increase in testicular T levels and alterations in genes involved in cell differentiation and meiosis in testes.	
Fish	Danio	Water	28 days	0.05,	~ PF 80d	Zebrafish exposed to BPAF at a concentration	(Yang, et

49

Species	Strain	Model	Time	Dose	Observations	Reference
	ratio			0.25 and 1 mg/L	of 1 mg/L showed acellular area in the testes with an increase in T levels in male and retardation of oocyte development in the female.	*al.*, 2016)
Mouse	ICR	*In vitro* oocyte	6, 9, 12, 15 and 18 h	2, 20, 50 and 100 μg/ml	BPAF exposure inhibited oocyte maturation at concentrations of 50 and 100 μg/ml and delayed cell cycle at a dose of 2 μg/ml. Further BPAF treatment induced spindle abnormalities, activated spindle assembly checkpoint at a dose of 50 μg/ml.	(Nakano, *et al.*, 2016)
Mouse		*In vitro* Spermatogonial cell line C18-4	24, 48 and 72 h	0.1, 1, 5, 10, and 25 μM	The BPAF exposure significantly decreased cell viability, altered nuclear morphology, increased γ-H2AX expression level, and perturbed cytoskeleton and cell cycle progression with EC20 ≈10 μM. Further, BPAF treatment at 25 μM induced the formation of multinucleated cells with active DNA synthesis and cells with dot-like structure.	(Liang, *et al.*, 2017)

Table 1.10. TBBPA and reproductive outcomes in experimental studies.

Animal	Strain	Exposure route	Time of exposure	Doses	Age at collection	Summary	Reference
Rat	SD	Oral gavage	10 weeks premating period, 2 weeks mating period, gestation and lactation	10, 100 and 1000 mg/kg	After mating/weaning	In SD rats, TBBPA exposure showed no effects on organ weight and sperm quality. Serum T4 levels were decreased in males and females of F0 and F1 generations and serum T3 levels were decreased in F0 males only at high dose groups. No changes in FSH levels were observed.	(ECB., 2012)
Mice	ICR	Dietary exposure	GD 0-PND 27	0.01%, 0.1% or 1.0% in diet	PND 27	In ICR mice received maternal dietary exposure through GD 0 to PND 27, no changes in testis, ovary or uterine weight were observed.	(Tada, et al., 2006)
Fish	Danio ratio	Water	30 days / 47 days	0.023-1.5 µM	Adult / Offspring ph 47 d	Adult zebra fish were exposed to waterborne TBBPA for 30 days, and their offsprings received TBBPA exposure up to 47 days. In F0 female fish, TBBPA exposure decreased egg production starting at 0.047 µM and increased premature oocytes at a dose of 1.5 µM. In offspring, exposure to 6 µM TBBPA resulted in embryo malformation.	(Kuiper, et al., 2007)
Rat	Wistar	Dietary exposure	Paternal and maternal exposure started 10 and 2 weeks before mating and ended in lactation	3, 10, 30, 100, 300, 1,000 and 3,000 mg/kg	Adult	Maternal and paternal TBBPA exposure resulted in decreases in circulating T4 levels and testis weight, an increase in circulating T3 levels at male offsprings, and a decrease in circulating T4 levels in female offsprings. In addition, the concentrations of TBBPA metabolites in plasma increased with increasing exposure levels.	(Van der Ven, et al., 2008)
Rat	SD	Dietary exposure	GD 10-PND 20	100, 1000 or 10,000 ppm	PND 77	In SD rats received the prenatal and postnatal exposure to TBBPA, no changes of testis, ovaries and uterus weights were	(Saegusa et al., 2009)

Mouse	CD1	Drinking water	Life time	35 μg/kg	PND 70	observed. A decreases in serum T3 levels was observed only at low exposure levels. In CD-1 mice, two-generation exposure to TBBPA resulted in decreases in testis weights, seminal vesicles weights and expression of the gene for the androgen receptor. Further, TBBPA exposure increased apoptotic cells and apoptotic genes expressions in seminiferous tubules. However, no changes in sperm parameters were observed.	(Zatecka, *et al.*, 2013)
Mouse	C57BL /6J	Drinking water	GD 0-PND 70	35 μg/kg	PND 70	C57Bl/6J mice were exposed to TBBPA during the GD 0 to PND 70. The TBBPA treatment significantly decreased protamine 1/protamine 2 ratio, increased total protamine/DNA ratio and number of TUNEL positive spermatozoa.	(Zatecka, *et al.*, 2014)
Rat	SD	Oral gavage	GD 0-GD 9	100, 300 and 1000 mg/kg	PND 60	In SD rats, exposure to TBBPA resulted in a decrease in circulating T4 levels in rats. Whereas no changes in sperm motility, concentration, and abnormal sperm percentage were observed in F0/1/2 generations.	(Cope, *et al.*, 2015)
Mouse	Wistar Han rats / B6C3F 1/N	Oral gavage	2 years	250, 500 and 1000 mg/kg	Adult	In 2-year TBBPA oral exposure, TBBPA increased uterine epithelial tumors including adenomas, adenocarcinomas, and malignant mixed Mullerian tumors in rats at doses of 500 and 1000 mg/kg. In the testes of treated male rats, atrophy of the germinal epithelium and testicular interstitial cell adenomas was observed (no significance).	(Dunnick, *et al.*, 2015)
Mouse		*In vitro* Sertoli	0-18 h	0-60 μM		In mouse Sertoli cells TM4, TBBPA treatment significantly increased cell	(Ogunbayo , *et al.*,

52

	cell line TM4			death starting at 10 μM and cellular Ca²⁺ levels starting at 5 μM. Further, TBBPA treatment inhibited sarcoplasmic/endoplasmic reticulum Ca²⁺-ATPases starting at 0.4 μM, and activated Ryanodine receptor Ca²⁺ channel starting at 2 μM.	2008)
Mouse	*In vitro* Leydig cell line MA-10	24 h	0-30 μM	TBBPA exposure significantly increased T levels at doses of 10 and 30 μM via multidrug resistance proteins. Further, 10 μM TBBPA exposure significantly induced the expression levels of StAR, Cyp11A1, and Cyp17 in Leydig cell line MA-10.	(Dankers, *et al.*, 2013)
Mouse	*In vitro* Leydig cell line MA-10	48 h	0.01–100 μM	TBBPA exposure significantly increased T levels at a dose of 30 μM, P4 levels and gene (5aRed1) at a dose of 10 μM in the MA-10 cells.	(Roelofs, *et al.*, 2015)
Mouse	*In vitro* Spermato gonial cell line C18-4	24, 48 and 72 h	0.1, 1, 5, 10, and 25 μM	The TBBPA exposure significantly decreased cell viability, altered nuclear morphology, increased γ-H2AX expression level, and perturbed cytoskeleton and cell cycle progression at a dose of 25 μM in spermatogonial cell line C18-4.	(Liang, *et al.*, 2017)

1.2 High-content analysis/screening and its applications in toxicology

1.2.1 Introduction

Over the past decade, high-content analysis (HCA) and high-content screening (HCS) has been one of the fastest growing fields in the cell biology and toxicology. HCA, which combines automated fluorescence microscopy with quantitative image analysis, enables the measurement of unbiased multiparametric data on the single cell level. HCA provides the temporal and spatial measurements of individual protein, organelle, and cell that are needed to fully understand biological consequence in response to environmental stimuli. This novel approach has been applied in drug discovery and development and stem cell biology (Bickle, 2010; Neumann *et al.*, 2010; Perlman *et al.*, 2004).

The main goal of employing HCA/HCS assays in toxicity risk assessment is to screen large numbers of commercial substances on the market and assess their hazards and risks for human and environment. Due to the impracticality of using traditional animal toxicity tests to evaluate the large numbers of chemicals, the transition from in *vivo* testing to *in vitro* toxicity pathway-based assays has been proposed in the landmark report "Toxicity Testing in the 21st Century: A Vision and a Strategy" (Krewski *et al.*, 2010).

To achieve this goal, the EPA initiated the ToxCast program, which used quantitative HTS and HCS approach to screen environmental chemicals. Most HCS assays are fit for microtiter plate-based format to screen a large number of chemicals with wide concentration range. The large-scale, multi-dimensional data enable the prioritization of chemicals for further study, characterization toxicity pathways and development the predictive model for human toxicity evaluation (Elmore *et al.*, 2014; Merrick *et al.*, 2015; Shukla *et al.*, 2010). So far, the program has tested over 1, 000 chemicals in over 700 assays that cover wide ranges of signaling

pathways (Attene-Ramos *et al.*, 2015; Belair *et al.*, 2016; Chandler *et al.*, 2011; Judson *et al.*, 2016; Karmaus *et al.*, 2016b; Tice *et al.*, 2013; Zang *et al.*, 2013). Further, the high-quality HCS data with advanced computational modeling were integrated to characterize the complex molecular pathways in response to chemical exposure and link those toxic pathways to adverse health outcomes at the higher levels of biological organizations (Auerbach *et al.*, 2016; Leung *et al.*, 2016).

Here, an overview of applications of HCA and HCS approach in the toxicological studies is provided. The key challenges that need addressing in the future are highlighted. The aims of this review include 1) provide the general principle of HCA/HCS assay development; 2) summarize the current applications of HCA/HCS in the studies of drug-induced liver injury (DILI), genotoxicity, neurotoxicity, and reproductive toxicity in various cell models; and 3) identify the current challenges and future study directions.

1.2.2 Principle of HCA/HCS assay development

The success of HCA/HCS assay mainly depends on the careful assay design and image analysis pipeline. The main goal for experiment design is to generate reproducible and scalable readouts with minimized experiment steps. The development of assay usually includes three steps: marker selection, image acquisition and processing, and data analysis.

1.2.2.1 Marker selection

A variety of fluorescent reagents, including immunoreagents that specifically recognize and combine to epitopes of the target protein, fluorescent dye/probe that can be taken by cells and concentrated in target organelle, and genetically encoded fluorescent proteins have become available in recent years to identify and quantify various molecules and organelles. It allows researcher to customize multiple endpoints and obtain unprecedented insight into complicated

55

cellular events. Further, the co-staining of cells with probe cocktail enabled to simultaneous measurement of multiple subcellular compartments and examination of the co-localization of target proteins. To achieve this goal, the optically compatible fluorophores with non-overlapping absorption and emission wavelengths must be carefully selected.

1.2.2.2 Image acquisition and processing

The rapid development of image acquisition equipment and image analysis software greatly facilitate the growth of the HCA. The automated imaging system allows researchers to image the corresponding region of cells in multiple wells without manual adjustment, which significantly reduces image acquisition time and bias. The advances of current image analysis software enable researchers to extract and quantify the multiple parameters on the object intensity, intensity distribution, shape, size, texture, and granularity from targeted objects in over thousands of images, which provides unbiased and multidimensional data and enables the robust statistical analysis. The main steps of image analysis include image acquisition, object segmentation, and feature extraction.

1.2.2.3 Image acquisition

The imaging platform in commercially available HCA and HCS microscopy can be broadly divided into two categories: confocal and wide field (Lee and Howell, 2006). Confocal imager gives better resolution, depth and image contrast, which is suitable for measuring subcellular structure, complex 3D structure or sample with high background signal. It reduces the light signal and requires longer image acquisition and higher cost in instruments, limiting its high-throughput capability. In contrast, wide field has higher image acquisition speed and provides stronger fluorescence signal, while it usually lacks resolution depth. In addition, the imaging channel number, objective magnification, and image acquisition number per well should

be considered. In the assay development, the tradeoff between image acquisition speed, image number, quality, and resolution are needed to be considered.

1.2.2.4 Object segmentation and feature extraction

Segmentation refers to the process of identifying target objects from image fields. After image acquisition, images usually are processed to reduce background noise and correct uneven illumination. Next, an intensity-based threshold is usually set to separate the primary object from the background. Other segmentation methods include applying the watershed algorithm, Gaussian mixture models, computing object shape, or identifying the intensity peak within the object. The success of object segmentation also depends on the selection of appropriate image features for targeted object identification (Peng, 2008). For example, nuclei are easily identified with DNA staining and usually set as a primary object to determine the cell localization. The objects that touched the border of the image usually are excluded from further analysis to prevent repeated count. Secondary or tertiary objects can be identified using mask or halo around the primary object with preselected pixel width or additional staining to determine the cell boundary.

Following object segmentation, feature extraction from subcellular compartments can be processed. Several high-content imaging systems provide built-in software for image analysis. Free open source software, such as ImageJ and CellProfiler are also available (Kamentsky *et al.*, 2011; Schneider *et al.*, 2012). Most analysis software can identify and quantify the size, shape, intensity, intensity distribution, and texture of the identified object. It is worth noting that partial features are less informative in the given biological condition, or redundant in similar biological meaning.

1.2.2.5 Statistical analysis

After feature extraction, a data analysis pipeline usually is set starting with row single cell-based data. A quality control step should be considered as an early step in the pipeline. Out-of-focus image, poor object segmentation, artifacts, and tracing errors should be checked and corrected. The data could be normalized between inter- or intra- plate to reduce data variability. Single cell-level data is usually aggregated to the well-level or treatment-level for further data analysis. The most common way for data aggregation is to calculate the arithmetic mean. While most readouts do not follow the normal distribution, the log transformation of data or the use of geometric mean are preferred in analysis. However, the data aggregation could potentially mask cellular heterogeneity and their differential cellular responses to chemical stimuli, especially when a phenotypic change only occurred in a subpopulation (Altschuler and Wu, 2010).

In single-cell data analysis, a large number of image-based features poses a great challenge to traditional analytical approaches that could be computationally intensive. To solve this problem, researchers usually reduce the number of features for analysis by selecting several physiologically-relevant features, which cannot fit for the complex multi-dimensional data analysis tasks to discriminate specific phenotype. The second approach for HCA data analysis is to employ an advanced computational algorithm to explore the intrinsic structure of high-dimensional data and transform the data into more compact and low-dimension level with less information lost.

1.2.2.6 Machine learning

ML refers to the algorithms that enable recognition and classification of the phenotype of interest from existing image and data. It aims to make accurate predictions from large datasets

with a small training set. Toxicology increasingly relies on automated fluorescence microscopy

and ML to capture massive sets of images that can be mined in multiple ways.

In general, it could be broadly categorized into supervised and unsupervised ML. In

supervised ML, after feature extraction, a small set of example data with user-defined classes are

used to train the ML-based software to learn the inherent structure within this data and

generating multiple rules to discriminate the phenotype of interest with others. Next, the ML-

based software can automatically infer these rules to classify millions of cells from HCA dataset.

This approach has been successfully implied in HCA, including providing phenotypic profiling

of human genome in cell division and multidimensional chemical profiling for drug development

(Fuller *et al.*, 2016; Loo *et al.*, 2007; Neumann*, et al.*, 2010; Singh *et al.*, 2010; Zhong *et al.*,

2012). However, this approach still requires the user-defined dataset to characterize the

phenotype of interest.

In contrast, unsupervised ML does not require predefined class and can cluster data

points based on the similarity of data structure, which is suitable for discovering aberrant

phenotypes without prior knowledge (de Ridder et al., 2013). To date, several open-source

software are available for ML–based HCA. Carpenter and her colleagues developed CellProfiler

Analyst equipped with multiple ML algorithms that could classify various biological phenotypes

(Dao et al., 2016). In addition, ilastik, an ML program that complements image analysis software

CellProfiler was developed to classify user-defined phenotype based on image pixel (Hennig et

al., 2017). Another valuable software is WND-CHARM (Weighted Neighbor Distances using a

Compound Hierarchy of Algorithms Representing Morphology) (Orlov et al., 2008). It can also

be used to analyze entire images without object segmentation and single-cell feature extraction.

Based on WND-CHARM, Uhlmann et.al. developed a new software named CP-CHARM that

provided more user-friendly ML platform by avoiding cell segmentation and image analysis

pipeline construction (Uhlmann *et al.*, 2016). Further, to overcome the limitations in

transformation across different datasets and feature representations on pixel level, deep ML that

uses more layers of features that forms a hierarchy is utilized by toxicologists and shows far

superior performance than classical algorithms (Kraus *et al.*, 2017).

1.2.3 The applications of HCA and HCS in toxicology

1.2.3.1 DILI

Hepatotoxicity is one of the major reasons for drug withdrawal from the market. In the

preclinical assessment of compounds, traditional animal testing showed poor predictability of

DILI in human (Olson *et al.*, 2000). *In vitro*, single-endpoint assays have been developed to

assess the chemical hepatotoxicity in humans, such as cell proliferation, mitochondrial

membrane potential (MMP), and plasma membrane permeability (PMP) (Farkas and

Tannenbaum, 2005). However, the single *in vitro* assay could not accurately predict the *in vivo*

toxicity. Over the decades, with the rapid development of imaging technology and image

analysis system, HCA and HCS are recognized as promising tools to evaluate the chemical

toxicity during drug research and development process (summarized in Table 1.11).

O'Brien et al. developed a quadprobe HCA assay in HepG2 cells to assess the

hepatotoxicity of 243 drugs with multiple markers, including cell count, nuclear morphology,

MMP, intracellular Ca^{2+} level and PMP, which showed high sensitivity (80%) and specificity

(90%) in detecting human hepatotoxicity (O'Brien *et al.*, 2006). Further, the high concordance

between *in vitro* hepatotoxicity detected by HCA assays and human toxicity data was reported in

the multiple studies (Chen *et al.*, 2014; Garside *et al.*, 2014; Persson *et al.*, 2013; Xu *et al.*,

2008). Among all validated HCA assays, cell number, nuclear morphology, MMP, MTP,

intracellular Ca^{2+} level, and ROS are commonly examined to elucidate molecular mechanisms in chemical-induced hepatocyte death. In certain assays, apoptosis, glutathione (GSH) level, lipid peroxidation, lysosome and mitochondrial activity were also measured simultaneously or separately (Abraham *et al.*, 2008; Anguissola *et al.*, 2014a; Chen*, et al.*, 2014; Dykens *et al.*, 2008; Garside*, et al.*, 2014; Saito *et al.*, 2016; Svingen *et al.*, 2017; Tolosa *et al.*, 2012; Xu*, et al.*, 2008; Ye *et al.*, 2007).

In the most assays, human liver carcinoma cell line HepG2 was employed as a model to predict human DILI. To further enhance the biological and physiological relevance of the HCA model, Xu et al. utilized the primary human hepatocyte cultured in a sandwich configuration to evaluate over 300 drugs and chemicals on multiple endpoints, including cell number, nuclear area, MMP, ROS and GSH levels. The data demonstrated high true-positive rate (50-60%) and low false-positive rate (0-5%) (Xu*, et al.*, 2008). As compared to the HepG2 cell line, the primary cells maintained more normal and balanced drug-metabolizing and transporter functions but showed the lower sensitivity, which could result from short exposure time, different marker selection, and low proliferation rate of primary cells (Bi *et al.*, 2006; Farkas and Tannenbaum, 2005). Similar findings were observed in the studies using primary rat or human hepatocytes (Chen*, et al.*, 2014; Garside*, et al.*, 2014). In addition, one study developed transfected HepG2 cells with high expression of P450 enzymes, and bioactive compounds exerted higher hepatotoxicity in the transfected cells, as compared to non-transfected cells (Tolosa *et al.*, 2013). Although the current HCA assays could not fully identify chemical hepatotoxicity due to the lack of full metabolic and immunological capacity in *in vitro* cell models, it already became a standard tool in the pharmaceutical industry for drug early screening because of its high throughput, high content and low cost (Persson and Hornberg, 2016).

In addition to direct hepatotoxicity, several assays were developed to evaluate the potential risk of phospholipidosis and steatosis due to long-term drug therapy. Phospholipidosis refers to phospholipid storage disorder that excessive lipid accumulated in the lysosome (Gross-Steinmeyer *et al.*, 2005). Most of the currently available assays only included the co-staining for nuclei, phospholipid, and lysosomes, which showed high sensitivity and specificity in screening drug-induced human phospholipidosis but the capability for HCS is still limited (LeCureux *et al.*, 2011; Schurdak *et al.*, 2007; Shahane *et al.*, 2014; van de Water *et al.*, 2011) (see Tables 1.12 and 1.13). One study developed HCA assays utilizing human pluripotent stem cell-derived hepatocytes to measure the cell count, nuclear morphology, phospholipid, lipid, MMP, and ROS and showed consistent classification of drug hepatotoxicity as previously published *in vitro* data (Pradip *et al.*, 2016). For steatosis, an abnormal lipid accumulation in the liver, Fujimura et al. first reported a single-endpoint imaging assay combined with gene expression analysis in primary rat hepatocytes to predict hepatosteatosis potentials of drugs (Fujimura *et al.*, 2009). Further, Donato et al. developed a HCA assay to simultaneously monitor the cell number, lipid accumulation, MMP and ROS in the HepG2 cells. This model could detect all known steatotic compounds and revealed that ROS was involved part of chemical-induced steatosis (Donato *et al.*, 2017).

1.2.3.2 Genotoxicity

Genotoxicity is defined as destructive effects on the genetic material, including heritable germline mutation and somatic cell mutation, which may result in cancer (Phillips and Arlt, 2009). *In vitro* micronucleus assay is a well-established genotoxicity assay to detect chromosome breaks induced by clastogens and whole chromosome loss induced by aneugens. The tradition micronucleus scoring is labor- and time-intensive due to manual operation, while micronuclei are

easily assessed using DNA stains and specific imaging algorithms in HCA assays. In Table 1.14, Diaz et al. developed an automated *in vitro* micronucleus assay in CHO-K1 cells. The cells were treated with 3 genotoxic compounds and 13 non-genotoxic compounds, fixed and stained with Hoechst. The micronucleus was automatically visualized and scored by fluorescence microscope and image analysis software, which showed high sensitivity (88%) and specificity (100%) in the detection of chemical genotoxicity (Diaz *et al.*, 2007). This assay was further employed in multiple cell models and showed high predictability of genotoxic chemicals (Mondal *et al.*, 2010; Westerink *et al.*, 2011; Ye *et al.*, 2014). However, more endpoints should be included to simultaneously explore the mechanisms for chemical genotoxicity.

γ-H2AX, a sensitive and early marker of DNA damage initiation, was recently employed in *in vitro* genotoxicity HTS and HCS. Garcia et al. developed an *in vitro* HCS assay on γ-H2AX in BEAS-2B cells, which showed high sensitivity (~ 90%) and specificity (84%) in screening genotoxic chemicals and was further applied to evaluate the genotoxicity of cigarette smoke (Garcia-Canton *et al.*, 2013a; Garcia-Canton *et al.*, 2013b; Garcia-Canton *et al.*, 2014). In addition, γ-H2AX was combined with multiple markers to monitor the complex cellular mechanisms in chemical-induced toxicity. Thompson et al. combined 8-OHdG, a marker of oxidative DNA damage, and γ-H2AX to evaluate the hexavalent chromium-induced genotoxicity in the intestine and revealed that oxidative DNA damage occurred at the lower exposure level, as compared to the initiation of DNA double-strand break (Thompson *et al.*, 2012). Anto et al. developed the HCA assay utilizing γ-H2AX, histone H3 and tubulin to monitor the chemical-induced DNA damage and cell cycle arrest in different phases (Ando *et al.*, 2014). In addition, Liang et al. developed the multi-parametric HCA assays combining DNA damage (γ-H2AX) with nuclear morphology, cell cycle progression (Hoechst), and cytoskeleton (F-actin). The data

63

revealed differential toxicities between BPA and its selected analogs, and it also showed a high correlation between DNA damage and cytoskeleton perturbation in germline cells (Liang, *et al.*, 2017).

1.2.3.3 Neurotoxicity

Accumulating evidence has demonstrated that exposure to the chemicals could induce the neurodevelopment disorder (Grandjean and Landrigan, 2006). The *in vitro* neural cell cultures HCA assays have been employed to study the effects of chemical exposure on specific cellular events during development of nervous system (Table 1.15). Neurite outgrowth, a determinant step in neuro development, has been extensively studied. HCA assays are available to quantify multiple parameters regarding the neurite outgrowth, including cell number, neurites number, area, length, and branchpoint in multiple neural cell lines, which discriminate the developmental neural toxicant with general cytotoxic compounds (Harrill *et al.*, 2010; Krug *et al.*, 2013; Radio *et al.*, 2008; Ryan *et al.*, 2016; Stiegler *et al.*, 2011; Wu *et al.*, 2016; Wu *et al.*, 2017). In addition, Jan et al. further assessed the apoptosis, intracellular Ca^{2+} levels, and MMP simultaneously with neurite outgrowth and revealed the differential neurotoxicities of nanoparticles (Jan *et al.*, 2008). Wu et al. incorporated specific markers for post mitosis and proliferation of hNP cells to evaluate the effects of 5 neurotoxins during human neural maturation (Wu, *et al.*, 2016). Although HCA of neurite phenotypic features provides a rapid and efficient tool for *in vitro* neurotoxicity screening, the cellular mechanisms were rarely examined in the current study. It remains unknown how *in vitro* data from HCA assays correlate with *in vivo* neurotoxicity data. Validation studies should be conducted using large sets of chemicals with doses relevant to the brain concentrations that produces toxicity in humans.

In the current chemical evaluations, *in vivo* reproductive toxicology test is time- and labor-consuming, expensive and requires extensive use of the animal. The EPA has initiated the ToxCast program, which applied more than 500 in silico and *in vitro* assays to evaluate the effects of environmental chemical exposure on various molecular and cellular targets. Further, the program applied computational toxicology that integrates computational modeling, ToxCast HTS data, and the Toxicity Reference Database to provide a predictive model to evaluate reproductive toxicants (Leung*, et al.*, 2016; Martin *et al.*, 2011; Reif *et al.*, 2010). Although several assays have shown some degree of predictability of chemical reproductive toxicity, there is no *in vitro* model in ToxCast program specifically targets on reproductive toxicity. Our lab developed a multiparametric HCA assay in mouse spermatogonial cells and applied this model to characterize the reproductive toxicity of bisphenol A and its selected analogs (Liang*, et al.*, 2017). In this HCA assay, cell number, nuclear morphology, and cell cycle progression (Hoechst), DNA synthesis (BrdU), DNA damage responses (γ-H2AX) and cytoskeleton (Phalloidin-stained F-actin) were measured. The data further revealed the differential toxicities between BPA and its analogs, in which BPAF exerted potent reproductive toxicity and induced multinucleated cells. This finding is further validated in the latest *in vivo* study that showed BPAF exposure uniquely impaired pregnancies and sexual development in rats, as compared to BPA at similar doses (Sutherland.*, et al.*, 2017). Although current HCA assays included multiple markers linked to functional disorder in testicular cells, biological markers for testicular functions, including steroidogenic activity, hormone receptor expression level, should be incorporated in the future HCA assays.

Although the HCA field has made tremendous progress in imaging hardware and analysis software, it stills faces several crucial challenges. First, consistency of image and data format is one of the challenging steps for HCA study. As the toxicological profiling of a large number of chemicals becomes more horizontally integrated across different research groups, it is important that multiple groups have easy access to the large-scale image-based data to improve the efficiency of data analysis and reproducibility of scientific research. However, due to the nature of imaging equipment types and the various data formats generated by different image analysis algorithms, the integration of HCA of datasets is still an overwhelming technical challenge and a major hindrance to the effective use of multiple imaging platforms. The common solution is to manually transfer images or data between multiple commercially available software, which is time consuming and non-productive. It would be essential for vendors to include the application programming interface to allow users to generate more common repositories. Image store and database management software are needed to provide access to the raw image and associated data. Further, HCS technologies generate the large scale of data on DNA, protein, or organelle structure within a single cell, whereas a toxicologist usually analyzes only 1–2 image-based features (Singh *et al.*, 2014a). The advanced computational approaches, such as machine learning, deep learning, and principal component analysis, are rarely used in the currently available studies to explore the multi-dimensional data and identify the rare phenotype within a cell population. In addition, the application of HCA on 3D cell culture or organ-on-chip are still limited due to the challenges in the diffusion of markers into multiple cellular layers, light penetration of imaging system, and 3D image analysis algorithms. Further, to validate the added

values of current 3D cell cultures in HCA, a large number of chemicals that have been screened in two-dimensional models should be tested in 3D cell culture.

1.2.5 Concluding remarks

The increasing reports of HCA and HCS in the literature within decades indicate that the automated microscopy platform combined with computational image analysis software is more accessible to the toxicologist. With the advanced biological model, image acquisition system, and analysis approach, HCA and HCS could serve as the first-tier screening for potential human toxicity, characterize the underlying molecular mechanism, and prioritize the chemicals for further comprehensive toxicological evaluation either *in vivo* or *in vitro*.

Table 1.11. HCA assays for detection of DILI.

Cell Model	Endpoints	Fluorophores	Conclusions	Resource
HepG2	nuclei MMP calcium PMP	Hoechst 33342 TMRM Fluo-4 AM TOTO-3	Cell number, nuclear area, intracellular Ca^{2+} concentration, MMP, and PMP were measured in the cells treated with 243 drugs for 72 h. The high concordance between human hepatotoxicity and *in vitro* cytotoxicity detected by HCS model was observed (80% sensitivity and 90% specificity).	(O'Brien, *et al.*, 2006)
HepG2	nuclei MMP apoptosis ROS GSH	Hoechst 33342 Rhodamine 123 PI Dihydroethidium 2,3-naphthalene-dicarboxaldehyde	Nuclear morphology, PMP, and MMP were measured in the cells cultured in a microfluidic device and treated with drugs for 24 h. In addition, ROS and GSH levels were examined separately. The HCS model would evaluate anticancer drugs and profile apoptosis factors.	(Ye, *et al.*, 2007)
HepG2	nuclei PMP MMP	Hoechst 33342 YOYO-1 TMRM	Nuclear morphology, PMP, and MMP were measured in the cells treated with quinolone antibiotics, thiazolidinediones, and statins for 72 h. This model could be used to rank compounds based on hepatotoxicity potential in humans.	(Abraham, *et al.*, 2008)
HepG2	nuclei MMP ROS GSH	DRAQ5 TMRM CM-H2DCFDA mBCl	Nuclei, intracellular lipids, ROS, MMP and GSH level were measured in cells treated with nefazodone, trazodone, and buspirone for 24 h. Data suggested the mitochondrial impairment induced by nefazodone potentially contributed to its hepatotoxicity.	(Dykens, *et al.*, 2008)
Primary human hepatocyte	nuclei MMP ROS GSH	DRAQ5 TMRM CM-H2DCFDA mBCl	Nuclei count, nuclear area, intracellular lipids, ROS, MMP and GSH level were measured in primary cells treated with over 300 drugs and chemicals. The testing modal exhibited high true-positive rate (50-60%) and low false-positive rate (0-5%).	(Xu, *et al.*, 2008)

HepG2	nuclei viability MMP lipid peroxidation calcium	Hoechst 33342 PI TMRM BODIPY 665/676 Fluo-4 AM	Cell viability, nuclear morphology, MMP, intracellular Ca^{2+} concentration and lipid peroxidation were determined in the cells treated with 78 compounds for 3 and 24 h. This assay classified injury degree for all compounds.	(Tolosa, *et al.*, 2012)
HepG2	nuclei lysosome PMP mitochondria	Hoechst 33342 LysoTracker Green TOTO-3 MitoTracker Orange	Nuclei count, nuclear area, plasma membrane integrity, lysosomal activity, MMP, and mitochondrial area were quantified in the cells treated with ~ 100 chemicals. The assays exhibited high specificity (90%) and moderate specificity (60%).	(Persson, *et al.*, 2013)
CYP adenoviral transfected HepG2	nuclei viability MMP calcium ROS	Hoechst 33342 PI TMRM Fluo-4 AM CellROX Deep Red	Cell viability, nuclear morphology, MMP, intracellular Ca^{2+} concentration and ROS were determined in the cells treated with 12 bioactivable and 3 non-bioactive compounds for 24 h. In the HCA assay, bioactivable compounds exerted higher hepatoxicities in the CYP transfected cells, as compared with normal cells.	(Tolosa, *et al.*, 2013)
HepG2	nuclei lysosome calcium MMP PMP	Hoechst 33342 LysoTracker Green Fluo-4 TMRM TOPRO-3	Nuclei count, nuclear morphology, MMP, intracellular Ca^{2+} concentration, PMP and lysosomal acidification were determined in the cells exposed to nanoparticles for 24 h. Combined with multiple cell lines representative of different organs, this platform would provide mechanistic insights for nanoparticle toxicity.	(Anguissola, *et al.*, 2014a)
Primary rat hepatocytes	nuclei DNA damage MMP lysosome	NA	Cell loss, nuclear morphology, DNA damage, MPM and lysosome mass were measured in the cells treated with 70 drugs for 1, 24 and 48 h. This testing strategy showed improved sensitivity (38%) and high specificity (100%) in hepatotoxicity detection.	(Chen, *et al.*, 2014)
	nuclei ROS	DAPI CM-H2DCFDA	Multiple endpoints were measured in cells treated with 108 drugs known to induce DILI and 36 negative drugs for 4, 24 and 48 h.	

Primary human hepatocytes	MMP mitosis apoptosis lipid cellular Stress phospholipidosis	TMRM p-Histone H3 Casapse-3 Neutral lipid dye red Anti-HSP70/72 green Phospholipid dye green	ROS generation assays showed the high sensitivity (41%) and specificity (86%). Further, the hierarchical clustering for all endpoints yields to the better sensitivity (58 %) and specificity (75%).	(Garside, *et al.*, 2014)
HePaRG / HepG2	nuclei ROS MMP GSH PMP	Hoechst 33342 / DRAQ5 CM-H2DCFDA TMRM mBCl YOYO-1	Nuclei number, nuclear area, ROS, GSH level and MMP were evaluated in the cells treated with 28 DILI and non-DILI compound for 24 h. This assay showed consistent results with a previously reported mechanism for DILI drugs.	(Saito, *et al.*, 2016)
HepG2	nuclei lysosome PMP mitochondria	Hoechst 33342 LysoTracker Green TOTO-3 MitoTracker Orange	Nuclei count, nuclear area, plasma membrane integrity, lysosomal activity, MMP, and mitochondrial area were evaluated in the cells treated with 8 mycotoxins for 24 and 72 h. This assay enabled the assessment and comparison of chemical hepatotoxicity.	(Svingen, *et al.*, 2017)

Table 1.12. HCA assays for detection of chemical-induced phospholipidosis.

Cell Model	Endpoints	Fluorophores	Conclusions	Resource
Primary Rat Hepatocytes / HepG2	nuclei	Hoechst 33342	Accumulation of phospholipid was measured in cells treated with 16 negative and positive compounds known to induce phospholipidosis. High degree of sensitivity (92%) and specificity (100%) were observed.	(Schurdak, *et al.*, 2007)
	phospholipid	ß-BODIPY C12-HPC		
	lysosomes	LysoTracker Red		
HepG2 / HuH-7 cells	nuclei	Hoechst 33342	Mean average intensity of LipidTox was quantified in cells exposed to 66 known phospholipidosis inducers and non-inducers. The concordances of HepG2 and HuH-7 cells in predicting phospholipidosis are 73% and 62 %, respectively.	(LeCureux, *et al.*, 2011)
	phospholipid	LipidTox		
HepG2	Nuclei	Hoechst 33342	Lysosomal phospholipid accumulation was quantified in the cells exposed to 56 reference compounds for 24 h. This *in vitro* HCA assay showed high sensitivity (88%) and specificity (80.6%).	(van de Water, *et al.*, 2011)
	cytoplasm	DRAQ5		
	phospholipid	NBD-PE		
	lysosomes	LysoTracker Red		
HepG2	nuclei	Hoechst 33342	Phospholipid induction was quantified in cells treated with 1280 compounds from the Library of Pharmacologically Active Compounds. This assay was enabled to identify known phospholipidosis inducers and identified several novel inducers.	(Shahane, *et al.*, 2014)
	phospholipid	LipidTox		
Human Pluripotent Stem Cell-Derived Hepatocytes	nuclei	Hoechst 33342	Cell count, nuclear morphology, lipids, phospholipids, MPM and ROS were measured in the cells treated with 3 known steatosis and phospholipidosis inducers and a negative control. The assay could characterize the compounds toxicities, which were consistent with degrees of injury published previously.	(Pradip, *et al.*, 2016)
	phospholipid	LipidTox Red phospholipidosis		
	lipids	LipidTox Green		
	PMP (live cell)	TOTO-3		
	ROS (live cell)	CM-H2DCFDA		

Table 1.13. HCA assays for detection of chemical-induced steatosis.

Cell Model	Endpoints	Fluorophores	Conclusions	Resource
Rat primary hepatocytes	lipid droplets	BODIPY® 558/568 C12	Accumulation of lipid was measured in the cells exposed to 6 positive reference compounds for 24 h. Combined with gene expression analysis, this method would be used to predict drug's potential for hepatosteatosis and elucidate its mechanisms.	(Fujimura, *et al.*, 2009)
HepG2	nuclei	Hoechst 33342	Cell viability, lipid accumulation, MMP, and ROS were determined in the cells treated with 16 steatotic compounds and 6 nonsteatotic compounds for 24 h. This *in vitro* approach could detect significant lipid accumulation in all steatotic compounds and induction of ROS in certain compounds.	(Donato *et al.*, 2012)
	lipid droplets	BODIPY493/503		
	ROS	2′,7′-dihydrodichlorofluorescein diacetate		
	MMP	tetramethyl rhodamine methyl ester		
	viability	propidium iodide		
Human Pluripotent Stem Cell-Derived Hepatocytes	nuclei	Hoechst 33342	Cell count, nuclear morphology, lipids, phospholipids, MPM and ROS, were measured in the cells treated with 3 known steatosis and phospholipidosis inducers and a negative control. The assay could characterize the compounds toxicities, which were consistent with degrees of injury published previously.	(Pradip, *et al.*, 2016)
	phospholipid	LipidTox Red phospholipidosis		
	lipids	LipidTox Green		
	PMP (live cell)	TOTO-3		
	ROS (live cell)	CM-H2DCFDA		

Table 1.14. HCA assays for detection of genotoxicity.

Cell Model	Endpoints	Fluorophores	Conclusions	Resource
CHO-K1 cells	micronucleus	Hoechst	Micronucleus and cell number were automatically scored in the cells treated with 33 genotoxic compounds and 13 non-genotoxic compounds for either 3 h with S9 or 24 h without S9. The assay showed high sensitivity (88%) and specificity (100%).	(Diaz, *et al.*, 2007)
CHO-K1 cells	micronucleus	Hoechst 33258	Induction of micronucleus was evaluated in the cells treated with 576 compounds or marketed drugs for 20 h. This assay demonstrated high predictability and capability to classify chemical toxicity.	(Mondal, *et al.*, 2010)
CHO-K1 and HepG2 cells	micronucleus	Hoechst 33342	Micronuclei were detected in the cells treated with 78 genotoxic or nongenotoxic chemicals for 24 h. The assays using CHO-K1 and HepG2 cells showed high sensitivity (80% and 60%) and specificity (88% for both).	(Westerink, *et al.*, 2011)
DU-145 cells	nuclei	DAPI	γ-H2AX foci were quantified in the cells treated with 14,400 compounds for 4 h alone or combined with radiation. This novel approach was enabled to identify two radiosensitizing compounds.	(Fu *et al.*, 2012)
	DNA damage	Anti- γ-H2AX antibody		
Caco-2 cells	nuclei / micronucleus	Hoechst 33342	Cell number, nuclear morphology, DNA damage, and micronucleus were measured in the cells treated with Cr (VI), hydrogen peroxide or rotenone for 2 to 24 h. This assay revealed that oxidative damage might involve in Cr (VI) genotoxicity.	(Thompson, *et al.*, 2012)
	DSB	Anti- γ-H2AX antibody		
	oxidative DNA damage	8-OHdG		
	cell body	SYTO Red		
BEAS-2B cells	nuclei	NA	Cell count and γ-H2AX frequency were determined in cells treated with various cigarette smoke toxicants and	(Garcia-Canton, *et al.*, 2013b)
	DNA damage	Anti- γ-H2AX antibodies		

73

			their mixture for 3 to 24 h. This model enabled quantify and compare the genotoxicity of tobacco products.	
BEAS-2B cells	nuclei	Hoechst	Cell count and γ-H2AX frequency were determined in the cells treated with 22 compounds for 4 h. The assay has high sensitivity and specificity (86–92% and 80–88% respectively).	(Garcia-Canton, *et al.*, 2013a)
	DNA damage	Anti- γ-H2AX antibodies		
CHO-k1 cells	micronucleus	Hoechst 33342	Cell count and micronucleus were evaluated in the cells treated with 44 compounds for 24 h without S9 and 3 h with S9. This assay showed high sensitivity (94%) and specificity (85%).	(Tilmant *et al.*, 2013)
HepG2 cells	nuclei	Hoechst 33342	DNA damage and cell cycle arrest were evaluated in the cells treated with 19 genotoxic and 7 non-genotoxic compounds for 1 or 24 h. This model could rapidly assess chemical genotoxicity and distinguish cell cycle arrest in different phases.	(Ando, *et al.*, 2014)
	DNA damage	Anti-γ-H2AX antibody		
	cell cycle	Anti-phospho-histone H3 antibody		
	cytoskeleton	Anti-tubulin antibody		
BEAS-2B cells	nuclei	Hoechst	Cell count and DNA damage were assessed in the cells exposed to whole mainstream cigarette smoke for 3 h. This assay could evaluate the genotoxicity of cigarette smoke at the air-liquid interface.	(Garcia-Canton, *et al.*, 2014)
	DNA damage	Anti- γ-H2AX antibody		
Human pluripotent stem cells	nuclei	DAPI	Nuclear translocation of SOX17 was monitored in the cells treated with 71 pharmaceutical compounds and 300 kinase inhibitors for 48 h. This model exhibited high sensitivity (97%) and specificity (92%) and high-throughput capacity.	(Kameoka *et al.*, 2014)
	transcription (teratogenic risk)	Anti-SOX17 antibody		

MGC-803 and A549 cells	micronucleus	Hoechst 33342	DNA damage was examined in the cells treated with 9 benzothiazoles for 24 h. This assay revealed some tested benzothiazoles had genotoxicity.	(Ye, *et al.*, 2014)
	mitochondria	MitoTracker Green		

Table 1.15. HCA assays for detection of neurotoxicity.

Cell Model	Endpoints	Fluorophores	Conclusions	Resource
NG108-15 murine neuroblastoma cells	nuclei apoptosis neurite outgrowth calcium MMP	Hoechst 33342 PI β-tubulin III Fluo-4 TMRM	Cell number, nuclear area, apoptosis, neurite outgrowth, MMP and cellular Ca^{2+} level were measured in the undifferentiated and differentiated neural cells treated with nanoparticles for 1.5, 6, and 24 h. The HCA assays differential cytotoxicity profiles of nanoparticles.	(Jan, *et al.*, 2008)
Neuroscreen-1 cells	nuclei neurite outgrowth	Hoechst 33342 β-tubulin III	Cell number, cell body, neurite number, and total neurite length were measured in the cells treated with 19 chemicals for 96 h. The results suggested this HCA assay would rapidly quantify chemical effects on neurite growth.	(Radio, *et al.*, 2008)
Primary rat hippocampal astrocytes Primary rat hippocampal neurons Rat PC12 cells	nuclei neurite outgrowth astrocyte	Hoechst β-tubulin III Glial fibrillary acidic protein	Total cell number, neurite length, astrocyte area and astrocyte count were quantified in the neurons/astrocytes co-cultures treated with acrylamide and H$_2$O$_2$. This HCA assay was successfully developed for quantification of multiple neuronal and astrocytic phenotypes for neurotoxicity assessment.	(Anderl *et al.*, 2009)
Human embryonic stem cell (hESC)-derived neural cells	nuclei neurite outgrowth	Hoechst 33342 β-tubulin III	Neuron density, neurites number, and total neurite length were measured in the cell treated with 5 chemicals for 2 to 24 h. This model showed comparable results with to other *in vitro* model and could serve as a tool to investigate the chemical effects of neurite growth.	(Harrill, *et al.*, 2010)
LUHMES human neuronal precursor cells	nuclei viable cell	Hoechst 33342 Resazurin	Viable cell number and neurite area were determined in the cells treated with 15 chemicals for 24 h. The results showed this HCA assay	(Stiegler, *et al.*, 2011)

	neurite area	Calcein-AM	could discriminate neurotoxic compounds from general cytotoxic compounds.	
Primary rat cortical neurons	nuclei	Hoechst 33258	Cell number, neurite, dendrite and axon length were measured in the cells treated with 4 chemicals for 22 h. The HCA assay could characterize the differential effects of neurotoxicants on the growth of axons and neurites.	(Harrill *et al.*, 2013)
	neurite outgrowth	β-tubulin III		
	dentrite and acon length	Microtubule associated protein 2		
LUHMES human neuronal precursor cells	nuclei	Hoechst 33342	Viable cell numbers and neurite area were determined in the cells treated with 40 chemicals for total 48 h. The results showed this HCA assay could discriminate neurotoxic compounds from general cytotoxic compounds.	(Krug, *et al.*, 2013)
	viable cell	Resazurin		
	neurite area	Calcein-AM		
Human neurons derived from induced pluripotent stem cells	nuclei	Hoechst 33342	Cell viability and multiple parameters for neurite outgrowth (e.g., the length of total outgrowth and a total number of branches) were assessed in the cells treated with 80 chemicals for 72 h. This HCA assay would screen, rank and prioritize compound neurotoxicity.	(Ryan, *et al.*, 2016)
	neurite outgrowth	Calcein-AM		
Human neural progenitor (hNP) cells	nuclei	Hoechst 33342	Cell number, neurite length, neurite number, branch point number, cell proliferation and mitosis were evaluated in the cells treated with 5 neurotoxins. This assay would examine the effects of neural developmental neurotoxins during human neural maturation.	(Wu, *et al.*, 2016)
	neurite outgrowth	β -tubulin III		
	post-mitotic neurons	HuC/D		
	proliferating hNP	SOX1		
Astrocyte-neuron co-cultures	nuclei	Hoechst 33342	Cell number, neurite length, neurite number, and branch point number were evaluated in the cells treated with chlorpyrifos. This assay revealed that astrocytes were protective against chlorpyrifos developmental neurotoxicity	(Wu, *et al.*, 2017)
	neuron cell/neurite outgrowth	β -tubulin III		
		MAP2		

1.3 Objectives, hypotheses, and specific aims

Given the data gaps of BPA analogs' reproductive toxicities and the demand for HCA assays of reproductive toxicant screening, the overall objectives of this dissertation were to (1) determine the adverse reproductive effects of BPA and its analogs, including BPS, BPAF and TBBPA, in *in vitro* testicular cell models and (2) develop and validate HCA assays in *in vitro* testicular cell models for characterizing and comparing testicular toxicities of environmental chemicals. To meet these objectives, the following hypotheses were developed: (1) BPA analogs will exert adverse effects on testicular cells and exhibit differential testicular toxicities, as compared to BPA; and (2) HCA assays for testicular toxicity evaluation will be able to quantitatively characterize and compare testicular toxicities of BPA and its analogs based on multiple features on a single-cell level. These hypotheses were addressed in the following Specific Aims:

Specific Aim for Chapter 2: To develop multi-parametric HCA assays and compare the testicular toxicities of BPA to its selected analogs in a spermatogonial cell line. The dose- and time-dependency of multiple endpoints that potentially lead to germ cell damage, including nuclear morphology, DNA synthesis, cell cycle progression, cytoskeletal integrity, and DNA damage responses were evaluated.

Specific Aim for Chapter 3: To develop ML-powered HCA approach in a testicular cell co-culture model for characterizing BPA and its analogs' testicular toxicities. This approach recognized and quantified multiple phenotypic changes in the co-culture model in response to chemical treatments.

Specific Aim for Chapter 4: To determine the cell-type specific toxicities of BPA and its analogs on multiple testicular cell types, including spermatogonial, Leydig, and Sertoli cell lines.

The HCA-based multi-dimensional toxicity profiling of BPA and its analogs in three cell types

were constructed and compared.

CHAPTER 2

HIGH-CONTENT ANALYSIS PROVIDES MECHANISTIC INSIGHTS INTO THE TESTICULAR TOXICITY OF BISPHENOL A AND SELECTED ANALOGS IN MOUSE SPERMATOGONIAL CELLS

2.1 Abstract

BPA, an endocrine-disrupting compound, was found to be a testicular toxicant in animal models. BPS, BPAF, and TBBPA were recently introduced to the market as alternatives to BPA. However, toxicological data of these compounds in the male reproductive system are currently limited. This study developed and validated an automated multi-parametric HCA using the C18-4 spermatogonial cell line as a model. These validated HCA assays, including nuclear morphology, DNA content, cell cycle progression, DNA synthesis, cytoskeleton integrity, and DNA damage responses, were applied to characterize and compare the testicular toxicities of BPA and 3 selected commercial available BPA analogs, BPS, BPAF, and TBBPA. HCA revealed BPAF and TBBPA exhibited higher spermatogonial toxicities as compared with BPA and BPS, including dose- and time-dependent alterations in nuclear morphology, cell cycle, DNA damage responses, and perturbation of the cytoskeleton. Our results demonstrated that this specific culture model together with HCA could be utilized for quantitative screening and discriminating of chemical-specific testicular toxicity in spermatogonial cells. It also provides a fast and cost-effective approach for the identification of environmental chemicals that could have detrimental effects on reproduction.

2.2 Introduction

BPA is an HPV chemical and worldwide used in food and beverage packaging materials, dental sealants and composite fillings, medical devices and thermal paper (Rochester, 2013). Human exposure to BPA occurs through ingestion, inhalation, and dermal contact from a variety of sources (Kang, *et al.*, 2006; Vandenberg, *et al.*, 2007). BPA and its metabolites are widely distributed in humans and animals (Calafat *et al.*, 2005; Melzer *et al.*, 2010), and were detected in more than 90% of urine samples from the United States population in the 2003-2004 and

2005-2006 National Health and Nutrition Examination Survey (Calafat, *et al.*, 2008; Lakind and

Naiman, 2011). As a known endocrine disruptor, BPA has been shown to interfere with

hormonal and homeostatic systems, and BPA levels in human urine have been correlated with

various diseases and adverse health outcomes (Braun *et al.*, 2011; Carwile and Michels, 2011;

Ehrlich *et al.*, 2012; Lang *et al.*, 2008; Lassen, *et al.*, 2014). BPA exposure has also been

associated with reproductive dysfunctions, including reduction of testicular weight and sperm

count, alterations of hormone levels, and impairment of spermatogenesis (Jin *et al.*, 2013;

Pacchierotti *et al.*, 2008; Sakaue *et al.*, 2001; Tiwari and Vanage, 2013; Wang *et al.*, 2016c). The

mechanism of action of BPA has been investigated with respect to its estrogenic activity, such as

effects on steroid hormone synthesis, and AR antagonism (Kitamura, *et al.*, 2005; Lee *et al.*,

2003; Vinggaard *et al.*, 2008; Zhang *et al.*, 2011). Due to public concern about these potential

adverse effects of BPA, usages of BPA in baby bottles, sippy cups, and infant formula packaging

were abandoned (FDA., 2013; FDA., 2012). As a result, the production of BPA analogs has

greatly increased and is expected to rise in the future. With inadequate data on their toxicities,

BPA analogs have gradually been used for the manufacture of a wide variety of consumer

products. However, because of their structural similarities with BPA, the safety of these analogs

is a subject of debate, and there is accumulating evidence that they also have the potential to be

endocrine disruptors (Usman and Ahmad, 2016). To date, the health risks of BPA analogs need

to be fully evaluated.

There are significant challenges to understanding the health risks associated with

thousands of diverse compounds entering the environment. Studying reproductive toxicity *in

vivo* is usually complicated, expensive, and time-consuming; they also involve the extensive

animal use, which significantly limits the number of chemicals to be tested. There is thus an

urgent need to develop effective and practical tools for early screening of chemicals with potential adverse effects using high-throughput, low-cost methodologies that ensure high predictability of human biological responses (Parks Saldutti *et al.*, 2013). Recently, *in vitro* testicular models have been introduced to environmental chemical safety assessment to improve the predictability of chemical-induced testicular toxicity in human and elucidate mechanisms of chemical toxicity (Harris *et al.*, 2015; Hofmann *et al.*, 2005a; Parks Saldutti, *et al.*, 2013; Wegner *et al.*, 2013; Wegner *et al.*, 2014; Yu *et al.*, 2003; Yu *et al.*, 2009; Yu *et al.*, 2005b). Some of these *in vitro* models form a testicular-like multilayered architecture that mimics *in vivo* characteristics of seminiferous tubules (Yu, *et al.*, 2003; Yu, *et al.*, 2005b). However, these *in vitro* primary testicular cell co-culture models still have the disadvantage of employing animals for the isolation of testicular cells. In addition, complicated isolation procedures lead to inconsistency of primary testicular cells (Wegner, *et al.*, 2013). In this study, a spermatogonial cell line (C18-4) was used to examine and compare the toxicity profiles of BPA and some of its analogs. The C18–4 germline cell line was previously established from type A spermatogonia isolated from 6-day-old mouse testes (Hofmann, *et al.*, 2005a; Hofmann *et al.*, 2005b; Kokkinaki *et al.*, 2009).

There is a need for improved *in vitro* methods to meet the challenges associated with the increasing push to predict the toxicity of chemicals. EPA has initiated a ToxCast project integrating *in vitro* high-content and high-throughput toxicity assessment to characterize the toxicological profiles of thousands of chemicals (Auerbach, *et al.*, 2016; Karmaus *et al.*, 2016a; Kavlock *et al.*, 2012; Paul Friedman *et al.*, 2016). HCA has been demonstrated to be particularly useful for toxicity testing and prediction as it enables measurements of multiple, early toxicological mechanisms by characterizing co-expression of multiple molecules, as well as

quantification and visualization of the spatial and temporal dynamic processes of cellular events. HCA has been successfully applied to the prediction of drug-induced human hepatotoxicity, and this highly specific and sensitive assay has shown high concordance with human data (O'Brien, *et al.*, 2006; Schoonen *et al.*, 2005; Xu*, et al.*, 2008; Xu *et al.*, 2004). Furthermore, the HCA enables comparisons of the effectiveness of various assay parameters, detects high-risk chemicals and the sequences of cellular events. By linking chemical-biological interactions with sequential key events at multiple biological responses, adverse outcome pathways provide a mechanism-based framework to support the hazard assessment of chemicals (Ankley *et al.*, 2010; Perkins *et al.*, 2015).

The purpose of this study was to develop an automated multi-parametric screening method and to optimize protocols for cell treatment, high-content imaging, and image analysis of the C18-4 spermatogonial cells. This validated HCA approach was applied to characterize and compare the testicular toxicities of BPA and three selected commercially available BPA analogs: BPS, BPAF, and TBBPA. Multiple cellular and molecular events that potentially lead to impaired male reproductive function were compared, including nuclear morphology, DNA content, cytoskeletal integrity, cell cycle, and DNA damage responses in a dose and time-dependent manner. Overall, our results demonstrated that this *in vitro* model combined with HCA could be utilized for a quantitative screening of chemical effects in spermatogonial cells and enable rapid and cost-effective measurement of the multidimensional biological profile of toxicity.

2.3 Materials and methods

2.3.1 Chemicals

Dulbecco's Modified Eagle Medium (DMEM), and Penicillin-Streptomycin were purchased from GE Healthcare Life Sciences (Logan, Utah). Fetal bovine serum (FBS), 2,2-bis(4-hydroxy-3-methylphenyl) propane (BPA, ≥99%), 4,4'-sulfonyldiphenol (BPS, 98%), 3,3',5,5'-tetrabromobisphenol A (TBBPA, 97%), and neutral red (NR) were purchased from Sigma-Aldrich (St Louis, Missouri). 4,4'-(hexafluoroisopropylidene) diphenyl (BPAF, 98%) was purchased from Alfa Aesar (Ward Hill, Massachusetts). The chemical structures of these compounds are shown in Figure 2.1 (Chen *et al.*, 2016a; Colnot *et al.*, 2014). 5-Bromo-2'-deoxyuridine (BrdU, 99%) was purchased from Thermo Scientific (Waltham, Massachusetts). Paraformaldehyde (4% in phosphate-buffered saline) was purchased from Boston Bioproducts (Ashland, Massachusetts).

2.3.2 Cell culture and treatment

The mouse C18-4 spermatogonial cell line was established from germ cells isolated from the testes of 6-day-old Balb/c mice. This cell line shows morphological features of type A spermatogonia, expresses germ cell–specific genes such as GFRA1, Dazl, and Ret, which are markers specific for germ cells in the testis (Hofmann*, et al.*, 2005a; Hofmann*, et al.*, 2005b). Cells were maintained in DMEM medium composed of 5% FBS, and 100 U/ml streptomycin and penicillin in a 33˚C, 5% CO_2 humidified environment in a sub-confluent condition with passaging every 3-4 days. When they reached 70-80% confluence, cells were inoculated with 1.2 $\times 10^4$ per well in a 96-well plate. Cells were cultured overnight and treated with various concentrations of BPA, BPS, BPAF and TBBPA for the indicated doses and time periods.

<u>2.3.4 Cell viability</u>

Cell viability was determined by measuring the capacity of cells to take up neutral red (NR). NR can be retained inside the lysosomes of viable cells, while the dye cannot be retained if the cells dies. Dye retention is proportional to the number of viable cells, and can be measured based on NR absorbance (Repetto *et al.*, 2008; Yu*, et al.*, 2009). Significant changes in cell viability were determined using a 1-way analysis of variance (1-way ANOVA) followed by Tukey-Kramer multiple comparison tests. Briefly, cells were treated with various concentrations of BPA, or BPS, (50, 100, 200 and 400 μM), and BPAF or TBBPA (25, 50, 75 and 100 μM) for different length of time (24-72 h). Cells treated with vehicle (0.05% DMSO) were used as the reference group with cell viability set as 100%. After treatments, the culture medium was removed and fresh medium containing NR (50 μg/ml) was added. Following 3 h incubation, cells were washed with phosphate buffered saline (PBS), and NR was eluted with 100 μl of a 0.5% acetic acid/50% ethanol solution. The plate was gently rocking on a plate shaker, and absorbance values were measured at 540 nm with a Synergy HT microplate reader (BioTek, VT). Cell viability was expressed as a percentage of the mean of vehicle controls after subtracting the background control.

<u>2.3.5 Fluorescence staining and image acquisition</u>

For cell cycle analysis, cells were incubated with BrdU (40 μM) for 3 h prior to fixation. Cells in the controls reached 100% confluence at the time of harvest. Cells were then fixed with 4% paraformaldehyde for 30 mins at room temperature, followed by three times washing with PBS. Cells were then acidified with a 4N HCl/ Triton X-100 solution for 30 min at room temperature. After neutralization with $Na_2B_4O_7$ solution for 10 min, cells were washed twice with PBS and blocked with 3% BSA in PBS. Cells were then incubated with a mouse anti-BrdU

antibody (Thermo Scientific, MA) in PBS/BSA/0.5% Tween 20 overnight at 4°C. After washing twice with PBS/BSA, cells were incubated with a goat anti-mouse DyLight 488 and the DNA staining dye Hoechst 33342 (Thermo Scientific, MA) in PBS/BSA solution for 90 min at room temperature.

For DNA damage responses and cytoskeleton analysis, cells treatments and fixation were the same as described above. After fixation, cells were permeabilized by 0.1% Triton X-100 in PBS, then incubated with mouse anti-phospho-Histone-H2AX (Ser139) (γ-H2AX) (Millipore, MA) in PBS/BSA/0.5% Tween 20 solution overnight at 4°C. After washing twice with PBS/BSA, cells were incubated with goat anti-mouse Dylight 650 (Thermo Scientific, MA), and Hoechst 33342 in PBS/BSA solution for 90 min at room temperature. Prior to image acquisition, cells were stained with Alexa Fluor 488 Phalloidin (Cell Signaling, MA) for F-actin staining for 30 min at room temperature.

Multichannel images were automatically acquired using an Arrayscan™ VTI HCS reader with HCS Studio™ 2.0 Target Activation BioApplication module (Thermo Scientific, MA). Forty-nine fields per well were acquired at 20x magnification using Hamamatsu ROCA-ER digital camera in combination with 0.63x coupler and Carl Zeiss microscope optics in auto-focus mode. Channel one (Ch1) applied the BGRFR 386_23 for Hoechst 33342 that was used for auto-focus, object identification, and segmentation. Image smoothing was applied to reduce object fragmentation prior to object detection in Ch1. Border objects were excluded. For BrdU staining, channel two (Ch2) applied the BGRFR 549_15 for BrdU. For F-actin and γ-H2AX staining, Ch2 applied the BGRFR 485_20 for F-actin, and channel three (Ch3) applied the BGRFR 650_13 for γ-H2AX.

<u>2.3.6 High-content images analysis</u>

Multi-Channel images were analyzed using HCS Studio[TM] 2.0 TargetActivation BioApplication. Change in nuclear morphology is an early event of the cellular response, and is associated with cellular functions (Elmore, 2007; Webster *et al.*, 2009; Zhivotosky and Orrenius, 2001). Single-cell based HCA provided multiple parameters to characterize the nucleus, including the number, nuclear area, shape, and total or average intensity. Nuclear shape measurement included P2A and length-width ratio (LWR) parameters. P2A is a shape measurement based on the ratio of the nuclear perimeter squared to 4π*nucleus area (perimeter^2/4 π * nucleus area), which evaluates nucleus smoothness. LWR measures the ratio of the length to the width of the nucleus, which evaluates nucleus roundness. For a fairly round and smooth object, the values for P2A and LWR are around 1.0. Total intensity was defined as total pixel intensities within a cell in the respective channel; the average intensity was defined as the total pixel intensities divided by the area of a cell in the respective channel. With 49 fields of each well, at least 5000 cells were analyzed per well and single-cell based data for each channel were exported for further statistical analysis. The experiments were performed with at least three biological replicates and repeated twice.

HCA-based cell cycle analysis was conducted as recently reported by Roukos et al. (Roukos *et al.*, 2015). The frequency distributions of total DNA intensity of all individual nuclei were calculated and plotted for each experimental condition in a custom script written in Python 3.5.2 (Python Software Foundation, OR; this script is freely available from the authors upon request). Cell cycle profiles with discrete sub-G1 (apoptotic cells), G0/1, S or G2/M populations in the controls and treatments were determined by the selections of appropriate thresholds of these gates as reported (Roukos*, et al.*, 2015).

2.3.7 Statistical analysis

All data obtained from the HCS Studio^{TM} 2.0 TargetActivation BioApplication were exported and further analysis was conducted using the JMP statistical analysis package (SAS Institute, North Carolina). Objects with nuclear area smaller than 50 μM^2 or larger than 800 μM^2 were excluded in order to remove cell debris and clumps. For each plate, the vehicle control showed consistent measurement for all endpoints tested. For intra-plate normalization, each sample value was normalized to the overall scaling factors, which was the mean of median values of vehicle control (0.05% DMSO) in each plate. The parameters from single-cell based imaging were quantified and averaged for each well condition. For the mega or multi-nuclei identification in the automatic HCA, nuclei with the enlarged nuclear area ($\geq$ 500 μm^2) and irregular nuclear shape (P2A $\geq$ 1.35) were identified, and the percentages were calculated. BrdU positive cells were set by the total intensity of BrdU in the control over 20,000 pixels. γ-H2AX positive cells were set by the total intensity of γ-H2AX in the control over 120,000 pixels. Data are presented as mean $\pm$ SD. Statistical significance was determined using 1-way ANOVA followed by Tukey-Kramer all pairs comparison. A P value less than 0.05 denoted a significant difference compared with the vehicle control (*).

To examine the relationship between the cytoskeleton and DNA damage responses, Spearman correlation analysis was conducted between the log-transformed total intensity of F-actin and log-transformed total intensity of γ-H2AX at 24, 48 and 72 h.

The 20% maximal effect concentration (EC20) and median lethal concentration (LC50) were calculated with a curve-fitting program using GraphPad Prism 5 (San Diego, CA). A dose-response curve fit was established based on the concentrations of chemicals that had a significant effect. The 4totored-parameter nonlinear regression curve fit was applied. Treatment

concentrations were $\log_{10}$ transformed. For cell viability (NR assay) and cell number data (HCA), the lowest value was set to be 0% and the highest value was set to be 100%. For other markers, the lowest value was set to be controls and the highest value was set to be a maximal effect at each time point.

2.4 Results

2.4.1 BPA and its analogs induced differential dose- and time-dependent cytotoxicity in spermatogonial cells

In order to select sub-lethal doses of BPA and its analogs for HCA analysis in spermatogonial cells, cell viability was measured using NR uptake assay. Figure 2.2 shows a significant dose- and time-dependent decreases in cell viability in spermatogonial cells treated with BPA and its analogs for 24 h and 48 h. BPAF reduced cell viability starting at a concentration of 25 μM, TBBPA reduced cell viability starting at a dose of 50 μM for 24 h and 25 μM for 48 h, while BPA and BPS reduced cell viability at a concentration of 100 μM for both 24 and 48 h exposure. This indicated that BPAF and TBBPA induced greater cytotoxicities, as compared with BPA and BPS. The LC50 values for 48 h were 42.16, 49.93, 132.7, 325.3 μM for BPAF, TBBPA, BPA, and BPS, respectively. The highest concentrations of 50 μM were selected for BPA and BPS, and 25 μM were selected for BPAF and TBBPA in the following HCA experiments.

2.4.2 BPA and its analogs altered nuclear morphology and cell number

Nuclear morphology has shown to be a sensitive endpoint compared with conventional cytotoxicity assays (Martin *et al.*, 2014). In this study, multiple parameters associated with nuclear morphology were measured. Figure 2.3A shows representative nuclear morphologies following 72 h treatments. Notable reductions of cell numbers and increases in mega or

multinucleated cell numbers were observed in the BPAF treatments at doses of 10 and 25 μM (arrows). Further quantification of the multinucleated cells using HCA demonstrated that BPAF treatment induced significant increases of multinucleated cells at doses of 25 μM for 24, 48 and 72 h (Supplementary Figure S2.1). No obvious morphological change was observed for the other tested compounds. As shown in Figure 2.3B-D, nuclear morphological parameters obtained from HCA, including nuclear area and nuclear shape, were compared in spermatogonial cells treated with various chemicals for 24, 48 and 72 h. Significant increases of nuclear area were observed in cells treated with 25 μM BPAF for 24, 48 and 72 h, and cells treated with 50 μM BPS and 25 μM TBBPA for 72 h. BPA significantly decreased LWR at a dose of 50 μM for 72 h. BPS significantly decreased LWR and P2A at a dose of 50 μM for 72 h. However, BPAF significantly increased LWR and P2A at concentrations of 25 μM for 24 h, 10 μM for 48 h. For 72 h, BPAF significantly increased LWR at 1 μM and P2A at 10 μM. TBBPA also induced significant increases of LWR at concentrations of 5, 10 and 25 μM and a significant increase of P2A at a concentration of 25 μM for 72 h.

As shown in Figure 2.4, BPAF and TBBPA reduced cell numbers starting at a dose of 25 μM for 24, 48 and 72 h. BPA and BPS reduced cell numbers at a dose of 50 μM for 24, 48 and 72 h. These numbers were lower than those observed with the NR assay. Notably, low doses of BPA (0.1 μM) and BPAF (0.1 and 5 μM) slightly increased cell numbers. These results suggested that for the detection of changes in cell numbers measured by HCA is more sensitive than the conventional NR uptake cytotoxicity assay.

2.4.3 BPA and its analogs affected DNA synthesis and cell cycle

The measurement of DNA content of individual cells enabled determination of the phases of the cell cycle, while the BrdU incorporation measured newly synthesized DNA. Figure 2.5A

shows representative images of BrdU incorporation after 72 h treatments. Most multinucleated cells in the BPAF treatment were BrdU positive cells (arrows). As shown in Figure 2.5B, BPAF (25 μM) significantly induced total DNA intensity, by 1.3-, 1.5- and 2.0-fold after 24, 48 and 72 h treatments as compared with the control, respectively. However, BPA, BPS, and TBBPA treatments show no observable change of DNA total intensity. Figure 2.5C showed that BPS of a concentration of 50 μM and BPA of concentrations of 10, 25, 50 μM significantly decreased BrdU positive cells for 24 and 48 h, respectively, suggesting inhibitory effects of DNA synthesis from those treatments. However, BPAF treatment induced significant increases in BrdU positive cells at all three time-points at a concentration of 25 μM as compared with the control. No change of BrdU incorporation was observed for the TBBPA treatment.

Histogram plots of total DNA intensity were generated and the percentages of cells in each phase of the cell cycle were determined. As shown in Figure 2.6, the DNA intensity histogram in control groups exhibited distinguishable 2N (G0/1 phase) and 4N DNA (G2/M phase) peaks. Significant changes in the DNA histogram plot such as decreases in G0/1, and increases of S and G2/M phases in the BPAF treatment were observed. As shown in Table 1, dynamic changes of cell cycle stages in the controls across time-points, such as increases of cells in G0/1 and decreases in cells in S phase after 48 and 72 h culture were observed as compared with the control after 24 h. Cell populations in G0/1 phase were significantly decreased with a BPAF treatment of 25 μM for 24 h, 10, 25 μM for 48 and 72 h, and a TBBPA treatment of 25 μM for 24, 48 and 72 h. Significant increases in the percentage of cells in S phase were observed when cells were treated with 25 μM BPAF for 24, 48 h, and 10, 25 μM for 72 h. On the contrary, significant decreases in the percentage of cells in S phase were observed after treatments with 10 and 25 μM TBBPA for 24 and 48 h, and after treatment with 10 μM for 72 h. Accumulations of

cells in G2/M phase were observed in cells treated with 10 µM BPA for 48 h, and 10 and 50 µM

BPS for 48 h. A similar pattern was observed with 25 µM BPAF for 24 h, 10 and 25 µM BPAF

for 48 h, and 25 µM BPAF for 72 h. Accumulations of cells in G2/M were also observed with 25

µM TBBPA for 24 and 72 h, and with doses of 5, 10 and 25 µM of TBBPA for 48 h. Significant

decreases in the percentages of cells in G2/M phase were observed with a BPA treatment of 50

µM for 24 h and of 10 µM for 72 h. A BPS treatment of 10 µM for 72 h had the same effect.

Finally, increases in the percentages of cells in sub-G1 phase, representing apoptotic cells, were

observed with BPA at a dose of 50 µM for 72 h, with BPAF treatment at doses of 10 and 25 µM

for 24 h, 25 µM for 48 h, 5and 10 µM for 72 h. TBBPA treatments of 25 µM for 48 h, and of 10,

25 µM for 72 h also increased the percentages of cells in apoptosis. Altogether, these results

indicated that BPAF and TBBPA treatments at higher concentrations led to an increase of cells

in the G2/M phase accompanied by an increase of apoptotic cells. Further, BPAF treatment

showed a unique increase of cells in S phase, which was consistent with our BrdU incorporation

results. On the contrary, BPA and BPS treatments led to a decrease in the number of cells in the

G2/M phase at doses of 10 or 50 µM.

2.4.4 BPA and its analogs disrupted the germ cell cytoskeleton

　　　The cytoskeleton provides a structural framework for the cell and serves as a scaffold that

determines cell shape and the organization of the cytoplasm (Sun *et al.*, 2011). Multi-parametric

HCA assays were developed to examine the effects of BPA and its analogs on the cytoskeleton

of the spermatogonial cells. As shown in Figure 2.7A, F-actin showed a regular organization

with aligned and tightly compacted structures in controls. However, BPAF and TBBPA

treatments induced actin aggregate as dot-like structures with highly condensed actin staining

(arrows). Further the number of dot-like structures of F-actin was quantified. Significant

increases in BPAF treatment at doses of 25 μM for 24, 48 and 72 h, and TBBPA treatment at

doses of 25 μM for 24 and 48 h were found. Significant decreases in dot-like structures were

observed in BPS treatment of 50 μM for 72 h (Supplementary Figure S2.2). These unique

structure changes were dose-dependently observed for the of BPAF and TBBPA treatments,

suggesting chemical-specific effects on the cytoskeleton. Dynamic changes of total intensity of

F-actin were further quantified as shown in Figure 2.7B. BPA and BPS (50 μM), BPAF and

TBBPA (25 μM) significantly increased total intensity of F-actin at 24, 48 and 72 h exposure

times. BPAF induced an approximate 2-fold increase in total intensity of F-actin at 48 and 72 h

exposure in comparison with other bisphenols. These data suggested that BPAF and TBBPA

could potentially impair F-actin polymerization, resulting in aberrant F-actin accumulation.

2.4.5 BPA and its analogs induced γ-H2AX expression, a marker for early DNA damage

To further explore the potential effects of BPA and its analogs on DNA integrity, γ-

H2AX expression was examined to assess early DNA damage responses in spermatogonial cells

after treatments with BPA and its analogs. As shown in Figure 2.7A, all tested compounds

induced various extent of γ-H2AX staining. BPAF induced γ-H2AX positive cells at a

concentration of 25 μM. For the quantification of γ-H2AX as shown in Figure 2.7C, BPA

treatment significantly increased the number of γ-H2AX positive cells at a concentration of 50

μM for 48 and 72 h. Both BPS (50 μM) and BPAF (25 μM) treatments significantly increased

the number of γ-H2AX positive cells after 24, 48 and 72 h exposure, as compared with the

control. TBBPA only induced γ-H2AX positive cells at a concentration of 25 μM for 72 h. BPAF

induced a higher number of γ-H2AX positive cells, with an increase of 2.5-, 3- and 5-fold for

exposures of 24, 48 and 72 h respectively as compared with the control. These data demonstrated

that BPAF showed greater genotoxic potency as observed by increased expression of the DNA damage response marker γ-H2AX.

To examine the relationship between the cytoskeleton and DNA damage responses, a Spearman correlation analysis was conducted based on the log-transformed total intensity of F-actin and γ-H2AX. The correlation coefficients (r) are summarized in Table 2. For all four chemicals tested, r was positive with P values of less than 0.0001, suggesting a significant and positive correlation between cytoskeleton perturbation and DNA damage responses. Thus, an increase in the intensity of F-actin staining was strongly correlated with an increase in the total intensity of γ-H2AX for 24 and 48 h exposure, and moderately correlated increase in the total intensity of γ-H2AX for 72 h, suggesting that cytoskeleton perturbation may co-occur with the DNA damage responses.

2.4.6 Comparison of EC20 values of BPA and its selected analogs for different endpoints

In order to clarify the relationship between doses of compounds, the magnitude, and type of cellular responses (endpoints), the EC20 values from different endpoints were calculated and are listed in Table 3. Similar to cell viability data obtained with the NR assay, the EC20 values of multiple endpoints obtained with the HCA were lower in all treatments, suggesting HCA-based assays identify potential targets of cytotoxic agents with improved sensitivity.

In BPA treatment, the endpoint with the lowest EC20 was cytoskeleton perturbation (7.5 μM), followed by cell number decrease (52.4 μM) and G2/M phase decrease (54.6 μM) after 24 h treatment. After 48 h treatment, the endpoint with the lowest EC20 was cytoskeleton perturbation (31.5 μM), followed by DNA damage responses (50.3 μM) and cell number decrease (50 μM). After 72 h treatment, the EC20 for multiple cellular responses was at the same dose level (50 μM). For the BPS treatment, the endpoint with the lowest EC20 was cytoskeleton

perturbation (4.5 μM), followed by DNA damage responses (31.0 μM), DNA synthesis

inhibition (36.9 μM) and cell number decrease (246.1 μM) after 24 h treatment. After 48 h

treatment, the endpoint with the lowest EC20 was DNA damage responses (20.5 μM) followed

by cytoskeleton perturbation (66.2 μM) and cell number decrease (81.4 μM). After 72 h

treatment, BPS induced nuclear shape changes, cell cycle arrest, and DNA damage responses all

at the same doses of 50 μM, while for cytoskeleton perturbation and nuclear area changes, the

EC20 values were around 100 μM. BPAF treatment induced a wide spectrum of cellular events

at a concentration of approximate 10 μM. These changes were independent of the time of

exposure, and include decreases in cell numbers, changes of cell number, nuclear morphology,

cell cycle perturbations, DNA synthesis facilitation, increased DNA damage responses and

cytoskeleton perturbations. The induction of apoptotic cells showed the lowest EC20 values (0.4

μM) after 72 h treatment. Among these endpoints, LWR consistently showed lower EC20 values

(6.1-7.6 μM), suggesting that alteration of nuclear roundness could serve as an early sensitive

marker of BPAF toxicity in C-18 spermatogonial cells. For the TBBPA treatment, the endpoints

with the lowest EC20 were S phase decrease (8.8 μM) followed by cytoskeleton perturbation

(10.1 μM), G2/M phase increase, and cell number decrease around 25 μM after 24 h treatment.

After 48 h treatment, the endpoint with the lowest EC20 was S phase decrease (5.7 μM) followed

by apoptosis increase (13.7 μM), cytoskeleton perturbation (24.4 μM), cell number decrease

(28.1 μM), G0/1 phase decrease (38 μM) and G2/M phase increase (52.2 μM). After 72 h

treatment, TBBPA treatment induced various cellular responses at a concentration of

approximately 25 μM (EC20), except for apoptosis increase. In summary, in comparison of the

EC20 values of four bisphenols, BPAF stood out markedly, with high cytotoxicity (EC20 values

ranging from 0.4 to 20 μM). TBBPA was identified as having an intermediate toxicity (EC20

96

values ranging from 0.3 to 47 μM). BPA and BPS were less cytotoxic (EC20 values from 4.5 to 250 μM) and the differences between these two compounds were minor.

2.5 Discussion

Despite increasing use of BPA analogs as BPA alternatives, there are still limited data available on their reproductive toxicities. Assessing reproductive toxins poses great challenges. Therefore it is urgent to develop an improved *in vitro* model to identify and assess critical biological events leading to adverse reproductive outcomes.

Cytotoxicity is a very complex process affecting multiple signaling pathways within cells. New approaches for toxicity characterization have focused on *in vitro* high-throughput and high-content assays, which enable measurement of early, sub-lethal indicators of cellular toxicity, as well as the determination of the sequences and patterns of cellular events. HCA has been an effective and sensitive tool for obtaining large quantities of robust data on the multiple effects of compounds as compared with conventional cytotoxicity assays like the NR assay. Several studies demonstrated that data obtained with HCA are concordant with drug-induced toxicity in humans (O'Brien, *et al.*, 2006; Schoonen, *et al.*, 2005; Xu, *et al.*, 2008). HCA has been widely used to assess chemical-induced mechanistic effects, and has been applied to drug discovery using specific cell type or three-dimensional cell culture models (Anguissola *et al.*, 2014b; Kameoka, *et al.*, 2014; Radio, *et al.*, 2008; Ramery and O'Brien, 2014; Sirenko *et al.*, 2015). In this study, a number of HCA-based assays and phenotypic read-outs were developed and validated, including characterizations of nuclear morphology, DNA content, cell cycle, cytoskeleton integrity, and DNA damage responses using a germline cell line.

The C18-4 germline cell line was selected as an *in vitro* cell model to evaluate the testicular toxicity of BPA and its selected analogs (Hofmann, *et al.*, 2005a; Hofmann, *et al.*,

2005b; Kokkinaki*, et al.*, 2009). Spermatogenesis is a complex process by which undifferentiated spermatogonial cells divide and mature, maintaining male fertility via the daily production of millions of spermatozoa in the testis. The foundation of this process lies in spermatogonial stem cells (SSCs), which undergo self-renewal and produce daughter cells by undergoing complicated differentiation processes (Oatley and Brinster, 2008). The immortalized C18-4 germline cells exhibited the morphological features of spermatogonial cells and expressed germ cell-specific proteins (Hofmann*, et al.*, 2005a). The C18-4 cells have been used to determine testicular signaling pathways (Golestaneh *et al.*, 2009; He *et al.*, 2008; Zhang *et al.*, 2013), and to characterize molecular mechanisms of reproductive toxicity of nanoparticles (Braydich-Stolle *et al.*, 2005; Braydich-Stolle *et al.*, 2010; Lucas *et al.*, 2012). In combination with the validated HCA assays, this *in vitro* model was suitable for quantitative screening of chemical effects in spermatogonial cells and enabled rapid and cost-effective assessment of reproductive toxicants.

Changes in nuclear morphology are general a reflection or a result of accumulation, of millions of cellular events taking place inside a cell, and known to be tightly associated with proliferation, gene expression, and protein synthesis (Versaevel *et al.*, 2012). The nucleus is surrounded by the nuclear envelope, which isolates chromosomes from the cytoplasm and typically has either an oval or round shape. Previous studies have demonstrated that the changes in nuclear morphology seen with HCA were sensitive markers for detecting cytotoxic effects (Martin*, et al.*, 2014; O'Brien*, et al.*, 2006; Persson*, et al.*, 2013). In the present study, BPA treatmentinduced alterations of nuclear shape (LWR) at non-cytotoxic doses, which is similar to previous findings in mouse embryonic fibroblasts (Dolinoy *et al.*, 2007; Gassman *et al.*, 2016). An *in vivo* study recently demonstrated that low-dose exposure to BPA (2μg/kg) induced germ

cell apoptosis in adult rats (Jin*, et al.*, 2013). Interestingly, BPAF induced a dose-dependent increase of multinucleated cells. Induction of abnormal testicular germ cells, such as multinucleated germ cells (MNGs), has been reported following gestational exposure to di-(n-butyl) phthalate (DBP) (Fisher *et al.*, 2003; Kleymenova *et al.*, 2005; Mahood *et al.*, 2007; Saffarini *et al.*, 2012). Ferrara and colleagues speculated that germ cells presenting DBP-induced MNGs might develop into carcinoma *in situ* (CIS) cells, the known precursors of testicular germ cell tumors (TGCT) in men (Ferrara *et al.*, 2006). Cell cycle analysis revealed that these BPAF-induced multinucleated cells were actively synthesizing DNA (BrdU), with increased numbers of cells in S and G2/M phase, suggesting these germline cells underwent abnormal proliferation. Further animal studies are needed to confirm whether BPAF has a testicular toxicity similar to DBP *in vivo.*

Assessment of the cell cycle status of individual cells is pivotal for the evaluation of cell cycle regulation in response to intracellular and extracellular cues. Cell cycle status and progression have traditionally been measured using population-based methods such as flow cytometry (Darzynkiewicz *et al.*, 2006; Sidhu *et al.*, 2006). Flow cytometry is generally dependent on the successful preparation of a single-cell suspension, which is not compatible with high-throughput and high-resolution cell imaging. HCA-based cell cycle analysis was recently reported by Roukos et al. (Roukos*, et al.*, 2015). Cell cycle profiles with discrete G1, S or G2/M populations were determined and these results were comparable to data obtained from flow cytometry analysis (Roukos*, et al.*, 2015). A protocol for the spermatogonial cell line was established, which was able to accurately segment the nuclei for DNA content quantification. The dynamic changes of the cell cycle in the control population at different time-points were observed (Table 1). Those percentage changes across the phases of the cell cycle are consistent

99

with the cellular growth status, exhibiting fast proliferation at an early time-point and then slowing down when cells reach 100% confluence for 72 h. This HCA-based cell cycle analysis allows us to be able to accurately segment the nuclei even when the C18-4 spermatogonial cells were at 100% confluence for 72 h. As an imaging-based method to probe the cell cycle phase of individual cells, HCA can be used to correlate phases with the subcellular localization or the co-expression levels of multiple DNA loci or proteins tagged with different fluorescent markers. This feature will be widely applied in the mechanistic toxicity studies to screen or identify potential mechanisms of action. As revealed in the cell cycle analysis using HCA-based DNA content histograms and BrdU incorporation assay, BPA and its analogs induced dose- and time-dependent alterations of the cell cycle with chemical-specific changes Previous *in vivo* studies showed that BPA disrupted meiosis I progression and altered the number of leptotene and diplotene spermatocytes percentages in rat testicular cells (Ali *et al.*, 2014; Liu *et al.*, 2013). Disruption of the cell cycle has been proposed to be a key event in BPA testicular toxicity (Ali*, et al.*, 2014; Liu*, et al.*, 2013). Our results demonstrated that BPA or BPS treatments at a concentration of 10 or 50 μM disrupted mitosis progression (G2/M phase). BPA induced a dose-dependent decrease of BrdU positive cells for 48 h, suggesting that HCA-based quantification of BrdU is a sensitive endpoint for the evaluation of the cell cycle in comparison to the cell cycle profiling from total DNA content histogram. It has been reported that BPA exposure caused diverse effects on the cell cycle. BPA treatment can inhibit cell proliferation and induced S and G2/M phase arrest in midbrain cells at 1×10^{-4} M (Liu*, et al.*, 2013). On the other side, low-dose BPA ($\leq 10^{-9}$ M) can promote cell proliferation in human seminoma cells though a G-protein-coupled non-classical membrane ER and induced cell proliferation and cell-cycle regulatory proteins in human breast cell lines (Bouskine *et al.*, 2009; Pfeifer *et al.*, 2015; Wu *et al.*, 2012).

The differences between our current observations and previous studies may be due to the different sensitivity to the endpoints tested in spermatogonial cells. For BPAF treatment, along with the significant changes in nuclear morphology, significant increases in S phase in both cell cycle profiling and BrdU labeling, and accumulation of cells in G2/M phase were observed in a dose-dependent manner. Again, HCA-based assessment of the cell cycle status of individual cells suggested that BPAF treatment could result in significant alterations of the cell cycle as compared with the treatment with BPA, BPS or TBBPA at similar dose ranges.

BPA has long been suspected to induce carcinogenesis (Keri *et al.*, 2007). Low doses of BPA have been reported to promote DNA damage, potentially contributing to breast cancer (Pfeifer*, et al.*, 2015). Several assays can measure and quantify cellular responses to DNA double-strand breaks. The proteins, such as γ–H2AX, ATM, CDKN1A, and TP53, involved in the early steps of the cellular response in sensing DNA damage and controlling progression, have been proposed as the top group of candidate biomarkers (Marchetti *et al.*, 2006). Due to the signal amplification of γH2AX foci at the site of DNA damage, the detection of γH2AX has been identified as an early sensitive cellular biomarker of DNA damage (Nikolova *et al.*, 2014; Rogakou *et al.*, 1998). In this study, a multi-parametric HCA assay along with the detection of γH2AX was developed. BPA and its analogs significantly altered the expression levels of γH2AX. It has been reported that BPA and its analogs induced DNA damages in a cell-type-specific and dose-dependent manner (Fic *et al.*, 2013; Lee *et al.*, 2013). BPA is able to induce DNA damage in spermatozoa (Liu, Duan et al. 2013), and in human breast cell line MCF-7 cells at the low concentration of 10 nM (Liu*, et al.*, 2013; Pfeifer*, et al.*, 2015). Other studies showed that BPA at a concentration of 100 μM did not induce γH2AX in a colorectal adenocarcinoma LSI174T cell line, but Bisphenol F did (Audebert *et al.*, 2011). Most significantly, among all

chemicals tested, BPAF showed significant induction of γH2AX at multiple time-points, suggesting a greater genotoxicity, as compared with other bisphenols.

The cytoskeleton, which serves as a scaffold that determines cell shape and the organization of the cytoplasm, plays a significant role in regulating cell shape, movement, cargo transportation and nuclear morphological modification (Sun*, et al.*, 2011). Disorganization of F-actin was found to induce germ cells dysfunction *in vivo* (Lie *et al.*, 2009). A BPA exposure of 200 μM induced the truncation and de-polymerization of F-actin with mislocalization of actin regulatory proteins in human Sertoli cells without the changes of the total F-actin fluorescence intensity (Xiao*, et al.*, 2014). HCA-based analysis of F-actin demonstrated that all four bisphenols showed the aberrant F-actin distribution in the cytoplasm (Figure 2.7B). These alterations in F-actin are highly correlated with the increased γ–H2AX expression, an early DNA damage responses marker (Table 2.3). It has been reported that alterations in the actin cytoskeleton were correlated with induction of γ–H2AX in human breast MCF-7 cells (Zhao *et al.*, 2015). In the present study, comparison of EC20 values indicated F-actin appeared an early cellular response marker for chemical-induced testicular toxicity, and that perturbation of the cytoskeleton could potentially be associated with other endpoints, such as change of nuclear morphology and cell cycle alterations.

One of the applications of HCA assays in drug discovery and toxicity testing is prioritizing and ranking compounds for their potential human toxicity. By comparing of EC20 values among four bisphenols, BPAF showed the highest germ cell cytotoxicity, followed by TBBPA, BPA, and BPS. Although the chemical structures of BPA and its analogs are similar, HCA demonstrated differential adverse effects of four bisphenols on multiple molecular and cellular events, suggesting that different mechanisms may promote cytotoxicity. Similar findings

were reported in previous *in vitro* studies, in which BPAF and TBBPA showed higher endocrine modulating potentials in human MCF7 breast cancer cells and Leydig cells, respectively, as compared with BPA (Lei *et al.*, 2016; Roelofs*, et al.*, 2015). BPS showed similar inhibitory effects with BPA on testosterone secretion in human fetal testes and induced more sensitive responses in mice testes (Eladak*, et al.*, 2015). The different levels of toxicities between BPA and its analogs could be dependent on their chemical structures. Perez et al. reported that the estrogenicity of BPA analogs in human breast cancer cells was influenced by the substitution at the bridging carbon between the two phenolic rings in human breast cancer cells (Perez *et al.*, 1998). In addition, for BPAF and TBBPA, introducing a halogen into the bisphenol structure could contribute to their higher toxicities. This is because the degree of halogenation in BPA analogs could alter activation of ERs and peroxisome proliferator–activated receptors (PPARs) (Riu *et al.*, 2011). By substituting different chemical groups and degree of halogenation, BPA and its analogs could exert differential toxicities via various receptor binding sites and binding affinities. In order to elucidate the potential structure-related toxicities, more BPA analogs will be included in future studies. Our *in vitro* data were also consistent with previous *in vivo* findings. BPA exposure ($\leq$ 50mg/kg) consistently induced impairments of sperm production and quality, and alteration of steroidogenesis (D'Cruz *et al.*, 2012; Tiwari and Vanage, 2013). Whereas BPS, BPAF and TBBPA exerted some adverse reproductive effects, including alterations of hormone levels, decreases in sperm count and changes of seminiferous epithelium morphology, Future study will be important to validate these findings (Feng*, et al.*, 2012; Kuriyama *et al.*, 2005; Ullah*, et al.*, 2016).

Several limitations of the *in vitro* HCA assay need to be considered. First, bioactivation might be required, but it is limited in our current *in vitro* cell culture model. It has been reported

that metabolites of BPA, such as 4-methyl-2, 4-bis (p-hydroxyphenyl) pent-1-ene, exhibited higher estrogenic potency as compared with BPA itself (Yoshihara *et al.*, 2004). Thus, metabolites of BPA and its analogs should be included in further experiments. Second, the duration of exposure might be insufficient. In order to mimic real-life exposure scenarios, chronic low-dose exposure to BPA and its analogs need to be considered. Third, the species-specific sensitivity for *in vitro* testing is critical to the interpretation of toxicity across species. It has been reported that BPA concentration required to impair testosterone production in human is about 100-fold lower than that in rodent fetal testis explants (Habert *et al.*, 2014). Thus, more cell lines or primary cells from different species, especially humans, would be helpful to extrapolate current *in vitro* findings to human health risk assessment.

In summary, multi-parametric HCA assays in germline cells were developed. The testicular toxicity of BPA and its analogs were compared. This multi-dimensional toxicological profiling revealed differential testicular toxicities of BPA and its analogs, whereas BPAF and TBBPA showed greater cytotoxicity, followed by BPA and BPS. Our findings also suggested that using the HCA platform with C18-4 spermatogonial cells could provide a rapid and cost-effective tool to gain insights into mechanisms of toxicity, and establish links between molecular pathways and accelerate safety testing of potential reproductive toxicants.
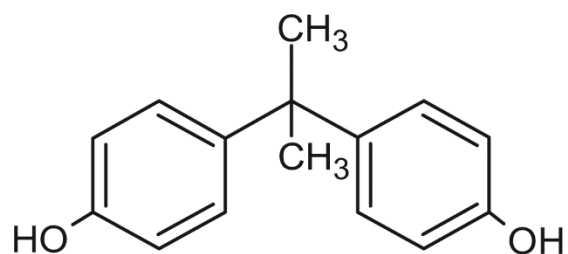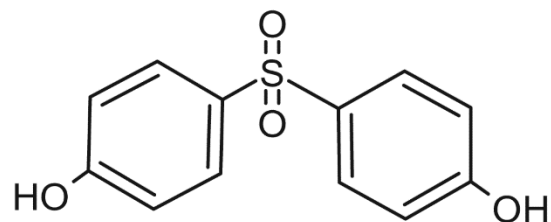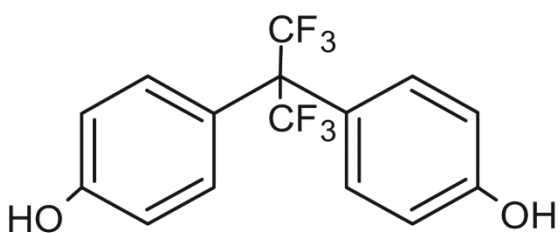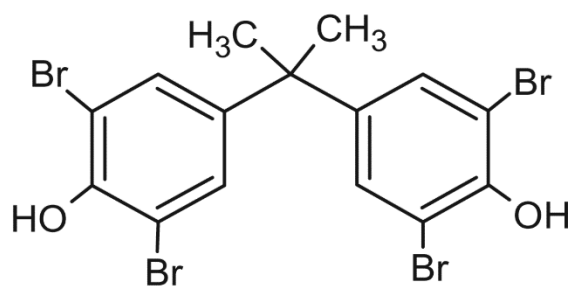
Figure 2.1. Chemical structures of BPA, BPS, BPAF, and TBBPA (Chen, *et al.*, 2016a; Colnot, *et al.*, 2014).
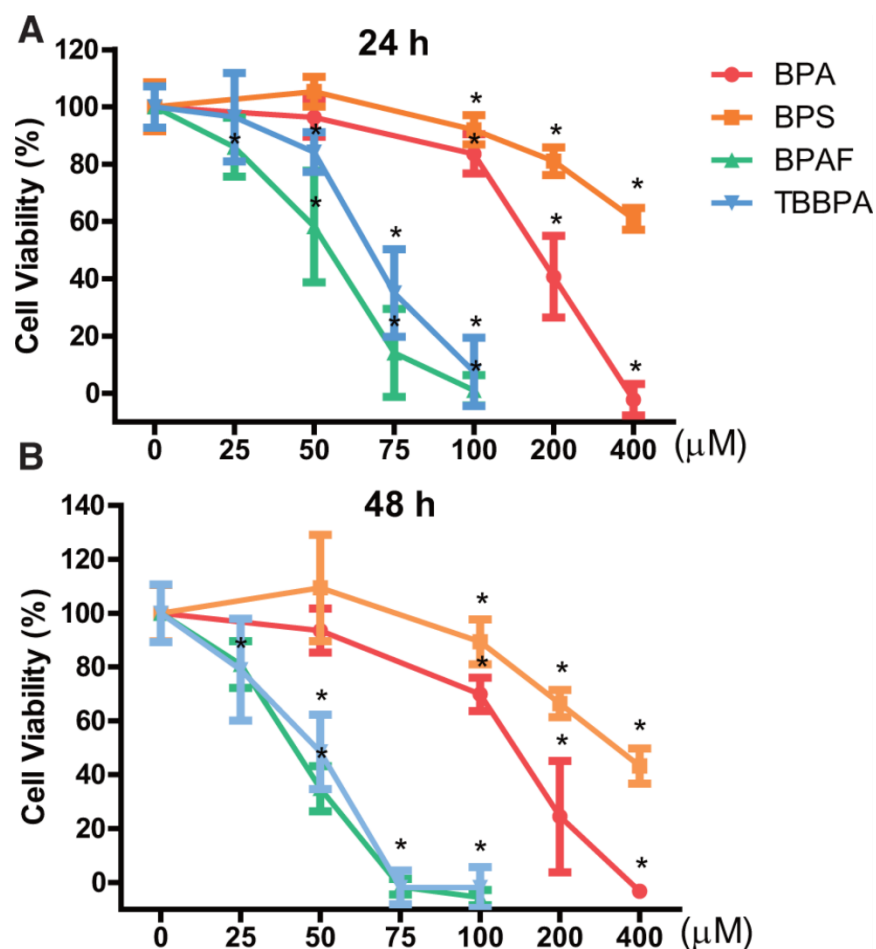
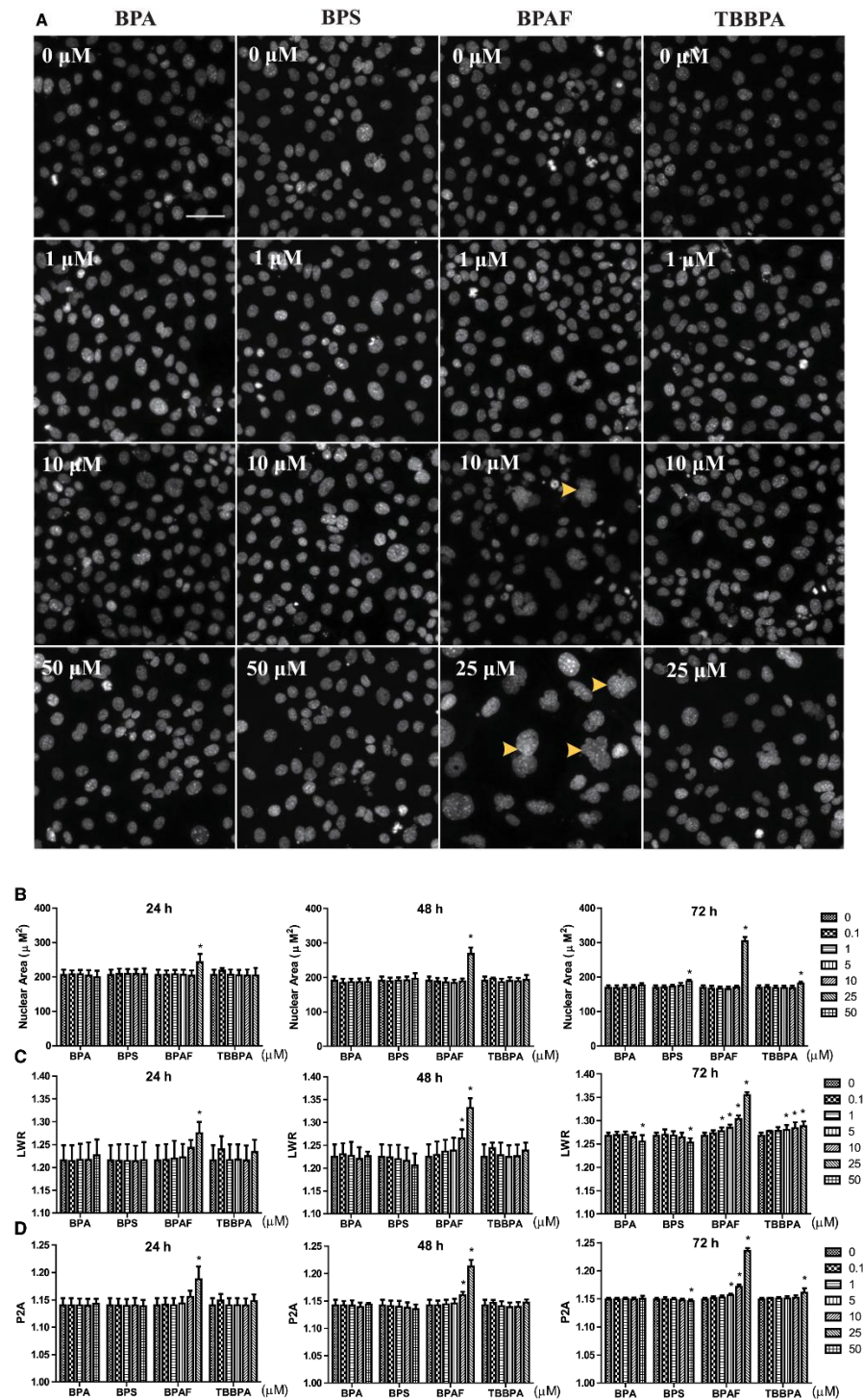Figure 2.2. Cell viability was determined by neutral red uptake assay in spermatogonial cells treated with BPA, BPS, BPAF and TBBPA. Cells were treated with various concentrations of BPA and BPS (50, 100, 200, and 400 μM), and BPAF and TBBPA (25, 50, 75, and 100 μM) for 24 (A) and 48 h (B). Cells treated with vehicle (0.05% DMSO) were used as vehicle controls (0). Data are presented as mean ± SD, n=10. Five replicates in two separate experiments were included. Statistical analysis was conducted by 1-way ANOVA followed by Tukey-Kramer multiple comparison (* P< 0.05).
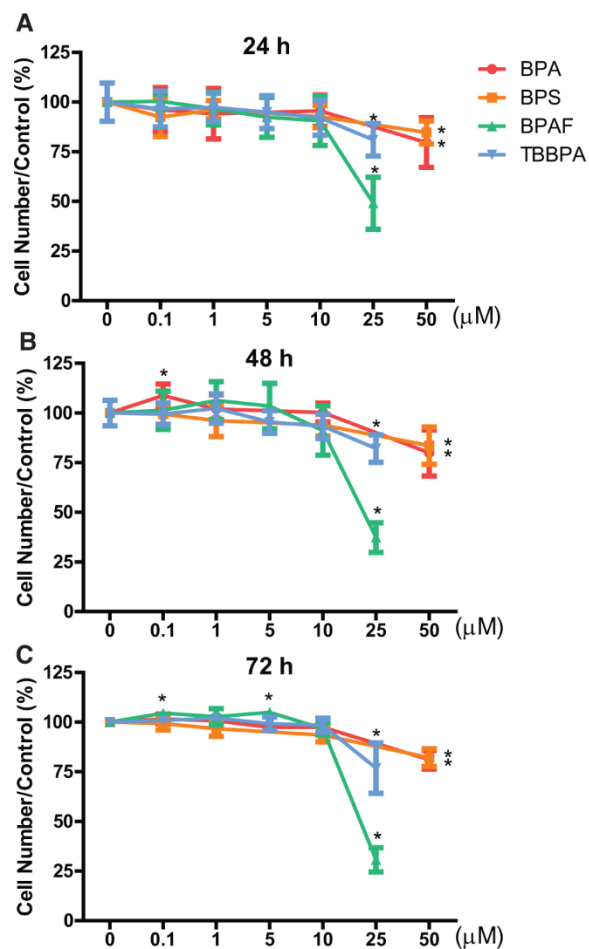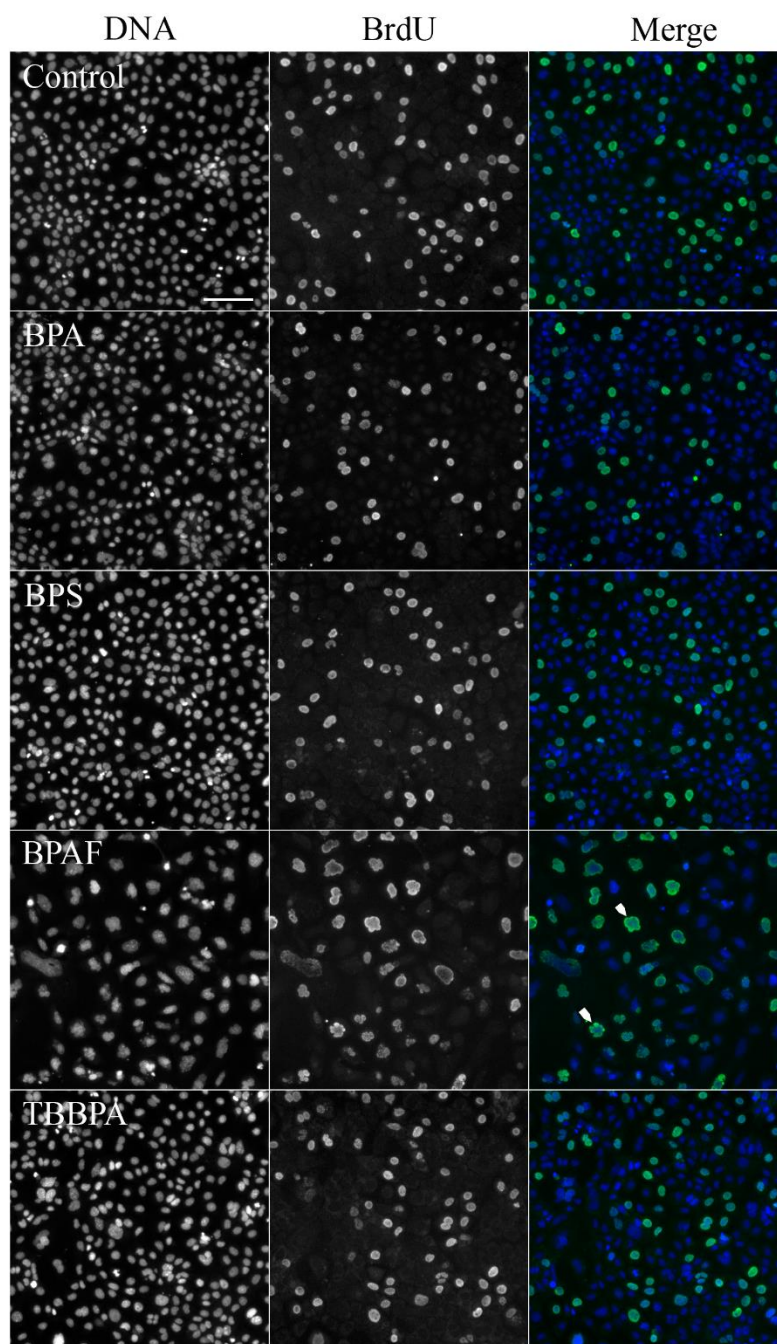
Figure 2.3. HCA of nuclear morphology of spermatogonial cells treated with BPA, BPS, BPAF and TBBPA. Cells were treated with various concentrations of BPA and BPS (0.1, 1, 10, and 50 μM), and BPAF and TBBPA (0.1, 1, 5, 10, and 25 μM). Cells treated with vehicle (0.05%

DMSO) were used as vehicle controls (0). The nuclei of spermatogonial cells were stained with

Hoechst 33342, and images were automatically obtained with a 20x objective, 49 fields per well.

A shows the representative images (40x) of controls and cells treated with BPA and BPS (1, 10,

and 50 µM), BPAF and TBBPA (1, 10, and 25 µM) for 72 h. Arrows indicate the multinucleated

cells. Scale bar = 50 µm. B-D shows the quantification of the absolute nuclear area (µm2),

nuclear shape, including LWR for nuclear roundness and P2A for smoothness. Data are

presented as mean ± SD, n=9. Three replicates in three separate experiments were included.

Statistical analysis was conducted by 1-way ANOVA followed by Tukey-Kramer multiple

comparison (* P< 0.05).

Figure 2.4. HCA of cell number of spermatogonial cells treated with BPA, BPS, BPAF and TBBPA. Cells were treated with various concentrations of BPA and BPS (0.1, 1, 10, and 50 µM), and BPAF and TBBPA (0.1, 1, 5, 10 and 25 µM) for 24 (A), 48 (B,) and 72 h (C). Cells treated with vehicle (0.05% DMSO) were used as vehicle controls (0). The nuclei of spermatogonial cells were stained with Hoechst 33342, and images were automatically obtained with a 20x objective, and 49 fields per well. The number of cells within 49 fields per well was counted. Data are presented as mean ± SD, n=9. Three replicates in three separate experiments were included. Statistical analysis was conducted by 1-way ANOVA followed by Tukey-Kramer multiple comparison (* P< 0.05).
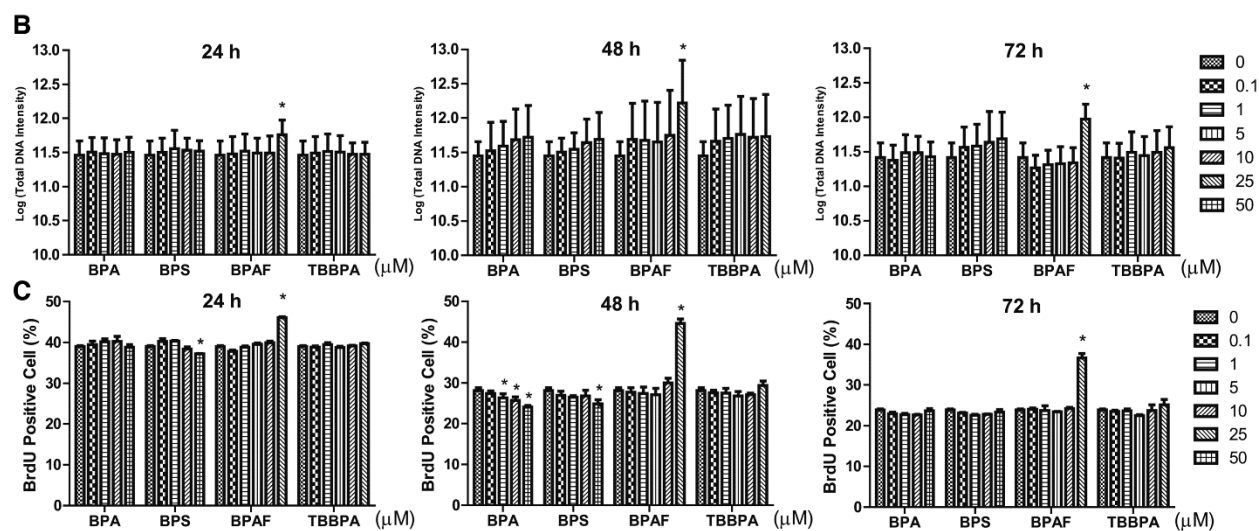
A

Figure 2.5. HCA of DNA content and synthesis of spermatogonial cells treated with BPA, BPS, BPAF and TBBPA. Cells were treated with various concentrations of BPA and BPS (0.1, 1, 10, and 50 μM), and BPAF and TBBPA (0.1, 1, 5, 10, and 25 μM) for 24, 48, and 72 h. Cells treated with vehicle (0.05% DMSO) were used as vehicle controls (0). The nuclei were stained with Hoechst 33342. Cells were incubated with BrdU (40 μM) for 3 h prior to cell fixation, and then stained with mouse anti-BrdU antibody and anti-mouse DyLight 488 for detection of BrdU incorporation (green). The nuclei were stained with Hoechst 33342 (blue). A shows the representative images of cells treated with BPA and BPS (50 μM), BPAF and TBBPA (25 μM) for 72 h. Arrows indicate the multinucleated cells with positive BrdU staining. Scale bar = 100 μm. B shows the quantification of log-transformed total DNA intensity. C shows the quantification of BrdU-positive cells. Data are presented as mean ± SD, n = 9. Three replicates in three separate experiments were included. Statistical analysis was conducted by 1-way ANOVA followed by Tukey-Kramer multiple comparison (* P< 0.05).
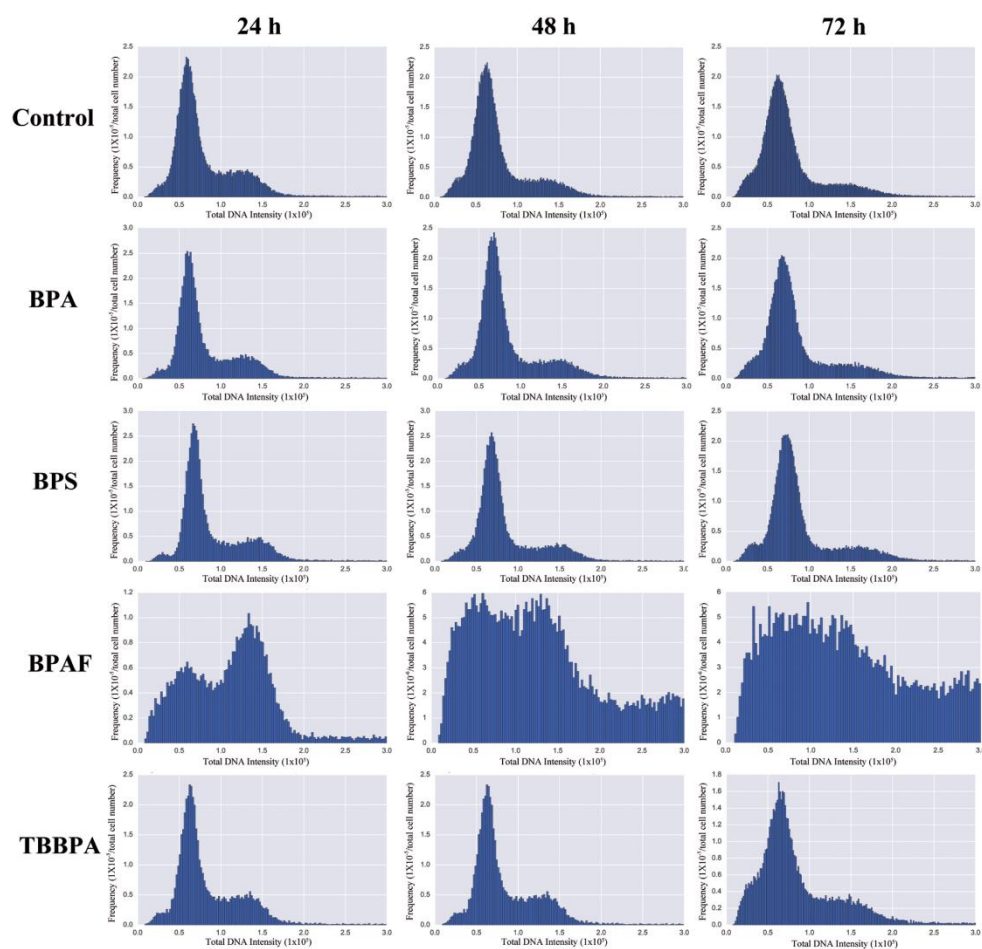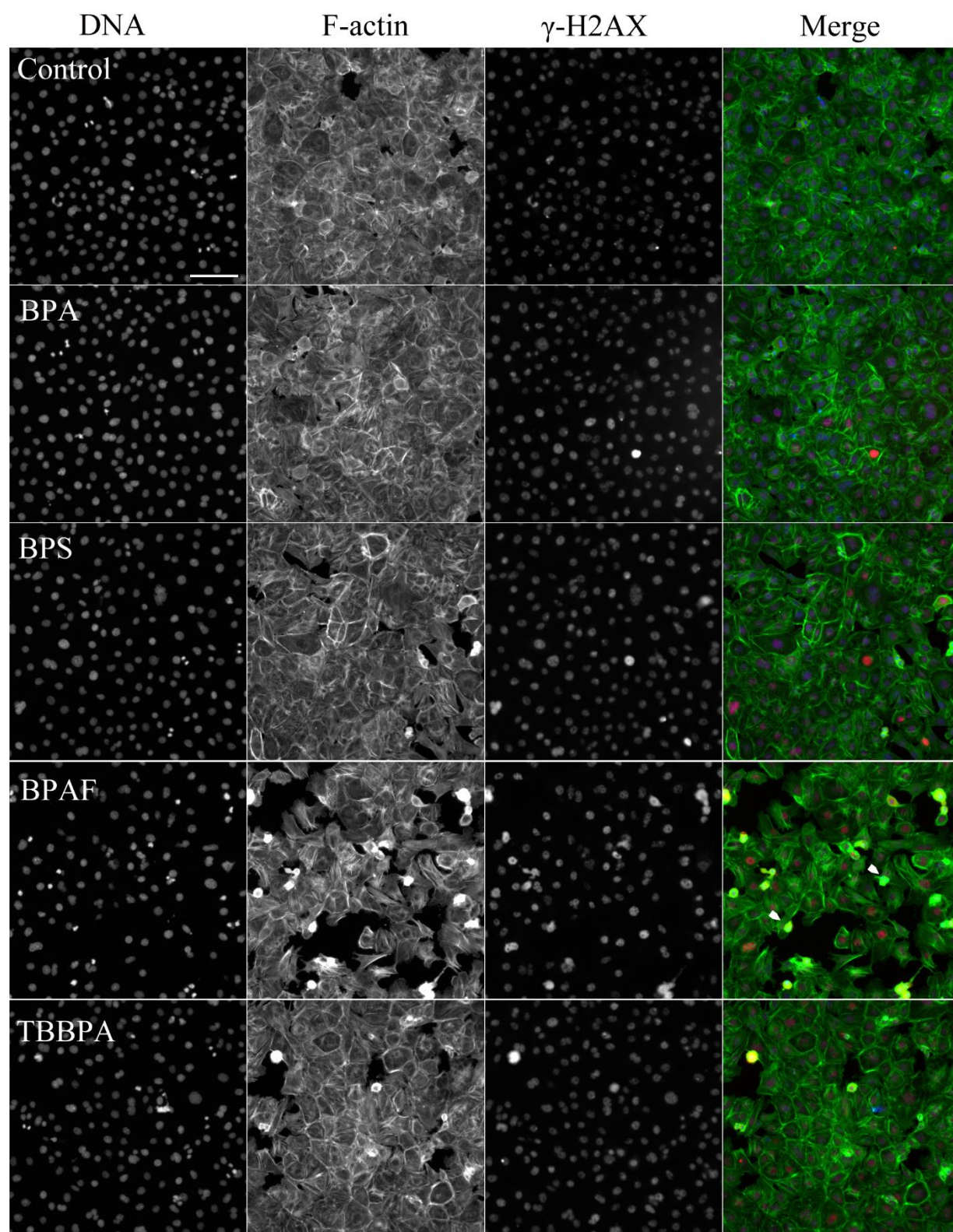
112

Figure 2.6. HCA of cell cycle of spermatogonial cells treated with BPA, BPS, BPAF and

TBBPA. The Representative DNA content histograms are shown in the vehicle controls (0.05%

DMSO vehicle) and treatments with BPA and BPS (50 µM), BPAF and TBBPA (25 µM) for 24,

48 and 72 h.

A

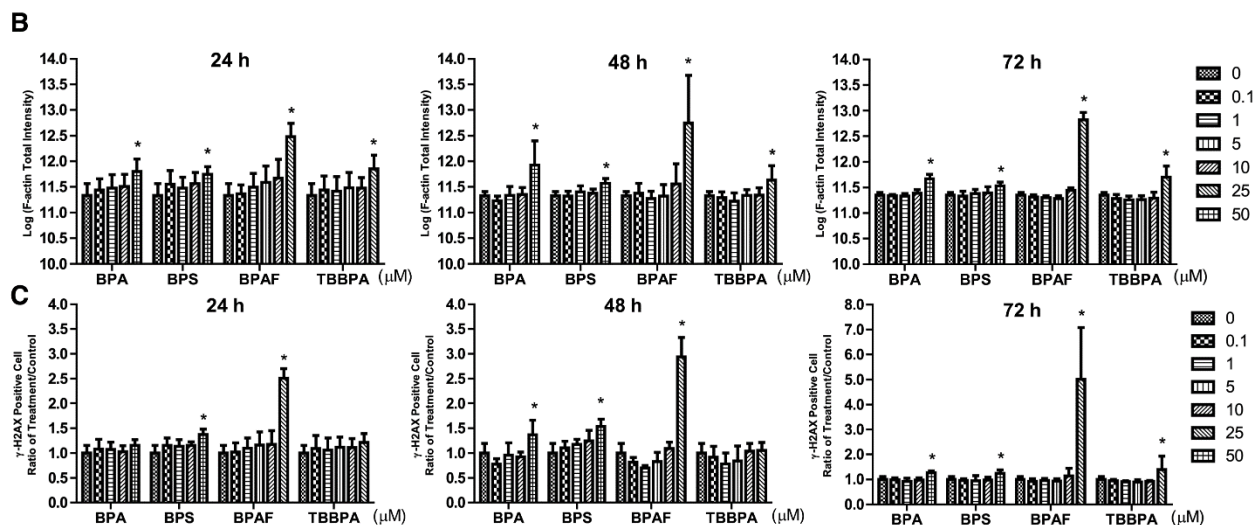|	DNA	F-actin	γ-H2AX	Merge

Control

BPA

BPS

BPAF

TBBPA

Figure 2.7. HCA of F-actin and γ-H2AX in spermatogonial cells treated with BPA, BPS, BPAF and TBBPA. Cells were treated with various concentrations of BPA and BPS (0.1, 1, 10, and 50 μM), and BPAF and TBBPA (0.1, 1, 5, 10, and 25 μM) for 24, 48, and 72 h. Cells treated with vehicle (0.05% DMSO) were used as vehicle controls (0). The nuclei were stained with Hoechst 33342 (blue), F-actin with Phalloidin staining (green), and γH2AX with a combination of primary anti-γ−H2AX and secondary Dylight 650 conjugated antibody (red). A shows the representative images of cells treated with BPA and BPS (50 μM), BPAF and TBBPA (25 μM) for 24 h. Arrows indicate dot-like structures. Scale bar = 100 μm. B-C demonstrated the quantification of the log-transformed total intensity of F-actin and positive γ-H2AX cells. Data are presented as mean ± SD, n=6. Three replicates in two separate experiments were included. Statistical analysis was conducted by 1-way ANOVA followed by Tukey-Kramer multiple comparison (* P< 0.05).

Table 2.1. HCA of cell cycle of spermatogonial cells treated with various concentrations of BPA, BPS, BPAF, and TBBPA for 24, 48, and 72 h.

	Dose (μM)	24 h				48 h				72 h			
		Sub G1(%)[a]	G0/1(%)	S (%)	G2/M (%)	Sub G1(%)[a]	G0/1(%)	S (%)	G2/M (%)	Sub G1(%)[a]	G0/1(%)	(%)S	G2/M (%)
BPA	0	3.5±1.1	64.6±1.7	12.6±0.8	18.1±1.7	5.2±1.5	67.4±1.6	12.0±0.7	13.0±1.1	5.6±1.0	70.7±1.7	9.9±1.4	12.9±1.0
	0.1	3.5±0.9	64.9±1.5	12.6±0.2	18.1±1.1	5.2±3.1	69.4±2.3	12.4±0.7	12.5±2.8	6.9±1.2	70.0±0.8	10.6±0.6	11.7±1.3
	1	4.4±2.1	62.5±1.5	12.9±0.8	18.9±1.9	5.9±1.5	67.9±1.2	12.1±0.6	13.6±1.8	6.5±1.1	70.7±2.1	9.3±2.1	12.2±1.0
	10	5.0±1.3	64.0±1.0	11.8±0.9	18.3±1.3	4.7±1.4	67.0±2.2	11.7±1.4	15.7±1.2*	6.8±0.6	70.6±3.1	11.3±2.6	9.8±1.2*
	50	4±1.3	65.8±3.0	13.5±0.6	15.3±1.3*	4.2±1.7	67.1±1.9	12.9±0.8	15.1±1.6	7.3±1.3*	67.5±3.1	11.0±1.7	13.1±1.9
BPS	0	3.5±1.1	64.6±1.7	12.6±0.8	18.1±1.7	5.2±1.5	67.4±1.6	12.0±0.7	13.0±1.1	5.6±1.0	70.7±1.7	9.9±1.4	12.9±1
	0.1	3.8±0.8	63.6±1.5	12.3±0.2	19.4±2.0	4.3±0.6	69.5±1.1	11.8±0.7	13.7±1.8	7.4±1.7	71.0±1.1	9.5±1.3	11.4±0.8
	1	3.6±0.7	62.9±2.0	12.6±0.5	20.0±1.1	3.7±1.8	68.4±1.8	11.7±0.5	15.0±1.6	6.5±0.6	71.9±1.8	9.6±1.4	11.3±1.1
	10	3.8±0.9	63.1±1.9	12.9±0.7	19.2±1.3	4.9±1.3	66.6±1.2	11.9±0.9	15.6±2.3*	8.7±5.0	70.1±1.9	10.2±1.5	10.2±2.8*
	50	3.9±1.1	63.7±1.3	13.0±0.8	18.6±1.6	5.9±3.4	65.9±2.5	11.2±0.9	16.0±1.9*	7.4±1.4	70.5±2.5	9.2±1.6	11.8±2.6
BPAF	0	3.5±1.1	64.6±1.7	12.6±0.8	18.1±1.7	5.2±1.5	67.4±1.6	12.0±0.7	13.0±1.1	5.6±1.0	70.7±1.7	9.9±1.4	12.9±1.0
	0.1	3.6±1.0	64.3±1.9	11.9±1.0	18.5±1.3	5.6±1.9	66.5±2.2	10.6±0.4	16.6±1.4	6.5±0.7	71.5±1.0	10.4±0.5	11.1±1.1
	1	3.3±0.7	65.1±1.4	13.5±0.5	17.3±2.0	5.4±1.4	68.1±2.0	11.5±1.4	14.0±2.1	7.7±1.1	67.9±3.3	10.9±1.1	12.8±1.2
	5	4.1±1.0	63.5±2.8	12.1±0.7	18.7±1.5	5.5±2.0	67.8±3.5	11.6±1.3	14.1±4.2	8.0±0.7*	70.0±1.0	10.3±1.2	11.2±1.1
	10	6.1±1.6*	62.2±1.8	12.3±0.8	18.5±1.2	8.4±4.1	59.7±1.5*	11.0±0.6	19.9±3.2*	12.1±2.5*	61.0±1.3*	13.1±2.1*	13.1±1.1
	25	7.6±1.9*	25.3±3.3*	14.9±1.6*	47.6±4.6*	9.7±1.7*	25.3±3.1*	15.2±1.4*	44.6±2.7*	6.8±2.5	26.4±3.0*	19.3±1.3*	48.3±5.1*
TBBPA	0	3.5±1.1	64.6±1.7	12.6±0.8	18.1±1.7	5.2±1.5	67.4±1.6	12.0±0.7	13.0±1.1	5.6±1.0	70.7±1.7	9.9±1.4	12.9±1.0
	0.1	4.9±2.0	62.4±1.7	12.9±0.7	19.1±2.0	4.1±1.9	69.1±1.9	11.4±0.4	14.8±3.3	7.4±1.2	71.0±0.5	10.3±0.4	10.8±0.9
	1	3.7±1.0	62.7±1.0	13.3±0.8	19.6±1.1	5.4±1.4	66.7±2.8	12.0±0.8	15.0±2.9	8.6±0.9	69.4±0.7	10.5±0.5	10.6±0.7
	5	4.3±1.5	62.9±1.7	13.2±0.7	18.7±0.9	3.4±1.1	67.6±1.6	11.9±0.6	16.3±2.0*	8.6±4.5	69.7±3.7	9.9±0.4	11.2±0.7
	10	4.2±1.5	66.3±1.7	11.0±1.1*	18.0±2.1	5.5±1.7	66.5±1.6	8.9±2.3*	18.1±1.4*	11.0±2.0*	67.7±1.6	6.7±0.6*	13.8±1.0
	25	4.7±1.0	60..3±0.9*	10.6±1.2*	23.5±0.9*	8.9±3.6*	63.2±3.3*	9.2±1.3*	17.7±2.0*	13.2±2.3*	57.5±8.0*	8.7±1.1	19.1±4.9*

Note: Percentage of each stage of cell cycle, including sub-G1 (apoptosis), G0/1, S and G2/M phase are presented as mean ±SD, n=6. Three replicates in two separate experiments were conducted. Statistical analysis was conducted by 1-way ANOVA followed by Tukey-Kramer multiple comparison (* P< 0.05). Cells treated with vehicle (0.05% DMSO) were used as vehicle controls (0).

Table 2.2. Correlation analysis between total intensity of F-actin and total intensity of γ-H2AX

Time	Correlation Coefficient									
	BPA		BPS		BPAF		TBBPA		All	
(h)	r	P	r	P	r	P	r	P	r	P
24	0.85	<0.0001	0.91	<0.0001	0.45	0.0384	0.75	<0.0001	0.76	<0.0001
48	0.82	<0.0001	0.89	<0.0001	0.74	0.0001	0.34	0.1295	0.75	<0.0001
72	0.42	0.0827	0.66	0.0027	0.48	0.0276	0.52	0.0152	0.50	<0.0001

Note: Spearman correlation analysis was conducted between the total intensity of F-actin and γ-H2AX in each cell (JMP statistical

analysis package, SAS Institute, Cary, North Carolina)

Table 2.3. EC20 values of BPA and its selected analogs from multiple endpoints.

		24 h				48 h				72 h			
	Dose (μM)	BPA	BPS	BPAF	TBBPA	BPA	BPS	BPAF	TBBPA	BPA	BPS	BPAF	TBBPA
Cell Viability [a]	EC_{20}	114.5	222.1	11.5	41.7	84	154.3	10.1	47.1	ND			
	CI	101.1-129.6	198.6-248.3	3.9-33.4	31.5-55.2	72.8-97.0	123.1-193.4	39.6-25.7	VW				
Cell Number	EC_{20}	52.4	246.1	13.3	27.8	50	81.4	13.9	28.1	52.5	64.8	15.7	23.6
	CI	26.1-105.4	26.2-2316	11.0-16.0	17.9-43.0	VW	36.6-180.8	11.6-16.6	21.4-36.9	47.7-57.9	47.9-87.7	13.9-17.6	21.8-25.5
Nuclear Area	EC_{20}	NS	NS	20.8	NS	NS	NS	18.1	NS	NS	108.1	12.5	26.4
	CI			VW				VW			54.3-215	VW	VW
P2A	EC_{20}	NS	NS	8.7	NS	NS	NS	8.3	NS	NS	-	7.7	33.8
	CI			7.8-9.9				7.4-9.2			-	6.5-9.1	25.8-44.3
LWR	EC_{20}	NS	NS	6.8	NS	NS	NS	7.6	NS	70.9	61.8	6.1	11.8
	CI			3.5-13.0				5.7-10.0		32.5-154.3	35.3-108.2	5.3-7.1	5.7-24.4
Cell Cycle (Sub G1)	EC_{20}	NS	NS	5.8	NS	NS	NS	6.3	13.7	-	NS	0.4	0.3
	CI			3.6-9.2				2.9-13.5	4.7-40.0	-		0.03-4.2	0.05-1.6
Cell Cycle (G0/1)	EC_{20}	NS	NS	11.4	-	NS	NS	10.1	38.0	NS	NS	9.8	18.9
	CI			6.1-21.3	-			VW	20.6-70.0			9.4-10.2	15.8-22.5
Cell Cycle (S)	EC_{20}	NS	NS	19.3	8.8	NS	NS	17.12	5.7	NS	NS	8.6	23.5
	CI			VW	VW			VW	VW			7.0-10.1	9.0-62.1
Cell Cycle (G2/M)	EC_{20}	54.6	NS	11.9	25.2	NS	-	9.8	52.2	NS	NS	12.0	24.7
	CI	VW		VW	VW		-	9.2-10.5	13.8-198.1			VW	21.7-28.1
BrdU	EC_{20}	NS	36.9	10.7	NS	-	78	10.4	NS	NS	NS	12.2	NS
	CI		15.8-86.2	8.6-13.3		-	12.9-472.4	VW				18.3-81.8	
γ-H2AX	EC_{20}	NS	31.0	10.9	NS	50.3	20.6	11.2	NS	60.2	56.6	11.3	26.1
	CI		9.5-101.1	8.7-13.7		VW	9.9-42.9	VW		VW	VW	VW	
F-actin	EC_{20}	7.5	4.5	7.8	10.1	31.5	66.2	10.2	24.4	47.0	99.4	10.9	24.6
	CI	1.7-34.0	0.7-28.6	5.5-11.1	5.8-20.5	12.4-80.0	36.2-121.1	VW	20.1-28.4	41.1-53.8	39.2-252.1	VW	VW

Notes. EC20: Values for dose causing 20% of the maximum response. CI: 95% confidence interval. NS: not significant. ND: not determined. VW: very wide. - : EC20 simulation failed (exceeded treatment concentration that decreased cell viability to 0%). Color code: red, increase; green, decrease. [a] Data from neutral red uptake assay.

118

CHAPTER 3

MACHINE LEARNING-POWERED HIGH CONTENT ANALYSIS TO CHARACTERIZE

PHENOTYPES ASSOCIATED WITH TOXICITIES OF BISPHENOL A AND ITS ANALOGS

BISPHENOL S, BISPHENOL AF, AND TETRABROMOBISPHENOL A IN A TESTICULAR

CELL CO-CULTURE MODEL

3.1 Abstract

High-content analysis (HCA) has emerged as a powerful tool for chemical toxicity profiling. A multi-parametric HCA in a spermatogonial cell line was previously developed to examine the testicular toxicities of BPA and its analogs, BPS, BPAF, and TBBPA. Due to the complexity of high-dimensional and large-scale HCA data, there are increasing demands for effective computational strategies to characterize and quantify phenotypic changes at a single-cell level. In this study, a machine learning (ML)-based HCA pipeline was developed to explore complex phenotypic changes. The toxicities of BPA and its analogs were characterized in a testicular cell co-culture model utilizing spermatogonial, Leydig, and Sertoli cell lines. In this ML-based phenotypic analysis, the treatments of BPA or its analogs resulted in the loss of spatial arrangement of 3D structure and accumulation of cells in M phase arrest in a dose- and time-dependent manner. Furthermore, BPAF induced accumulation of multinucleated cells, which was associated with an increase in DNA damage response and impairment in cellular actin filaments. These results showed that BPAF and TBBPA exerted toxicity at lower doses, as compared with BPA and BPS on multiple endpoints in the co-cultures. In summary, an ML-based HCA approach was developed in a testicular cell co-culture model and reflected complex phenotypic changes and characterized testicular toxicities of BPA and its analogs. It allowed for an in-depth analysis of multi-dimensional HCA data and unbiased quantitative analysis of phenotypes of interest.

3.2 Introduction

With recent advances in automated fluorescence microscopy and quantitative image analysis software, HCA enables the measurement of unbiased multiparametric data at the single-cell level and provides temporal and spatial measurements of various cellular events that are

120

associated with adverse health outcomes (Buchser *et al.*, 2004; Mattiazzi Usaj *et al.*, 2016;

Zanella *et al.*, 2010). This approach has been used to prioritize chemical toxicity for further

study, characterize adverse outcome pathways and develop predictive models for toxicity

evaluation in humans (Elmore*, et al.*, 2014; Merrick*, et al.*, 2015; Shukla*, et al.*, 2010). The EPA

initiated the ToxCast program using *in vitro* HTS and HCS to profile and predict the toxicity of

thousands of environmental chemicals (Krewski*, et al.*, 2010; Martin*, et al.*, 2011; Paul

Friedman*, et al.*, 2016). Although HCA provides large-scale, image-based data, the analysis of

these data become a major bottleneck. Quantification of the cellular phenotype usually depends

on manual parameter adjustment, which is time- and labor-extensive with low reproducibility

among different experiments (Sommer and Gerlich, 2013). Thus, there are increasing demands

for advanced computational strategies to explore the inherent structure of multidimensional data

and provide an unbiased assessment of versatile phenotypes in large-scale image data sets.

Supervised ML has emerged as a powerful approach to classify cellular heterogeneity using non-

linear multi-parametric algorithms in HCA data (Altschuler and Wu, 2010; Sommer and Gerlich,

2013). The algorithms could learn from the small training dataset with predefined classes and

automatically infers the rules to classify full datasets. Although this approach has been applied to

examine the dynamic changes of genome and proteome in single cell imaging (Chong *et al.*,

2015; Neumann*, et al.*, 2010), its application in toxicology has not yet been fully explored.

We previously established and validated a battery of HCA assays in the spermatogonial

cell line C18-4 and revealed the differential testicular toxicities of BPA and its analogs,

including BPS, BPAF, and TBBPA(Liang*, et al.*, 2017). BPA is a HPV chemical and is used

widely in consumer products, thermal paper, medical devices, and dental sealants (Rochester,

2013). Exposure to BPA is widespread and occurs mainly through ingestion, inhalation and

dermal exposure (Kang, *et al.*, 2006; Vandenberg, *et al.*, 2007). BPA has been detected in more than 90% of urine samples from the general population in the U.S. (Calafat, *et al.*, 2008; Lakind and Naiman, 2011). , BPA is an endocrine disruptor that has known reproductive and developmental toxicity in animal models (Peretz, *et al.*, 2014; Richter, *et al.*, 2007; Rochester, 2013; vom Saal, *et al.*, 2007). Due to concerns about the ubiquitous exposure to BPA and its potential adverse effects on human, the uses of BPA in baby bottles and infant food packaging have been abandoned and its application in the thermal paper is restricted (EU., 2016; FDA., 2013; FDA., 2012). The structural analogs of BPA have been introduced into the market as BPA substitutes or used as crosslinking agents and flame retardants in the plastics industry. Although there is a general lack of production data for BPA analogs, the usage of these chemicals is expected to rise globally. With high structural similarity, these analogs could potentially exhibit similar estrogen potencies and comparable reproductive toxicities with BPA. Emerging evidence indicates that BPA analogs can be detected in food and human urine samples and they interact with various physiological receptors (Driffield, *et al.*, 2008; Kitamura, *et al.*, 2005; Liao and Kannan, 2013; Liao, *et al.*, 2012b; Stossi, *et al.*, 2014). However, toxicological data on BPA analogs are still limited.

Although using spermatogonial cell line provides mechanistic insights into the testicular toxicities of BPA and its analogs, it lacks multicellular complexity and an organ-like structure to fully mimic the physiological conditions present in *vivo*. Sertoli and Leydig cells play critical roles in regulating and supporting spermatogenesis and maintaining the structure and functions of the testis (Haywood, *et al.*, 2003; Lui, *et al.*, 2003; Payne, 1990). The primary testicular cell co-culture model that employs germ, Sertoli and Leydig cells with extracellular matrix (ECM) has been reported to exhibit a testicular-like multilayered architecture. This model demonstrated

differential metabolic capacity, inflammatory responses and differential toxicogenomic responses to phthalates exposures (Harris*, et al.*, 2015; Harris *et al.*, 2016a; Harris *et al.*, 2016b; Yu*, et al.*, 2009; Yu*, et al.*, 2005b). Recently, our laboratory developed an animal-free, *in vitro* testicular cell co-culture model utilizing mouse spermatogonial (C18-4), Sertoli (TM4) and Leydig (TM3) cell lines, which exhibited unique 3D *in vivo* structure as compared to single cell type cultures, and enabled us to classify reproductive toxic substances with high specificity and sensitivity (Yin *et al.*, 2017)

The purpose of this study is to develop a supervised ML-based HCA to characterize phenotypes associated with the testicular toxicities of BPA and its structural analogs, BPS, BPAF and TBBPA in a testicular cell co-culture model. A wide spectrum of adverse endpoints that are linked to functional disorders in testicular cells was measured, including nuclear morphology, DNA synthesis, DNA damage and cytoskeleton structure using established HCA assays. A phenotype recognition pipeline using supervised ML in high-content images and data was developed to classify the phenotypic changes in the co-cultures in response to chemical exposure. BPA and its analogs induced phenotypic 3D structural changes and M phase arrest in a dose-dependent manner. BPAF treatment uniquely induced the formation of multinucleated cells. Overall, by integrating the ML approach with established HCA assays, phenotypic changes were quantitatively identified in the co-cultures treated with BPA and its analogs. Their differential toxicities were observed in this large multivariate dataset based on an ML algorithm. This ML-based HCA approach provided an in-depth analysis of a high-content dataset and enabled us to rapidly and objectively perform phenotypic screening for future toxicity evaluation.

3.3 Materials and methods

3.3.1 Chemicals

Dulbecco's Modified Eagle Medium (DMEM), Modified Eagle's Medium/ Nutrient Mixture F-12 (DME/F12), horse serum and penicillin-streptomycin were purchased from GE Healthcare Life Sciences (Logan, Utah). FBS, 4,4'-(propane-2,2-diyl) diphenol (BPA, ≥99%), 4,4'-sulfonyldiphenol (BPS, 98%), 2,2',6,6'-tetrabromo-4,4'-isopropylidenediphenol (TBBPA, 97%), and neutral red (NR) were purchased from Sigma-Aldrich (St Louis, Missouri). Nu-Serum was purchased from BD BioScience (Redford, Massachusetts). 4-[1,1,1,3,3,3-hexafluoro-2-(4-hydroxyphenyl)propan-2-yl]phenol (BPAF, 98%) was purchased from Alfa Aesar (Ward Hill, Massachusetts). BrdU (99%) was purchased from Thermo Scientific (Waltham, Massachusetts). 4% Paraformaldehyde was purchased from Boston Bioproducts (Ashland, Massachusetts).

3.3.2 Establishment of a testicular cell co-culture model and treatment

The testicular cell co-culture model was established as reported previously (Yin*, et al.*, 2017). Briefly, the mouse C18-4 spermatogonial cell line was established from germ cells isolated from testes of 6-day-old Balb/c mice. This cell line shows morphological features of type A spermatogonia and expresses testicular germ cell–specific genes such as Gfra1, Dazl and Ret (Hofmann*, et al.*, 2005a). The mouse TM3 Leydig and TM4 Sertoli cell lines were purchased from ATCC. C18-4 cells were maintained in DMEM supplemented with 5% FBS, and 100 U/ml streptomycin and penicillin in a 33˚C, 5% CO2 humidified environment in a sub-confluent condition with passaging every 3-4 days. TM3 and TM4 cells were cultured in DME/F12 supplemented with 1.25% FBS, 2.5 % horse serum, and 100 U/ml streptomycin and penicillin at 37˚C, 5% CO2 in a sub-confluent condition with passaging every 2-3 days. When the cells reached 70-80% confluence, a total of 1.5×10^4 cells per well were inoculated in a 96-well plate.

The percentage of each cell type in the co-culture model was 80%, 15%, and 5% for the spermatogonial, Sertoli, and Leydig cell, respectively. The co-cultures were maintained in DMEM supplemented with 2.5% Nu-serum, and 100 U/ml streptomycin and penicillin in a 33˚C, 5% CO_2 humidified environment. After overnight culture, the co-cultures reached 100% confluence and were treated with various doses of BPA, BPS, BPAF and TBBPA for indicated doses and time periods.

3.3.3 NR dye uptake assay

Cell viability was determined by NR uptake assay based on the ability of the viable cell to incorporate NR dye into the lysosomes (Repetto, *et al.*, 2008). The co-cultures were treated with various doses of BPA, or BPS, (25, 50, 100, 200 and 400 μM), and BPAF or TBBPA (2.5, 5, 10, 25 and 50 μM) for 24, 48 and 72 h. The co-cultures treated with vehicle (0.05% DMSO) were defined as the vehicle controls. After treatments, the culture medium was replaced by fresh medium containing NR (50 μg/ml). After 3 h incubation, the co-cultures were washed with PBS, and NR was eluted with 100 μl of a 0.5% acetic acid/50% ethanol solution. The plate was gently shaking, and absorbance values were measured at 540 nm with a Synergy HT microplate reader (BioTek, VT). Cell viability is presented as a percentage of the mean of vehicle controls after subtracting background reading.

3.3.4 Fluorescence staining and image acquisition

For DNA synthesis and cell cycle analysis, the co-cultures were treated with various doses of BPA, or BPS (5, 10, 25, 50, and 100 μM), and BPAF or TBBPA (1, 2.5, 5, 10, and 15 μM) for 24, 48 and 72 h. BrdU incorporation, cell fixation, BrdU and DNA staining followed the previously described (Liang, *et al.*, 2017). For DNA damage responses and cytoskeleton

analysis, cell treatments and fixation were the same as described above. γ-H2AX and F-actin staining followed the methods described in the previous study.

Multi-channel images were automatically acquired using an Arrayscan™ VTI HCS reader (Thermo Scientific, MA). A total of 49 fields per well were acquired at 20x and 40X magnification using a Hamamatsu ROCA-ER digital camera in combination with 0.63x coupler and Carl Zeiss microscope optics in auto-focus mode. Ch1 applied the BGRFR 386_23 for Hoechst 33342 that was used for auto-focus, object identification, and segmentation. Border objects were excluded. For BrdU staining, Ch2 applied the BGRFR 549_15 for BrdU. For F-actin and γ-H2AX staining, Ch2 applied the BGRFR 485_20 for F-actin, and Ch3 applied the BGRFR 650_13 for γ-H2AX.

3.3.5 High-content images analysis

Multi-channel images were analyzed using HCS StudioTM 2.0 TargetActivation BioApplication. Multi-parameters of nuclei were characterized in HCA, including nuclei number, nuclear area, shape, and total DNA intensity. The total intensity of BrdU, γ-H2AX, and F-actin of the individual cell was also quantified. Nuclear shape measurement included P2A, a ratio of the nuclear perimeter squared to 4π*nucleus area (perimeter^2/4 π * nuclear area) to evaluate nuclear smoothness, and nuclear length to width (LWR) to measure nuclear roundness. For a fairly round and smooth object, the values for P2A and LWR are around 1.0. Total intensity was defined as total pixel intensities within a cell in the respective channel. With forty-nine 20x images acquired from each well, at least 1000 cells were analyzed per well, and single-cell based data were extracted for further analysis. The experiments were performed with at least four biological replicates and repeated twice.

For ML-based HCA as illustrated in Figure 3.1, the multi-channel images acquired from the Arrayscan™ VTI HCS reader were analyzed using an open-source software CellProfiler (Broad Institute, MA) (Carpenter *et al.*, 2006). The processing pipeline includes cell segmentation, localization, and measurement of multiple features from a single cell. The pipeline identified the nuclei from the Hoechst 33342 (nuclei) channel and used the nuclei as a primary object to assist in the identification of secondary objects, including F-actin and γ-H2AX in each cell. The pipeline measures more than 200 cellular features, including size, shape, intensity, and texture of nuclei, intensity, and texture of F-actin, and intensity of γ-H2AX in a single cell. The pipeline is freely available from the authors upon request. For nuclear area and shape measurement, multiple features were extracted, such as object area, perimeter, eccentricity, and orientation. For object intensity, various intensity statistics, such as integrated intensity, mean intensity, maximal or minimal pixel intensity within an object or on an object edge, were measured. To quantify the object texture, Haralick texture features that derived from a co-occurrence matrix were employed to calculate the occurrence of pairs of pixels with specific intensity values and spatial relationship in an image. The texture features described homogeneity, local variation, randomness and contrast of object texture. Supervised ML was performed with the CellProfiler Analyst with the "RandomForest Classifier" algorithm (Broad Institute, MA) (Jones *et al.*, 2008). The random forest is an ensemble learning method by constructing decision trees with an averaged prediction, which is robust in high-dimensional data analysis with low bias (Breiman, 2001). In the current study, three phenotypic changes in the co-cultures were quantified. First, the multinucleated cells, a unique toxicity marker for BPAF observed in spermatogonial cells in the previous study, was examined in the current testicular cell co-culture model. As shown in Figure 1, the multinucleated phenotype was identified as a cell with giant

127

nuclei and irregular nuclear contour. HCA-based cell cycle analysis revealed BPAF significantly induced G2/M phase arrest. However, this DNA histogram could not determine the exact M phase. Mitotic phenotypes were identified as a cell with small condensed nuclei with a round shape (prometaphase), condensed nuclei with shallow concavities (metaphase), and nuclei with separated and aligned chromosomes (anaphase, telophase, and late telophase). Last, the formation of 3D structure was observed in the co-cultures at 48, 72 and 96 h at 100% confluence, and the treatment with BPA and its analogs resulted in the disturbance of these structures. Cells with phenotypic 3D structure have stretching F-actin bundles across the cytoplasm. During the training process, a small set of unclassified objects were manually sorted into two classes, including non-multinucleated cells and multinucleated cells, cells not in and in M phase, and cells with and without stretching F-actin filaments. The maximum number of features was set as 20 in order to generate rules for phenotypic classification, and those features were automatically selected by random forest to capture subtle differences between classes. The phenotype classification was based on the images acquired by Arrayscan™ VTI HCS reader, and multiple features were measured by CellProfiler. The input features included values describing nuclei size, shape, DNA intensity and texture, F-actin intensity and texture, and γ-H2AX intensity on a single-cell level. For multinucleated cells and M phase cells, the training set was established by visual examination of images in the nuclei channel. For a cell with stretching F-actin filaments, the initial manual classification during the training process was based on multi-channel images, including nuclei, F-actin and γ-H2AX. Results were presented as the number of cells in predefined classes and the total cell number per image field. The field-based data were averaged for the well-based condition.

Data obtained from the HCS Studio™ 2.0 TargetActivation BioApplication,

CellProfiler and CellProfiler Analyst were exported and further analyzed using the JMP

statistical analysis package (SAS Institute, North Carolina). To remove cell clumps, the nuclei

with area larger than 1000 μM^2 was excluded. For each plate, the vehicle control showed

consistent measurement for all endpoints tested. For intra-plate normalization, data were

normalized to the overall scaling factors, which was the mean of medians of vehicle controls in

each plate. The single cell-based data were averaged for the well-based condition. BrdU positive

cells were set by the total intensity of BrdU in the control over 25,000 pixels. γ-H2AX positive

cells were set by the total intensity of γ-H2AX in the control over 120,000 pixels. LC50 were

calculated using nonlinear regression curve fit on GraphPad Prism 5 (San Diego, California). To

examine the correlation between the cytoskeleton and DNA damage responses in multinucleated

cells, the Spearman correlation analysis was conducted between the total intensity of F-actin and

γ-H2AX for 24, 48, and 72 h using cell-based data. Data are presented as mean ± SD. Statistical

significance was determined using 1-way ANOVA followed by Tukey-Kramer all pairs

comparison. A p-value less than 0.05 denoted a significant difference compared to the vehicle

control (*).

3.4 Results

3.4.1 BPA and its analogs induced time and dose-dependent cytotoxicity in the testicular cell co-culture model.

To determine the appropriate concentrations of BPA and its analogs in HCA experiments,

cell viability was measured by NR uptake assay. Figure 3.2 shows dose-and time-dependent

decreases in cell viability in the co-cultures treated with BPA and its analogs for 24 (A), 48 (B),

and 72 h (C). BPA and BPS treatments significantly decreased cell viability starting at doses of 200 and 400 μM, respectively, for 24 h, and 100 μM for 48 and 72 h. BPAF and TBBPA significantly reduced cell viability starting at concentrations of 5 and 25 μM, respectively, for 24, 48, and 72 h. The LC50 values for 72 h were 8.5, 16.8, 150.2, and 625.8 μM for BPAF, TBBPA, BPA, and BPS respectively. In the following HCA experiments, the highest concentration was selected as 100 μM for BPA and BPS treatments, and 15 μM for BPAF and TBBPA treatments.

3.4.2 BPA and its analog altered nuclear morphology and cell number in the testicular cell co-culture model.

Nuclear morphology was considered to be a sensitive endpoint to detect chemical toxicity in HCA assays (Martin, *et al.*, 2014; O'Brien, *et al.*, 2006). In HCA, multiple morphological parameters of nuclei, including nuclear area, roundness (LWR) and smoothness (P2A) were measured. Figure 3A shows representative images of nuclear morphology after 48 h with or without treatments. Notable decreases in cell numbers were observed in all four chemical treatments. Furthermore, multinucleation (arrow) were observed after BPAF treatment at a dose of 5 μM (Figure 3.3A). As shown in Figure 3.3B, nuclear morphology was quantified in the co-cultures treated with BPA and its analogs after 24, 48 and 72 h. Significant increases in nuclear area were observed in the co-cultures treated with BPAF at a dose of 10 μM for 24 h, 5 to 15 μM for 48 h, and 5 and 10 μM for 72 h, TBBPA at a dose of 15 μM for 24, 48, and 72 h, BPA at 100 μM for 24, 48 and 72 h, and BPA and BPS at a dose of 100 μM for 72 h. Significant decreases in nuclear area were observed in the co-cultures treated with BPA starting at 10 μM for 24 h, and 10 to 50 μM for 48 h. BPA treatment significantly reduced LWR starting at 50 μM for 24 h, at 25 μM for 48 and 72 h and reduced P2A at a dose of 50 μM for 24 h, 50 and 100 μM for 48 and 72 h. BPS treatment significantly decreased LWR and P2A at doses of 50 and 100 μM for 24, 48

and 72 h. BPAF significantly increased LWR and P2A at a dose of 5 μM for 24 and 48 h, 2.5 and 5 μM for 72 h, and decreased LWR and P2A at a dose of 15 μM for 72 h. TBBPA treatment significantly increased P2A at a dose of 15 μM for 24 and 48 h, and decreased LWR and P2A at doses of 15 μM for 72 h. The differential nuclear area alterations in 50 and 100 μM BPA treatments might reflect 3D structure loss at 100 μM, while the differential nuclear morphological changes of BPAF treatments at 5 and 15 μM could be explained by an early adaptive response to low-dose treatment and loss of cellular homeostasis at high-dose treatment.

In Figure 3.3C-E, BPA and BPS treatments significantly reduced cell number at a dose of 100 μM for 24 h, and at doses of 50 and 100 μM for 48 and 72 h. BPAF treatment decreased cell numbers starting at 2.5 μM for 24, 48, and 72 h, while TBBPA reduced cell number starting at 10 μM for 24, 48, and 72 h. These data indicate that cell number counting in HCA is more sensitive than traditional NR uptake cytotoxicity assay.

To quantify the multinucleated cells in the co-cultures treated with various compounds, a supervised ML-based HCA of imaging data was applied. In Figure 3.3F, BPAF treatment significantly induced multinucleated cells at a dose of 5 μM for 24, 48, and 72 h, whereas BPA, BPS, and TBBPA treatments did not induce notable changes of multinucleated cells. In order to elucidate how the multinucleation related to other pathologic feature, a supervised ML was applied to classify the HCA imaging dataset into multinucleated cells and non- multinucleated cells. Utilizing Spearman correlation analysis, the association of multinucleation with DNA damage responses and F-actin was examined. As shown in Figure 3G, there is a higher positive correlation between total F-actin and γ-H2AX intensity in the multinucleated cells, as compared to those in non-multinucleated cells with BPAF treatment at a dose of 5 μM for 24, 48, and 72 h.

Thus, the data suggest that cytoskeleton perturbation might co-occur with DNA damage in the multinucleated cells.

3.4.3 BPA and its analog perturbed DNA synthesis and induced M phase arrest in the testicular cell co-culture model.

Cell cycle progression is essential for germ cell renewal and progeny cell production (De Rooij and Russell, 2000). We previously developed an HCA assay to measure DNA synthesis and cell cycle progression (Liang, *et al.*, 2017). Figure 3.4A shows representative images of BrdU incorporation. Notable decreases in BrdU positive cells were observed after 24 h treatments with BPA, BPS, BPAF and TBBPA treatments after 24 h treatment. After BPAF treatment, multinucleated cells exhibited BrdU positive staining at a dose of 5 μM (arrow). Significant decreases in BrdU positive cells were observed in the co-cultures treated with BPA at a dose of 100 μM for 24 and 48 h, BPS at a dose of 100 μM for 24 h, BPAF at doses of 5, 10, and 15 μM for 24 h, 10 and 15 μM for 48, and 15 μM for 72 h, and TBBPA at doses of 10 and 15 μM at 24 h, and 15 μM for 48 and 72 h, which suggested inhibition of DNA synthesis due to the chemical treatments. BPAF treatment induced BrdU positive cells at a dose of 10 μM for 72 h (Figure 3.4B). Interestingly, BPAF treatment at a dose of 10 μM inhibited DNA synthesis in the early periods but promoted it at longer exposure periods, suggesting the potential of BPAF-induced abnormal DNA synthesis after longer exposure times.

In addition, BPA and its analogs perturbed cell cycle progression in the co-cultures in a dose-and time-dependent manner (Supplementary Figure S3.1). To identify the effects of BPA and its analogs on mitosis progression, a supervised ML approach was conducted, and various phenotypic features of M phase were extracted. Various mitotic phenotypes, including the nucleus in pro-metaphase (pro meta), metaphase (meta), anaphase (ana), telophase (telo) and

late-telophase (late-telo) were observed in the co-cultures (Figure 3.4C). Significant inductions of cells in M phase were observed in the co-cultures treated with BPA and BPS at a dose of 100 μM for 48 and 72 h, BPAF at a dose of 10 μM for 24 h, and at doses of 10 and 15 μM for 48 and 72 h, and TBBPA at a dose of 15 μM for 24, 4,8 and 72 h. These results suggested that BPA and its analogs induced M phase arrest in the co-cultures.

3.4.4 BPA and its analogs perturbed the F-actin cytoskeleton and induced phenotypic 3D structure changes, and DNA damage responses in the testicular cell co-culture model.

F-actin structures are involved in various cellular processes including germ cell nuclei remodeling, cytoplasm reduction, and cell movement during spermatogenesis (Niedenberger *et al.*, 2013). In Sertoli cells, parallel actin bundles form ectoplasmic specialization (ES) to provide an immunological barrier for germ cells and regulate elongated spermatids orientation and spermatozoa release (Cheng and Mruk, 2002; Setchell, 2008; Wong *et al.*, 2008). As shown in Figure 3.5A, F-actin filaments in the untreated co-cultures exhibited two typical patterns, including cortical actin filaments adjacent to the cell edge and thick stress fiber bundles through the cytosol. The cells with stretching F-actin bundles in the cytoplasm further formed unique cord-like structures in the co-cultures. BPA, BPAF, and TBBPA treatments dramatically perturbed these structures and induced gel-like networks of cross-branched actin filaments, whereas BPS treatment did not induce notable changes. Figure 3.5B shows the quantification of log-transformed total intensity of F-actin. Significant increases in total intensity of F-actin were observed in the co-cultures treated with 50 and 100 μM BPA for 24 and 48 h, 100 μM BPA for 72 h, 100 μM BPS for 24 and 48 h, 5, 10 and 15 μM BPAF for 24, 48 and 72 h, and 10 and 15 μM TBBPA for 24 and 48 h, and 5 to 15 μM TBBPA for 72 h.

In order to quantify phenotypic 3D structure in the co-cultures and its response to chemical perturbation, the cells with stretching F-actin bundles across the cytosol were quantified based on a supervised ML approach. Figure 3.5C shows time-dependent increases of cellular phenotypic 3D structure in the controls for 24, 48, and 72 h, indicating the formation of 3D structure in the co-cultures. As shown in Figure 3.5D, significance decreases in this phenotype were observed in the co-cultures treated with BPA at a dose of 100 μM for 24 h, 50 and 100 μM for 48 and 72 h, BPS at a dose of 100 μM for 72 h, BPAF at doses of 2.5, 5, 10 and 15 μM for 24 and 48 h, 5, 10 and 15 μM for 72 h, and TBBPA at doses of 10 and 15 μM for 24, 48, and 72 h.

γ-H2AX, a marker for early DNA damage responses, was measured in HCA experiment to assess genotoxicity of BPA and its analogs in the co-cultures. As shown in Figure 3.5E, the percentages of γ-H2AX positive cells were significantly induced by BPAF treatment at doses of 10 and 15 μM for 24 h, and 5 to 15 μM for 48 and 72 h, and TBBPA treatment at a dose of 15 μM for 24, 48, and 72 h. BPA and BPS treatments did not show observable changes of γ-H2AX positive cells.

3.5 Discussion

Although current HCA has emerged as a powerful tool to provide multiparametric data for toxicity profiling, exploration of data content still lags behind. Conventional analysis of high-content data focuses on one or two image-related features and generates population-averaged readouts that simply reflect alterations of feature distribution in each replicate sample (Singh *et al.*, 2014b). In addition, the aggregation of single cell-level data usually masks phenotypic heterogeneity within cells, especially when a phenotypic change only occurs in a small specific subpopulation (Altschuler and Wu, 2010). Although certain phenotypes could be identified by a

single parameter threshold, many unusual phenotypes require the assessment of multiple parameters of cells (Jones *et al.*, 2009). Therefore, it is essential to employ an advanced computational approach to integrate multi-dimensional HCA data on a single-cell level to precisely quantify complex phenotypes of interest. ML that selects and integrates multiple features for automatic phenotypic classification has been used to unbiasedly score various phenotypes in millions of cells (Bakal *et al.*, 2007; Loo*, et al.*, 2007; Neumann *et al.*, 2006). Object pixel intensity, texture features, and morphology are incorporated and analyzed in ML to determine the complex pattern of phenotypes of interest and differentiate them from others. This reduces the work-load of manual adaption of parameter sets and increases objectivity, consistency, and accuracy in phenotype annotation in large data sets by using a few training samples (Sommer and Gerlich, 2013; Tarca *et al.*, 2007). In recent years, ML has been combined with HCA to generate phenotypic profiling in multiple cell lines to evaluate physiological responses to genetic or chemical stimuli (Conrad and Gerlich, 2010; Fuchs *et al.*, 2010; Leonard *et al.*, 2015; Mata *et al.*, 2016; Schmitz *et al.*, 2010). In this study, a supervised ML-based HCA pipeline was developed to characterize phenotypic changes in the testicular cell co-cultures and applied to evaluate the testicular toxicities of BPA and its analogs.

Sertoli and Leydig cells play critical roles in maintaining spermatogenesis and reproductive functions by providing physiological and nutritional support for germ cell mitosis, meiosis, and movement. These two cell types have been employed in various co-culture systems to improve the physical relevance of *in vitro* models and examine reproductive toxicities of various chemicals. Recently, we combined the C18-4 spermatogonial cell line with the TM3 Leydig cell line and the TM4 Sertoli cell line to construct an animal-free testicular cells co-culture model to mimic *in vivo* testicular structure (Yin*, et al.*, 2017). The Leydig cell line TM3

and Sertoli cell line TM4 were previously established from the testes of immature BALB/c mice and exhibited distinct morphology and growth response to hormones as primary Leydig and Sertoli cells, respectively (Mather, 1980). By incorporation of testicular somatic cells, this co-culture model showed distinct cord-like structures and high specificity and high sensitivity in the classification of reproductive toxicants (Yin, *et al.*, 2017).

Nuclear morphological features have been suggested as useful indicators in various adverse cellular events (Eidet *et al.*, 2014; Ikeguchi *et al.*, 1999). In HCA assays, quantitative assessment of multiple nuclear parameters has been demonstrated as a sensitive marker for detecting early cytotoxic effects. In the present study, quantification of nuclear morphology revealed that BPA treatment significantly altered the nuclear area at a non-lethal dose, which is consistent with previous *in vivo* studies that exposure to BPA induced abnormal nuclear morphology in rat mammary gland and mice testes (Ibrahim *et al.*, 2016; Takao *et al.*, 1999). In addition, significant changes in P2A and LWR in the cells treated with BPA and BPS could be detected at lower doses in the co-cultures, as compared with single cell culture. These data suggested that alteration of nuclear morphology in the co-cultures could be a sensitive endpoint in the detection of chemical toxicity.

In our previous study, threshold gating to the nuclear area and P2A was applied to quantify the subpopulation of multinucleated cells but the detection rate was low. In this study, an ML-based phenotypic classification was developed based on multiple subcellular features extracted from morphology, texture, and intensity. These results revealed a dose- and time-dependent induction of multinucleated cells in the co-cultures treated with BPAF was consistent with visual examinations. The induction of multinucleated gonocytes has been reported to be a reproductive toxicity marker in animal models and human exposed to environmental chemicals,

including DBP, BPA, andrographolide, and aflatoxin (Akbarsha and Murugaian, 2000; Barlow *et al.*, 2004; Faridha *et al.*, 2007; Gallegos-Avila *et al.*, 2010; Mylchreest *et al.*, 2002; Takao*, et al.*, 1999). Although the underlying mechanism of multinucleated cell formation is still unclear, Faridha et al. reported that generation of multinucleated spermatids occurred through the opening of the cytoplasmic bridge and merging among multiple cells (Faridha*, et al.*, 2007). In addition, p190RhoGAP, an actin stress fiber regulator, has been demonstrated to induce a multinucleated phenotype in overexpression condition (Su *et al.*, 2003). Furthermore, the perturbation of cytoskeleton texture co-occurred with the formation of multi-nucleated cells, which could be explained by the alteration of compressive forces driven by perinuclear actin networks (Chen *et al.*, 2015a). As compared to non-multinucleated cells in the same treatment condition, multinucleated cells exhibited a higher correlation between cytoskeleton perturbation and DNA damage responses on a single-cell level, showing the unique biological characteristics of these cells. It has been reported that DNA damage induced dramatic alterations in nuclear and cytoplasmic actin, and F-actin polymerization served as a negative modulator in DNA damage responses (Belin *et al.*, 2015; Chang *et al.*, 2015; Wang *et al.*, 2013; Zuchero *et al.*, 2012). In a future study, the underlying mechanism of BPAF-induced multinucleated cells in the spermatogonial cells and co-cultures should be examined.

M phase progression is one of the most important events for successful cell reproduction, in which replicated chromosomes are segregated into two daughter cells (Nurse, 1990). Identification and quantification of cell populations in M phase usually requires additional staining by using mitotic specific markers, such as anti-phosphorylated (ser10) H3 in HCA assays (Lyman *et al.*, 2011). In our previous study, we developed an HCA approach to generate a cell cycle profile with discrete SubG1, G0/1, S, and G2/M phases in a spermatogonial cell line

(Liang, *et al.*, 2017). However, it could not provide quantification of the cell population in M phase. Blasi et al. recently reported a label-free quantification of mitotic cell cycle phase by applying supervised ML to multi-dimensional features of single cells (Blasi *et al.*, 2016). An ML analysis pipeline in the co-cultures was established, which was able to precisely recognize and quantify the cells in M phase based on morphological, textural and intensity features extracted from multi-channel staining. It has shown M phase arrest in the co-cultures treated with BPA and its analogs in a dose- and time- dependent manner, which provide in-depth mechanistic views of chemical effects on cell cycle progression. In previous studies, exposure to BPA significantly perturbed spermiogenesis in animal models and inhibited cell proliferation in the Sertoli cell line TM4 and the Leydig cell line TM3 (Ali, *et al.*, 2014; Boudalia, *et al.*, 2014; Chen, *et al.*, 2016c; Liu, *et al.*, 2013). Current results showed that BPA, BPS, and TBBPA treatments induced M phase arrest with decreased DNA synthesis, which suggested an anti-proliferative effect of these compounds. In addition, BPAF treatment induced DNA synthesis and increased the cell population at S phase in the co-cultures at 72 h, suggesting that abnormal cell proliferation occurred.

Actin, as one of a major component of the cytoskeleton, has been shown to play essential roles in cell movement, cargo transportation, acrosome reactions and nuclear modification during spermatogenesis (Kierszenbaum and Tres, 2004; Sun, *et al.*, 2011). Alteration of F-actin intensity is a sensitive indicator for monitoring the adverse effects of BPA. However, quantification of F-actin total intensity cannot reflect spatial alterations of F-actin filament in the cytoplasm and complex 3D structures in the co-cultures. In the co-culture model, two types of F-actin fibers were observed, including dense cortex F-actin on the cell edge and stretching F-actin filaments across cytosol that assembled to form the 3D structure. The ML approach was applied

138

to recognize and quantify the cells with stretching F-actin bundles across the cytosol and demonstrated it significant decreases of this specific phenotype in the co-cultures treated with different chemicals. In the previous study, a combination of cell-type specific markers and HCA cytoskeleton analysis revealed Sertoli cells exhibited stretching F-actin bundles in the co-cultures (Yin, *et al.*, 2017). Within Sertoli cells, parallel actin bundle formed ectoplasmic specialization, which participates in spermatid head formation, cell movement, elongated spermatids orientation and spermatozoa release. Damage to Sertoli cells often resulted in germ cell degeneration and loss (Vidal and Whitney, 2014). Thus, the alteration of cells with stretching F-actin filaments suggested a potential loss of Sertoli cells and perturbation of 3D structure in the co-cultures. These observations are consistent with previous *in vivo* studies showing that BPA or its analogs altered seminiferous tubules morphology in animal models.

In HCA assays to assess chemical genotoxicity, γ-H2AX has recently emerged as a highly specific and sensitive cellular marker to monitor initiation of DNA damages (Ando, *et al.*, 2014; Fu, *et al.*, 2012; Garcia-Canton, *et al.*, 2013a). Studies have shown that exposure to BPA or BPS induced DNA damage responses in germ cells (Chen, *et al.*, 2016b; Liu, *et al.*, 2014a). In addition, the genotoxicity of BPA and its analogs have been detected in multiple cell lines and follow a cell-type-specific and chemical-specific manner. In the co-cultures, BPA and BPS treatment did not induce γ-H2AX expression. The possible explanations of inconsistency between the co-cultures and previous single cell type cultures could be due to differential biotransformation of BPA and its analogs, and DNA damage repair capacity among different cell models. In human breast cancer cells, BPA was able to induce γ-H2AX at a low dose of 10 nM, while in the HepG2 cell line, BPA did not induce γ-H2AX even at a dose of 100 μM, but bisphenol F did (Audebert, *et al.*, 2011; Pfeifer, *et al.*, 2015). For the other two compounds tested

in the co-cultures, BPAF treatment significantly induced DNA damage response starting at 5 µM and TBBPA induced a higher degree of DNA damage response at a dose of 15 µM, suggesting higher genotoxicity, as compared to BPA.

In the current study, a similar toxicity ranking of BPA and its analogs in the co-culture and spermatogonial cell culture was observed, in which BPAF exerted the highest toxicity, followed by TBBPA, BPA, and BPS. This *in vitro* finding was further supported by an *in vivo* study that BPAF exposure uniquely impaired pregnancies and sexual development in rats at doses of ~80 and ~280 mg/kg, whereas BPA exposure did not alter these reproductive endpoints at similar levels (Sutherland*., et al.*, 2017). Given the similarity of these two chemicals' *in vitro* ER and AR activities, *in vivo* disposition and excretion, their differential reproductive toxicity both *in vitro* and *in vivo* potentially suggest that BPAF might partially exert its adverse effects on the reproductive system in an estrogen-independent manner. Also, recent data demonstrated that TBBPA did not interact with ER α/β or AR in a panel of *in vitro* bioassays, but it showed higher toxicity in both testicular cell models, as compared with BPA (Molina-Molina*, et al.*, 2013). Future studies will be critical to validate current findings and elucidate the mechanism of action.

This ML-based HCA in a testicular cell co-culture model still has several limitations. First, although current supervised ML can recognize rare phenotypes of interest, it still requires user-defined examples. Un-supervised ML should be applied in a future study to fully explore morphological deviation that has not been discovered by researchers. Second, the metabolic capacity of the current co-culture model is still unclear. The absence of metabolic capability usually is one of the barriers for the utilization of *in vitro* models. Previous studies have shown that glucuronidation was a major metabolic pathway for BPA and its analogs and it reduced the endocrine activities of the conjugated chemicals (Skledar and Masic, 2016). While it has been

reported that one of the metabolites of BPA, 4-Methyl-2,4-bis(4-hydroxyphenyl)pent-1-ene (MBP) exerted higher estrogenic activity *in vitro* and *in vivo*, as compared to BPA (Baker and Chandsawangbhuwana, 2012; Okuda *et al.*, 2010). Thus, it is critical to characterize the metabolic capabilities and kinetics of BPA and its analogs in co-cultures. Third, although the current HCA assays include multiple markers linked to a functional disorder in testicular cells, biological markers for testicular functions, including steroidogenic activity and hormone receptor expression level, should be incorporated in any future HCA assays.

In summary, an ML-based HCA approach in a testicular cell co-culture model was developed to classify multiple cellular phenotypes and to characterize the testicular toxicity of BPA and its analogs. The advanced ML approach demonstrated phenotypic changes of complex 3D structures and mitotic progression in response to chemical exposure and revealed unique BPAF-induced multinucleated cells in the co-cultures. Utilizing ML, the added value of HCA to classify multiple cellular phenotypes and characterize compound specific testicular toxicities of BPA and its analogs were explored. By integrating machine-learning based approaches with established HCA algorithms, it should be possible to uncover multi-dimensional data and quantify phenotypic changes in a large-scale environmental chemical exposure.
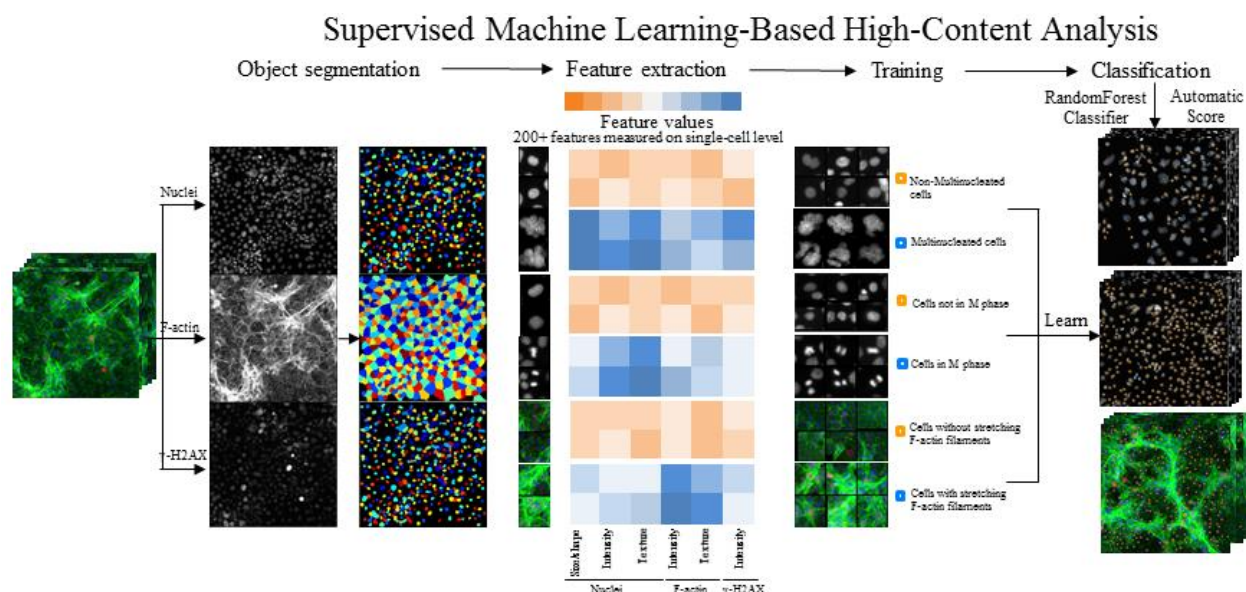
Figure 3.1. ML-based high-content and phenotypic analysis in the co-culture.

The diagram illustrates the four steps in the ML process. First, object identification and segmentation were conducted in multi-channel (nuclei, cytoskeleton, and γ-H2AX) image using CellProfiler. Second, over 200 quantitative features were extracted, including size, shape, intensity, the texture of the nuclei, intensity, and texture of F-actin, and intensity of γ-H2AX in a single cell. The orange-blue gradient represents various features values (one per column) for a single cell. Then, a small training sample was developed by users with the manual classification of a certain phenotype in CellProfiler Analyst. Then, ML algorithm was trained to discriminate different phenotypes based on multiple features of the classified cells. Last, ML infer classification rules to score all cells in the experiment and calculate cell number in each class.
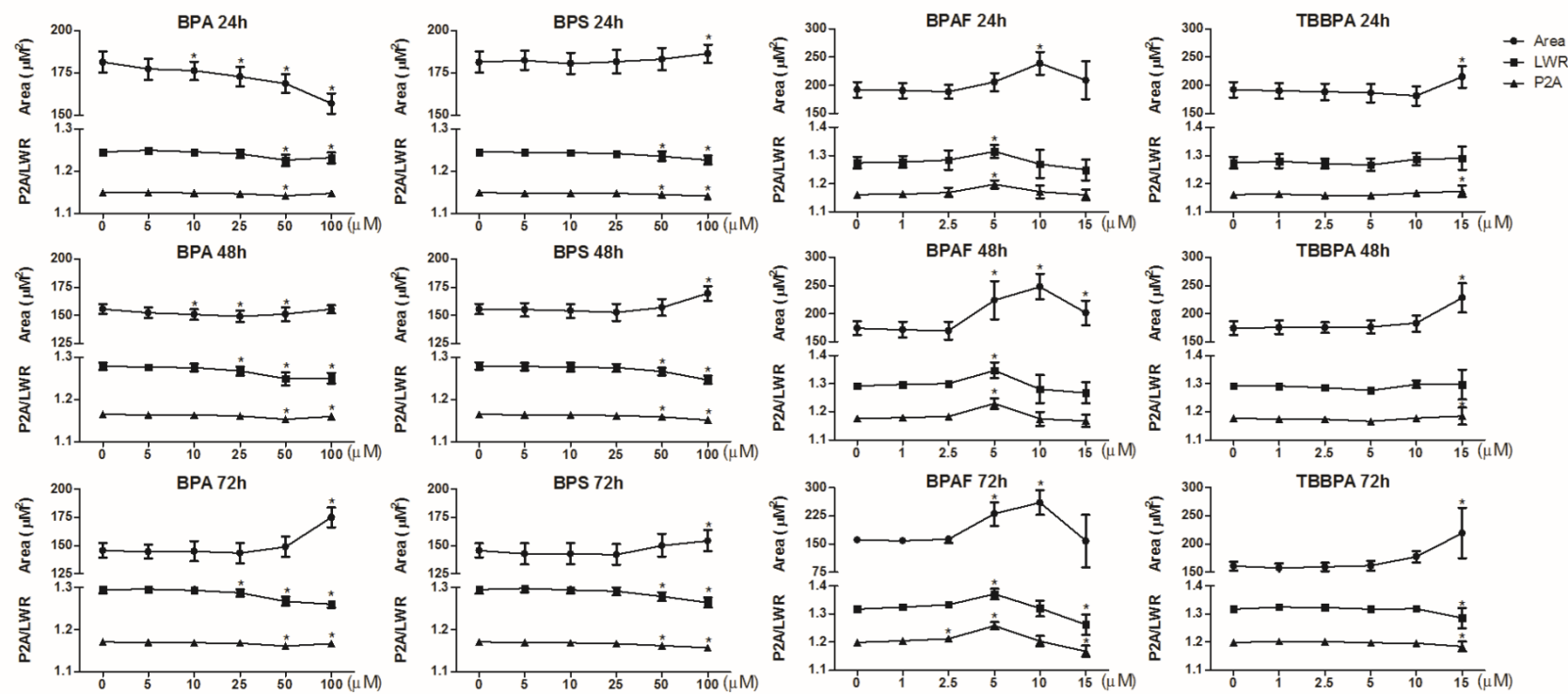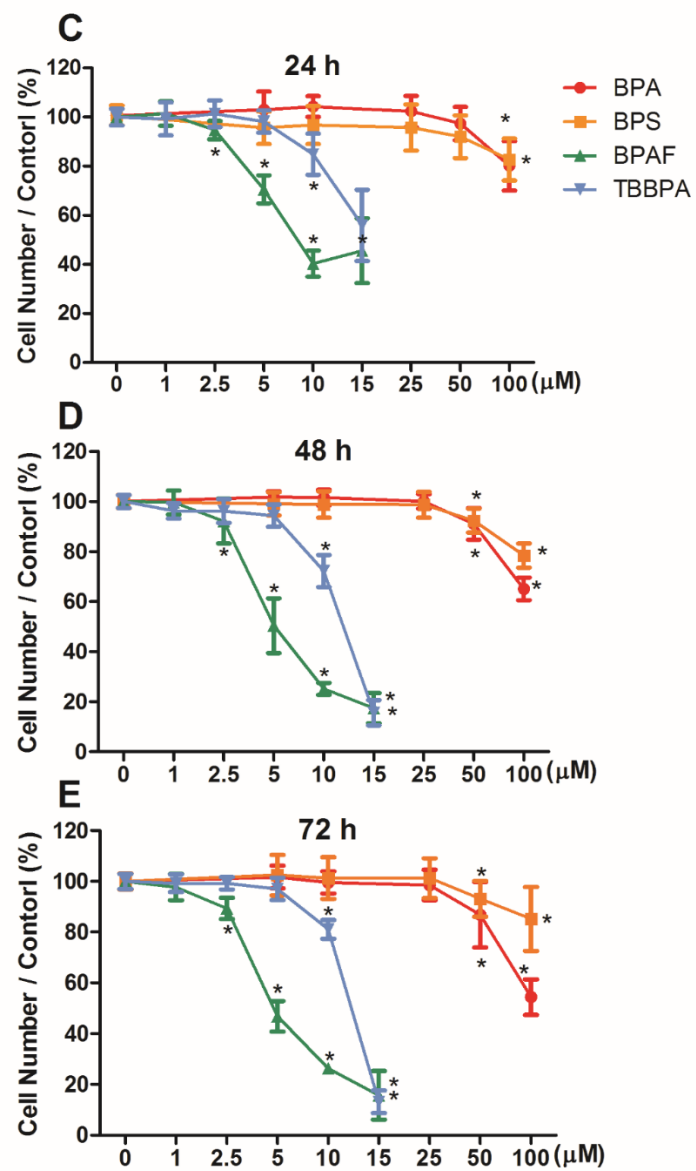
142
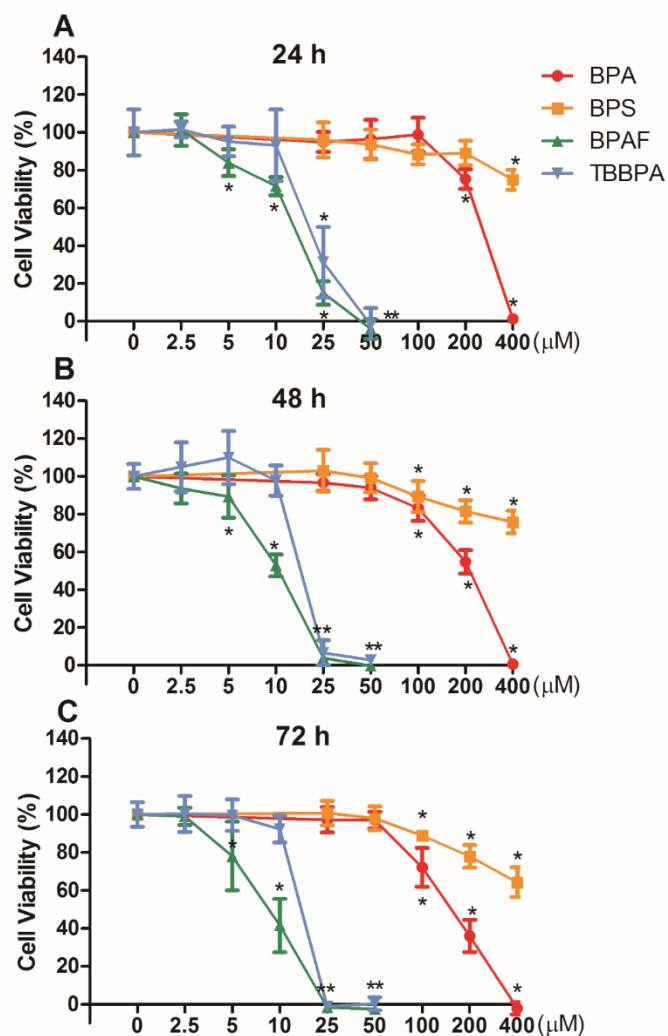
Figure 3.2. Cell viability was determined by NR uptake assay in the co-cultures treated with BPA, BPS, BPAF, and TBBPA. Co-cultures were treated with various concentrations of BPA and BPS (25, 50, 100, 200 and 400 μM), and BPAF and TBBPA (2.5, 5, 10, 25 and 50 μM) for 24 (A), 48 (B), and 72 h (C). Cells treated with vehicle (0.05% DMSO) were used as vehicle controls (0 μM). Data are expressed as mean ± SD, n=8. Four replicates in two independent experiments were included. Statistical analysis was conducted by 1-way ANOVA followed by Tukey-Kramer multiple comparison (*P<0.05)
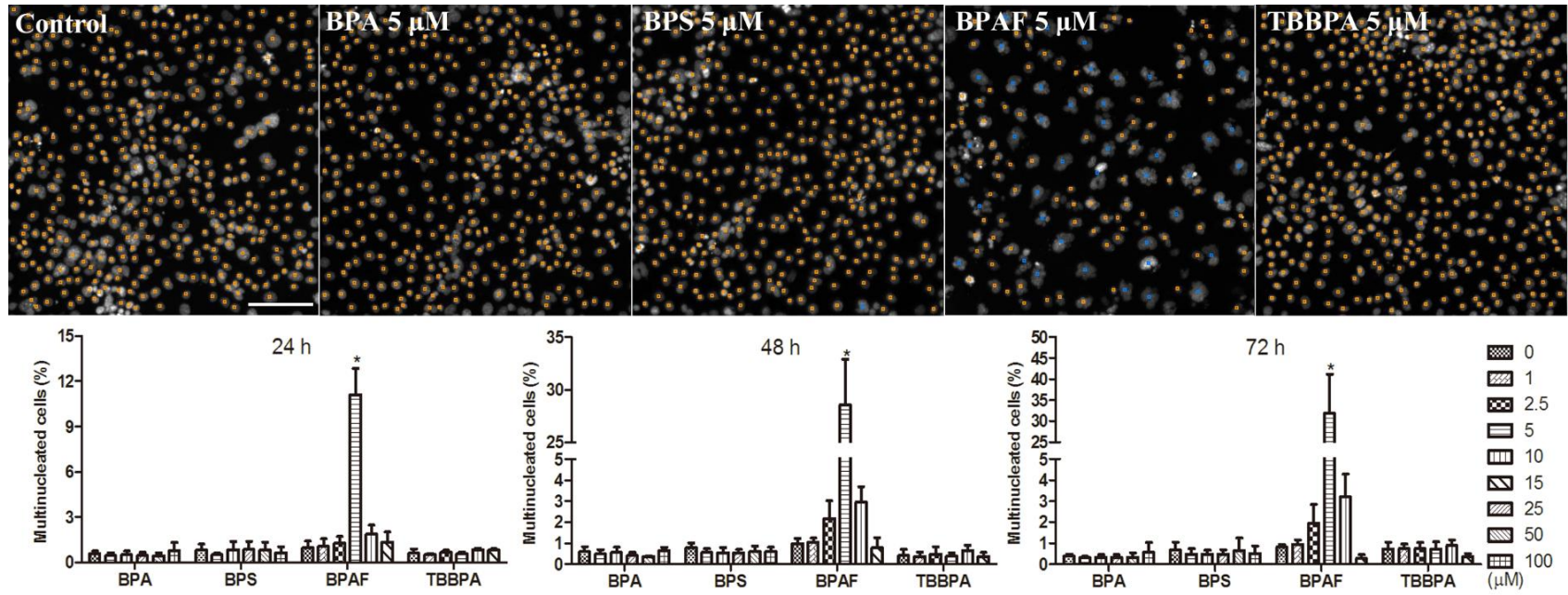
A

B

C

24 h

Cell Number / Contorl (%)

BPA
BPS
BPAF
TBBPA

D

48 h

Cell Number / Contorl (%)

E

72 h

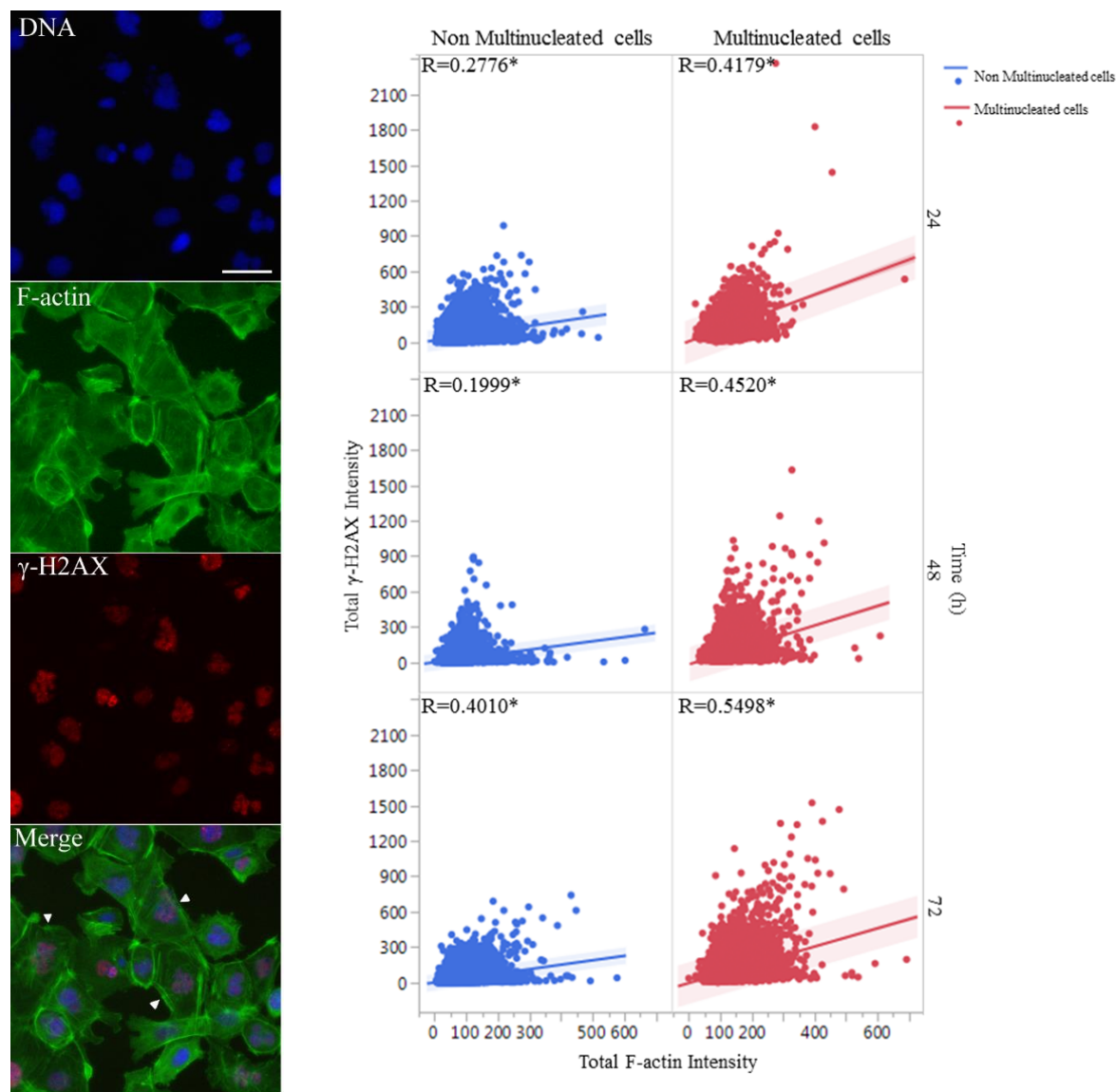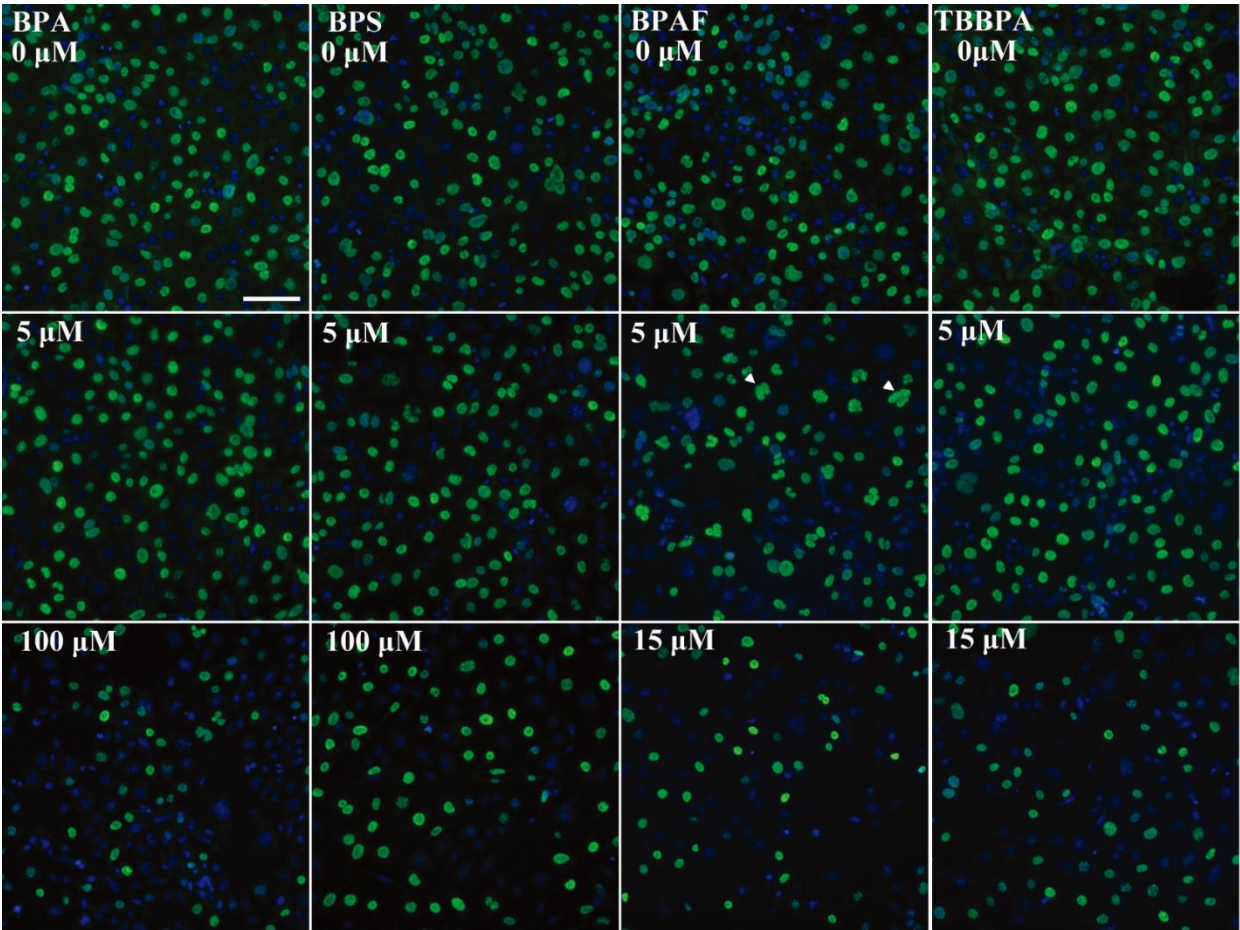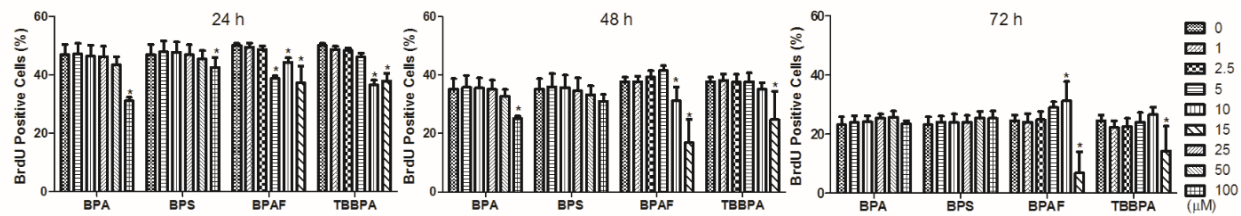Cell Number / Contorl (%)
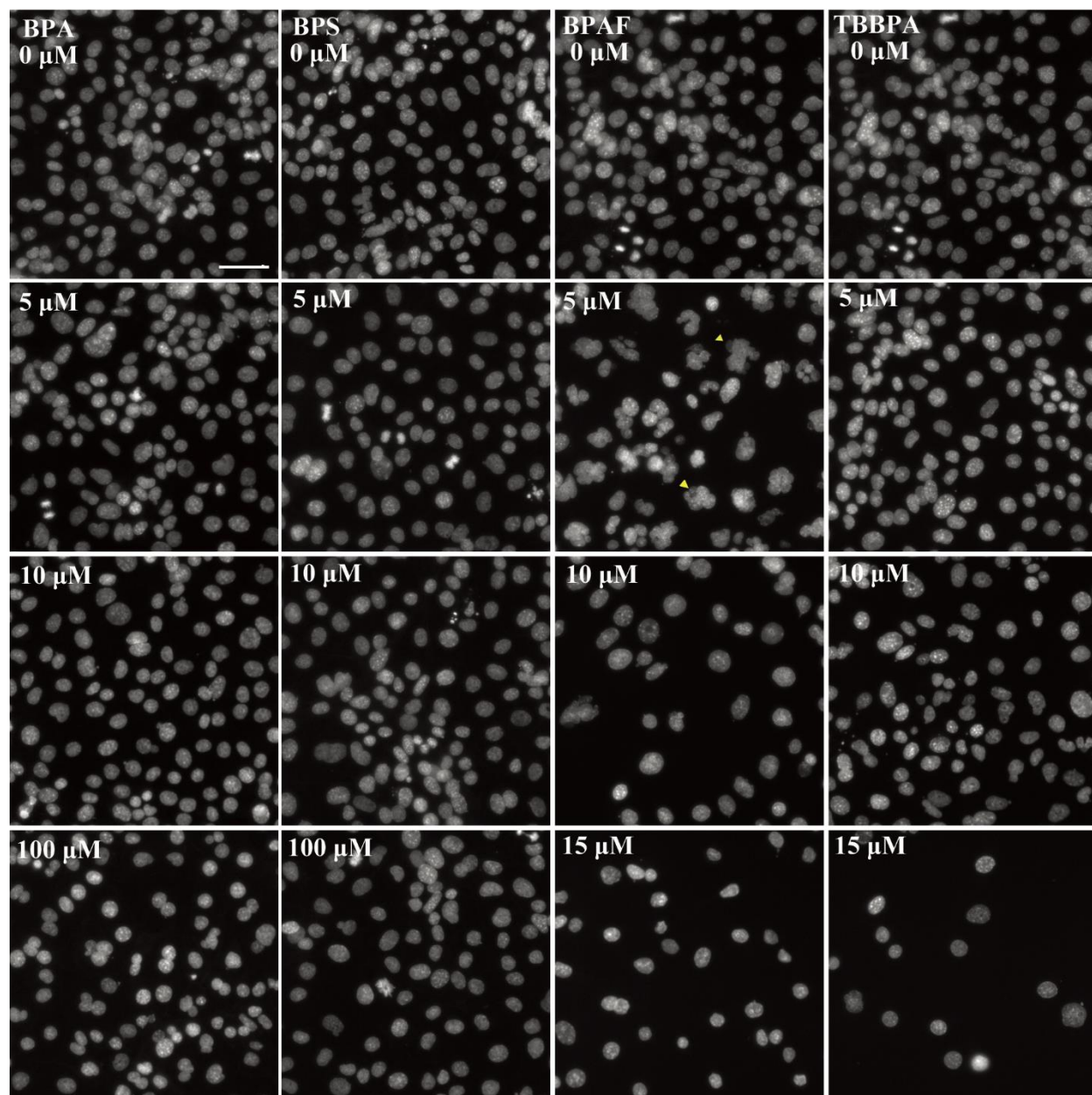
F

G

Figure 3.3. Characteristic changes of nuclear morphology and cell number in the co-cultures. Co-cultures were treated with various concentrations of BPA and BPS (5, 10, 25, 50 and 100 μM), and BPAF and TBBPA (1, 2.5, 5, 10, and 15 μM) for 24, 48, and 72 h. Cells treated with vehicle (0.05% DMSO) were used as vehicle controls (0 μM). The nuclei were stained with Hoechst 33342, and images were automatically acquired with 20X and 40X objectives, and 49 fields per

well. A shows the representative images (40X) of controls and cells treated with BPA and BPS (5, 10 and 100 µM), BPAF and TBBPA (5, 10 and 15 µM) for 48 h. Arrows indicated the multinucleated cells. Scale bar = 50 µm. B shows the quantification of the absolute nuclear area (µm²), LWR for nuclear roundness, and P2A for nuclear smoothness. C-E shows the quantification of cell number in each condition. F shows the representative images (20X) of multinucleated cell classification in control and the cells treated with BPA, BPS, BPAF and TBBPA (5 µM) for 48 h, and quantification of multinucleated cell number using ML-based HCA. Using CellProfiler Analyst, multinucleated cells are automatically recognized and labeled with blue color. Non-multinucleated cells are labeled with orange color. Scale bar = 100 µm. Data are presented as mean ± SD, n=16. Four replicates in 4 independent experiments were included. Statistical analysis was conducted by 1-way ANOVA followed by Tukey-Kramer multiple comparison (*P<0.05). G shows Spearman correlation analysis of total F-actin intensity and total γ-H2AX intensity between non-multinucleated and multinucleated cells at a single cell level. (*P<0.05). Shaded area indicates 95% confident area. Arrows indicated the multinucleated cells with positive γ-H2AX foci staining in the nuclear and aberrant cytoskeleton distribution in the cytoplasm. Scale bar = 50 µm.
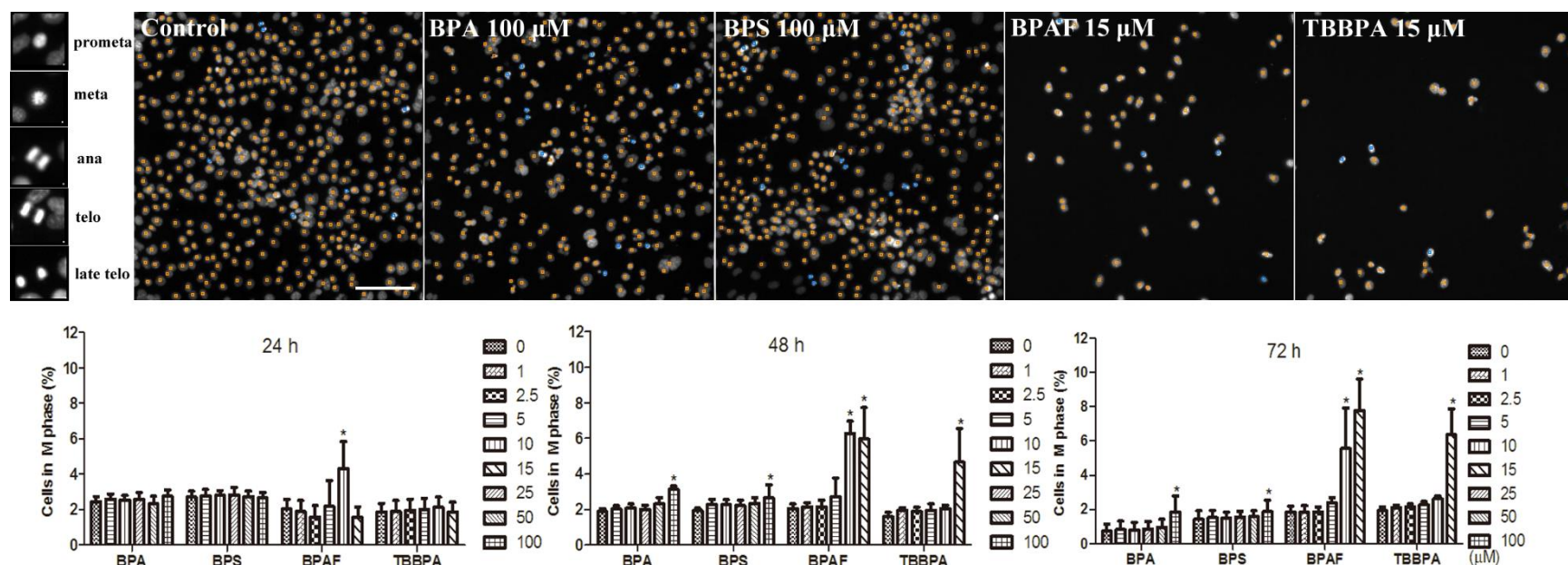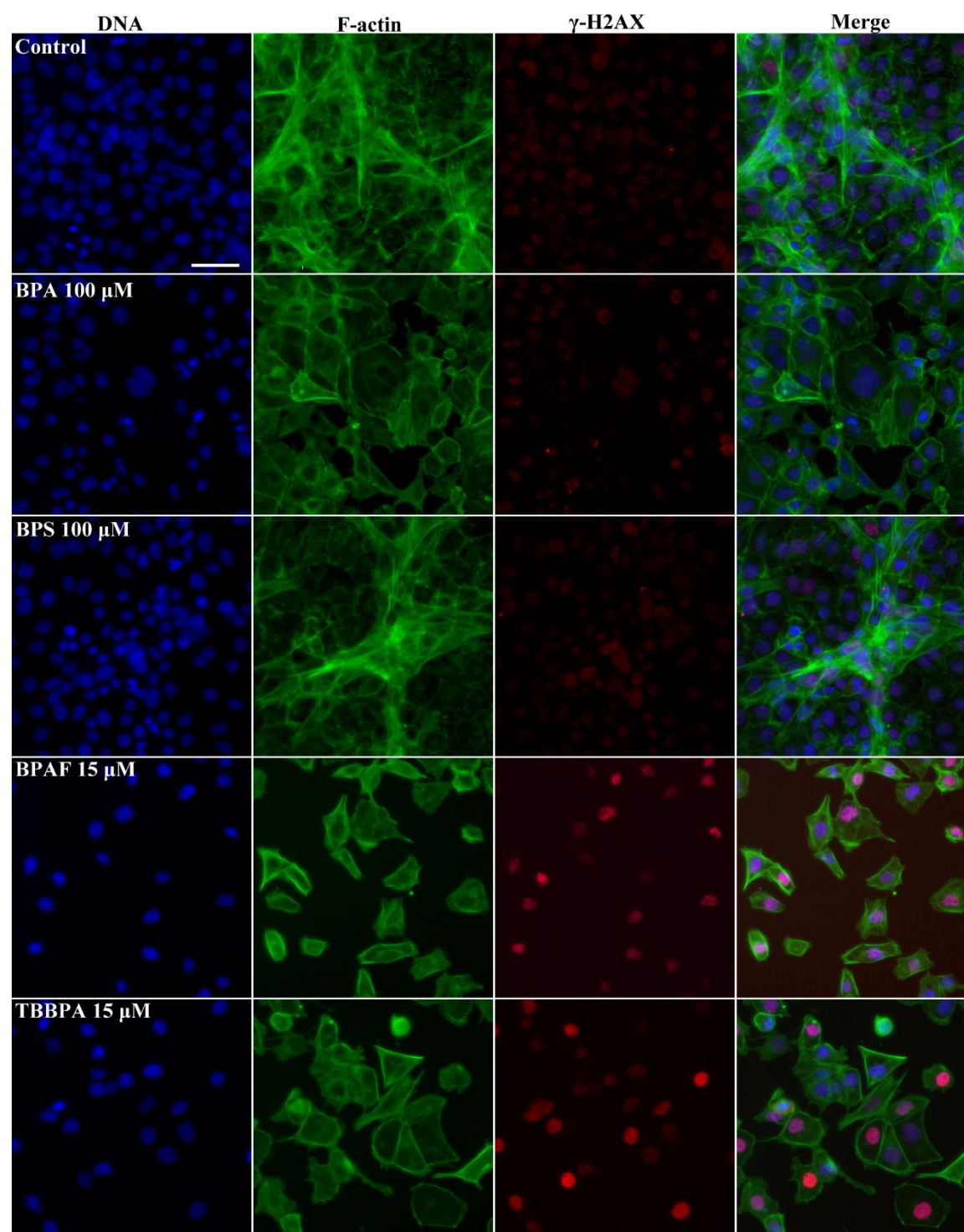
A

B

C

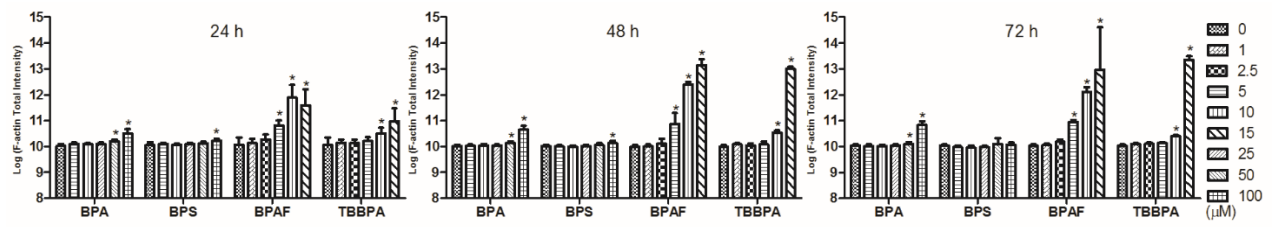Figure 3.4. Characteristic changes of DNA synthesis and cell population in mitosis phase in the co-culture.

Co-cultures were treated with various concentrations of BPA and BPS (5, 10, 25, 50 and 100 μM), and BPAF and TBBPA (1, 2.5, 5, 10, and 15 μM) for 24, 48, and 72 h. Cells treated with vehicle (0.05% DMSO) were used as vehicle controls (0 μM). The nuclei were stained with Hoechst 33342 (blue). Cells were incubated with BrdU (40 μM) for 3 h prior to cell fixation, and then stained with mouse anti-BrdU antibody and anti-mouse DyLight 488 for detection of BrdU incorporation (green). A shows the representative images (20X) of controls and the cells treated with BPA and BPS (100 μM), BPAF (5 and 15 μM) and TBBPA (15 μM) for 24 h. Arrows indicated the multinucleated cells with active DNA synthesis. Scale bar = 100 μm. B shows the quantification of BrdU-positive cells.

C shows the representative images (20X) of ML-based mitotic cell classification in control and cells treated with BPA and BPS (100 μM), and BPAF and TBBPA (15 μM) for 48 h, the image of nuclei in prometaphase, metaphase, anaphase and late-anaphase and the quantification of cells in M phase. Using CellProfiler Analyst, cells in M phase are automatically recognized and labeled with blue color. Cells not in M phase are labeled with orange color. Scale bar = 100 μm. Data are presented as mean ± SD, n=8. Four replicates in two independent experiments were included. Statistical analysis was conducted by 1-way ANOVA followed by Tukey-Kramer multiple comparison (*P<0.05).
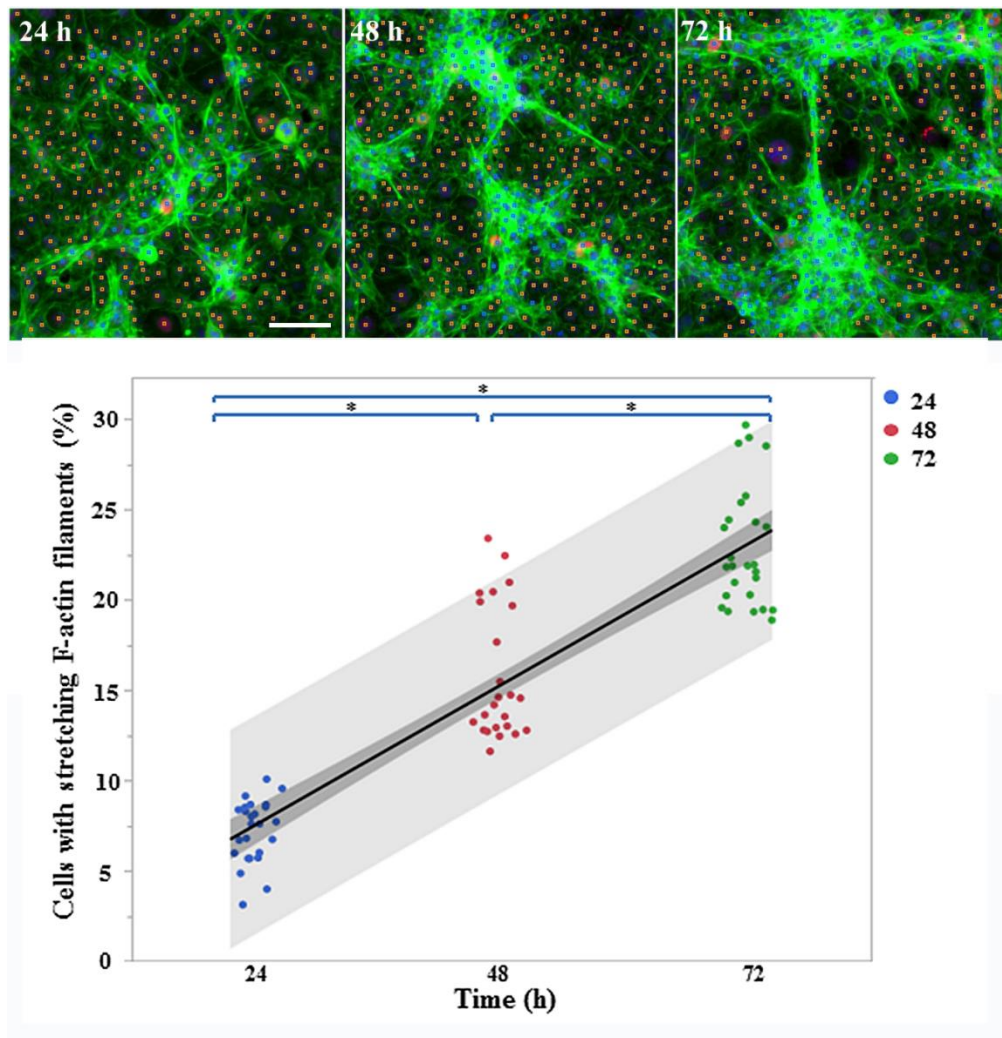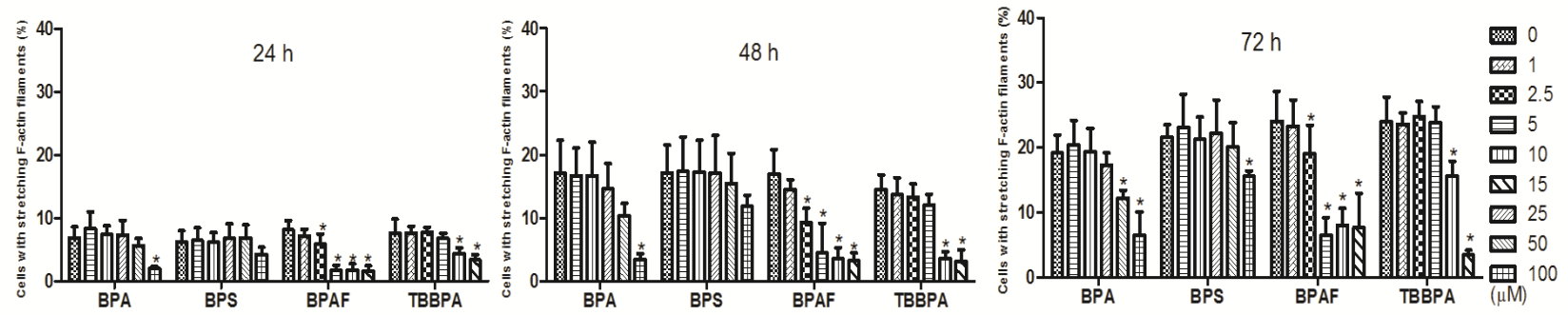
A

DNA	F-actin	γ-H2AX	Merge

Control

BPA 100 μM

BPS 100 μM

BPAF 15 μM

TBBPA 15 μM

B

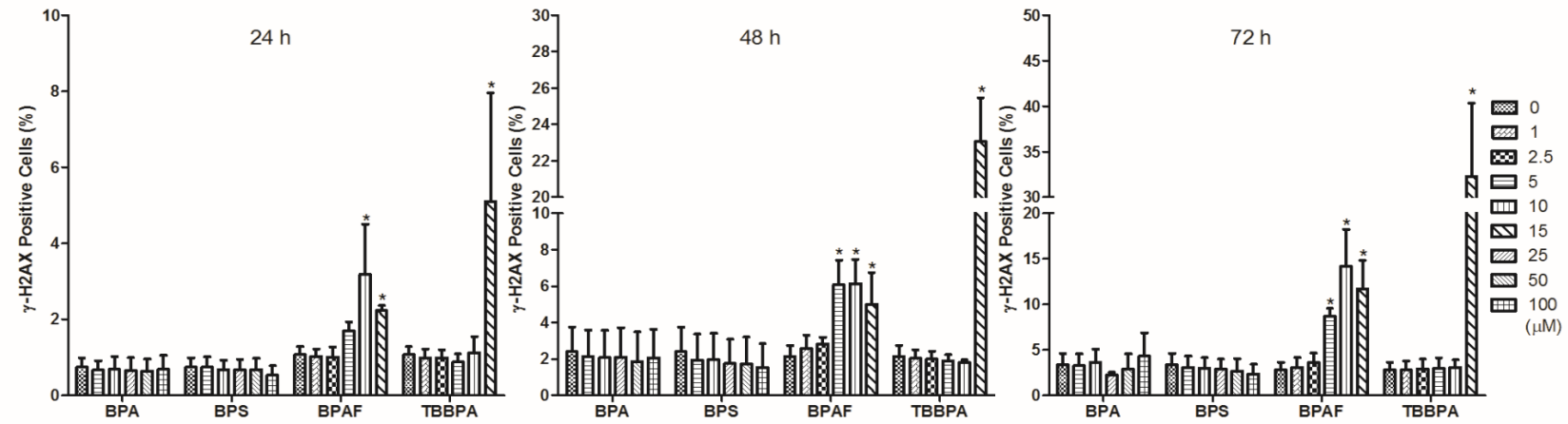

C

154

D

E

155

Figure 3.5. Characteristic changes of cytoskeleton and DNA damage responses in the co-culture. Co-cultures were treated with various concentrations of BPA and BPS (5, 10, 25, 50 and 100 μM), and BPAF and TBBPA (1, 2.5, 5, 10, and 15 μM) for 24, 48, and 72 h. Cells treated with vehicle (0.05% DMSO) were used as vehicle controls (0 μM). The nuclei were stained with Hoechst 33342 (blue), F-actin with Phalloidin staining (green), and γ-H2AX with a combination of primary anti-γ−H2AX and secondary Dylight 650 conjugated antibody (red). A shows the representative image (40X) of co-cultures treated with BPA and BPS (100 μM), BPAF (5 and 15 μM) and TBBPA (15 μM) for 48 h. Scale bar = 50 μm. B demonstrates the quantification of log-transformed F-actin total intensity. C shows the representative images (20X) of ML-based classification of cells with stretching F-actin filaments in vehicle controls for 24, 48 and 72 h, and quantification of cells with stretching F-actin filaments in vehicle controls for 24, 48 and 72 h. Using CellProfiler Analyst, cells with stretching F-actin filaments are automatically recognized and labeled with blue color. Cells without stretching F-actin filaments are labeled with orange color. Scale bar = 100 μm. Linear regression fit across multiple doses was performed. Shaded area indicates 95% confident area. D shows quantification of cells with stretching F-actin filaments in co-cultures. E shows the quantification of positive γ-H2AX cells. Data are presented as mean ± SD, n=8. Four replicates in two independent experiments were included. Statistical analysis was conducted by 1-way ANOVA followed by Tukey-Kramer multiple comparison (*P<0.05).

CHAPTER 4

COMPARATIVE HIGH-CONTENT ANALYSIS ON TOXICITY PROFILING OF BPA AND

ITS ANALOGS BISPHENOL S, BISPHENOL AF, AND TETRABROMOBISPHENOL A IN

MOUSE SPERMATOGONIAL CELLS, LEYDIG CELLS, AND SERTOLI CELLS

Liang, S., Yin, L., Yu, X. To be submitted to *Toxicological Sciences*.

4.1 Abstract

Spermatogenesis is supported by SCCs and multiple somatic cell populations in the testis. BPA, an EDC, was found to be a testicular toxicant in animal models. Some of its structural analogs have been introduced to the market but were shown to have similar or higher estrogen potency, as compared with BPA. EDCs are able to interact with ERs and ARs that are expressed on Leydig and Sertoli cells, which makes these two cell types potential targets of EDCs' testicular toxicities. To determine cell-specific toxicities of BPA and its analogs, HCA assays were utilized to measure multiple adverse endpoints that are related to testicular cell dysfunction, including cell number, nuclear morphology, DNA synthesis, cell cycle progression, DNA damage, cytoskeleton, DNA methylation and autophagy to generate chemical toxicity profile of these chemicals in spermatogonial cells, Sertoli cells and Leydig cells. The non-supervised hierarchical cluster analysis on multiparametric HCA features revealed differential toxicity profiles of BPA and its analogs in three types of testicular cells. BPA and BPS exerted higher toxicities in Sertoli and Leydig cells, as compared with spermatogonial cells. BPAF showed a distinct toxicity profile among three cell types at different doses. Leydig cells showed high resistance to TBBPA toxicity. In summary, our current comparative HCA-based toxicity profiling revealed the cell-type specific toxicities of BPA and its analogs in different testicular cells. It also provides mechanistic insight into the *in vivo* testicular toxicity of BPA and its analogs.

4.2 Introduction

There are increasing public concerns regarding the adverse reproductive effects of environmental chemical exposure (Jenardhanana *et al.*, 2016; Leung*, et al.*, 2016). Recent studies have noted the declining trend of human semen quality in certain areas and have revealed that

exposure to environmental contaminants is one of the major causes of male reproductive dysfunction (Jeng, 2014; Knez, 2013; Nordkap *et al.*, 2012; Skakkebaek *et al.*, 2016). Spermatogenesis refers to the complex developmental process from SSCs to mature sperms. The foundation of this process relies on the spermatogonial cells, which undergo self-renewal to maintain a germ cell population or differentiation to form gametes (Oatley and Brinster, 2008). In addition, the Sertoli cells present in seminiferous tubules and interstitial Leydig cells, along with peritubular myoid cells and blood vessels play essential roles in maintaining a microenvironmental niche to support spermatogenesis (Jan *et al.*, 2012; Oatley and Brinster, 2012). Sertoli cells provide the physical, nutritional and immunological supports for germ cell differentiation and movement (Hai *et al.*, 2014). Leydig cells secrete T under the control of LH to support meiosis and spermiogenesis (Ruwanpura *et al.*, 2010). Due to the complex cell-cell interactions, chemical-induced damage of Sertoli cells or Leydig cells has been reported to result in germ cell degeneration and loss (Vidal and Whitney, 2014).

To determine the target cell population and elucidate the underlying mechanism for chemical reproductive toxicity, establishment of *in vitro* testicular models in which spermatogonial cells, Sertoli cells, Leydig cells or testicular cell co-cultures can be maintained and proliferate is in high demand. To date, immortalized mouse germ,Sertoli and Leydig cell lines have been developed and used as *in vitro* testicular cell models to examine their cell-cell interaction and the effects of toxins on testis development (Braydich-Stolle*, et al.*, 2010; Chapin *et al.*, 1988; Chen *et al.*, 2013; Hofmann*, et al.*, 2005a; Hu *et al.*, 2013; Mather, 1980). In addition, co-culture models that retain several testicular cell populations have been developed to mimic *in vivo* testicular responses and to examine the mechanisms of chemical–induced germ cells loss (Gray, 1986; Gregotti *et al.*, 1992; Harris*, et al.*, 2015; Harris*, et al.*, 2016a; Harris*, et*

al., 2016b; Williams and Foster, 1987; Yu *et al.*, 2005a; Yu, *et al.*, 2009; Yu *et al.*, 2008).

Further, with advances in image acquisition and analysis, HCA has emerged as a powerful tool in toxicology. It provides unbiased multi-dimensional data at the single cell level, which enables temporal and spatial measurements of the complex cellular network in response to chemical stimuli (Mattiazzi Usaj, *et al.*, 2016; Persson *et al.*, 2014; Singh, *et al.*, 2014a). The EPA initiated the ToxCast program using *in vitro* HCS and HCA assays to predict chemical reproductive toxicity *in vivo* (Leung, *et al.*, 2016; Martin, *et al.*, 2011; Reif, *et al.*, 2010). This approach was also applied to generate multi-parametric toxicity profiles and discriminate cell-type specific toxicities of hundreds of chemicals (Kremb and Voolstra, 2017; Malik *et al.*, 2014).

BPA is an HPV chemical and is commonly used in various consumer products (Rochester, 2013). The main routes of BPA exposure include ingestion, inhalation, and dermal contact (Kang, *et al.*, 2006; Vandenberg, *et al.*, 2007). Detectable levels of BPA have been found in over 90% of the United States population (Calafat, *et al.*, 2008; Lakind and Naiman, 2011). As an endocrine disruptor, BPA acts through various physiological receptors and exerts reproductive toxicities in animal models (Peretz, *et al.*, 2014; Richter, *et al.*, 2007; Rochester, 2013; vom Saal, *et al.*, 2007). Due to the concern about its widespread exposure and potential reproductive hazards in humans, the uses of BPA in consumer products are gradually abandoned (EU., 2016; FDA., 2013; FDA., 2012). Its structural analogs have been introduced into the market as alternatives to BPA or sharing similar applications in manufacturing. With the high degree of structural similarity, BPA analogs may pose similar adverse reproductive effects. Limited data have demonstrated that exposure to BPA analogs affect reproductive functions, including decreased sperm quality, perturbed steroidogenesis, and testicular morphology in animal models (Chen, *et al.*, 2016b; Cope, *et al.*, 2015; Eladak, *et al.*, 2015; Li, *et al.*, 2016a; Yang, *et al.*,

160

2016). In previous study, we utilized HCA assays and observed that BPA and its analogs differentially perturbed DNA synthesis and cell cycle progression, induced DNA damage response and aberrant cytoskeleton (Liang, *et al.*, 2017). An ML–powered HCA pipeline was developed to examine phenotypic changes in a testicular cell co-culture model treated with BPA and its analogs, which revealed that chemical treatment resulted in the loss of phenotypic 3D structure and M phase arrest, and BPAF treatment uniquely induced multinucleated cells. However, without cell-specific markers, the kinetic changes in populations of specific testicular cell type remains unclear. It has been reported that BPS and BPAF exerted similar or higher estrogen potency, as compared to BPA (Mesnage *et al.*, 2017; Rochester and Bolden, 2015). As endocrine disruptors, BPA and some of its analogs could potentially interact with ERs or ARs on Leydig and Sertoli cells, and exert more prominent testicular toxicities on these two cell types, as compared with spermatogonial cells.

The purpose of this study is to utilize multiparametric HCA assays to comparatively examine the selective toxicity of BPA, BPS, BPAF, and TBBPA on spermatogonial, Leydig, and Sertoli cell lines. In this study, a wide spectrum of adverse endpoints that are related to testicular cell dysfunction was measured, including cell number, nuclear morphology, DNA synthesis, cell cycle progression, early DNA damage response, cytoskeleton structure, DNA methylation, and autophagy. WeUnsupervised hierarchical cluster analysis on multiple HCA features was conducted. Distinct toxicity profiles of BPA and its analogs in three testicular types were observed. These findings indicated the specific cell target for chemical testicular toxicity and provided mechanistic information for the interpretation of *in vivo* reproductive toxicity studies of BPA and its analogs.

4.3 Materials and methods

4.3.1 Chemicals

DMEM, DME/F12, FBS, horse serum and penicillin-streptomycin were purchased from GE Healthcare Life Sciences (Logan, Utah). 4,4'-(propane-2,2-diyl) diphenol (BPA, ≥99%), 4,4'-sulfonyldiphenol (BPS, 98%), and 2,2',6,6'-tetrabromo-4,4'-isopropylidenediphenol (TBBPA, 97%) were obtained from Sigma-Aldrich (St Louis, Missouri). Nu-Serum was purchased from BD BioScience (Redford, Massachusetts). 4-[1,1,1,3,3,3-hexafluoro-2-(4-hydroxyphenyl)propan-2-yl]phenol (BPAF, 98%) was obtained from Alfa Aesar (Ward Hill, Massachusetts). BrdU (99%) was purchased from Thermo Scientific (Waltham, Massachusetts). 4% Paraformaldehyde was purchased from Boston Bioproducts (Ashland, Massachusetts).

4.3.2 Cell culture and treatment

The mouse C18-4 spermatogonial cell line was established from germ cells isolated from the testes of 6-day-old Balb/c mice. This cell line exhibits morphological features of type A spermatogonia and expresses testicular germ cell–specific genes such as Gfra1, Dazl and Ret (Hofmann et al., 2005). Mouse Leydig TM3 and Sertoli TM4 cell lines were purchased from ATCC. The spermatogonial cells were maintained in DMEM supplemented with 5% FBS, and 100 U/ml streptomycin and penicillin in a 33˚C, 5% CO2 humidified environment in a sub-confluent condition with passaging every 3-4 days. The Leydig and Sertoli cells were cultured in DME/F12 supplemented with 1.25% FBS, 2.5 % horse serum, and 100 U/ml streptomycin and penicillin at 37˚C, 5% CO2 in a sub-confluent condition with passaging every 2-3 days. When cells reached 70-80% confluence, the spermatogonial cells were inoculated with 1.2 x10^4 per well, and Leydig and Sertoli cells were inoculated with 1.6 x10^4 per well in a 96-well plate. Cells

162

were cultured overnight at 70-80% confluence and treated with various concentrations of BPA, BPS, BPAF and TBBPA for the indicated time periods.

<u>4.3.3 Fluorescence staining and image acquisition</u>

For DNA methylation, autophagy, and cell cycle analysis, each cell type was treated with various doses of BPA, or BPS (5, 50 and 100 μM), and BPAF or TBBPA (1, 5 and 10 μM) for 24 and 48 h. Cells were incubated with BrdU (40μM) for 3 h prior to fixation. Then, the cells were fixed with 4% paraformaldehyde for 30 min at room temperature, followed by washing 3 times with PBS. After fixation, cells were permeabilized by 0.1% Triton X-100 in PBS, blocked with PBS/3% BSA, and incubated with a rabbit anti-light chain 3B (LC3B) antibody and a mouse anti-methyl CpG binding protein 1 (MBD1) in PBS/BSA/0.5% Tween 20 overnight at 4 °C. After washing twice with PBS/BSA, cells were incubated with anti-mouse Dylight 488 and anti-rabbit Dylight 650, and Hoechst 33342 in PBS/BSA solution for 1.5 h at room temperature. After image acquisition for MBD1 and LC3B staining, cells were acidified with 4N HCL/Triton X-100 solution, neutralized with $Na_2B_4O_7$ solution, blocked with PBS/3% BSA, and incubated with a mouse anti-BrdU antibody in PBS/BSA/0.5% Tween 20 overnight at 4 °C. After washing three times with PBS/BSA, cells were incubated with a goat anti-mouse Dylight 488 and Hoechst 33342 in PBS/BSA solution for 1.5 h at room temperature. For DNA damage responses and cytoskeleton analysis, cell treatments and fixation were the same as described above. γ-H2AX and F-actin staining followed the protocol reported previously (Liang, *et al.*, 2017).

Multi-channel images were automatically acquired using an Arrayscan™ VTI HCS reader (Thermo Scientific, Massachusetts). 49 fields per well were acquired at 20x and 40X magnification using a Hamamatsu ROCA-ER digital camera in combination with a 0.63x coupler and Carl Zeiss microscope optics in auto-focus mode. Ch1 applied the BGRFR 386_23

for Hoechst 33342 that was used for auto-focus, object identification, and segmentation. Border objects were excluded. For MBD 1 and LC3B staining, Ch2 applied the BGRFR 485_20 for MBD1, and Ch3 applied the BGRFR 650_13 for LC3B. For BrdU staining, Ch2 applied the BGRFR 549-15 for BrdU. For F-actin and γ-H2AX staining, Ch2 applied the BGRFR 485_20 for F-actin, and Ch3 applied the BGRFR 650_13 for γ-H2AX.

4.3.4 High-content image analysis

Multi-channel images were analyzed using HCS StudioTM 2.0 TargetActivation BioApplication. Multi-parameters of nuclei were characterized in HCA, including the nuclei number, nuclear area, shape, and total DNA intensity. The total intensity of BrdU, γ-H2AX, F-actin, MBD 1 and LC3B of each individual cell was also quantified in HCA. Nuclear shape measurements included P2A (nuclear perimeter^2/4 π * nuclear area) to evaluate nuclear smoothness, and LWR (nuclear length/width) to measure nuclear roundness. For a fairly round and smooth object, the values for P2A and LWR are close to 1. Total intensity was defined as total pixel intensities within a cell in the respective channel. With 49 fields of each well, at least 1000 cells were analyzed per well, and single-cell based data were exported for further analysis. The experiments were performed with at least four biological replicates and repeated twice.

HCA-based cell cycle analysis was conducted as previously described (Liang, *et al.*, 2017). Briefly, the histogram of total DNA intensity of each replicate in various experimental conditions was constructed in a custom script written in Python 2.7.12 (Python Software Foundation, OR; this script is freely available from the authors upon request). The input data were gated using the nuclear area and total DNA intensity to exclude cell debris and clumps. Cell populations in sub-G1 (apoptotic cells), G0/1, S, and G2/M in the controls and treatments were quantified by the appropriate selection of the gating threshold.

Data obtained from the HCS Studio™ 2.0 TargetActivation BioApplication were exported and further analyzed using the JMP statistical analysis package (SAS Institute, North Carolina). Nuclei with an area larger than 1000 μM^2 were excluded to remove cell clumps. For each plate, the vehicle control showed consistent measurements for all endpoints tested. For intra-plate normalization, data were normalized to the overall scaling factor, which was the mean of medians of vehicle controls in each plate. The single cell-based data were averaged for the well-based condition. BrdU positive cells were set by the total intensity of BrdU in the control over 25,000 pixels. γ-H2AX positive cells were set by the total intensity of γ-H2AX in the control over 140,000 pixels. Data are presented as the mean ± SD. Statistical significance was determined using 1-way ANOVA followed by Tukey-Kramer all pairs comparison. A P value less than 0.05 denoted a significant difference compared to the vehicle control (*). A non-supervised hierarchical cluster analysis with Ward's minimum variance was conducted on 13 HCA features measured in multiple treatment conditions for 48 h to examine whether the multiparametric data could be used to discriminate the specific toxicity of the chemical in three testicular cells. For each feature, the data were first averaged to fold changes over the mean of the controls. Next, fold-change data were normalized to a value between -1 and 1 by dividing the absolute number of maximum fold differences between the treatments and the controls after subtracting 1. The complete output of cluster analysis is shown as the value change (-1 to 1) indicated calorimetrically.

4.4 Results

4.4.1 BPA and its analogs differentially decreased cell number in spermatogonial cells (C18-4), Leydig cells (TM3), and Sertoli cells (TM4).

Cell number measured in HCA was reported to be a sensitive endpoint to reflect the conspicuous difference in chemical toxicities (O'Brien, *et al.*, 2006). Figure 4.1A shows representative images of nuclei staining following 24 h treatments. Notable induction of multinucleated cells was observed in spermatogonial cells treated with BPAF at a dose of 5 μM and Sertoli cells treated with BPAF at a dose of 10 μM. The quantification of nuclear morphology demonstrated exposure to BPA and its analogs induced significant changes in nuclear morphology in a dose- and time-dependent manner (Figure S4.1). After BPA treatment, Leydig and Sertoli cells exhibited similar morphological changes of nuclei, while spermatogonial cells showed less of a response. After BPS and TBBPA treatment, Leydig cells showed a sensitive response, including significant changes in nuclear area, P2A, and LWR, at non-cytotoxic doses. After BPAF treatment, all three types of cells exhibited similar nuclear morphological changes, including inductions of nuclear area, P2A, and LWR, at different doses (Supplementary Fig. S4.1). In Figure 4.1B, the cell number in different cell types treated with BPA and its analogs for 24 and 48 h were measured. BPA treatment significantly decreased cell numbers at doses of 50 and 100 μM for 24 and 48 h in spermatogonial cells, at a dose of 100 μM for 24 h, 50, and 100 μM for 48 h in both Leydig and Sertoli cells. BPS treatment significantly reduced cell numbers at doses of 50 and 100 μM for 24 h in three cell types, 100 μM for 48 h in spermatogonial cells, and 50 and 100 μM for 48 h in Leydig and Sertoli cells. BPAF treatment significantly reduced cell numbers at doses of 5 and 10 μM for 24 and 48 h in spermatogonial and Leydig cells, at a dose of 10 μM for 24 h, and 5 and 10 μM for 48 h in Sertoli cells. TBBPA

166

treatment decreased cell numbers at doses of 5 and 10 μM for 24 and 48h in spermatogonial cells, at a dose of 10 μM for 48 h in Leydig cells, and for 24 and 48 h in Sertoli cells. Significant increases in cell number were observed in Sertoli cells treated with BPA at a dose of 5 μM for 24 h and spermatogonial cells treated with BPS at a dose of 5 μM for 48 h.

4.4.2 BPA and its analogs differentially altered the DNA synthesis and cell cycle progression in spermatogonial cells (C18-4), Leydig cells (TM3), and Sertoli cells (TM4).

Cell cycle analysis is a fundamental approach for evaluating chemical toxicity and differentiating cellular response to specific chemical (Chan *et al.*, 2013; Lyman*, et al.*, 2011). We previously developed multiparametric HCA assays to measure DNA synthesis and cell cycle progression in cells (Liang, et al., 2017). Figure 4.2A shows representative images of BrdU incorporation after 24 h treatment. As shown in Figure 4.2B, BPA treatment significantly decreased the number of BrdU positive cells at doses of 50 and 100 μM after 24 and 48 h in spermatogonial cells, for 24 h in Leydig and Sertoli cells, and 100 μM for 48 h in Leydig cells. BPS treatment significantly reduced DNA synthesis at doses of 50 and 100 μM for 24 and 48 h in spermatogonial and Leydig cells, 24 h in Sertoli cells, and a dose of 100 μM for 48 h in Sertoli cells. BPAF treatment significantly decreased the number of BrdU positive cells in spermatogonial cells at a dose of 10 μM, in Leydig and Sertoli cells at a dose of 5 μM for 24 h. Significant inductions of BrdU positive cells were observed in the C18-4 cells treated with BPAF at doses of 5 and 10 μM for 48 h, Leydig treated with BPAF at a dose of 10 μM for 24 and 48 h, and Sertoli cells treated with BPAF at a dose of 10 μM for 48 h. TBBPA treatment reduced the number of BrdU positive cells at doses of 5 and 10 μM for 24 h in spermatogonial cells, at a dose of 10 μM for 24 h in Sertoli cells, and for 48 h in spermatogonial cells. No notable change in DNA synthesis was observed in TBBPA-treated Leydig cells.

167

Total DNA intensity histograms were constructed, and percentage of cell in each cell cycle phase was quantified. As shown in Figure 4.2C, in spermatogonial cells, significant decreases in cell population in the G0/1 phase were observed after BPA treatment at a dose of 100 μM for 24 and 48 h, BPAF treatment at doses of 5 and 10 μM for 24 and 48 h, and TBBPA treatment at doses of 5 and 10 μM for 24 h and 10 μM for 48 h. Inductions of G2/M phase were observed in the cells treated with BPA at a dose of 100 μM, BPAF at doses of 5 and 10 μM, and TBBPA at a dose of 10 μM for 24 and 48 h. Significant decreases in S phase population were observed after BPA treatment at a dose of 100 μM for 24 h, BPS treatment at doses of 50 and 100 μM for 24 h and 100 μM for 48 h, BPAF treatment at doses of 5 and 10 μM for 24 h, and TBBPA treatment at a dose of 10 μM for 24 and 48 h. Increases in the percentage of cells in S phase was observed in BPAF treatment at a dose of 5 μM for 48 h. Increases in the percentage of cells in subG1 were observed after BPA treatment at 100 μM for 48 h and BPAF treatment at 5 μM for 24 and 48 h.

In Leydig cells, significant increases in the percentage of cells in G0/1 phase and decreases in the percentage of cells in G2/M phase were observed after BPA and BPS treatment at doses of 50 and 100 μM for 24 and 48 h, and reductions of cells in G0/1 phase and induction of cells in G2/M phase were observed after BPAF treatment at a dose of 10 μM for 24 and 48 h. A significant decrease in percentage of cells in S phase was observed after BPA treatment at a dose of 100 μM for 24 h, 50 and 100 μM for 48 h, BPS treatment at doses of 50 and 100 μM for 24 and 48 h, and TBBPA treatment at a dose of 10 μM for 24 h. In contrast, accumulation of cells in the S phase was observed after BPAF treatment at a dose of 10 μM for 48 h, accompanied with significant increases in the percentages of cells in sub-G1 phase.

168

In Sertoli cells, significant decreases in the cell population in G0/1 phase and increases in the percentage of cells in G2/M phase were observed after BPA and BPS treatment at a dose of 100 μM for 24 h, 50 and 100 μM for 48 h, BPAF treatment at a dose of 10 μM for 24 h, 5 and 10 μM for 48 h, and TBBPA treatment at a dose of 10 μM for 24 and 48 h. Significant decreases in the percentage of cells in S phase were observed after BPA and BPS treatment at a dose of 100 μM for 24 h, 50 and 100 μM for 48 h, and TBBPA treatment at a dose of 10 μM for 24 and 48 h. An accumulation of cells in S phase was observed after BPAF treatment at a dose of 10 μM. In addition, increases in the percentages of cells in sub-G1 phase were observed after BPAF treatment at 5 μM for 24 and 48 h, and TBBPA treatment at doses of 5 and 10 μM for 24 h.

4.4.3 BPA and its analog differentially perturbed the cytoskeleton and induced early DNA damage responses in spermatogonial cells (C18-4), Leydig cells (TM3), and Sertoli cells (TM4).

F-actin, as a major component of the cytoskeleton, is involved in cell movement, cargo transportation, acrosome reactions and nuclear modification during spermatogenesis (Sun*, et al.*, 2011; Wong*, et al.*, 2008). As shown in Figure 4.3A, different cell types exhibited a distinct F-actin filament structure. In spermatogonial cells, two F-actin structures are observed, including cortical actin filaments adjacent to the cell edge and scattered actin fibers across cytoplasm. In Leydig cells, diffuse F-actin fibers are observed without clear cortical actin filaments at the cell edge. In Sertoli cells, the thick F-actin filaments that forms bundles across the cytoplasm or multiple cells are observed. After treatment, these actin structures are disturbed and gel-like networks of cross-branched actin filaments were formed in treated cells. As shown in Figure 4.3B, BPA treatment significantly increased the log-transformed total F-actin intensity at a dose of 100 μM for 24 h in spermatogonial cells, and 50 and 100 μM for 24 and 48 h in spermatogonial, Leydig and Sertoli cells.

169

BPS treatment significantly increased total intensity of F-actin at a dose of 100 μM for 24 and 48 h in spermatogonial cells, 50 and 100 μM after 24 h in Leydig cells, 24 and 48 h in Sertoli cells, and 5 to 100 μM for 48 h in Leydig cells. After BPAF treatment, significant increases in total intensity of F-actin were observed at a dose of 10 μM for 24 and 48 h in spermatogonial cells, 24 h in Sertoli cells, 5 and 10 μM for 24 h in Leydig cells, 48 h in Sertoli cells, and 1, 5, and 10 μM for 48 h in Leydig cells. After TBBPA treatment, inductions of total intensity of F-actin were observed at a dose of 10 μM for 24 and 48 h in spermatogonial and Sertoli cells, and 1, 5, and 10 μM for 48 h in Leydig cells.

γ-H2AX is a highly specific and sensitive cellular marker to monitor the initiation of DNA damages and is increasingly applied in HCA to examine chemical genotoxicity (Ando, *et al.*, 2014; Garcia-Canton, *et al.*, 2013a; Garcia-Canton, *et al.*, 2013b). As shown in Figure 4.3C, after BPA treatment, significant increases in γ-H2AX positive cells were observed at a dose of 100 μM for 24 and 48 h in spermatogonial cells, 24 h in Sertoli cells, and 50 and 100 μM for 48 h in Leydig and Sertoli cells. After BPS treatment, accumulation of γ-H2AX positive cells was observed at a dose of 100 μM for 24 and 48 h in spermatogonial cells, 50 and 100 μM for 24 and 48 h in Sertoli cells, and for 48 h in Leydig cells. BPAF treatment significantly induced γ-H2AX positive cells at a dose of 10 μM for 24 h in Leydig and Sertoli cells, 5 and 10 μM for 24 and 48 h in spermatogonial cells, and 48 h at Leydig and Sertoli cells. TBBPA treatment significantly increased the number of γ-H2AX positive cells at a dose of 10 μM for 24 and 48 h in spermatogonial and Sertoli cells.

4.4.4 BPA and its analogs differentially induced DNA methylation and activated autophagy in spermatogonial cells (C18-4), Leydig cells (TM3), and Sertoli cells (TM4).

DNA methylation is a heritable epigenetic modification and shows a distinct pattern in germ cell development (Trasler, 2009). In our HCA experiment, MBD1, a transcriptional repressor that binds to single methylated CpGs as a monomer, was used to quantify the methylation status of cells treated with BPA and its analogs. Figure 4.4A shows the representative images for MBD-1 and LC3B co-staining in three cell types with various treatment conditions after 24 h exposure. As shown in Figure 4.4B, after BPA treatment, the total intensity of MBD1 was significantly increased at doses of 50 and 100 μM for 24 h in spermatogonial cells, 48 h in Sertoli cells, 100 μM for 24 h in Leydig and Sertoli cells, and 48 h in spermatogonial and Leydig cells. After BPS treatment, a significant induction of total intensity of MBD1 was observed at a dose of 100 μM in spermatogonial cells and 50 and 100 μM in Leydig and Sertoli cells for 24 and 48 h. BPAF treatment significantly induced total intensity of MBD1 at a dose of 10 μM for 24 h and 5 and 10 μM for 48 h in all three cell types. TBBPA treatment increased the total intensity of MBD1 at a concentration of 10 μM for 24 h and 48 h in spermatogonial cells, and 48 h in Sertoli cells.

Autophagy plays an essential role in the regulation of cell survival by degrading and recycling cytoplasmic components to maintain cellular homeostasis (Baehrecke, 2005; Gallagher *et al.*, 2016). Here, an autophagosome membrane protein LC3B was employed to monitor autophagy activity in cells. In Figure 4.4C, BPA treatment significantly increased the total intensity of LC3B at doses of 50 and 100 μM for 24 h in spermatogonial cells, 48 h for Leydig and Sertoli cells, 100 μM for 24 h in Leydig and Sertoli cells, and 48 h in spermatogonial cells. BPS treatment significantly increased total intensity of LC3B at a dose of 100 μM for 24 h in spermatogonial cells, and 50 and 100 μM for 24 and 48 h in Leydig and Sertoli cells. BPAF treatment induced LC3B expression at a dose of 10 μM after 24 h in spermatogonial and Sertoli

cells, 5 and 10 μM after 24 h in Leydig cells, and 48 h for all cell types. TBBPA treatment

significantly increased the LC3B level at a dose of 10 μM after 24 h in spermatogonial cells, and

48 h in spermatogonial and Sertoli cells.

4.4.5 Non-supervised hierarchical cluster analysis of multi-parametric HCA data in

spermatogonial cells (C18-4), Leydig cells (TM3), and Sertoli cells (TM4).

In order to compare the testicular toxicity profiles among BPA and its analogs in

spermatogonial, Leydig, and Sertoli cells, a non-supervised two-dimensional hierarchical cluster

analysis was conducted based on 13 features measured in in three cell types after 48 h of

treatment, including cell number, nuclear area, P2A, LWR, DNA synthesis (BrdU positive cells),

cell population in subG1 phase, G0/1 phase, S phase and G2/M phase, DNA damage response (γ-

H2AX positive cells), total intensity of F-actin, MBD1, and LC3B. Based on the multiparametric

HCA data, the cluster analysis was able to group datasets that shared similar patterns across a

number of cell features. Figure 4.5 illustrates the differential toxicity profile of tested compounds

in spermatogonial, Sertoli, and Leydig cells. The treatment conditions (cell type with specific

concentration of tested chemical) at the top cluster (cluster A) showed a similar toxicity profile

with vehicle controls, suggesting none or minor toxicity of tested chemicals in cells at specific

doses. Cluster A included the three cell types treated with vehicle controls, spermatogonial cells

treated with BPA and BPS at doses of 5 and 50 μM, BPAF at a dose of 1 μM, TBBPA at doses

of 1 and 5 μM, Sertoli cells treated with BPA and BPS at a dose of 5 μM, BPAF at a dose of 1

μM, TBBPA at doses of 1 and 5 μM, and Leydig cells treated with BPA at doses of 5 and 50 μM,

BPS at a dose of 5 μM, BPAF at a dose of 1 μM, and TBBPA at doses of 1, 5, and 10 μM.

Cluster B contained spermatogonial cells treated with BPA and BPS at a dose of 100 μM, and

Leydig and Sertoli cells treated with BPAF at a dose of 5 μM. Cluster C included Leydig cells

172

treated with BPA at a dose of 100 μM and BPS at doses of 50 and 100 μM. Cluster D included

Sertoli cells treated with BPA and BPS at doses of 50 and 100 μM, and TBBPA at a dose of 10

μM. Cluster E included spermatogonial cells treated with BPAF and TBBPA at a dose of 10 μM.

Cluster F-I only contained single treatment condition, including spermatogonial cells treated with

BPAF at doses of 5 and 10 μM and Leydig and Sertoli cells treated with BPAF at a dose of 10

μM.

4.5 Discussion

Spermatogonial cells are the foundation of continual spermatogenesis by maintaining

agerm cell population and supporting gametes production in testis (Oatley and Brinster, 2008). In

addition, spermatogenesis is regulated and supported by Sertoli and Leydig cells, as well as other

cell types in the testis. Injury of these cell types will consequently result in testicular damage and

reproductive dysfunction. Previous studies demonstrated that exposure to BPA induced a wide

spectrum of adverse effects on the male reproductive system in animal models (Chen*, et al.*,

2016b; Cope*, et al.*, 2015; Feng*, et al.*, 2012; Peretz*, et al.*, 2014; Yamasaki*, et al.*, 2004).

Limited data have suggested that some BPA analogs exhibited similar estrogen potencies with

BPA and exerted testicular toxicities in animal models (Chen*, et al.*, 2016a; Mesnage*, et al.*,

2017; Rochester and Bolden, 2015). As endocrine disruptors, these chemicals could interfere

with hormone receptors expressed on Leydig or Sertoli cells, consequently resulting in disruption

of hormone homeostasis, testicular structure, and spermatogenesis. Thus, a comparison of

chemical toxicity in different testicular cell types could help to identify cell type-specific

toxicity, elucidate the functional significance of targeted cells, and extrapolate *in vitro* toxicity

data to human risk assessment.

In our previous study, we developed and validated HCA assays in spermatogonial cell line C18-4 to characterize the testicular toxicity of BPA and its analogs (Liang, *et al.*, 2017). The C18-4 cell line exhibited morphological features of type A spermatogonia and expressed germ cell-specific genetic markers (Hofmann, *et al.*, 2005a). This cell line has been applied in multiple studies to examine signaling pathways involved in germ cell development and to characterize the reproductive toxicity of nanoparticles (Braydich-Stolle, *et al.*, 2005; Braydich-Stolle, *et al.*, 2010; Golestaneh, *et al.*, 2009; He, *et al.*, 2008; Zhang, *et al.*, 2013). In order to compare the cell type-specific toxicity of tested chemicals, Leydig and Sertoli cell lines were included in the current HCA experiments. These two cell lines were isolated from pre-pubertal mouse gonads and they expressed multiple hormone receptors as primary Sertoli cells and Leydig cells, respectively (Mather, 1980). The Leydig cell line TM3 has often been used to assess chemical effects on steroidogenic activity (Chen *et al.*, 2015b; Komatsu *et al.*, 2008). The Sertoli cell line TM4 has been used as a testicular toxicity model to investigate adverse effects of chemical exposure on blood-testis-barrier (BTB) stability (Reis *et al.*, 2015). By incorporating TM3 and TM4 cells, our laboratory constructed an *in vitro* testicular co-culture model that showed the 3D structure and high sensitivity and specificity in reproductive toxicant screening, which suggested essential roles of Sertoli and Leydig cells in supporting and maintaining testicular functions (Yin, *et al.*, 2017).

The HCA approach has been widely applied in toxicological studies to provide toxicity profiling for large numbers of environmental chemicals, elucidate adverse-outcome pathways, and prioritize chemical for future in-depth study. The adoption of HCA for toxicity testing allows measurement of various chemicals with a wide dose range and on different cell types, which provides a cost-effective tool for chemical screening. Furthermore, with simultaneous

measurement of multiple cellular markers on a single cell, HCA can generate complex multivariate toxicity profiles and hazard ranking of chemicals among different cell models. It has been reported that HCA could identify selective toxicity of over 2000 compounds on neural stem cells and cortical neurons (Malik, *et al.*, 2014). Anguissola et.al reported an HCS platform for *in vitro* screening of nanomaterial toxicity in seven different types of organ cells (Anguissola, *et al.*, 2014a). In addition, Kremb et.al conducted HCA on multiple cellular markers to generate unique cytological profiling fingerprints, and construct structure–activity relationships and the mechanism of action of 720 natural products (Kremb and Voolstra, 2017). These advances provide evidence that HCA could be an efficient tool for screening for cell-type specific toxicity of chemicals.

In the previous study, we developed a cell cycle analysis approach based on a histogram of total DNA intensity in the spermatogonial cell line, which showed accurate segmentation of cell cycles and high capability with high-content image analysis (Liang, et al., 2017). In this study, the same approach was applied to examine the chemical effects on cell cycle progression in three testicular cell types. The data revealed that BPA and its analogs perturbed cell cycle progression in a cell-and chemical-specific manner. Our results demonstrated that BPA and its analogs induced G2/M phase arrest in both spermatogonial cells and Leydig cells. However, in Sertoli cells, BPA and BPS treatment induced G0/1 phase arrest. It has been reported that different signaling pathways are involved in cell cycle arrest in various phases. Chemical modulation of cyclin-dependent kinases complexes are able to induce G2/M phase arrest, while for chemicals affecting the calmodulin-dependent protein kinase-II, G1 phase arrest is observed in the cell population (Malumbres and Barbacid, 2005; Morris *et al.*, 1998). Thus, the differential alterations of cell cycle progression in multiple testicular cells may suggest a distinct cellular

175

mechanism underlying chemical toxicity. In addition, BPAF treatment induced multinucleated cells in spermatogonial and Sertoli cells, and abnormal DNA synthesis and cell proliferation in all three types of cells. Induction of multinucleated cells in testes has been reported to be a reproductive toxicity marker in animal models exposed to various environmental chemicals (Faridha, *et al.*, 2007; Gallegos-Avila, *et al.*, 2010; Mylchreest, *et al.*, 2002; Takao, *et al.*, 1999). Further, the multinucleated gonocytes have been reported failing during completion of postnatal mitosis and leading to testicular dysgenesis *in vivo* (Barlow, *et al.*, 2004; Kleymenova, *et al.*, 2005). Among these chemicals, DBP, an endocrine disruptor, induced multinucleated gonocytes and aggregation of Leydig cells in testes (Barlow, *et al.*, 2004; Mahood *et al.*, 2005; Mylchreest, *et al.*, 2002). Although the detailed mechanism of DBP testicular toxicity remains unclear, current data suggest BPAF might act through similar pathways with DBP to induce testicular damage.

The spermatogenesis includes multiple cellular events to generate mature sperms, which including dramatic cell morphology change and cell movement within seminiferous tubules. F-actin, as one of the major components of the cytoskeleton, has been shown to play important roles in cell movement, cell connection, and cargo transportation in testis development (Sun, *et al.*, 2011; Vogl, 1989). In Sertoli cells, F-actin forms parallel actin bundles in ES that are located between adjacent Sertoli cells and adhesion between Sertoli cells and germ cells to regulate movement and release of spermatids (Cheng and Mruk, 2009; Setchell, 2008). In the present study, the distinct pattern of the F-actin cytoskeleton among three cell types and alteration of these structures after chemical treatment were observed in a dose-dependent manner. The significant induction of total intensity of F-actin further suggests aberrant F-actin accumulation within cells. In an *in vivo* study, BPA treatment induced aberrant actin distribution, which

176

contributed to the cytokinesis failure in porcine oocytes (Berger, *et al.*, 2016). Exposure to BPA induced the truncation and de-polymerization of actin via perturbing localization of actin regulatory proteins in Sertoli cells, which provides cellular mechanisms for BPA-induced BTB damage (Xiao, *et al.*, 2014).

Another molecular mechanism that has been suggested to be involved in BPA reproductive toxicity is DNA damage (Ferris, *et al.*, 2016; Meeker *et al.*, 2010; Tiwari *et al.*, 2012). γ-H2AX, an early cellular DNA damage response marker, has recently been applied in HCA to screen for genotoxicity of chemicals (Ando, *et al.*, 2014; Garcia-Canton, *et al.*, 2013a; Garcia-Canton, *et al.*, 2013b). In this study, BPA and its analogs differentially induced DNA damage responses in a cell type-specific manner. Overall, spermatogonial and Sertoli cells showed early responses to DNA damage at lower doses, as compared with Leydig cells. This could be explained by differential biotransformation of BPA and its analogs, and DNA damage repair capacity among different cell types. In *in vitro* studies, BPA treatment induced γ-H2AX at a low dose of 10 nM in human breast cancer cells, while in HepG2 cells, BPA was extensively metabolized and did not increase γ-H2AX even at a dose of 100 μM (Audebert, *et al.*, 2011; Pfeifer, *et al.*, 2015). In addition, BPAF did not induce γ-H2AX in HepG2 and chicken DT40 cells, while it significantly increased the number of γ-H2AX positive cells in a spermatogonial cell line and testicular cells co-cultures (Fic, *et al.*, 2013; Lee, *et al.*, 2013; Liang, *et al.*, 2017).

Epigenetics refers to heritable changes in gene expression without alteration of the DNA sequence. DNA methylation, as one of the major processes of epigenetic alterations, has been reported to show a unique pattern in testis development (Oakes *et al.*, 2007). In an epidemiological study, DNA methylation of multiple loci has been associated with decreased sperm concentration and quality (Houshdaran *et al.*, 2007). There is increasing evidence to

177

indicate aberrant epigenetic alterations contribute to BPA-induced reproductive dysfunction (Bromer *et al.*, 2010; Doshi *et al.*, 2011; Tang *et al.*, 2012). It has been reported that neonatal exposure to BPA induced hypermethylation of the ER promoter region in rat testes (Doshi*, et al.*, 2011). In the current study, BPA and its analogs increased the expression level of MBD 1, a transcriptional repressor, in three testicular cell types, suggesting aberrant methylation occurred.

In addition, autophagic activity was measured simultaneously in three types of cells. As a highly conserved process to degrade and recycle cytoplasmic constituents, autophagy is essential for cell proliferation and differentiation and serves as a cell survival mechanism in nutrition-starved cells (Mizushima and Komatsu, 2011; Mizushima and Levine, 2010). In addition, studies have shown that autophagy plays an active role in cell death by excessive degradation of the cytoplasm to induce apoptosis (Baehrecke, 2005; Marino *et al.*, 2014). Induction of autophagy has been observed in spermatogonial cells or spermatocytes exposed to environmental chemicals (Liu *et al.*, 2014b; Liu *et al.*, 2015a; Zhang *et al.*, 2016). Here the expression level of an autophagosome membrane protein, LC3B, was examined to monitor autophagic activity and found that BPA and its analogs differentially activated autophagy in spermatogonial, Sertoli, and Leydig cells. It has been reported that activation of autophagy acted as a protective role against BPA-induced neurodegeneration via AMPK and mTOR pathways at doses of 40 and 400 μg (Agarwal et al., 2015). BPA treatment induced autophagy and apoptosis concurrently in rat testes at a dose of 50 mg/kg (Quan*, et al.*, 2016a). Thus, the activation of autophagy in testicular cells might serve as an early protective mechanism against BPA toxicity at low doses, while involved in apoptosis at high doses.

In the current study, chemical treatment induced a wide spectrum of adverse cellular events in cells. It has been reported that autophagy activation is closely related to cell cycle arrest

178

(Mathiassen *et al.*, 2017). Further, the perturbation of actin cytoskeleton could result in failure in autophagosome transportation and cytokinesis (Eggert *et al.*, 2006; Kast and Dominguez, 2017). The induction of DNA damage led to dramatic alterations in nuclear and cytoplasmic actin, and F-actin polymerization served as a negative modulator in DNA damage responses (Belin, *et al.*, 2015; Chang, *et al.*, 2015; Wang, *et al.*, 2013; Zuchero, *et al.*, 2012). Thus, these cellular adverse events might be closely connected to each other and eventually lead to cell death. Future study should be conducted to examine the causal and temporal relationships between these events.

In toxicology, one of the applications of HCA is to prioritize and rank chemical toxicity (Elmore, *et al.*, 2014; Merrick, *et al.*, 2015; Shukla, *et al.*, 2010). Multiple adverse endpoints that were related to testicular cell dysfunction in HCA experiments were monitored. However, it is impossible using single *in vitro* assay to sufficiently evaluate and rank chemical toxicity. To compare the testicular toxicity of BPA and its analogs in spermatogonial, Sertoli, and Leydig cells, a non-supervised hierarchical cluster analysis was conducted on multiple parameters measured in HCA experiments. The cluster analysis demonstrated higher toxicities of BPA and BPS in Sertoli and Leydig cells, as compared to spermatogonial cells. As an EDC, BPA has been reported to interact with various physiological receptors, such as ER α/β, estrogen-related receptor γ, AR, and thyroid hormone receptor (Dong, *et al.*, 2011; Gould, *et al.*, 1998; Kuiper, *et al.*, 1998; Matsushima, *et al.*, 2007; Okada, *et al.*, 2008; Richter, *et al.*, 2007; Tokarz, *et al.*, 2013; Wozniak, *et al.*, 2005). The Leydig and Sertoli cell lines used in the present study expressed functional ERs and ARs, and showed active responses to natural hormones (Lin *et al.*, 2014; Mather, 1980; McGuinness and Shaw, 2010). These results suggested the differential toxicological profiles of BPA or BPS in three types of cells could result from their endocrine potency. After BPAF treatment, spermatogonial cells treated with BPAF at doses of 5 and 10

179

μM, Leydig and Sertoli cell treated with BPAF at a dose of 10 μM showed distinct cluster with other treatment conditions, which might reflect its unique toxicity, including formation of multinucleated cells at specific doses, and abnormal cell proliferation and DNA synthesis under those treatment conditions. Furthermore, although three cell types treated with BPAF at a dose of 10 μM were assigned into different clusters, they showed similar toxicity profiles, suggesting the estrogen potency of BPAF might or might not be partially involved in adverse effects on endpoints measured in the current study. Interestingly, cluster analysis clearly discriminated TBBPA-treated spermatogonial cells, Sertoli cells, and Leydig cells. Among all three cell types, spermatogonial cells appeared to be the target for TBBPA, while Leydig cells were highly resistant to TBBPA toxicity, followed by Sertoli cells. Given the controversial evidence on TBBPA's estrogenic activity in limited *in vitro* studies, our results suggested TBBPA does not primarily target Leydig or Sertoli cells in testes (Colnot*, et al.*, 2014). In addition, these results might provide cellular mechanisms for interpreting TBBPA *in vivo* reproductive toxicity. Although high testicular toxicity of TBBPA was previously observed in *in vitro* spermatogonial cells and a testicular co-culture model, its *in vivo* toxicity remains controversial (Cope*, et al.*, 2015; Liang*, et al.*, 2017; Saegusa*, et al.*, 2009; Tada*, et al.*, 2006; Van der Ven*, et al.*, 2008). Cope, et al. only observed the decrease in T4 level in SD rats exposed to TBBPA at a dose of 1000 mg/kg. Whereas no changes in sperm motility, concentration, or percentage of abnormal sperm were observed in multiple generations (Cope*, et al.*, 2015). Our current data suggested that somatic cells (Sertoli cells) that formed BTB and interstitial cells (Leydig cells) are resistant to TBBPA toxicity. Thus, TBBPA potentially could not penetrate through BTB to affect germ cells and exert less effects on testicular hormone homeostasis.

As compared to the previous study, similar toxicity ranking of BPA and its analogs was observed in spermatogonial cells, Sertoli cells, and Leydig cells, respectively. However, BPAF and TBBPA exhibited toxicity at much lower doses in spermatogonial cells (Liang, *et al.*, 2017). As an endocrine disruptor, BPA or its analog could mimic naturally occurring hormones and interfere with physiological receptors. Traditional FBS contains high protein content and multiple hormones, including FSH, T, P4, and LH to support cell growth, which could potentially exert agonist or antagonist effects on BPA or its analogs in testicular cells. To reduce the effects of protein contents and hormones, reduced serum or serum-free cell culture conditions are increasingly required in current research. In this study, Nu-serum, a cost-effective FBS alternative, was employed in the current cell culture system. As compared to FBS, Nu-serum reduced the various hormone levels and protein content and has been shown to successfully support cell growth in a large variety of cell types (Culty *et al.*, 1992; Medh *et al.*, 1992). Thus, the differential toxicity of BPAF and TBBPA in the two cell culture conditions could result from their competitive binding with natural hormones or nonspecific binding with protein contents, which significantly affected the total concentration of the chemical at the target site.
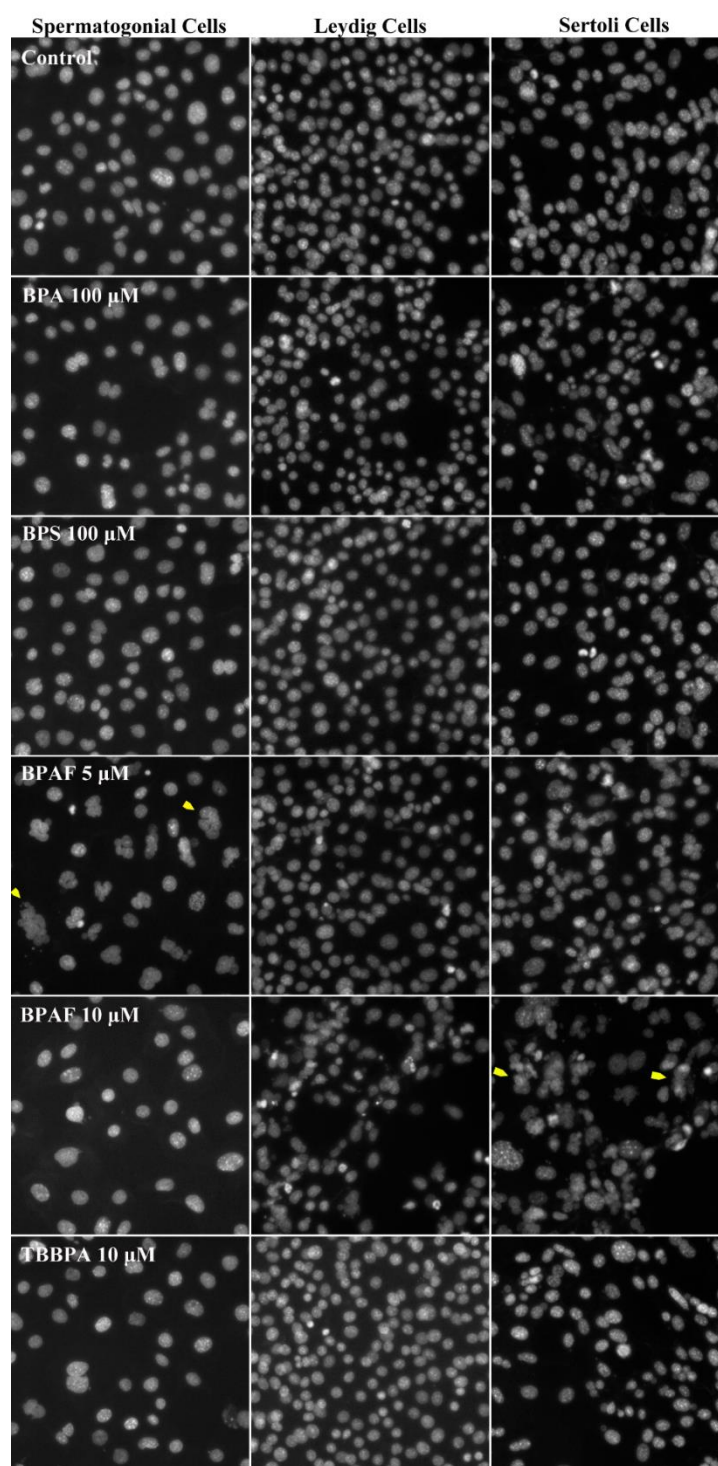
In summary, by utilizing HCA assays in spermatogonial, Sertoli, and Leydig cells, multiple adverse effects of BPA and its analogs on different testicular cell types were characterized. The non-supervised hierarchical cluster analysis combined with HCA-based toxicity profiling identified chemical cell-type specific toxicity, which provided substantial evidence for BPA analogs' testicular toxicities and multidimensional information for toxicity classification. In the future, more endpoints that are closely related to *in vivo* reproductive function will be included, such as steroidogenesis and hormone receptor expression. More

compounds will be examined to construct reproductive toxicological profiles and provide

mechanistic information for prediction of biological targets of reproductive toxins.

A

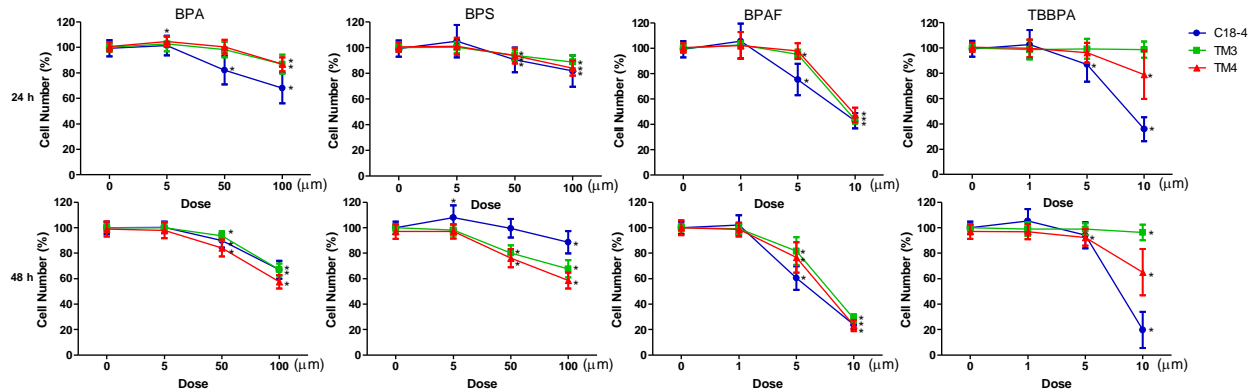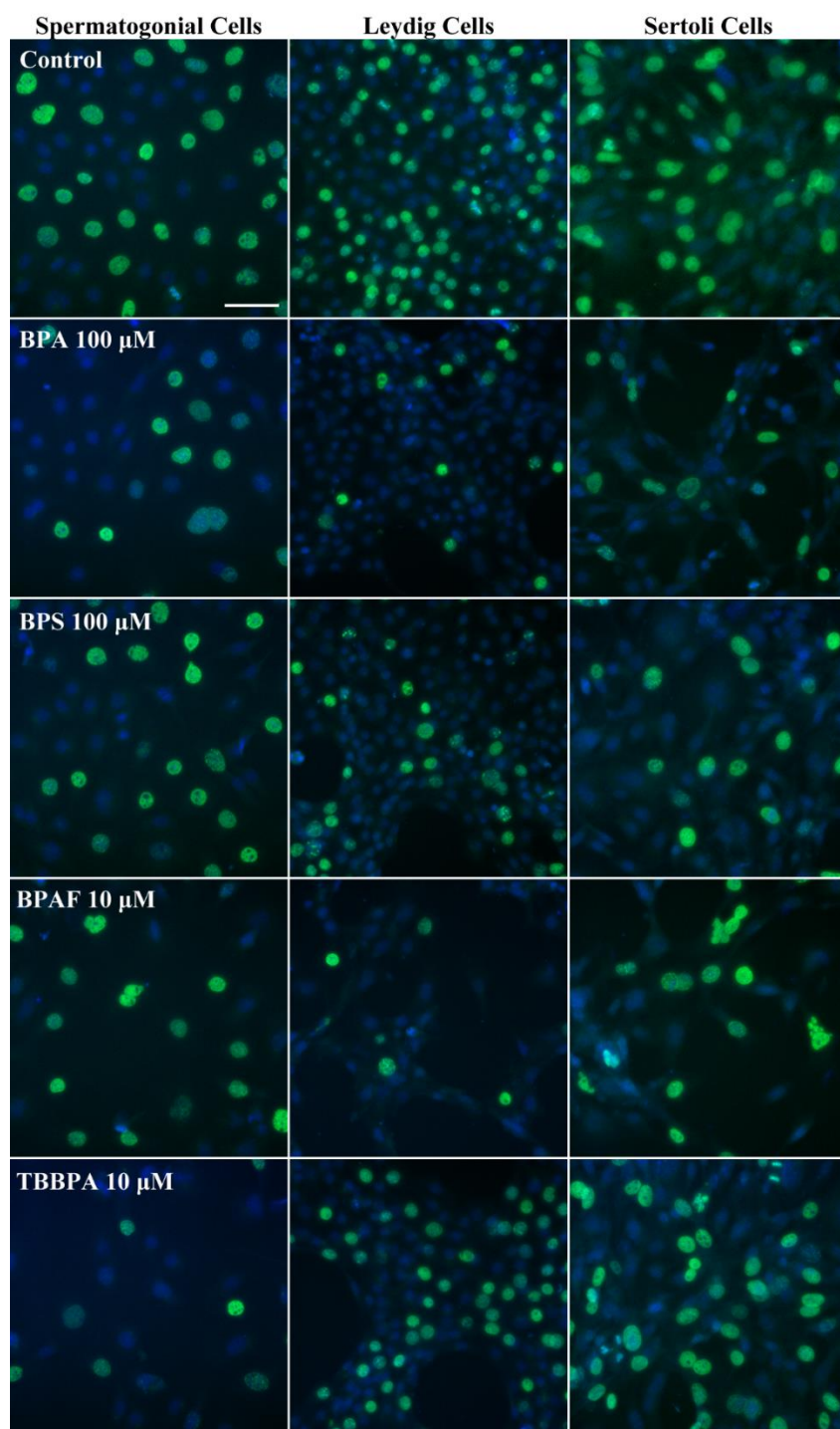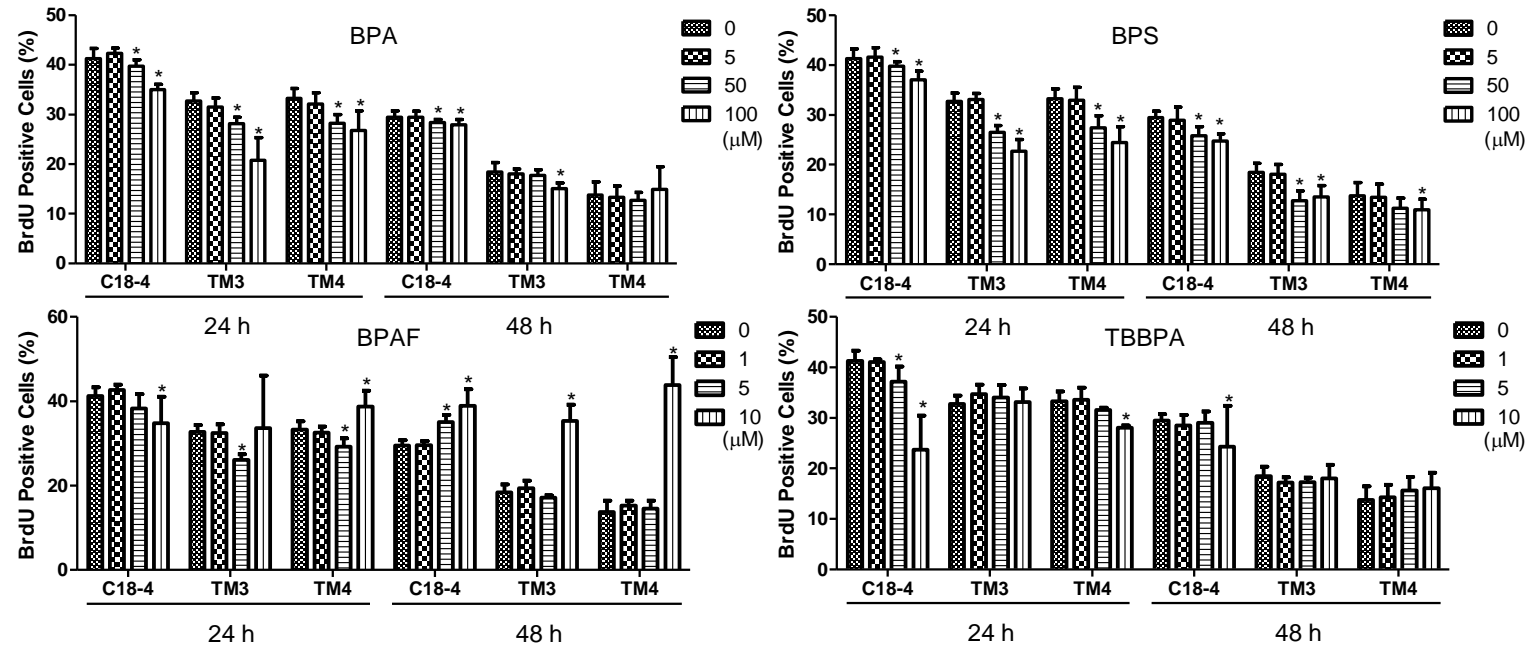|	Spermatogonial Cells	Leydig Cells	Sertoli Cells
Control			
BPA 100 μM			
BPS 100 μM			
BPAF 5 μM			
BPAF 10 μM			
TBBPA 10 μM			

B

Figure 4.1. HCA of cell number of spermatogonial cells, Leydig cells, and Sertoli cells treated with BPA, BPS, BPAF, and TBBPA. Cells were treated with various concentrations of BPA and BPS (5, 50, and 100 μM), and BPAF and TBBPA (1, 5, and 10 μM) for 24 and 48 h. Cells treated with 0.05% DMSO were used as vehicle control (0 μM). The nuclei of co-cultures were stained with Hoechst 33342, and images were automatically acquired with 20X and 40X objectives, and 49 fields per well. A shows the representative images (40X) of controls and cells treated with BPA and BPS (100 μM), BPAF (5 and 10 μM) and TBBPA (10 μM) for 24 h. Arrows indicated the multinucleated cells. Scale bar = 50 μm. B shows the quantification of cell number. Data ae presented as mean ± SD, n=16. Four replicates in four independent experiments were included. Statistical analysis was conducted by 1-way ANOVA followed by Tukey-Kramer multiple comparison (*P<0.05).

A

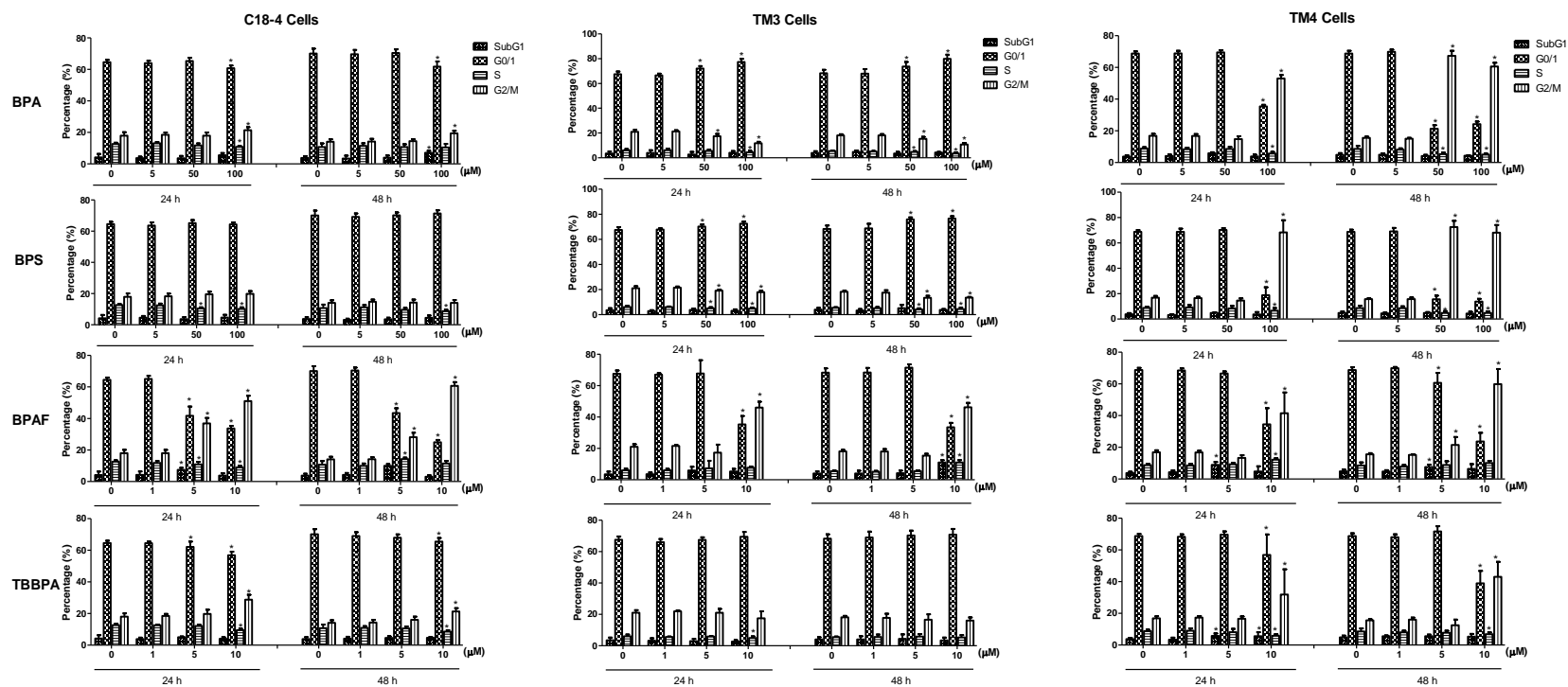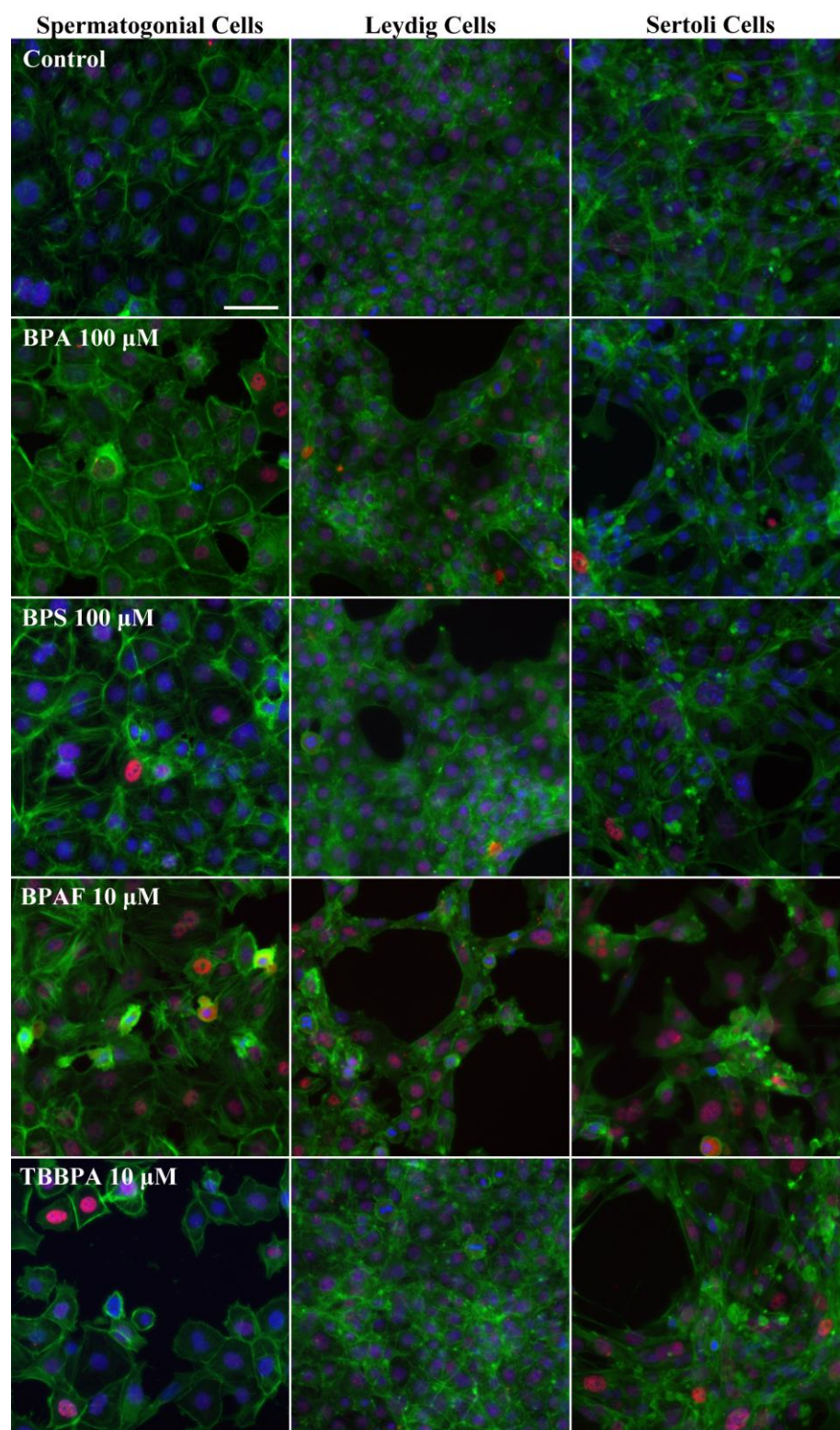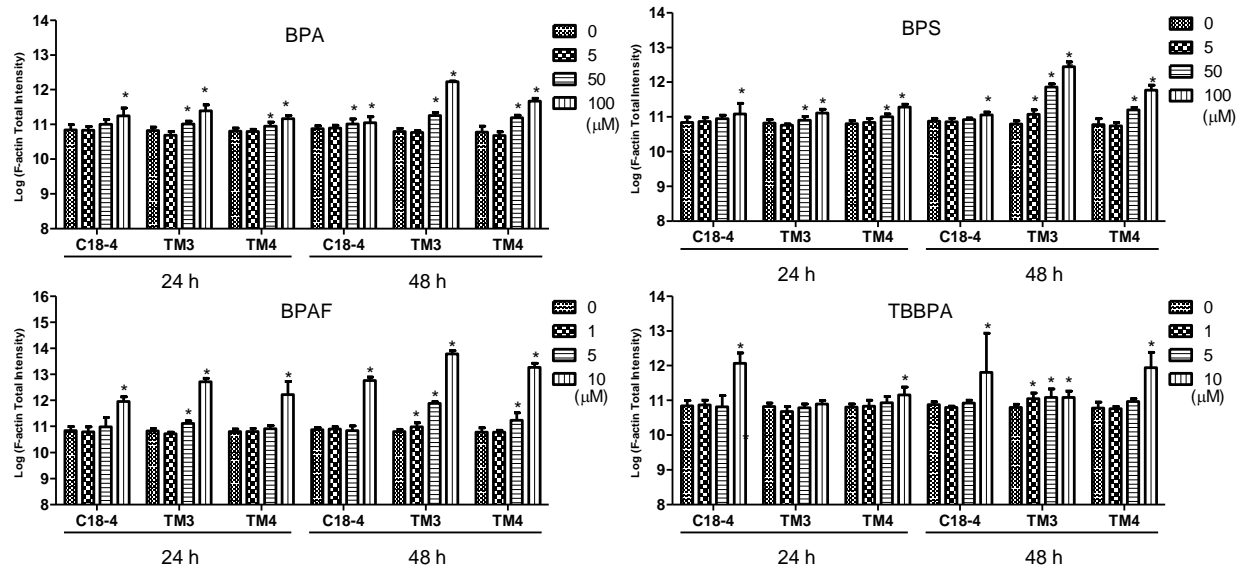|	Spermatogonial Cells	Leydig Cells	Sertoli Cells
Control			
BPA 100 μM			
BPS 100 μM			
BPAF 10 μM			
TBBPA 10 μM			

B

C

Figure 4.2. HCA of DNA synthesis and cell cycle progression of spermatogonial cells, Leydig cells, and Sertoli cells treated with BPA, BPS, BPAF, and TBBPA. Cells were treated with various concentrations of BPA and BPS (5, 50, and 100 μM), and BPAF and TBBPA (1, 5, and 10 μM) for 24 and 48 h. Cells treated with 0.05% DMSO were used as vehicle control (0 μM). The nuclei were stained with Hoechst 33342 (blue). Cells were incubated with BrdU (40 μM) for 3 h prior to cell fixation, and then stained with mouse anti-BrdU antibody and anti-mouse DyLight 488 for detection of BrdU incorporation (green). A shows the representative images (40X) of controls and cells treated with BPA and BPS (100 μM), BPAF and TBBPA (10 μM) for 24 h. Scale bar = 50 μm. B shows the quantification of BrdU-positive cells. C shows the quantification of the percentage of each cell cycle phase, including subG1, G0/1, S and G2/M phase. Data are presented as mean ± SD, n=8. Four replicates in two independent experiments were included. Statistical analysis was conducted by 1-way ANOVA followed by Tukey-Kramer multiple comparison (*P<0.05).

A

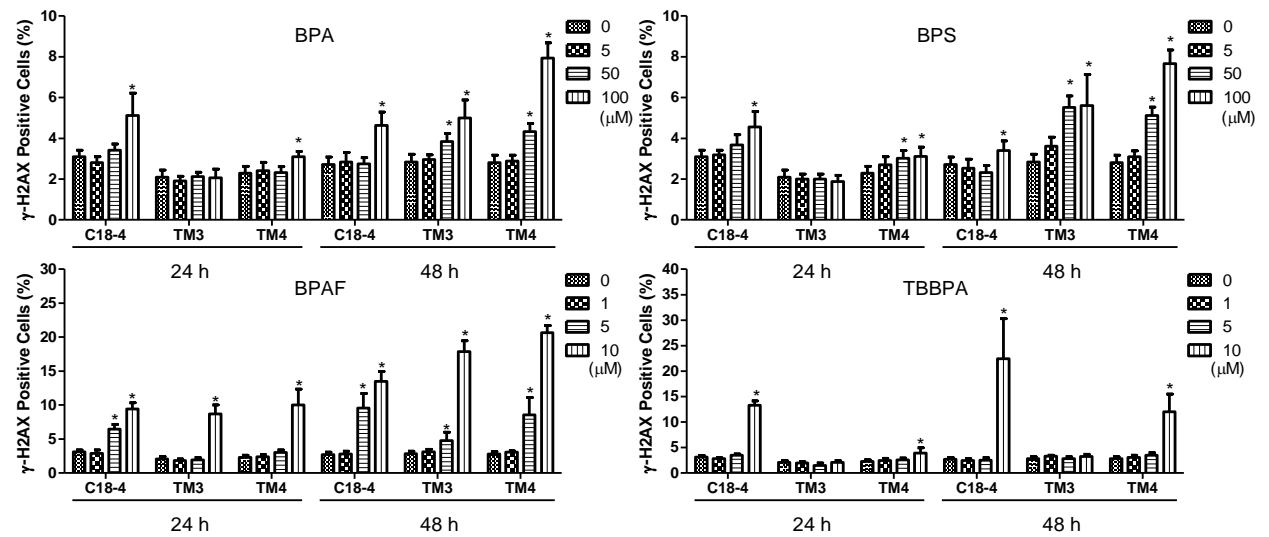| | Spermatogonial Cells | Leydig Cells | Sertoli Cells |

B

C

Figure 4.3. HCA of cytoskeleton and DNA damage responses of spermatogonial cells, Leydig

cells, and Sertoli cells treated with BPA, BPS, BPAF, and TBBPA. Cells were treated with

190

various concentrations of BPA and BPS (5, 50, and 100 μM), and BPAF and TBBPA (1, 5, and 10 μM) for 24 and 48 h. Cells treated with 0.05% DMSO were used as vehicle control (0 μM). The nuclei were stained with Hoechst 33342 (blue), F-actin with Phalloidin staining (green), and γ-H2AX with a combination of primary anti-γ−H2AX and secondary Dylight 650 conjugated antibody (red). A shows the representative images (40X) of controls and cells treated with BPA and BPS (100 μM), BPAF and TBBPA (10 μM) for 24 h. Scale bar = 50 μm. B demonstrates the quantification of log-transformed total intensity of F-actin. C shows the quantification of positive γ-H2AX cells. Data are presented as mean ± SD, n=8. Four replicates in two independent experiments were included. Statistical analysis was conducted by 1-way ANOVA followed by Tukey-Kramer multiple comparison (*P<0.05).
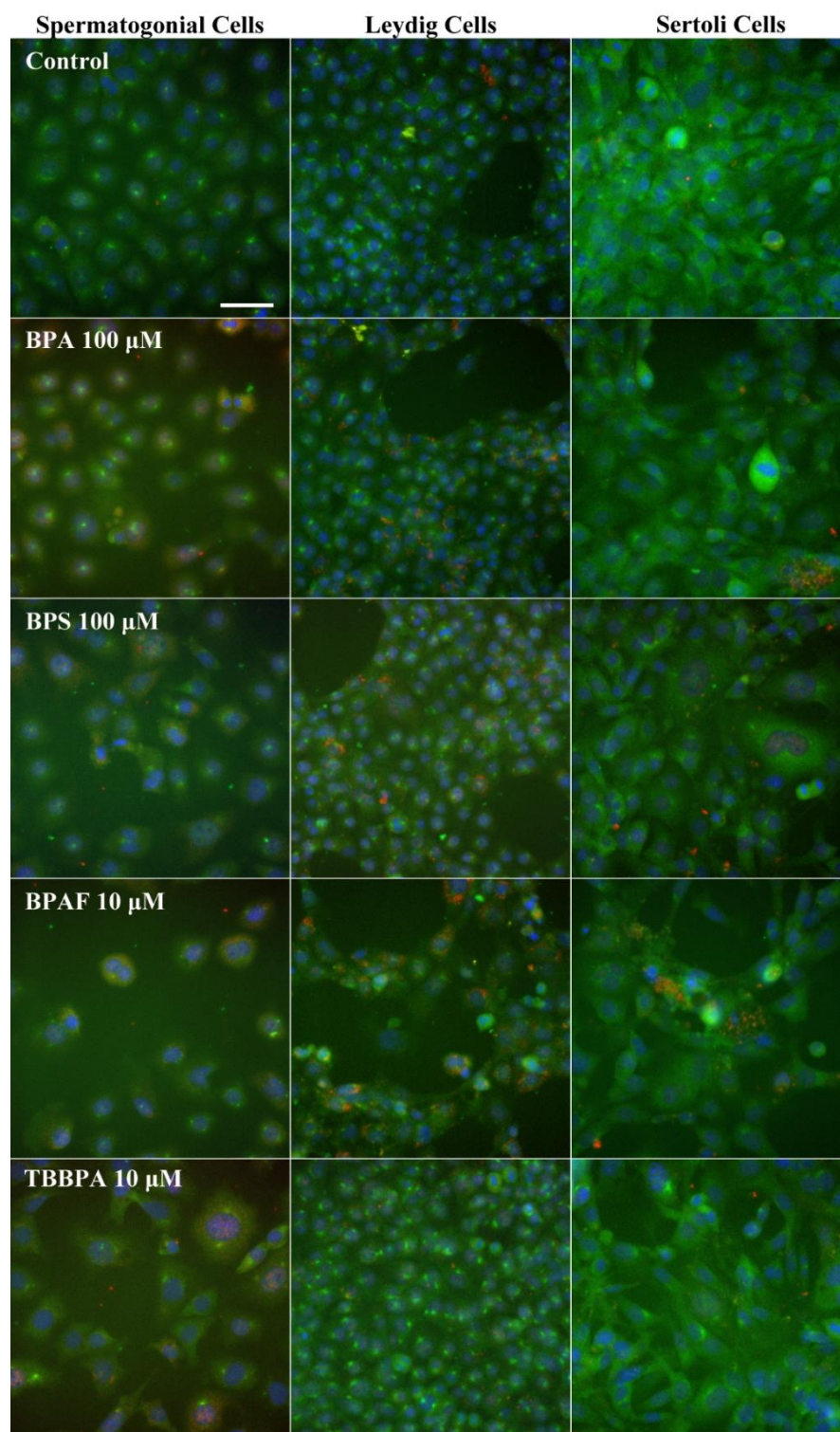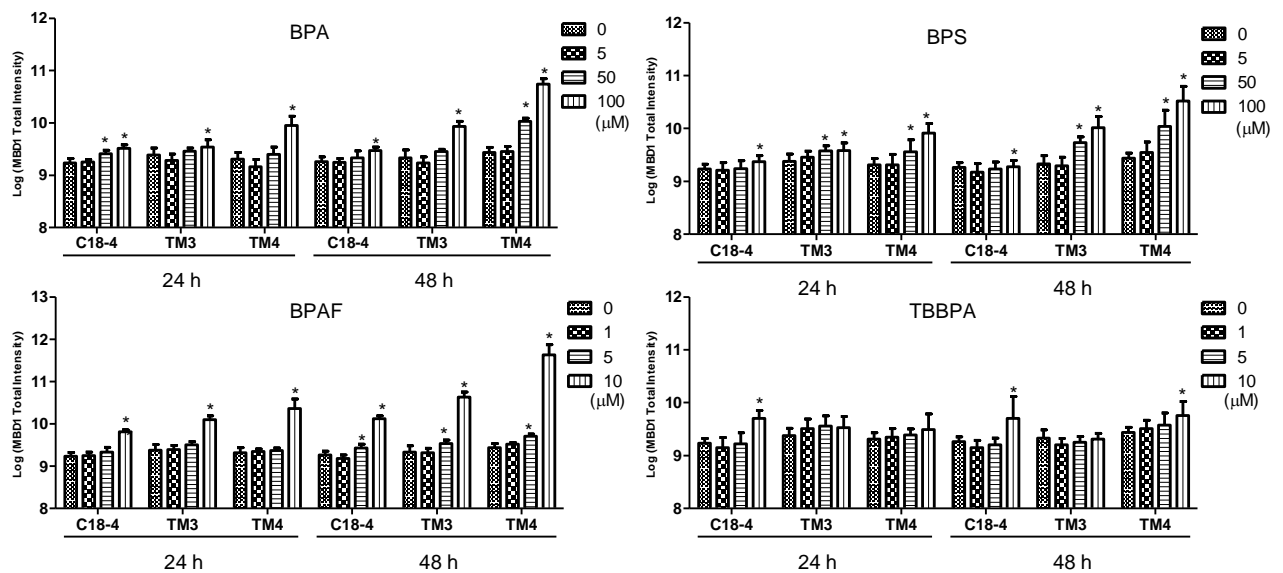
A

Spermatogonial Cells	Leydig Cells	Sertoli Cells

Control

BPA 100 µM

BPS 100 µM

BPAF 10 µM

TBBPA 10 µM

B

C

Figure 4.4. HCA of DNA methylation and autophagic activity of spermatogonial cells, Leydig

cells, and Sertoli cells treated with BPA, BPS, BPAF, and TBBPA. Cells were treated with

193

various concentrations of BPA and BPS (5, 50, and 100 µM), and BPAF and TBBPA (1, 5, and 10 µM) for 24 and 48 h. Cells treated with 0.05% DMSO were used as vehicle control (0 µM). The nuclei were stained with Hoechst 33342 (blue), MBD1 with a combination of primary anti-MBD1 and secondary Dylight 488 conjugated antibody (green), and LC3B with a combination of primary anti-LC3B and secondary Dylight 650 conjugated antibody (red). A shows the representative images (40X) of controls and cells treated with BPA and BPS (100 µM), BPAF and TBBPA (10 µM) for 24 h. Scale bar = 50 µm. B demonstrates the quantification of log-transformed MBD1 total intensity. C shows the quantification of log-transformed LC3B total intensity. Data are presented as mean ± SD, n=8. Four replicates in two independent experiments were included. Statistical analysis was conducted by 1-way ANOVA followed by Tukey-Kramer multiple comparison (*P<0.05).
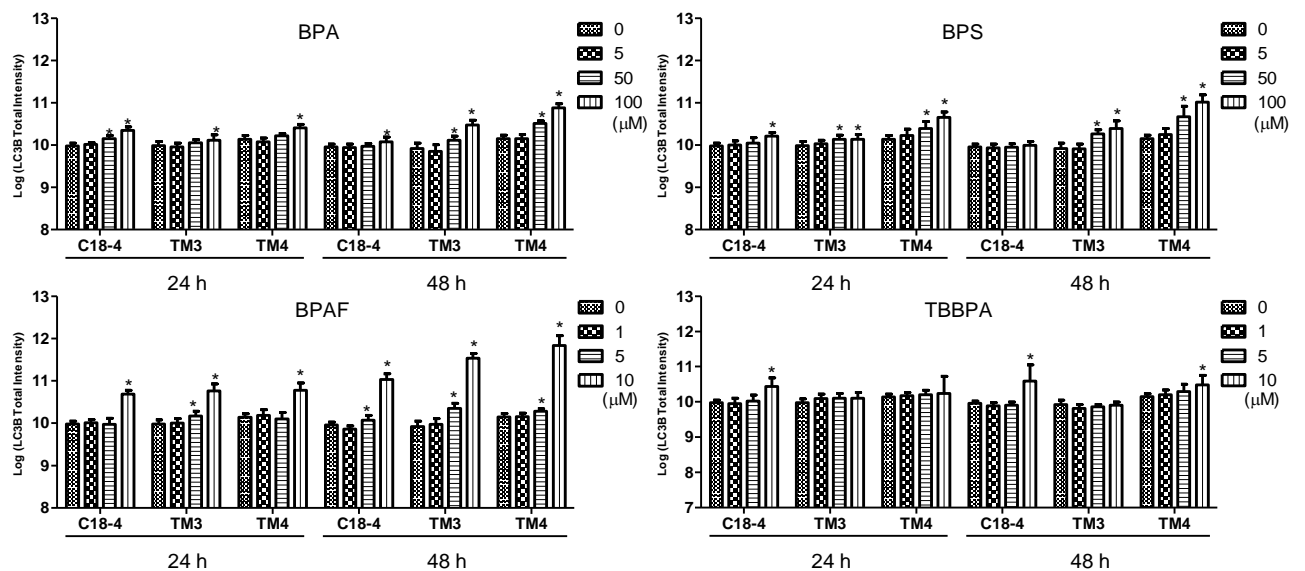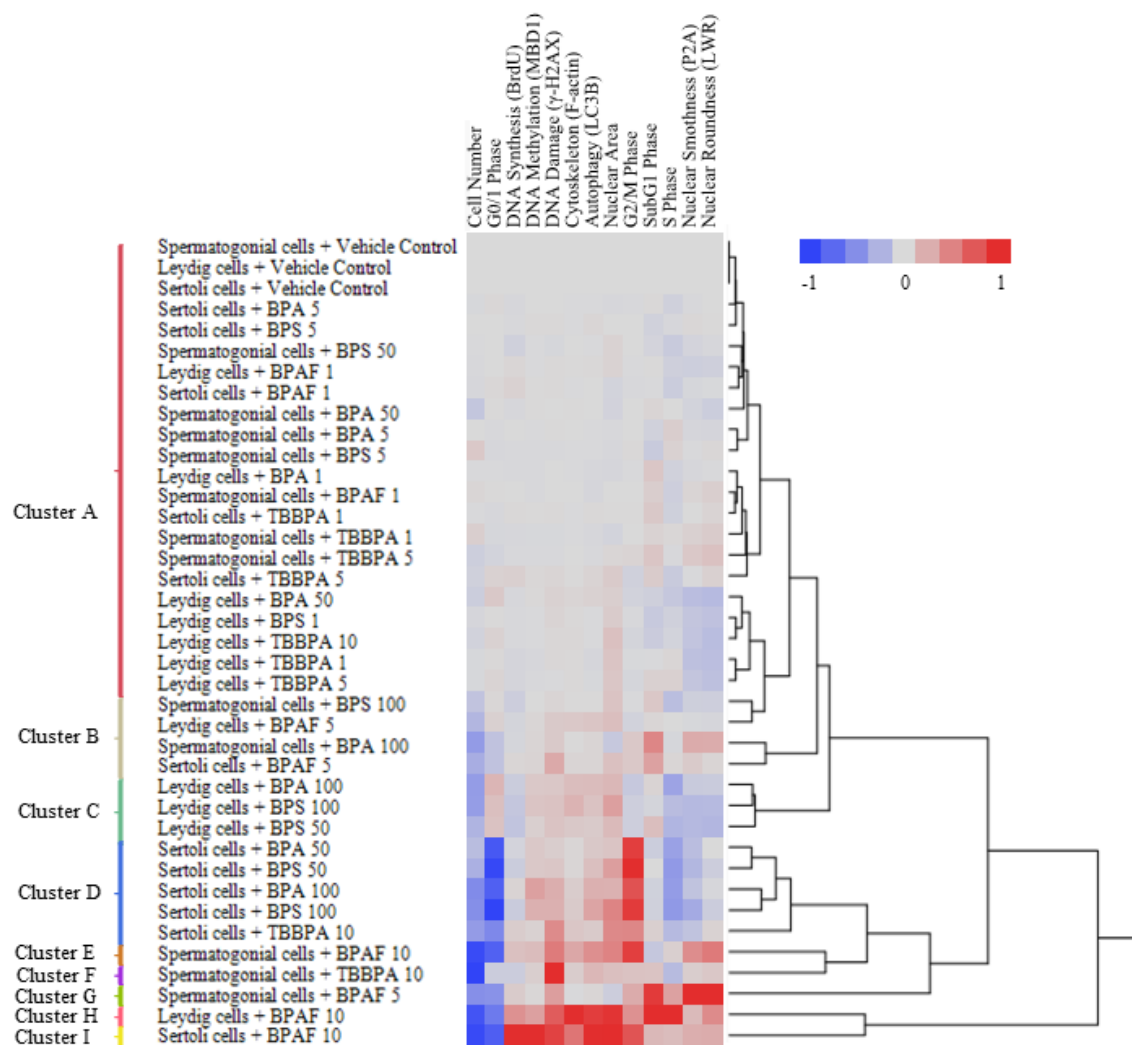
Figure 4.5.

Hierarchical cluster analysis of toxicological profiles of spermatogonial cells, Leydig cells, and Sertoli cells treated with BPA, BPS, BPAF, and TBBPA. Cells were treated with various concentrations of BPA and BPS (5, 50, and 100 μM), and BPAF and TBBPA (1, 5, and 10 μM) for 48 h. A total of 13 features measured in HCA assays were normalized to value from -1 to 1, indicating negative (blue) or positive (red) deviation from the mean of vehicle controls (value=0, gray). A non-supervised two-dimensional hierarchical clustering analysis was conducted on the normalized data using Ward's minimum variance in the JMP statistical analysis pack.

CHAPTER 5

CONCLUSIONS AND FUTURE DIRECTIONS

5.1 Conclusions

This dissertation work was dedicated to the development of HCA assays for reproductive toxicity assessment and characterization of testicular toxicities of BPA and its analogs in spermatogonial cells, Sertoli cells, Leydig cells, and a testicular cell co-culture model. This research project developed and validated HCA assays to simultaneously quantify multiple endpoints related to testicular cell dysfunction, i.e., cell cycle progression, DNA damage, and the cytoskeleton. Next, an ML-powered HCA substantially increased our capabilities of high-content data analysis and understanding of complex phenotypic changes in a testicular cell co-culture model. These results revealed differential testicular toxicities of BPA and its analogs in multiple testicular cell models. Last, a comparative HCA-based toxicity profiling revealed cell-type specific toxicities of BPA and its analogs in spermatogonial, Sertoli and Leydig cells. The major findings and conclusions were summarized below:

In Chapter 2, HCA assays in a spermatogonial cell line were developed and validated to measure multiple endpoints related to testicular cell dysfunction, including cell number, nuclear morphology, cell cycle progression, DNA damage responses, and the cytoskeleton. The HCA revealed higher spermatogonial toxicities of BPAF and TBBPA, as compared to BPA and BPS, on multiple endpoints in spermatogonial cells. These finding greatly improved our understanding of the potential testicular toxicities of BPA analogs. Our HCA approach could be utilized as a

fast and cost-effective tool for identification, screening, and discrimination of the reproductive hazards of environmental chemicals.

The ML-powered HCA in the testicular cell co-culture model in Chapter 3 characterized various phenotypic changes in the co-cultures and characterized testicular toxicities of BPA and its analogs. The supervised ML provided an effective computational strategy and multi-dimensional analysis of high-content image and data from current HCA assays. The phenotypic analysis revealed that BPA and its analogs induced phenotypic 3D structure loss and M phase arrest in the co-cultures. In addition, BPAF induced unique multinucleated cells. ML-based HCA provided in-depth analysis of high-content data and a new approach for characterizing and screening for testicular toxicities of environmental chemicals.

Chapter 4 demonstrated the cell-type specific toxicities of BPA and its analogs in spermatogonial, Leydig, and Sertoli cell lines. HCA assays showed these chemicals affected a wide spectrum of endpoints related to testicular cell dysfunctions, i.e., cell cycle progression, DNA damage, cytoskeleton, autophagy and DNA methylation in three types of testicular cells. The multi-parameter toxicity profile combined with non-supervised hierarchical cluster analysis demonstrated that BPA and its analogs showed cell-type specific toxicity among three types of testicular cells. These results imply that BPA and BPS may target Sertoli and Leydig cells. BPAF exhibited unique toxicity, including multinucleated cells, abnormal DNA synthesis, and aberrant cell cycle progression in three types of testicular cells at different doses. Leydig cells showed high resistance to TBBPA toxicity. The comparative toxicity profiling of BPA and its analogs also provided mechanistic information for *in vivo* toxicity data interpretation and extrapolation in risk assessment.

Together, the findings from this research can aid in identifying toxicity pathways in chemical-induced testicular toxicity, providing fast and cost-efficient screening for potential reproductive toxicants, and prioritizing chemicals based on multi-dimensional data for human risk assessment.

5.2 Future directions

The present HCA assays revealed differential testicular toxicities of BPA and its analogs in multiple single testicular cell type cultures and a testicular cell co-culture model. The present studies serve as a starting point for establishing an HCA-based *in vitro* testicular toxicity model and raising the awareness of BPA analogs' toxicities. To make HCA results more relevant to *in vivo* studies and human exposure, future studies should include low doses that reflect the internal concentrations that induced the adverse reproductive effects in animal models or humans. *In vivo* studies should be conducted to validate current *in vitro* findings. The metabolic capacity of current *in vitro* testicular cell models should be evaluated. The characterization of metabolic capabilities of each testicular cell line and the co-culture model and kinetic biotransformation of bisphenols could greatly improve interoperability of current results. To improve the ability of this model to capture biological pathways that may be perturbed by chemical in testis, future studies should include more reproductive-related endpoints. Besides the general endpoints used in the current study, additional markers that assess steroidogenesis activity and hormone receptor expression level should be considered. In addition, because current works demonstrated the cell-type specific toxicities of BPA and its analogs in multiple single cell cultures, cell-type specific markers for spermatogonial, Leydig, and Sertoli cells should be incorporated to monitor the dynamic changes in cell subpopulations in the co-culture model after chemical treatment. In data analysis, to further explore the multidimensional high-content data, non-supervised ML could be

used to automatically discover previously unappreciated phenotypes. A deep learning approach that uses more layers of image features to form hierarchical classification also should be considered to overcome the current limitations in transformation across datasets and feature representations on a pixel level.

The present HCA assays revealed that BPA and its analogs induced a wide spectrum of adverse effects on testicular cells. However, the detailed mechanisms of chemical-induced cell cycle arrest, DNA damage responses, cytoskeleton perturbation, aberrant DNA methylation and autophagy activation remain to be investigated. Signaling pathways involved in those adverse effects should be elucidated using gain-and loss-of-function approaches. As an endocrine disruptor, BPA could interact with multiple physiological receptors (Peretz, *et al.*, 2014; Richter, *et al.*, 2007; Rochester, 2013; vom Saal, *et al.*, 2007). Some of its analogs have been reported to exert similar or higher estrogen potency, as compared with BPA (Mesnage, *et al.*, 2017; Rochester and Bolden, 2015). The potential interactions of bisphenols and hormone receptors on different testicular cell lines and their toxic consequences need to be determined. In addition, present high-content image and ML-based HCA revealed BPAF treatment uniquely induced multinucleated cells in spermatogonial and Sertoli cells and the co-cultures. Although this phenotypic change has been reported in testes treated with various environmental chemicals, the underlying mechanism should be elucidated in future (Akbarsha and Murugaian, 2000; Barlow, *et al.*, 2004; Faridha, *et al.*, 2007; Gallegos-Avila, *et al.*, 2010; Mylchreest, *et al.*, 2002; Takao, *et al.*, 1999).

Efforts are needed to develop and apply HCA assays to evaluate testicular toxicity of environmental chemical and to advance a mechanistic understanding of the effects of environmental chemical on human reproductive health. Research incorporating both

reproduction-related endpoints and advanced image analysis approaches is necessary to fully

explore the value of HCA in reproductive toxicity testing.

REFERENCES

Abraham, V. C., Towne, D. L., Waring, J. E., Warrior, U., and Burns, D. J. (2008). Application of a high-content multiparameter cytotoxicity assay to prioritize compounds based on toxicity potential in humans. *J Biomol Screen* **13**(6), 527-537, 10.1177/1087057108318428.

Agarwal, S., Tiwari, S. K., Seth, B., Yadav, A., Singh, A., Mudawal, A., Chauhan, L. K. S., Gupta, S. K., Choubey, V., Tripathi, A., Kumar, A., Ray, R. S., Shukla, S., Parmar, D., and Chaturvedi, R. K. (2015). Activation of Autophagic Flux against Xenoestrogen Bisphenol-A-induced Hippocampal Neurodegeneration via AMP kinase (AMPK)/Mammalian Target of Rapamycin (mTOR) Pathways. *J Biol Chem* **290**(34), 21163-21184, 10.1074/jbc.M115.648998.

Akbarsha, M. A., and Murugaian, P. (2000). Aspects of the male reproductive toxicity/male antifertility property of andrographolide in albino rats: effect on the testis and the cauda epididymidal spermatozoa. *Phytother Res* **14**(6), 432-5.

Akin, L., Kendirci, M., Narin, F., Kurtoglu, S., Saraymen, R., Kondolot, M., Kocak, S., and Elmali, F. (2015). The endocrine disruptor bisphenol A may play a role in the aetiopathogenesis of polycystic ovary syndrome in adolescent girls. *Acta Paediatr* **104**(4), E171-E177, 10.1111/apa.12885.

Akingbemi, B. T., Sottas, C. M., Koulova, A. I., Klinefelter, G. R., and Hardy, M. P. (2004). Inhibition of testicular steroidogenesis by the xenoestrogen bisphenol a is associated with reduced pituitary luteinizing hormone secretion and decreased steroidogenic enzyme gene expression in rat Leydig cells. *Endocrinology* **145**(2), 592-603, 10.1210/en.2003-1174.

Ali, S., Steinmetz, G., Montillet, G., Perrard, M. H., Loundou, A., Durand, P., Guichaoua, M. R., and Prat, O. (2014). Exposure to low-dose bisphenol A impairs meiosis in the rat seminiferous tubule culture model: a physiotoxicogenomic approach. *Plos One* **9**(9), e106245, 10.1371/journal.pone.0106245.

Altschuler, S. J., and Wu, L. F. (2010). Cellular Heterogeneity: Do Differences Make a Difference? *Cell* **141**(4), 559-563, 10.1016/j.cell.2010.04.033.

Anderl, J. L., Redpath, S., and Ball, A. J. (2009). A neuronal and astrocyte co-culture assay for high content analysis of neurotoxicity. *J Vis Exp* doi: 10.3791/1173(27), 10.3791/1173.

Ando, M., Yoshikawa, K., Iwase, Y., and Ishiura, S. (2014). Usefulness of monitoring gamma-H2AX and cell cycle arrest in HepG2 cells for estimating genotoxicity using a high-content analysis system. *J Biomol Screen* **19**(9), 1246-54, 10.1177/1087057114541147.

Anguissola, S., Garry, D., Salvati, A., O'Brien, P. J., and Dawson, K. A. (2014a). High content analysis provides mechanistic insights on the pathways of toxicity induced by amine-modified polystyrene nanoparticles. *Plos One* **9**(9), e108025, 10.1371/journal.pone.0108025.

Anguissola, S., Garry, D., Salvati, A., O'Brien, P. J., and Dawson, K. A. (2014b). High Content Analysis Provides Mechanistic Insights on the Pathways of Toxicity Induced by Amine-Modified Polystyrene Nanoparticles. *PloS one* **9**(9), 10.1371/journal.pone.0108025.

Ankley, G. T., Bennett, R. S., Erickson, R. J., Hoff, D. J., Hornung, M. W., Johnson, R. D., Mount, D. R., Nichols, J. W., Russom, C. L., Schmieder, P. K., Serrrano, J. A., Tietge, J. E., and Villeneuve, D. L. (2010). Adverse Outcome Pathways: A Conceptual Framework to Support Ecotoxicology Research and Risk Assessment. *Environ Toxicol Chem* **29**(3), 730-741, 10.1002/etc.34.

Asimakopoulos, A. G., Xue, J. C., De Carvalho, B. P., Iyer, A., Abualnaja, K. O., Yaghmoor, S. S., Kumosani, T. A., and Kannan, K. (2016). Urinary biomarkers of exposure to 57 xenobiotics and its association with oxidative stress in a population in Jeddah, Saudi Arabia. *Environ Res* **150**, 573-581, 10.1016/j.envres.2015.11.029.

Attene-Ramos, M. S., Huang, R. L., Michael, S., Witt, K. L., Richard, A., Tice, R. R., Simeonov, A., Austin, C. P., and Xia, M. H. (2015). Profiling of the Tox21 Chemical Collection for Mitochondrial Function to Identify Compounds that Acutely Decrease Mitochondrial Membrane Potential. *Environ Health Persp* **123**(1), 49-56, 10.1289/ehp.1408642.

Audebert, M., Dolo, L., Perdu, E., Cravedi, J. P., and Zalko, D. (2011). Use of the gamma H2AX assay for assessing the genotoxicity of bisphenol A and bisphenol F in human cell lines. *Arch Toxicol* **85**(11), 1463-1473, 10.1007/s00204-011-0721-2.

Auerbach, S., Filer, D., Reif, D., Walker, V., Holloway, A. C., Schlezinger, J., Srinivasan, S., Svoboda, D., Judson, R., Bucher, J. R., and Thayer, K. A. (2016). Prioritizing Environmental Chemicals for Obesity and Diabetes Outcomes Research: A Screening Approach Using ToxCast (TM) High-Throughput Data. *Environ Health Persp* **124**(8), 1141-1154, 10.1289/ehp.1510456.

Baehrecke, E. H. (2005). Autophagy: dual roles in life and death? *Nat Rev Mol Cell Biol* **6**(6), 505-10, 10.1038/nrm1666.

Bakal, C., Aach, J., Church, G., and Perrimon, N. (2007). Quantitative morphological signatures define local signaling networks regulating cell morphology. *Science* **316**(5832), 1753-1756, 10.1126/science.1140324.

Baker, M. E., and Chandsawangbhuwana, C. (2012). 3D Models of MBP, a Biologically Active Metabolite of Bisphenol A, in Human Estrogen Receptor alpha and Estrogen Receptor beta. *Plos One* **7**(10), ARTN e46078 10.1371/journal.pone.0046078.

Barbonetti, A., Castellini, C., Di Giammarco, N., Santilli, G., Francavilla, S., and Francavilla, F. (2016). In vitro exposure of human spermatozoa to bisphenol A induces pro-oxidative/apoptotic mitochondrial dysfunction. *Reprod Toxicol* **66**, 61-67, 10.1016/j.reprotox.2016.09.014.

Barlow, N. J., McIntyre, B. S., and Foster, P. M. D. (2004). Male reproductive tract lesions at 6, 12, and 18 months of age following in utero exposure to di(n-butyl) phthalate. *Toxicol Pathol* **32**(1), 79-90, 10.1080/01926230490265894.

Belair, D. G., Schwartz, M. P., Knudsen, T., and Murphy, W. L. (2016). Human iPSC-derived endothelial cell sprouting assay in synthetic hydrogel arrays. *Acta Biomater* **39**, 12-24, 10.1016/j.actbio.2016.05.020.

Belin, B. J., Lee, T., and Mullins, R. D. (2015). DNA damage induces nuclear actin filament assembly by Formin-2 and Spire-1/2 that promotes efficient DNA repair. *Elife* **4**, ARTN e07735 10.7554/eLife.07735.

Berger, A., Ziv-Gal, A., Cudiamat, J., Wang, W., Zhou, C. Q., and Flaws, J. A. (2016). The effects of in utero bisphenol A exposure on the ovaries in multiple generations of mice. *Reprod Toxicol* **60**, 39-52, 10.1016/j.reprotox.2015.12.004.

Bi, Y. A., Kazolias, D., and Duignan, D. B. (2006). Use of cryopreserved human hepatocytes in sandwich culture to measure hepatobiliary transport. *Drug Metab Dispos* **34**(9), 1658-1665, 10.1124/dmd.105.009118.

Bickle, M. (2010). The beautiful cell: high-content screening in drug discovery. *Anal Bioanal Chem* **398**(1), 219-226, 10.1007/s00216-010-3788-3.

Blasi, T., Hennig, H., Summers, H. D., Theis, F. J., Cerveira, J., Patterson, J. O., Davies, D., Filby, A., Carpenter, A. E., and Rees, P. (2016). Label-free cell cycle analysis for high-throughput imaging flow cytometry. *Nat Commun* **7**, ARTN 10256   10.1038/ncomms10256.

Boudalia, S., Berges, R., Chabanet, C., Folia, M., Decocq, L., Pasquis, B., Abdennebi-Najar, L., and Canivenc-Lavier, M. C. (2014). A multi-generational study on low-dose BPA exposure in Wistar rats: Effects on maternal behavior, flavor intake and development. *Neurotoxicol Teratol* **41**, 16-26, 10.1016/j.ntt.2013.11.002.

Bouskine, A., Nebout, M., Brucker-Davis, F., Benahmed, M., and Fenichel, P. (2009). Low Doses of Bisphenol A Promote Human Seminoma Cell Proliferation by Activating PKA and PKG via a Membrane G-Protein-Coupled Estrogen Receptor. *Environ Health Persp* **117**(7), 1053-1058, 10.1289/ehp.0800367.

Braun, J. M., Kalkbrenner, A. E., Calafat, A. M., Yolton, K., Ye, X. Y., Dietrich, K. N., and Lanphear, B. P. (2011). Impact of Early-Life Bisphenol A Exposure on Behavior and Executive Function in Children. *Pediatrics* **128**(5), 873-882, 10.1542/peds.2011-1335.

Braydich-Stolle, L., Hussain, S., Schlager, J. J., and Hofmann, M. C. (2005). In vitro cytotoxicity of nanoparticles in mammalian germline stem cells. *Toxicol Sci* **88**(2), 412-419, 10.1093/toxsci/kfi256.

Braydich-Stolle, L. K., Lucas, B., Schrand, A., Murdock, R. C., Lee, T., Schlager, J. J., Hussain, S. M., and Hofmann, M. C. (2010). Silver Nanoparticles Disrupt GDNF/Fyn kinase Signaling in Spermatogonial Stem Cells. *Toxicol Sci* **116**(2), 577-589, 10.1093/toxsci/kfq148.

Breiman, L. (2001). Random forests. *Mach Learn* **45**(1), 5-32, Doi 10.1023/A:1010933404324.

Brewer, G. D. (2009). Science and Decisions Advancing Risk Assessment. *Science* **325**(5944), 1075-1076, 10.1126/science.1175150.

Bromer, J. G., Zhou, Y., Taylor, M. B., Doherty, L., and Taylor, H. S. (2010). Bisphenol-A exposure in utero leads to epigenetic alterations in the developmental programming of uterine estrogen response. *Faseb J* **24**(7), 2273-80, 10.1096/fj.09-140533.

205

Buchser, W., Collins, M., Garyantes, T., Guha, R., Haney, S., Lemmon, V., Li, Z., and Trask, O. J. (2004). Assay Development Guidelines for Image-Based High Content Screening, High Content Analysis and High Content Imaging. In *Assay Guidance Manual* (G. S. Sittampalam, N. P. Coussens, K. Brimacombe, A. Grossman, M. Arkin, D. Auld, C. Austin, J. Baell, B. Bejcek, T. D. Y. Chung, J. L. Dahlin, V. Devanaryan, T. L. Foley, M. Glicksman, M. D. Hall, J. V. Hass, J. Inglese, P. W. Iversen, S. D. Kahl, M. Lal-Nag, Z. Li, J. McGee, O. McManus, T. Riss, O. J. Trask, Jr., J. R. Weidner, M. Xia, and X. Xu, Eds.) doi, Bethesda (MD).

Calafat, A. M., Kuklenyik, Z., Reidy, J. A., Caudill, S. P., Ekong, J., and Needham, L. L. (2005). Urinary concentrations of bisphenol A and 4-nonylphenol in a human reference population. *Environ Health Persp* **113**(4), 391-395.

Calafat, A. M., Ye, X. Y., Wong, L. Y., Reidy, J. A., and Needham, L. L. (2008). Exposure of the US population to bisphenol A and 4-tertiary-octylphenol: 2003-2004. *Environ Health Persp* **116**(1), 39-44, 10.1289/ehp.10753.

Calhoun, K. C., Padilla-Banks, E., Jefferson, W. N., Liu, L. W., Gerrish, K. E., Young, S. L., Wood, C. E., Hunt, P. A., VandeVoort, C. A., and Williams, C. J. (2014). Bisphenol A Exposure Alters Developmental Gene Expression in the Fetal Rhesus Macaque Uterus. *Plos One* **9**(1), ARTN e85894 10.1371/journal.pone.0085894.

Camacho, L., Basavarajappa, M. S., Chang, C. W., Han, T., Kobets, T., Koturbash, I., Surratt, G., Lewis, S. M., Vanlandingham, M. M., Fuscoe, J. C., da Costa, G. G., Pogribny, I. P., and Delclos, K. B. (2015). Effects of oral exposure to bisphenol A on gene expression and global genomic DNA methylation in the prostate, female mammary gland, and uterus of NCTR Sprague-Dawley rats. *Food Chem Toxicol* **81**, 92-103, 10.1016/j.fct.2015.04.009.

Carignan, C. C., Abdallah, M. A. E., Wu, N., Heiger-Bernays, W., McClean, M. D., Harrad, S., and Webster, T. F. (2012). Predictors of Tetrabromobisphenol-A (TBBP-A) and Hexabromocyclododecanes (HBCD) in Milk from Boston Mothers. *Environ Sci Technol* **46**(21), 12146-12153, 10.1021/es302638d.

Carpenter, A. E., Jones, T. R., Lamprecht, M. R., Clarke, C., Kang, I. H., Friman, O., Guertin, D. A., Chang, J. H., Lindquist, R. A., Moffat, J., Golland, P., and Sabatini, D. M. (2006). CellProfiler: image analysis software for identifying and quantifying cell phenotypes. *Genome Biol* **7**(10), ARTN R100 10.1186/gb-2006-7-10-r100.

Carwile, J. L., and Michels, K. B. (2011). Urinary bisphenol A and obesity: NHANES 2003-2006. *Environ Res* **111**(6), 825-830, 10.1016/j.envres.2011.05.014.

Chan, G. K. Y., Kleinheinz, T. L., Peterson, D., and Moffat, J. G. (2013). A Simple High-Content Cell Cycle Assay Reveals Frequent Discrepancies between Cell Number and ATP and MTS Proliferation Assays. *Plos One* **8**(5), ARTN e63583 10.1371/journal.pone.0063583.

Chandler, K. J., Barrier, M., Jeffay, S., Nichols, H. P., Kleinstreuer, N. C., Singh, A. V., Reif, D. M., Sipes, N. S., Judson, R. S., Dix, D. J., Kavlock, R., Hunter, E. S., and Knudsen, T. B. (2011). Evaluation of 309 Environmental Chemicals Using a Mouse Embryonic Stem Cell Adherent Cell Differentiation and Cytotoxicity Assay. *Plos One* **6**(6), ARTN e18540 10.1371/journal.pone.0018540.

Chang, C. Y., Leu, J. D., and Lee, Y. J. (2015). The Actin Depolymerizing Factor (ADF)/Cofilin Signaling Pathway and DNA Damage Responses in Cancer. *Int J Mol Sci* **16**(2), 4095-4120, 10.3390/ijms16024095.

Chapin, R. E., Gray, T. J., Phelps, J. L., and Dutton, S. L. (1988). The effects of mono-(2-ethylhexyl)-phthalate on rat Sertoli cell-enriched primary cultures. *Toxicol Appl Pharmacol* **92**(3), 467-79.

Chen, B., Co, C., and Ho, C. C. (2015a). Cell shape dependent regulation of nuclear morphology. *Biomaterials* **67**, 129-136, 10.1016/j.biomaterials.2015.07.017.

Chen, D., Kannan, K., Tan, H. L., Zheng, Z. G., Feng, Y. L., Wu, Y., and Widelka, M. (2016a). Bisphenol Analogues Other Than BPA: Environmental Occurrence, Human Exposure, and Toxicity-A Review. *Environ Sci Technol* **50**(11), 5438-5453, 10.1021/acs.est.5b05387.

Chen, G. L., Zhang, S. B., Jin, Y. X., Wu, Y., Liu, L., Qian, H. F., and Fu, Z. W. (2015b). TPP and TCEP induce oxidative stress and alter steroidogenesis in TM3 Leydig cells. *Reprod Toxicol* **57**, 100-110, 10.1016/j.reprotox.2015.05.011.

Chen, M. J., Tung, C. W., Shi, Q., Guo, L., Shi, L. M., Fang, H., Borlak, J., and Tong, W. D. (2014). A testing strategy to predict risk for drug-induced liver injury in humans using high-content screen assays and the 'rule-of-two' model. *Arch Toxicol* **88**(7), 1439-1449, 10.1007/s00204-014-1276-9.

Chen, X., Liu, Y. N., Zhou, Q. H., Leng, L., Chang, Y., and Tang, N. J. (2013). Effects of Low Concentrations of Di-(2-ethylhexyl) and Mono-(2-ethylhexyl) Phthalate on Steroidogenesis Pathways and Apoptosis in the Murine Leydig Tumor Cell Line MLTC-1. *Biomed Environ Sci* **26**(12), 986-989, 10.3967/bes2013.034.

Chen, Y. C., Shu, L., Qiu, Z. Q., Lee, D. Y., Settle, S. J., Hee, S. Q., Telesca, D., Yang, X., and Allard, P. (2016b). Exposure to the BPA-Substitute Bisphenol S Causes Unique Alterations of Germline Function. *Plos Genet* **12**(7), ARTN e1006223
10.1371/journal.pgen.1006223.

Chen, Z., Zuo, X., He, D., Ding, S., Xu, F., Yang, H., Jin, X., Fan, Y., Ying, L., Tian, C., and Ying, C. (2017). Long-term exposure to a 'safe' dose of bisphenol A reduced protein acetylation in adult rat testes. *Sci Rep* **7**, 40337, 10.1038/srep40337.

Chen, Z. J., Zhang, K. S., Ge, L. C., Liu, H., Chen, L. K., Du, J., and Wang, H. S. (2016c). Signals involved in the effects of bisphenol A (BPA) on proliferation and motility of Leydig cells: a comparative proteomic analysis. *Toxicol Res-Uk* **5**(6), 1573-1584, 10.1039/c6tx00258g.

Cheng, C. Y., and Mruk, D. D. (2002). Cell junction dynamics in the testis: Sertoli-germ cell interactions and male contraceptive development. *Physiol Rev* **82**(4), 825-874, 10.1152/physrev.00009.2002.

Cheng, C. Y., and Mruk, D. D. (2009). An intracellular trafficking pathway in the seminiferous epithelium regulating spermatogenesis: a biochemical and molecular perspective. *Crit Rev Biochem Mol* **44**(5), 245-263, 10.1080/10409230903061207.

Chong, Y. T., Koh, J. L. Y., Friesen, H., Duffy, S. K., Cox, M. J., Moses, A., Moffat, J., Boone, C., and Andrews, B. J. (2015). Yeast Proteome Dynamics from Single Cell Imaging and Automated Analysis (vol 161, pg 1413, 2015). *Cell* **162**(1), 221-221, 10.1016/j.cell.2015.06.047.

Chouhan, S., Yadav, S. K., Prakash, J., Westfall, S., Ghosh, A., Agarwal, N. K., and Singh, S. P. (2015). Increase in the expression of inducible nitric oxide synthase on exposure to bisphenol A: A possible cause for decline in steroidogenesis in male mice. *Environ Toxicol Phar* **39**(1), 405-416, 10.1016/j.etap.2014.09.014.

Colnot, T., Kacew, S., and Dekant, W. (2014). Mammalian toxicology and human exposures to the flame retardant 2,2',6,6'-tetrabromo-4,4'-isopropylidenediphenol (TBBPA): implications for risk assessment. *Arch Toxicol* **88**(3), 553-573, 10.1007/s00204-013-1180-8.

Conrad, C., and Gerlich, D. W. (2010). Automated microscopy for high-content RNAi screening. *J Cell Biol* **188**(4), 453-461, 10.1083/jcb.200910105.

Cope, R. B., Kacew, S., and Dourson, M. (2015). A reproductive, developmental and neurobehavioral study following oral exposure of tetrabromobisphenol A on Sprague-Dawley rats. *Toxicology* **329**, 49-59, 10.1016/j.tox.2014.12.013.

Culty, M., Nguyen, H. A., and Underhill, C. B. (1992). The hyaluronan receptor (CD44) participates in the uptake and degradation of hyaluronan. *J Cell Biol* **116**(4), 1055-62.

D'Cruz, S. C., Jubendradass, R., Jayakanthan, M., Rani, S. J. A., and Mathur, P. P. (2012). Bisphenol A impairs insulin signaling and glucose homeostasis and decreases steroidogenesis in rat testis: An in vivo and in silico study. *Food Chem Toxicol* **50**(3-4), 1124-1133, 10.1016/j.fct.2011.11.041.

Dallaire, R., Ayotte, P., Pereg, D., Dery, S., Dumas, P., Langlois, E., and Dewailly, E. (2009). Determinants of Plasma Concentrations of Perfluorooctanesulfonate and Brominated Organic Compounds in Nunavik Inuit Adults (Canada). *Environ Sci Technol* **43**(13), 5130-5136, 10.1021/es9001604.

Dankers, A. C., Roelofs, M. J., Piersma, A. H., Sweep, F. C., Russel, F. G., van den Berg, M., van Duursen, M. B., and Masereeuw, R. (2013). Endocrine disruptors differentially target ATP-binding cassette transporters in the blood-testis barrier and affect Leydig cell testosterone secretion in vitro. *Toxicol Sci* **136**(2), 382-91, 10.1093/toxsci/kft198.

Dao, D., Fraser, A. N., Hung, J., Ljosa, V., Singh, S., and Carpenter, A. E. (2016). CellProfiler Analyst: interactive data exploration, analysis and classification of large biological image sets. *Bioinformatics* **32**(20), 3210-3212, 10.1093/bioinformatics/btw390.

Darzynkiewicz, Z., Huang, X., and Okafuji, M. (2006). Detection of DNA strand breaks by flow and laser scanning cytometry in studies of apoptosis and cell proliferation (DNA replication). *Methods in Molecular Biology* **314**, 81-93, 10.1385/1-59259-973-7:081.

de Freitas, A. T. A. G., Ribeiro, M. A., Pinho, C. F., Peixoto, A. R., Domeniconi, R. F., and Scarano, W. R. (2016). Regulatory and junctional proteins of the blood-testis barrier in human Sertoli cells are modified by monobutyl phthalate (MBP) and bisphenol A (BPA) exposure. *Toxicol in Vitro* **34**, 1-7, 10.1016/j.tiv.2016.02.017.

de Ridder, D., de Ridder, J., and Reinders, M. J. (2013). Pattern recognition in bioinformatics. *Brief Bioinform* **14**(5), 633-47, 10.1093/bib/bbt020.

De Rooij, D. G., and Russell, L. D. (2000). All you wanted to know about spermatogonia but were afraid to ask. *Journal of Andrology* **21**(6), 776-798.

Dekant, W., and Voelkel, W. (2008). Human exposure to bisphenol A by biomonitoring: Methods, results and assessment of environmental exposures. *Toxicol Appl Pharm* **228**(1), 114-134, 10.1016/j.taap.2007.12.008.

Delclos, K. B., Camacho, L., Lewis, S. M., Vanlandingham, M. M., Latendresse, J. R., Olson, G. R., Davis, K. J., Patton, R. E., da Costa, G. G., Woodling, K. A., Bryant, M. S., Chidambaram, M., Trbojevich, R., Juliar, B. E., Felton, R. P., and Thorn, B. T. (2014). Toxicity Evaluation of Bisphenol A Administered by Gavage to Sprague Dawley Rats From Gestation Day 6 Through Postnatal Day 90. *Toxicol Sci* **139**(1), 174-197, 10.1093/toxsci/kfu022.

Diaz, D., Scott, A., Carmichael, P., Shi, W., and Costales, C. (2007). Evaluation of an automated in vitro micronucleus assay in CHO-K1 cells. *Mutat Res* **630**(1-2), 1-13, 10.1016/j.mrgentox.2007.02.006.

Dolinoy, D. C., Huang, D., and Jirtle, R. L. (2007). Maternal nutrient supplementation counteracts bisphenol A-induced DNA hypomethylation in early development. *Proc Natl Acad Sci U S A* **104**(32), 13056-61, 10.1073/pnas.0703739104.

Donato, M. T., Gomez-Lechon, M. J., and Tolosa, L. (2017). Using high-content screening technology for studying drug-induced hepatotoxicity in preclinical studies. *Expert Opin Drug Discov* **12**(2), 201-211, 10.1080/17460441.2017.1271784.

Donato, M. T., Tolosa, L., Jimenez, N., Castell, J. V., and Gomez-Lechon, M. J. (2012). High-Content Imaging Technology for the Evaluation of Drug-Induced Steatosis Using a Multiparametric Cell-Based Assay. *J Biomol Screen* **17**(3), 394-400, 10.1177/1087057111427586.

Dong, S., Terasaka, S., and Kiyama, R. (2011). Bisphenol A induces a rapid activation of Erk1/2 through GPR30 in human breast cancer cells. *Environ Pollut* **159**(1), 212-218, 10.1016/j.envpol.2010.09.004.

Doshi, T., Mehta, S. S., Dighe, V., Balasinor, N., and Vanage, G. (2011). Hypermethylation of estrogen receptor promoter region in adult testis of rats exposed neonatally to bisphenol A. *Toxicology* **289**(2-3), 74-82, 10.1016/j.tox.2011.07.011.

Driffield, M., Harmer, N., Bradley, E., Fernandes, A. R., Rose, M., Mortimer, D., and Dicks, P. (2008). Determination of brominated flame retardants in food by LC-MS/MS: diastereoisomer-specific hexabromocyclododecane and tetrabromobisphenol A. *Food Addit Contam A* **25**(7), 895-903, 10.1080/02652030701882999.

Dunnick, J. K., Sanders, J. M., Kissling, G. E., Johnson, C. L., Boyle, M. H., and Elmore, S. A. (2015). Environmental Chemical Exposure May Contribute to Uterine Cancer Development:

Studies with Tetrabromobisphenol A. *Toxicol Pathol* **43**(4), 464-473, 10.1177/0192623314557335.

Dykens, J. A., Jamieson, J. D., Marroquin, L. D., Nadanaciva, S., Xu, J. H. J., Dunn, M. C., Smith, A. R., and Will, Y. (2008). In vitro assessment of mitochondrial dysfunction and cytotoxicity of nefazodone, trazodone, and buspirone. *Toxicol Sci* **103**(2), 335-345, 10.1093/toxsci/kfn056.

ECB. (2012). European union risk assessment report―2,2′,6,6′-tetrabromo-4,4′-isopropylidenediphenol (tetrabromobisphenol-A or TBBP-A) (CAS: 79-94-7) Part II―human health, vol 63, EUR 22161 EN. Institute for Health and Consumer Protection, European Chemicals Bureau, European Commission Joint Research Centre, 4th Priority List, Luxembourg: Office for Official Publications of the European Communities. In (I. f. H. a. C. Protection, Ed.) Eds.), Vol. 63, pp. 1-157.

Eggert, U. S., Mitchison, T. J., and Field, C. M. (2006). Animal cytokinesis: From parts list to mechanisms. *Annu Rev Biochem* **75**, 543-566, 10.1146/annurev.biochem.74.082803.133425.

Ehrlich, S., Williams, P. L., Missmer, S. A., Flaws, J. A., Berry, K. F., Calafat, A. M., Ye, X. Y., Petrozza, J. C., Wright, D., and Hauser, R. (2012). Urinary Bisphenol A Concentrations and Implantation Failure among Women Undergoing in Vitro Fertilization. *Environ Health Persp* **120**(7), 978-983, 10.1289/ehp.1104307.

Eidet, J. R., Pasovic, L., Maria, R., Jackson, C. J., and Utheim, T. P. (2014). Objective assessment of changes in nuclear morphology and cell distribution following induction of apoptosis. *Diagn Pathol* **9**, Artn 92 10.1186/1746-1596-9-92.

Eladak, S., Grisin, T., Moison, D., Guerquin, M. J., N'Tumba-Byn, T., Pozzi-Gaudin, S., Benachi, A., Livera, G., Rouiller-Fabre, V., and Habert, R. (2015). A new chapter in the

bisphenol A story: bisphenol S and bisphenol F are not safe alternatives to this compound. *Fertil Steril* **103**(1), 11-21, 10.1016/j.fertnstert.2014.11.005.

Elmore, S. (2007). Apoptosis: A review of programmed cell death. *Toxicol Pathol* **35**(4), 495-516, 10.1080/01926230701320337.

Elmore, S. A., Ryan, A. M., Wood, C. E., Crabbs, T. A., and Sills, R. C. (2014). FutureTox II: Contemporary Concepts in Toxicology: "Pathways to Prediction: In Vitro and In Silico Models for Predictive Toxicology". *Toxicol Pathol* **42**(5), 940-942, 10.1177/0192623314537135.

EPA, U. S. (1993). Bisphenol A (CASRN 80-05-7). *http://www.epa.gov/iris/subst/0356.htm* doi.

EU. (2016). amending Annex XVII to Regulation (EC) No 1907/2006 of the European Parliament and of the Council concerning the Registration, Evaluation, Authorisation and Restriction of Chemicals (REACH) as regards bisphenol A. 2016/2235. Available at: http://eur-lex.europa.eu/legal-content/EN/TXT/PDF/?uri=CELEX:32016R2235&from=EN. Accessed April 13, 2017.

Faridha, A., Faisal, K., and Akbarsha, M. A. (2007). Aflatoxin treatment brings about generation of multinucleate giant spermatids (symplasts) through opening of cytoplasmic bridges: Light and transmission electron microscopic study in Swiss mouse. *Reprod Toxicol* **24**(3-4), 403-408, 10.1016/j.reprotox.2007.04.071.

Farkas, D., and Tannenbaum, S. R. (2005). In vitro methods to study chemically-induced hepatotoxicity: A literature review. *Curr Drug Metab* **6**(2), 111-125, Doi 10.2174/1389200053586118.

FDA. (2012). Indirect Food Additives: Polymers. 21 CFR 177. 41899 -41902. Available at: https://federalregister.gov/a/2012-17366. Accessed June 2, 2016.

214

FDA. (2013). Indirect Food Additives: Adhesives and Components of Coatings. 21 CFR 175.

41840 -41843. Available at: https://federalregister.gov/a/2013-16684. Accessed June 2, 2016.

Feng, Y. X., Yin, J., Jiao, Z. H., Shi, J. C., Li, M., and Shao, B. (2012). Bisphenol AF may cause

testosterone reduction by directly affecting testis function in adult male rats. *Toxicol Lett* **211**(2),

201-209, 10.1016/j.toxlet.2012.03.802.

Ferguson, K. K., Peterson, K. E., Lee, J. M., Mercado-Garcia, A., Blank-Goldenberg, C., Tellez-

Rojo, M. M., and Meeker, J. D. (2014). Prenatal and peripubertal phthalates and bisphenol A in

relation to sex hormones and puberty in boys. *Reprod Toxicol* **47**, 70-76,

10.1016/j.reprotox.2014.06.002.

Ferrara, D., Hallmark, N., Scott, H., Brown, R., McKinnell, C., Mahood, I. K., and Sharpe, R. M.

(2006). Acute and long-term effects of in utero exposure of rats to di(n-butyl) phthalate on

testicular germ cell development and proliferation. *Endocrinology* **147**(11), 5352-62,

10.1210/en.2006-0527.

Ferris, J., Favetta, L. A., and King, W. A. (2015). Bisphenol A Exposure during Oocyte

Maturation in vitro Results in Spindle Abnormalities and Chromosome Misalignment in Bos

taurus. *Cytogenet Genome Res* **145**(1), 50-58, 10.1159/000381321.

Ferris, J., Mahboubi, K., MacLusky, N., King, W. A., and Favetta, L. A. (2016). BPA exposure

during in vitro oocyte maturation results in dose-dependent alterations to embryo development

rates, apoptosis rate, sex ratio and gene expression. *Reprod Toxicol* **59**, 128-38,

10.1016/j.reprotox.2015.12.002.

Fic, A., Zegura, B., Dolenc, M. S., Filipic, M., and Masic, L. P. (2013). Mutagenicity and DNA

Damage of Bisphenol a and Its Structural Analogues in Hepg2 Cells. *Arh Hig Rada Toksiko*

64(2), 189-200, 10.2478/10004-1254-64-2013-2319.

Fisher, J. S., Macpherson, S., Marchetti, N., and Sharpe, R. M. (2003). Human 'testicular dysgenesis syndrome': a possible model using in-utero exposure of the rat to dibutyl phthalate. *Hum Reprod* **18**(7), 1383-1394, 10.1093/humrep/deg273.

Fu, S. B., Yang, Y., Tirtha, D., Yen, Y., Zhou, B. S., Zhou, M. M., Ohlmeyer, M., Ko, E. C., Cagan, R., Rosenstein, B. S., Chen, S. H., and Kao, J. (2012). gamma-H2AX Kinetics as a Novel Approach to High Content Screening for Small Molecule Radiosensitizers. *Plos One* **7**(6), ARTN e38465 10.1371/journal.pone.0038465.

Fuchs, F., Pau, G., Kranz, D., Sklyar, O., Budjan, C., Steinbrink, S., Horn, T., Pedal, A., Huber, W., and Boutros, M. (2010). Clustering phenotype populations by genome-wide RNAi and multiparametric imaging. *Mol Syst Biol* **6**, 370, 10.1038/msb.2010.25.

Fujimura, H., Murakami, N., Kurabe, M., and Toriumi, W. (2009). In vitro assay for drug-induced hepatosteatosis using rat primary hepatocytes, a fluorescent lipid analog and gene expression analysis. *J Appl Toxicol* **29**(4), 356-363, 10.1002/jat.1420.

Fuller, J. A., Berlinicke, C. A., Inglese, J., and Zack, D. J. (2016). Use of a Machine Learning-Based High Content Analysis Approach to Identify Photoreceptor Neurite Promoting Molecules. *Adv Exp Med Biol* **854**, 597-603, 10.1007/978-3-319-17121-0_79.

Furr, J. R., Lambright, C. S., Wilson, V. S., Foster, P. M., and Gray, L. E. (2014). A Short-term In Vivo Screen Using Fetal Testosterone Production, a Key Event in the Phthalate Adverse Outcome Pathway, to Predict Disruption of Sexual Differentiation. *Toxicol Sci* **140**(2), 403-424, 10.1093/toxsci/kfu081.

Gallagher, L. E., Williamson, L. E., and Chan, E. Y. (2016). Advances in Autophagy Regulatory Mechanisms. *Cells* **5**(2), 10.3390/cells5020024.

Gallegos-Avila, G., Ancer-Rodriguez, J., Niderhauser-Garcia, A., Ortega-Martinez, M., and Jaramillo-Rangel, G. (2010). Multinucleation of spermatozoa and spermatids in infertile men chronically exposed to carbofuran. *Reprod Toxicol* **29**(4), 458-60, 10.1016/j.reprotox.2010.03.007.

Gamez, J. M., Penalba, R., Cardoso, N., Bernasconi, P. S., Carbone, S., Ponzo, O., Pandolfi, M., Scacchi, P., and Reynoso, R. (2015). Exposure to a low dose of bisphenol A impairs pituitary-ovarian axis in prepubertal rats Effects on early folliculogenesis. *Environ Toxicol Phar* **39**(1), 9-15, 10.1016/j.etap.2014.10.015.

Gamez, J. M., Penalba, R., Cardoso, N., Ponzo, O., Carbone, S., Pandolfi, M., Scacchi, P., and Reynoso, R. (2014). Low dose of bisphenol A impairs the reproductive axis of prepuberal male rats. *J Physiol Biochem* **70**(1), 239-246, 10.1007/s13105-013-0298-8.

Ganesan, S., and Keating, A. F. (2016). Bisphenol A-Induced Ovotoxicity Involves DNA Damage Induction to Which the Ovary Mounts a Protective Response Indicated by Increased Expression of Proteins Involved in DNA Repair and Xenobiotic Biotransformation. *Toxicol Sci* **152**(1), 169-180, 10.1093/toxsci/kfw076.

Garcia-Canton, C., Anadon, A., and Meredith, C. (2013a). Assessment of the in vitro γH2AX assay by High Content Screening as a novel genotoxicity test. *Mutation Research/Genetic Toxicology and Environmental Mutagenesis* **757**(2), 158-166.

Garcia-Canton, C., Anadon, A., and Meredith, C. (2013b). Genotoxicity evaluation of individual cigarette smoke toxicants using the in vitro gammaH2AX assay by high content screening. *Toxicol Lett* **223**(1), 81-7, 10.1016/j.toxlet.2013.08.024.

Garcia-Canton, C., Errington, G., Anadon, A., and Meredith, C. (2014). Characterisation of an aerosol exposure system to evaluate the genotoxicity of whole mainstream cigarette smoke using

the in vitro gammaH2AX assay by high content screening. *BMC Pharmacol Toxicol* **15**, 41, 10.1186/2050-6511-15-41.

Garside, H., Marcoe, K. F., Chesnut-Speelman, J., Foster, A. J., Muthas, D., Kenna, J. G., Warrior, U., Bowes, J., and Baumgartner, J. (2014). Evaluation of the use of imaging parameters for the detection of compound-induced hepatotoxicity in 384-well cultures of HepG2 cells and cryopreserved primary human hepatocytes. *Toxicol in Vitro* **28**(2), 171-181, 10.1016/j.tiv.2013.10.015.

Gassman, N. R., Coskun, E., Jaruga, P., Dizdaroglu, M., and Wilson, S. H. (2016). Combined Effects of High-Dose Bisphenol A and Oxidizing Agent (KBrO) on Cellular Microenvironment, Gene Expression, and Chromatin Structure of Ku70-deficient Mouse Embryonic Fibroblasts. *Environ Health Perspect* doi: 10.1289/EHP237, 10.1289/EHP237.

Ge, L. C., Chen, Z. J., Liu, H. Y., Zhang, K. S., Liu, H., Huang, H. B., Zhang, G., Wong, C. K. C., Giesy, J. P., Du, J., and Wang, H. S. (2014). Involvement of activating ERK1/2 through G protein coupled receptor 30 and estrogen receptor alpha/beta in low doses of bisphenol A promoting growth of Sertoli TM4 cells. *Toxicol Lett* **226**(1), 81-89, 10.1016/j.toxlet.2014.01.035.

Geens, T., Roosens, L., Neels, H., and Covaci, A. (2009). Assessment of human exposure to Bisphenol-A, Triclosan and Tetrabromobisphenol-A through indoor dust intake in Belgium. *Chemosphere* **76**(6), 755-760, 10.1016/j.chemosphere.2009.05.024.

Goldstone, A. E., Chen, Z., Perry, M. J., Kannan, K., and Louis, G. M. B. (2015). Urinary bisphenol A and semen quality, the LIFE Study. *Reprod Toxicol* **51**, 7-13, 10.1016/j.reprotox.2014.11.003.

Golestaneh, N., Beauchamp, E., Fallen, S., Kokkinaki, M., Uren, A., and Dym, M. (2009). Wnt signaling promotes proliferation and stemness regulation of spermatogonial stem/progenitor cells. *Reproduction* **138**(1), 151-162, 10.1530/Rep-08-0510.

Gould, J. C., Leonard, L. S., Maness, S. C., Wagner, B. L., Conner, K., Zacharewski, T., Safe, S., McDonnell, D. P., and Gaido, K. W. (1998). Bisphenol A interacts with the estrogen receptor alpha in a distinct manner from estradiol. *Mol Cell Endocrinol* **142**(1-2), 203-214, Doi 10.1016/S0303-7207(98)00084-7.

Grandjean, P., and Landrigan, P. J. (2006). Developmental neurotoxicity of industrial chemicals. *Lancet* **368**(9553), 2167-78, 10.1016/S0140-6736(06)69665-7.

Gray, T. J. (1986). Testicular toxicity in vitro: Sertoli-germ cell co-cultures as a model system. *Food Chem Toxicol* **24**(6-7), 601-5.

Gregotti, C., Dinucci, A., Costa, L. G., Manzo, L., Scelsi, R., Berte, F., and Faustman, E. M. (1992). Effects of Thallium on Primary Cultures of Testicular Cells. *J Toxicol Env Health* **36**(1), 59-69.

Gross-Steinmeyer, K., Stapleton, P. L., Tracy, J. H., Bammler, T. K., Lehman, T., Strom, S. C., and Eaton, D. L. (2005). Influence of Matrigel-overlay on constitutive and inducible expression of nine genes encoding drug-metabolizing enzymes in primary human hepatocytes. *Xenobiotica* **35**(5), 419-438, 10.1080/00498250500137427.

Gurmeet, K. S. S., Rosnah, I., Normadiah, M. K., Das, S., and Mustafa, A. M. (2014). Detrimental Effects of Bisphenol a on Development and Functions of the Male Reproductive System in Experimental Rats. *Excli J* **13**, 151-160.

Habert, R., Muczynski, V., Grisin, T., Moison, D., Messiaen, S., Frydman, R., Benachi, A., Delbes, G., Lambrot, R., Lehraiki, A., N'Tumba-Byn, T., Guerquin, M. J., Levacher, C.,

Rouiller-Fabre, V., and Livera, G. (2014). Concerns about the widespread use of rodent models for human risk assessments of endocrine disruptors. *Reproduction* **147**(4), R119-29, 10.1530/REP-13-0497.

Hai, Y. A., Hou, J. M., Liu, Y., Liu, Y., Yang, H., Li, Z., and He, Z. P. (2014). The roles and regulation of Sertoli cells in fate determinations of spermatogonial stem cells and spermatogenesis. *Semin Cell Dev Biol* **29**, 66-75, 10.1016/j.semcdb.2014.04.007.

Harrill, J. A., Freudenrich, T. M., Machacek, D. W., Stice, S. L., and Mundy, W. R. (2010). Quantitative assessment of neurite outgrowth in human embryonic stem cell-derived hN2 (TM) cells using automated high-content image analysis. *Neurotoxicology* **31**(3), 277-290, 10.1016/j.neuro.2010.02.003.

Harrill, J. A., Robinette, B. L., Freudenrich, T., and Mundy, W. R. (2013). Use of high content image analyses to detect chemical-mediated effects on neurite sub-populations in primary rat cortical neurons. *Neurotoxicology* **34**, 61-73, 10.1016/j.neuro.2012.10.013.

Harris, S., Hermsen, S. A. B., Yu, X. Z., Hong, S. W., and Faustman, E. M. (2015). Comparison of toxicogenomic responses to phthalate ester exposure in an organotypic testis co-culture model and responses observed in vivo. *Reprod Toxicol* **58**, 149-159, 10.1016/j.reprotox.2015.10.002.

Harris, S., Shubin, S. P., Wegner, S., Van Ness, K., Green, F., Hong, S. W., and Faustman, E. M. (2016a). The presence of macrophages and inflammatory responses in an in vitro testicular co-culture model of male reproductive development enhance relevance to in vivo conditions. *Toxicol in Vitro* **36**, 210-215, 10.1016/j.tiv.2016.08.003.

Harris, S., Wegner, S., Hong, S. W., and Faustman, E. M. (2016b). Phthalate metabolism and kinetics in an in vitro model of testis development. *Toxicol in Vitro* **32**, 123-131, 10.1016/j.tiv.2015.12.002.

Hass, U., Christiansen, S., Boberg, J., Rasmussen, M. G., Mandrup, K., and Axelstad, M. (2016). Low-dose effect of developmental bisphenol A exposure on sperm count and behaviour in rats. *Andrology-Us* **4**(4), 594-607, 10.1111/andr.12176.

Haywood, M., Spaliviero, J., Jimemez, M., King, N. J., Handelsman, D. J., and Allan, C. M. (2003). Sertoli and germ cell development in hypogonadal (hpg) mice expressing transgenic follicle-stimulating hormone alone or in combination with testosterone. *Endocrinology* **144**(2), 509-17, 10.1210/en.2002-220710.

He, Z. P., Jiang, J. J., Kokkinaki, M., Golestaneh, N., Hofmann, M. C., and Dym, M. (2008). GDNF upregulates c-fos transcription via the Ras/ERK1/2 pathway to promote mouse spermatogonial stem cell proliferation. *Stem Cells* **26**(1), 266-278, 10.1634/stemcells.2007-0436.

Heinala, M., Ylinen, K., Tuomi, T., Santonen, T., and Porras, S. P. (2017). Assessment of Occupational Exposure to Bisphenol A in Five Different Production Companies in Finland. *Ann Work Expo Health* **61**(1), 44-55, 10.1093/annweh/wxw006.

Helmestam, M., Davey, E., Stavreus-Evers, A. L., and Olovsson, M. (2014). Bisphenol A affects human endometrial endothelial cell angiogenic activity in vitro. *Reprod Toxicol* **46**, 69-76, 10.1016/j.reprotox.2014.03.002.

Hennig, H., Rees, P., Blasi, T., Kamentsky, L., Hung, J., Dao, D., Carpenter, A. E., and Filby, A. (2017). An open-source solution for advanced imaging flow cytometry data analysis using machine learning. *Methods* **112**, 201-210, 10.1016/j.ymeth.2016.08.018.

Hines, C. J., Jackson, M. V., Deddens, J. A., Clark, J. C., Ye, X., Christianson, A. L., Meadows, J. W., and Calafat, A. M. (2017). Urinary bisphenol A (BPA) concentrations among workers in industries that manufacture and use BPA in the USA. *Annals of Work Exposures and Health* **61**(2), 164-182.

Hofmann, M. C., Braydich-Stolle, L., Dettin, L., Johnson, E., and Dym, M. (2005a). Immortalization of mouse germ line stem cells. *Stem Cells* **23**(2), 200-210, 10.1634/stemcells.2003-0036.

Hofmann, M. C., Braydich-Stolle, L., and Dym, M. (2005b). Isolation of male germ-line stem cells; influence of GDNF. *Dev Biol* **279**(1), 114-124, 10.1016/j.ydbio.2004.12.006.

Houshdaran, S., Cortessis, V. K., Siegmund, K., Yang, A., Laird, P. W., and Sokol, R. Z. (2007). Widespread Epigenetic Abnormalities Suggest a Broad DNA Methylation Erasure Defect in Abnormal Human Sperm. *Plos One* **2**(12), ARTN e1289 10.1371/journal.pone.0001289.

Hu, Y. H., Dong, C. C., Chen, M. J., Lu, J., Han, X. M., Qiu, L. L., Chen, Y. S., Qin, J. J., Li, X. C., Gu, A. H., Xia, Y. K., Sun, H., Li, Z., and Wang, Y. B. (2013). Low-dose monobutyl phthalate stimulates steroidogenesis through steroidogenic acute regulatory protein regulated by SF-1, GATA-4 and C/EBP-beta in mouse Leydig tumor cells. *Reprod Biol Endocrin* **11**, Artn 72 10.1186/1477-7827-11-72.

Ibrahim, M. A. A., Elbakry, R. H., and Bayomy, N. A. (2016). Effect of bisphenol A on morphology, apoptosis and proliferation in the resting mammary gland of the adult albino rat. *Int J Exp Pathol* **97**(1), 27-36, 10.1111/iep.12164.

Ikeguchi, M., Sakatani, T., Endo, K., Makino, M., and Kaibara, N. (1999). Computerized nuclear morphometry is a useful technique for evaluating the high metastatic potential of colorectal adenocarcinoma. *Cancer* **86**(10), 1944-1951, Doi 10.1002/(Sici)1097-0142(19991115)86:10<1944::Aid-Cncr10>3.0.Co;2-2.

Jan, E., Byrne, S. J., Cuddihy, M., Davies, A. M., Volkov, Y., Gun'ko, Y. K., and Kotov, N. A. (2008). High-content screening as a universal tool for fingerprinting of cytotoxicity of nanoparticles. *Acs Nano* **2**(5), 928-938, 10.1021/nn7004393.

Jan, S. Z., Hamer, G., Repping, S., de Rooij, D. G., van Pelt, A. M. M., and Vormer, T. L. (2012). Molecular control of rodent spermatogenesis. *Bba-Mol Basis Dis* **1822**(12), 1838-1850, 10.1016/j.bbadis.2012.02.008.

Jenardhanana, P., Panneerselvama, M., and Mathur, P. P. (2016). Effect of environmental contaminants on spermatogenesis. *Semin Cell Dev Biol* **59**, 126-140, 10.1016/j.semcdb.2016.03.024.

Jeng, H. A. (2014). Exposure to endocrine disrupting chemicals and male reproductive health. *Front Public Health* **2**, 55, 10.3389/fpubh.2014.00055.

Ji, K., Hong, S., Kho, Y., and Choi, K. (2013). Effects of Bisphenol S Exposure on Endocrine Functions and Reproduction of Zebrafish. *Environ Sci Technol* **47**(15), 8793-8800, 10.1021/es400329t.

Jin, P., Wang, X., Chang, F., Bai, Y., Li, Y., Zhou, R., and Chen, L. (2013). Low dose bisphenol A impairs spermatogenesis by suppressing reproductive hormone production and promoting germ cell apoptosis in adult rats. *Journal of Biomedical Research* **27**(2), 135-44, 10.7555/JBR.27.20120076.

Jones, T. R., Carpenter, A. E., Lamprecht, M. R., Moffat, J., Silver, S. J., Grenier, J. K., Castoreno, A. B., Eggert, U. S., Root, D. E., Golland, P., and Sabatini, D. M. (2009). Scoring diverse cellular morphologies in image-based screens with iterative feedback and machine learning. *P Natl Acad Sci USA* **106**(6), 1826-1831, 10.1073/pnas.0808843106.

Jones, T. R., Kang, I. H., Wheeler, D. B., Lindquist, R. A., Papallo, A., Sabatini, D. M., Golland, P., and Carpenter, A. E. (2008). CellProfiler Analyst: data exploration and analysis software for complex image-based screens. *Bmc Bioinformatics* **9**, Artn 482 10.1186/1471-2105-9-482.

Judson, R., Houck, K., Martin, M., Richard, A. M., Knudsen, T. B., Shah, I., Little, S., Wambaugh, J., Setzer, R. W., Kothiya, P., Phuong, J., Filer, D., Smith, D., Reif, D., Rotroff, D., Kleinstreuer, N., Sipes, N., Xia, M. H., Huang, R. L., Crofton, K., and Thomas, R. S. (2016). Analysis of the Effects of Cell Stress and Cytotoxicity on In Vitro Assay Activity Across a Diverse Chemical and Assay Space (vol 152, pg 323, 2016). *Toxicol Sci* **153**(2), 409-409, 10.1093/toxsci/kfw148.

Kalb, A. C., Kalb, A. L., Cardoso, T. F., Fernandes, C. G., Corcini, C. D., Varela, A. S., and Martinez, P. E. (2016). Maternal Transfer of Bisphenol A During Nursing Causes Sperm Impairment in Male Offspring. *Arch Environ Con Tox* **70**(4), 793-801, 10.1007/s00244-015-0199-7.

Kamentsky, L., Jones, T. R., Fraser, A., Bray, M. A., Logan, D. J., Madden, K. L., Ljosa, V., Rueden, C., Eliceiri, K. W., and Carpenter, A. E. (2011). Improved structure, function and compatibility for CellProfiler: modular high-throughput image analysis software. *Bioinformatics* **27**(8), 1179-80, 10.1093/bioinformatics/btr095.

Kameoka, S., Babiarz, J., Kolaja, K., and Chiao, E. (2014). A High-Throughput Screen for Teratogens Using Human Pluripotent Stem Cells. *Toxicol Sci* **137**(1), 76-90, 10.1093/toxsci/kft239.

Kang, J. H., Kondo, F., and Katayama, Y. (2006). Human exposure to bisphenol A. *Toxicology* **226**(2-3), 79-89, 10.1016/j.tox.2006.06.009.

Kang, S. Y., Song, J. Y., and Cho, H. H. (2014). Gene expression analysis of uterine smooth muscle cells exposed to bisphenol A. *Toxicology and Environmental Health Sciences* **6**(4), 261-267.

Karmaus, A. L., Filer, D. L., Martin, M. T., and Houck, K. A. (2016a). Evaluation of food-relevant chemicals in the ToxCast high-throughput screening program. *Food Chem Toxicol* **92**, 188-96, 10.1016/j.fct.2016.04.012.

Karmaus, A. L., Toole, C. M., Filer, D. L., Lewis, K. C., and Martin, M. T. (2016b). High-Throughput Screening of Chemical Effects on Steroidogenesis Using H295R Human Adrenocortical Carcinoma Cells. *Toxicol Sci* **150**(2), 323-332, 10.1093/toxsci/kfw002.

Kast, D. J., and Dominguez, R. (2017). The Cytoskeleton-Autophagy Connection. *Curr Biol* **27**(8), R318-R326, 10.1016/j.cub.2017.02.061.

Kavlock, R., Chandler, K., Houck, K., Hunter, S., Judson, R., Kleinstreuer, N., Knudsen, T., Martin, M., Padilla, S., Reif, D., Richard, A., Rotroff, D., Sipes, N., and Dix, D. (2012). Update on EPA's ToxCast Program: Providing High Throughput Decision Support Tools for Chemical Risk Management. *Chem Res Toxicol* **25**(7), 1287-1302, 10.1021/tx3000939.

Kendziorski, J. A., and Belcher, S. M. (2015). Strain-specific induction of endometrial periglandular fibrosis in mice exposed during adulthood to the endocrine disrupting chemical bisphenol A. *Reprod Toxicol* **58**, 119-130, 10.1016/j.reprotox.2015.08.001.

Keri, R. A., Ho, S. M., Hunt, P. A., Knudsen, K. E., Soto, A. M., and Prins, G. S. (2007). An evaluation of evidence for the carcinogenic activity of bisphenol A. *Reprod Toxicol* **24**(2), 240-252, 10.1016/j.reprotox.2007.06.008.

Kierszenbaum, A. L., and Tres, L. L. (2004). The acrosome-acroplaxome-manchette complex and the shaping of the spermatid head. *Arch Histol Cytol* **67**(4), 271-84.

Kim, H. R., Kim, Y. S., Yoon, J. A., Lyu, S. W., Shin, H., Lim, H. J., Hong, S. H., Lee, D. R., and Song, H. (2014). Egr1 is rapidly and transiently induced by estrogen and bisphenol A via activation of nuclear estrogen receptor-dependent ERK1/2 pathway in the uterus. *Reprod Toxicol* **50**, 60-67, 10.1016/j.reprotox.2014.10.010.

Kitamura, S., Suzuki, T., Sanoh, S., Kohta, R., Jinno, N., Sugihara, K., Yoshihara, S., Fujimoto, N., Watanabe, H., and Ohta, S. (2005). Comparative study of the endocrine-disrupting activity of bisphenol A and 19 related compounds. *Toxicol Sci* **84**(2), 249-259, 10.1093/toxsci/kfi074.

Kleymenova, E., Swanson, C., Boekelheide, K., and Gaido, K. W. (2005). Exposure in utero to di(n-butyl) phthalate alters the vimentin cytoskeleton of fetal rat sertoli cells and disrupts sertoli cell-gonocyte contact. *Biol Reprod* **73**(3), 482-490, 10.1095/biolreprod.104.037184.

Knez, J. (2013). Endocrine-disrupting chemicals and male reproductive health. *Reprod Biomed Online* **26**(5), 440-8, 10.1016/j.rbmo.2013.02.005.

Knez, J., Kranvogl, R., Breznik, B. P., Voncina, E., and Vlaisavljevic, V. (2014). Are urinary bisphenol A levels in men related to semen quality and embryo development after medically assisted reproduction? *Fertil Steril* **101**(1), 215-+, 10.1016/j.fertnstert.2013.09.030.

Kokkinaki, M., Lee, T. L., He, Z. P., Jiang, J. J., Golestaneh, N., Hofmann, M. C., Chan, W. Y., and Dym, M. (2009). The Molecular Signature of Spermatogonial Stem/Progenitor Cells in the 6-Day-Old Mouse Testis. *Biol Reprod* **80**(4), 707-717, 10.1095/biolreprod.108.073809.

Komatsu, T., Tabata, M., Kubo-Irie, M., Shimizu, T., Suzuki, K., Nihei, Y., and Takeda, K. (2008). The effects of nanoparticles on mouse testis Leydig cells in vitro. *Toxicol in Vitro* **22**(8), 1825-1831, 10.1016/j.tiv.2008.08.009.

Kotwicka, M., Skibinska, I., Piworun, N., Jendraszak, M., Chmielewska, M., and Jedrzejczak, P. (2016). Bisphenol A modifies human spermatozoa motility in vitro. *Journal of Medical Science* **85**(1), 39-45.

Kraus, O. Z., Grys, B. T., Ba, J., Chong, Y., Frey, B. J., Boone, C., and Andrews, B. J. (2017). Automated analysis of high-content microscopy data with deep learning. *Mol Syst Biol* **13**(4), ARTN 924 10.15252/msb.20177551.

Kremb, S., and Voolstra, C. R. (2017). High-resolution phenotypic profiling of natural products-induced effects on the single-cell level. *Sci Rep* **7**, 44472, 10.1038/srep44472.

Krewski, D., Acosta, D., Andersen, M., Anderson, H., Bailar, J. C., Boekelheide, K., Brent, R., Charnley, G., Cheung, V. G., Green, S., Kelsey, K. T., Kerkvliet, N. I., Li, A. A., McCray, L., Meyer, O., Patterson, R. D., Pennie, W., Scala, R. A., Solomon, G. M., Stephens, M., Yager, J., Zeise, L., and Assess, S. C. T. T. (2010). Toxicity Testing in the 21st Century: A Vision and a Strategy. *J Toxicol Env Heal B* **13**(2-4), 51-138, 10.1080/10937404.2010.483176.

Krug, A. K., Balmer, N. V., Matt, F., Schonenberger, F., Merhof, D., and Leist, M. (2013). Evaluation of a human neurite growth assay as specific screen for developmental neurotoxicants. *Arch Toxicol* **87**(12), 2215-2231, 10.1007/s00204-013-1072-y.

Kuiper, G. G. J. M., Lemmen, J. G., Carlsson, B., Corton, J. C., Safe, S. H., van der Saag, P. T., van der Burg, P., and Gustafsson, J. A. (1998). Interaction of estrogenic chemicals and phytoestrogens with estrogen receptor beta. *Endocrinology* **139**(10), 4252-4263, DOI 10.1210/en.139.10.4252.

Kuiper, R. V., van den Brandhof, E. J., Leonards, P. E. G., van der Ven, L. T. M., Wester, P. W., and Vos, J. G. (2007). Toxicity of tetrabromobisphenol A (TBBPA) in zebrafish (Danio rerio) in a partial life-cycle test. *Arch Toxicol* **81**(1), 1-9, 10.1007/s00204-006-0117-x.

Kuriyama, S. N., Talsness, C. E., Grote, K., and Chahoud, I. (2005). Developmental exposure to low-dose PBDE-99: Effects on male fertility and neurobehavior in rat offspring. *Environ Health Persp* **113**(2), 149-154, 10.1289/ehp.7421.

Lai, D. Y., Kacew, S., and Dekant, W. (2015). Tetrabromobisphenol A (TBBPA): Possible modes of action of toxicity and carcinogenicity in rodents. *Food Chem Toxicol* **80**, 206-214, 10.1016/j.fct.2015.03.023.

Lakind, J. S., and Naiman, D. Q. (2011). Daily intake of bisphenol A and potential sources of exposure: 2005-2006 National Health and Nutrition Examination Survey. *J Expo Sci Env Epid* **21**(3), 272-279, 10.1038/jes.2010.9.

Lang, I. A., Galloway, T. S., Scarlett, A., Henley, W. E., Depledge, M., Wallace, R. B., and Melzer, D. (2008). Association of urinary bisphenol A concentration with medical disorders and laboratory abnormalities in adults. *Jama-J Am Med Assoc* **300**(11), 1303-1310, DOI 10.1001/jama.300.11.1303.

Lassen, T. H., Frederiksen, H., Jensen, T. K., Petersen, J. H., Joensen, U. N., Main, K. M., Skakkebaek, N. E., Juul, A., Jorgensen, N., and Andersson, A. M. (2014). Urinary Bisphenol A Levels in Young Men: Association with Reproductive Hormones and Semen Quality. *Environ Health Persp* **122**(5), 478-484, 10.1289/ehp.1307309.

LeCureux, L., Cheng, C. S., Herbst, J., Reilly, T. P., Lehman-McKeeman, L., and Otieno, M. (2011). Evaluation and validation of multiple cell lines and primary mouse macrophages to predict phospholipidosis potential. *Toxicol in Vitro* **25**(8), 1934-43, 10.1016/j.tiv.2011.06.017.

Lee, H. J., Chattopadhyay, S., Gong, E. Y., Ahn, R. S., and Lee, K. (2003). Antiandrogenic effects of bisphenol A and nonylphenol on the function of androgen receptor. *Toxicol Sci* **75**(1), 40-46, 10.1093/toxsci/kfg150.

Lee, S., and Howell, B. J. (2006). High-content screening: emerging hardware and software technologies. *Methods Enzymol* **414**, 468-83, 10.1016/S0076-6879(06)14025-2.

Lee, S., Liu, X., Takeda, S., and Choi, K. (2013). Genotoxic potentials and related mechanisms of bisphenol A and other bisphenol compounds: A comparison study employing chicken DT40 cells. *Chemosphere* **93**(2), 434-440, 10.1016/j.chemosphere.2013.05.029.

Lee, S. H., Kang, S. M., Choi, M. H., Lee, J., Park, M. J., Kim, S. H., Lee, W. Y., Hong, J., and Chung, B. C. (2014). Changes in steroid metabolism among girls with precocious puberty may not be associated with urinary levels of bisphenol A. *Reprod Toxicol* **44**, 1-6, 10.1016/j.reprotox.2013.03.008.

Lei, B., Xu, J., Peng, W., Wen, Y., Zeng, X., Yu, Z., Wang, Y., and Chen, T. (2016). In vitro profiling of toxicity and endocrine disrupting effects of bisphenol analogues by employing MCF-7 cells and two-hybrid yeast bioassay. *Environ Sci Technol* doi: 10.1002/tox.22234, 10.1002/tox.22234.

Leonard, A. P., Cameron, R. B., Speiser, J. L., Wolf, B. J., Peterson, Y. K., Schnellmann, R. G., Beeson, C. C., and Rohrer, B. (2015). Quantitative analysis of mitochondrial morphology and membrane potential in living cells using high-content imaging, machine learning, and morphological binning. *Bba-Mol Cell Res* **1853**(2), 348-360, 10.1016/j.bbamcr.2014.11.002.

Leung, M. C. K., Phuong, J., Baker, N. C., Sipes, N. S., Klinefelter, G. R., Martin, M. T., McLaurin, K. W., Setzer, R. W., Darney, S. P., Judson, R. S., and Knudsen, T. B. (2016). Systems Toxicology of Male Reproductive Development: Profiling 774 Chemicals for Molecular Targets and Adverse Outcomes. *Environ Health Persp* **124**(7), 1050-1061, 10.1289/ehp.1510385.

Li, J., Sheng, N., Cui, R. N., Feng, Y. X., Shao, B., Guo, X. J., Zhang, H. X., and Dai, J. Y. (2016a). Gestational and lactational exposure to bisphenol AF in maternal rats increases testosterone levels in 23-day-old male offspring. *Chemosphere* **163**, 552-561, 10.1016/j.chemosphere.2016.08.059.

Li, M., Yang, Y. J., Yang, Y., Yin, J., Zhang, J., Feng, Y. X., and Shao, B. (2013). Biotransformation of Bisphenol AF to Its Major Glucuronide Metabolite Reduces Estrogenic Activity. *Plos One* **8**(12), ARTN e83170 10.1371/journal.pone.0083170.

Li, Q., Davila, J., Kannan, A., Flaws, J. A., Bagchi, M. K., and Bagchi, I. C. (2016b). Chronic Exposure to Bisphenol A Affects Uterine Function During Early Pregnancy in Mice. *Endocrinology* **157**(5), 1764-74, 10.1210/en.2015-2031.

LI, Y.-h., Fei, D., Fen, Y., ZHOU, X.-y., PAN, H.-j., Yang, L., and Runsheng, L. (2015). Pubertal exposure to bisphenol A affects the reproduction of male mice and sex ratio of offspring. *Journal of Reproduction and Contraception* **26**(1), 14-21.

Li, Y. C., Zhang, W. C., Liu, J., Wang, W. X., Li, H., Zhu, J. L., Weng, S. Z., Xiao, S. H., and Wu, T. T. (2014). Prepubertal bisphenol A exposure interferes with ovarian follicle development and its relevant gene expression. *Reprod Toxicol* **44**, 33-40, 10.1016/j.reprotox.2013.09.002.

Liang, S., Yin, L., Shengyang Yu, K., Hofmann, M. C., and Yu, X. (2017). High-Content Analysis Provides Mechanistic Insights into the Testicular Toxicity of Bisphenol A and Selected Analogues in Mouse Spermatogonial Cells. *Toxicol Sci* **155**(1), 43-60, 10.1093/toxsci/kfw178.

Liao, C. Y., and Kannan, K. (2013). Concentrations and Profiles of Bisphenol A and Other Bisphenol Analogues in Foodstuffs from the United States and Their Implications for Human Exposure. *J Agr Food Chem* **61**(19), 4655-4662, 10.1021/jf400445n.

Liao, C. Y., and Kannan, K. (2014). A Survey of Alkylphenols, Bisphenols, and Triclosan in Personal Care Products from China and the United States. *Arch Environ Con Tox* **67**(1), 50-59, 10.1007/s00244-014-0016-8.

Liao, C. Y., Liu, F., Alomirah, H., Loi, V. D., Mohd, M. A., Moon, H. B., Nakata, H., and Kannan, K. (2012a). Bisphenol S in Urine from the United States and Seven Asian Countries: Occurrence and Human Exposures. *Environ Sci Technol* **46**(12), 6860-6866, 10.1021/es301334j.

Liao, C. Y., Liu, F., Guo, Y., Moon, H. B., Nakata, H., Wu, Q., and Kannan, K. (2012b). Occurrence of Eight Bisphenol Analogues in Indoor Dust from the United States and Several Asian Countries: Implications for Human Exposure. *Environ Sci Technol* **46**(16), 9138-9145, 10.1021/es302004w.

Liao, C. Y., Liu, F., and Kannan, K. (2012c). Bisphenol S, a New Bisphenol Analogue, in Paper Products and Currency Bills and Its Association with Bisphenol A Residues. *Environ Sci Technol* **46**(12), 6515-6522, 10.1021/es300876n.

Lie, P. P. Y., Mruk, D. D., Lee, W. M., and Cheng, C. Y. (2009). Epidermal growth factor receptor pathway substrate 8 (Eps8) is a novel regulator of cell adhesion and the blood-testis barrier integrity in the seminiferous epithelium. *Faseb J* **23**(8), 2555-2567, 10.1096/fj.06-070573.

Lin, J., Zhu, J., Li, X., Li, S. Q., Lan, Z. J., Ko, J., and Lei, Z. M. (2014). Expression of Genomic Functional Estrogen Receptor 1 in Mouse Sertoli Cells. *Reprod Sci* **21**(11), 1411-1422, 10.1177/1933719114527355.

Liu, C., Duan, W., Li, R., Xu, S., Zhang, L., Chen, C., He, M., Lu, Y., Wu, H., Pi, H., Luo, X., Zhang, Y., Zhong, M., Yu, Z., and Zhou, Z. (2013). Exposure to bisphenol A disrupts meiotic

progression during spermatogenesis in adult rats through estrogen-like activity. *Cell Death Dis* **4**, ARTN e67610.1038/cddis.2013.203.

Liu, C., Duan, W. X., Zhang, L., Xu, S. C., Li, R. Y., Chen, C. H., He, M. D., Lu, Y. H., Wu, H. J., Yu, Z. P., and Zhou, Z. (2014a). Bisphenol A exposure at an environmentally relevant dose induces meiotic abnormalities in adult male rats. *Cell Tissue Res* **355**(1), 223-232, 10.1007/s00441-013-1723-6.

Liu, K., Zhang, G., Wang, Z., Liu, Y., Dong, J., Dong, X., Liu, J., Cao, J., Ao, L., and Zhang, S. (2014b). The protective effect of autophagy on mouse spermatocyte derived cells exposure to 1800MHz radiofrequency electromagnetic radiation. *Toxicol Lett* **228**(3), 216-24, 10.1016/j.toxlet.2014.05.004.

Liu, M. L., Wang, J. L., Wei, J., Xu, L. L., Yu, M., Liu, X. M., Ruan, W. L., and Chen, J. X. (2015a). Tri-ortho-cresyl phosphate induces autophagy of rat spermatogonial stem cells. *Reproduction* **149**(2), 163-70, 10.1530/REP-14-0446.

Liu, X. Q., Miao, M. H., Zhou, Z. J., Gao, E. S., Chen, J. P., Wang, J. T., Sun, F., Yuan, W., and Li, D. K. (2015b). Exposure to bisphenol-A and reproductive hormones among male adults. *Environ Toxicol Phar* **39**(2), 934-941, 10.1016/j.etap.2015.03.007.

Loo, L. H., Wu, L. F., and Altschuler, S. J. (2007). Image-based multivariate profiling of drug responses from single cells. *Nat Methods* **4**(5), 445-453, 10.1038/Nmeth1032.

Lucas, B. E., Fields, C., Joshi, N., and Hofmann, M. C. (2012). Mono-(2-ethylhexyl)-phthalate (MEHP) affects ERK-dependent GDNF signalling in mouse stem-progenitor spermatogonia. *Toxicology* **299**(1), 10-9, 10.1016/j.tox.2012.04.011.

Lui, W. Y., Mruk, D., Lee, W. M., and Cheng, C. Y. (2003). Sertoli cell tight junction dynamics: Their regulation during spermatogenesis. *Biol Reprod* **68**(4), 1087-1097, 10.1095/biolreprod.102.010371.

Lyman, S. K., Crawley, S. C., Gong, R., Adamkewicz, J. I., McGrath, G., Chew, J. Y., Choi, J., Holst, C. R., Goon, L. H., Detmer, S. A., Vaclavikova, J., Gerritsen, M. E., and Blake, R. A. (2011). High-Content, High-Throughput Analysis of Cell Cycle Perturbations Induced by the HSP90 Inhibitor XL888. *Plos One* **6**(3), ARTN e17692 10.1371/journal.pone.0017692.

Mahood, I. K., Hallmark, N., McKinnell, C., Walker, M., Fisher, J. S., and Sharpe, R. M. (2005). Abnormal Leydig cell aggregation in the fetal testis of rats exposed to Di (n-butyl) phthalate and its possible role in testicular dysgenesis. *Endocrinology* **146**(2), 613-623, 10.1210/en.2004-0671.

Mahood, I. K., Scott, H. M., Brown, R., Hallmark, N., Walker, M., and Sharpe, R. M. (2007). In utero exposure to di(n-butyl) phthalate and testicular dysgenesis: comparison of fetal and adult end points and their dose sensitivity. *Environ Health Perspect* **115 Suppl 1**, 55-61, 10.1289/ehp.9366.

Malik, N., Efthymiou, A. G., Mather, K., Chester, N., Wang, X. T., Nath, A., Rao, M. S., and Steiner, J. P. (2014). Compounds with species and cell type specific toxicity identified in a 2000 compound drug screen of neural stem cells and rat mixed cortical neurons. *Neurotoxicology* **45**, 192-200, 10.1016/j.neuro.2014.10.007.

Malumbres, M., and Barbacid, M. (2005). Mammalian cyclin-dependent kinases. *Trends Biochem Sci* **30**(11), 630-41, 10.1016/j.tibs.2005.09.005.

Mansur, A., Adir, M., Yerushalmi, G., Hourvitz, A., Gitman, H., Yung, Y., Orvieto, R., and Machtinger, R. (2016). Does BPA alter steroid hormone synthesis in human granulosa cells in vitro? *Hum Reprod* **31**(7), 1562-1569, 10.1093/humrep/dew088.

Mao, Z. X., Xia, W., Chang, H. L., Huo, W. Q., Li, Y. Y., and Xu, S. Q. (2015). Paternal BPA exposure in early life alters Igf2 epigenetic status in sperm and induces pancreatic impairment in rat offspring. *Toxicol Lett* **238**(3), 30-38, 10.1016/j.toxlet.2015.08.009.

Marchetti, C., Walker, S. A., Odreman, F., Vindigni, A., Doherty, A. J., and Jeggo, P. (2006). Identification of a novel motif in DNA ligases exemplified by DNA ligase IV. *DNA Repair (Amst)* **5**(7), 788-98, 10.1016/j.dnarep.2006.03.011.

Marino, G., Niso-Santano, M., Baehrecke, E. H., and Kroemer, G. (2014). Self-consumption: the interplay of autophagy and apoptosis. *Nat Rev Mol Cell Bio* **15**(2), 81-94, 10.1038/nrm3735.

Martin, H. L., Adams, M., Higgins, J., Bond, J., Morrison, E. E., Bell, S. M., Warriner, S., Nelson, A., and Tomlinson, D. C. (2014). High-Content, High-Throughput Screening for the Identification of Cytotoxic Compounds Based on Cell Morphology and Cell Proliferation Markers. *Plos One* **9**(2), 10.1371/journal.pone.0088338.

Martin, M. T., Knudsen, T. B., Reif, D. M., Houck, K. A., Judson, R. S., Kavlock, R. J., and Dix, D. J. (2011). Predictive Model of Rat Reproductive Toxicity from ToxCast High Throughput Screening. *Biol Reprod* **85**(2), 327-339, 10.1095/biolreprod.111.090977.

Mata, G., Radojevic, M., Smal, I., Morales, M., Meijering, E., and Rubio, J. (2016). Automatic Detection of Neurons in High-Content Microscope Images Using Machine Learning Approaches. *I S Biomed Imaging* doi, 330-333.

Mather, J. P. (1980). Establishment and characterization of two distinct mouse testicular epithelial cell lines. *Biol Reprod* **23**(1), 243-52.

Mathiassen, S. G., De Zio, D., and Cecconi, F. (2017). Autophagy and the Cell Cycle: A

Complex Landscape. *Front Oncol* **7**, ARTN 51

10.3389/fonc.2017.00051.

Matsushima, A., Kakuta, Y., Teramoto, T., Koshiba, T., Liu, X. H., Okada, H., Tokunaga, T.,

Kawabata, S., Kimura, M., and Shimohigashi, Y. (2007). Structural evidence for endocrine

disruptor bisphenol a binding to human nuclear receptor ERR gamma. *J Biochem* **142**(4), 517-

524, 10.1093/jb/mvm158.

Matsushima, A., Liu, X. H., Okada, H., Shimohigashi, M., and Shimohigashi, Y. (2010).

Bisphenol AF Is a Full Agonist for the Estrogen Receptor ER alpha but a Highly Specific

Antagonist for ER beta. *Environ Health Persp* **118**(9), 1267-1272, 10.1289/ehp.0901819.

Mattiazzi Usaj, M., Styles, E. B., Verster, A. J., Friesen, H., Boone, C., and Andrews, B. J.

(2016). High-Content Screening for Quantitative Cell Biology. *Trends Cell Biol* **26**(8), 598-611,

10.1016/j.tcb.2016.03.008.

McGuinness, M. P., and Shaw, R. A. (2010). Functional estrogen receptors in the nucleus and

plasma membrane of TM3 Leydig cell line. *Faseb J* **24**.

Medh, R. D., Santell, L., and Levin, E. G. (1992). Stimulation of Tissue Plasminogen-Activator

Production by Retinoic Acid - Synergistic Effect on Protein-Kinase-C Mediated Activation.

Blood **80**(4), 981-987.

Meeker, J. D., Ehrlich, S., Toth, T. L., Wright, D. L., Calafat, A. M., Trisini, A. T., Ye, X. Y.,

and Hauser, R. (2010). Semen quality and sperm DNA damage in relation to urinary bisphenol A

among men from an infertility clinic. *Reprod Toxicol* **30**(4), 532-539,

10.1016/j.reprotox.2010.07.005.

Melzer, D., Rice, N. E., Lewis, C., Henley, W. E., and Galloway, T. S. (2010). Association of Urinary Bisphenol A Concentration with Heart Disease: Evidence from NHANES 2003/06. *Plos One* **5**(1), ARTN e867310.1371/journal.pone.0008673.

Merrick, B. A., Paules, R. S., and Tice, R. R. (2015). Intersection of toxicogenomics and high throughput screening in the Tox21 program: an NIEHS perspective. *Int J Biotechnol* **14**(1), 7-27, 10.1504/IJBT.2015.074797.

Mesnage, R., Phedonos, A., Arno, M., Balu, S., Christopher Corton, J., and Antoniou, M. N. (2017). Transcriptome profiling reveals bisphenol A alternatives activate estrogen receptor alpha in human breast cancer cells. *Toxicol Sci* doi: 10.1093/toxsci/kfx101, 10.1093/toxsci/kfx101.

Miao, M. H., Yuan, W., Yang, F., Liang, H., Zhou, Z. J., Li, R. S., Gao, E. S., and Li, D. K. (2015). Associations between Bisphenol A Exposure and Reproductive Hormones among Female Workers. *Int J Env Res Pub He* **12**(10), 13240-13250, 10.3390/ijerph121013240.

Minguez-Alarcon, L., Gaskins, A. J., Chiu, Y. H., Williams, P. L., Ehrlich, S., Chavarro, J. E., Petrozza, J. C., Ford, J. B., Calafat, A. M., Hauser, R., and Team, E. S. (2015). Urinary bisphenol A concentrations and association with in vitro fertilization outcomes among women from a fertility clinic. *Hum Reprod* **30**(9), 2120-2128, 10.1093/humrep/dev183.

Mizushima, N., and Komatsu, M. (2011). Autophagy: Renovation of Cells and Tissues. *Cell* **147**(4), 728-741, 10.1016/j.cell.2011.10.026.

Mizushima, N., and Levine, B. (2010). Autophagy in mammalian development and differentiation. *Nature Cell Biology* **12**(9), 823-830.

Molina-Molina, J. M., Amaya, E., Grimaldi, M., Saenz, J. M., Real, M., Fernandez, M. F., Balaguer, P., and Olea, N. (2013). In vitro study on the agonistic and antagonistic activities of

bisphenol-S and other bisphenol-A congeners and derivatives via nuclear receptors. *Toxicol Appl Pharm* **272**(1), 127-136, 10.1016/j.taap.2013.05.015.

Mondal, M. S., Gabriels, J., McGinnis, C., Magnifico, M., Marsilje, T. H., Urban, L., Collis, A., Bojanic, D., Biller, S. A., Frieauff, W., Martus, H. J., Suter, W., and Bentley, P. (2010). High-content micronucleus assay in genotoxicity profiling: initial-stage development and some applications in the investigative/lead-finding studies in drug discovery. *Toxicol Sci* **118**(1), 71-85, 10.1093/toxsci/kfq181.

Moore-Ambriz, T. R., Acuna-Hernandez, D. G., Ramos-Robles, B., Sanchez-Gutierrez, M., Santacruz-Marquez, R., Sierra-Santoyo, A., Pina-Guzman, B., Shibayama, M., and Hernandez-Ochoa, I. (2015). Exposure to bisphenol A in young adult mice does not alter ovulation but does alter the fertilization ability of oocytes. *Toxicol Appl Pharm* **289**(3), 507-514, 10.1016/j.taap.2015.10.010.

Morris, T. A., DeLorenzo, R. J., and Tombes, R. M. (1998). CaMK-II inhibition reduces cyclin D1 levels and enhances the association of p27kip1 with Cdk2 to cause G1 arrest in NIH 3T3 cells. *Exp Cell Res* **240**(2), 218-27, 10.1006/excr.1997.3925.

Mylchreest, E., Sar, M., Wallace, D. G., and Foster, P. M. D. (2002). Fetal testosterone insufficiency and abnormal proliferation of Leydig cells and gonocytes in rats exposed to di(n-butyl) phthalate. *Reprod Toxicol* **16**(1), 19-28, Pii S0890-6238(01)00201-5 Doi 10.1016/S0890-6238(01)00201-5.

Naderi, M., Wong, M. Y. L., and Gholami, F. (2014). Developmental exposure of zebrafish (Danio rerio) to bisphenol-S impairs subsequent reproduction potential and hormonal balance in adults. *Aquat Toxicol* **148**, 195-203, 10.1016/j.aquatox.2014.01.009.

Nakamura, D., Yanagiba, Y., Duan, Z. W., Ito, Y., Okamura, A., Asaeda, N., Tagawa, Y., Li, C. M., Taya, K., Zhang, S. Y., Naito, H., Ramdhan, D. H., Kamijima, M., and Nakajima, T. (2010). Bisphenol A may cause testosterone reduction by adversely affecting both testis and pituitary systems similar to estradiol. *Toxicol Lett* **194**(1-2), 16-25, 10.1016/j.toxlet.2010.02.002.

Nakano, K., Nishio, M., Kobayashi, N., Hiradate, Y., Hoshino, Y., Sato, E., and Tanemura, K. (2015). Comparison of the effects of BPA and BPAF on oocyte spindle assembly and polar body release in mice. *Zygote* doi: 10.1017/S0967199415000027, 1-9, 10.1017/S0967199415000027.

Nakano, K., Nishio, M., Kobayashi, N., Hiradate, Y., Hoshino, Y., Sato, E., and Tanemura, K. (2016). Comparison of the effects of BPA and BPAF on oocyte spindle assembly and polar body release in mice. *Zygote* **24**(2), 172-180, 10.1017/S0967199415000027.

Nanjappa, M. K., Simon, L., and Akingbemi, B. T. (2012). The Industrial Chemical Bisphenol A (BPA) Interferes with Proliferative Activity and Development of Steroidogenic Capacity in Rat Leydig Cells. *Biol Reprod* **86**(5), ARTN 135
10.1095/biolreprod.111.095349.

Neumann, B., Held, M., Liebel, U., Erfle, H., Rogers, P., Pepperkok, R., and Ellenberg, J. (2006). High-throughput RNAi screening by time-lapse imaging of live human cells. *Nat Methods* **3**(5), 385-390, 10.1038/Nmeth876.

Neumann, B., Walter, T., Heriche, J. K., Bulkescher, J., Erfle, H., Conrad, C., Rogers, P., Poser, I., Held, M., Liebel, U., Cetin, C., Sieckmann, F., Pau, G., Kabbe, R., Wunsche, A., Satagopam, V., Schmitz, M. H. A., Chapuis, C., Gerlich, D. W., Schneider, R., Eils, R., Huber, W., Peters, J. M., Hyman, A. A., Durbin, R., Pepperkok, R., and Ellenberg, J. (2010). Phenotypic profiling of the human genome by time-lapse microscopy reveals cell division genes. *Nature* **464**(7289), 721-727, 10.1038/nature08869.

Niedenberger, B. A., Chappell, V. K., Kaye, E. P., Renegar, R. H., and Geyer, C. B. (2013). Nuclear localization of the actin regulatory protein Palladin in sertoli cells. *Mol Reprod Dev* **80**(5), 403-13, 10.1002/mrd.22174.

Nikolova, T., Dvorak, M., Jung, F., Adam, I., Kramer, E., Gerhold-Ay, A., and Kaina, B. (2014). The gamma H2AX Assay for Genotoxic and Nongenotoxic Agents: Comparison of H2AX Phosphorylation with Cell Death Response. *Toxicol Sci* **140**(1), 103-117, 10.1093/toxsci/kfu066.

Nordkap, L., Joensen, U. N., Jensen, M. B., and Jorgensen, N. (2012). Regional differences and temporal trends in male reproductive health disorders: Semen quality may be a sensitive marker of environmental exposures. *Mol Cell Endocrinol* **355**(2), 221-230, 10.1016/j.mce.2011.05.048.

Nurse, P. (1990). Universal Control Mechanism Regulating Onset of M-Phase. *Nature* **344**(6266), 503-508, DOI 10.1038/344503a0.

O'Brien, P. J., Irwin, W., Diaz, D., Howard-Cofield, E., Krejsa, C. M., Slaughter, M. R., Gao, B., Kaludercic, N., Angeline, A., Bernardi, P., Brain, P., and Hougham, C. (2006). High concordance of drug-induced human hepatotoxicity with in vitro cytotoxicity measured in a novel cell-based model using high content screening. *Arch Toxicol* **80**(9), 580-604, 10.1007/s00204-006-0091-3.

Oakes, C. C., La Salle, S., Smiraglia, D. J., Robaire, B., and Trasler, J. M. (2007). A unique configuration of genome-wide DNA methylation patterns in the testis. *P Natl Acad Sci USA* **104**(1), 228-233, 10.1073/pnas.0607521104.

Oatley, J. A., and Brinster, R. L. (2008). Regulation of Spermatogonial Stem Cell Self-Renewal in Mammals. *Annu Rev Cell Dev Bi* **24**, 263-286, 10.1146/annurev.cellbio.24.110707.175355.

Oatley, J. M., and Brinster, R. L. (2012). The Germline Stem Cell Niche Unit in Mammalian Testes. *Physiol Rev* **92**(2), 577-595, 10.1152/physrev.00025.2011.

Ogunbayo, O. A., Lai, P. F., Connolly, T. J., and Michelangeli, F. (2008). Tetrabromobisphenol A (TBBPA), induces cell death in TM4 Sertoli cells by modulating Ca(2+) transport proteins and causing dysregulation of Ca(2+) homeostasis. *Toxicol in Vitro* **22**(4), 943-952, 10.1016/j.tiv.2008.01.015.

Okada, H., Tokunaga, T., Liu, X. H., Takayanagi, S., Matsushima, A., and Shimohigashi, Y. (2008). Direct evidence revealing structural elements essential for the high binding ability of bisphenol A to human estrogen-related receptor-gamma. *Environ Health Persp* **116**(1), 32-38, 10.1289/ehp.10587.

Okuda, K., Takiguchi, M., and Yoshihara, S. (2010). In vivo estrogenic potential of 4-methyl-2,4-bis(4-hydroxyphenyl)pent-1-ene, an active metabolite of bisphenol A, in uterus of ovariectomized rat. *Toxicol Lett* **197**(1), 7-11, 10.1016/j.toxlet.2010.04.017.

Olson, H., Betton, G., Robinson, D., Thomas, K., Monro, A., Kolaja, G., Lilly, P., Sanders, J., Sipes, G., Bracken, W., Dorato, M., Van Deun, K., Smith, P., Berger, B., and Heller, A. (2000). Concordance of the toxicity of pharmaceuticals in humans and in animals. *Regul Toxicol Pharm* **32**(1), 56-67, DOI 10.1006/rtph.2000.1399.

Orlov, N., Shamir, L., Macura, T., Johnston, J., Eckley, D. M., and Goldberg, I. G. (2008). WND-CHARM: Multi-purpose image classification using compound image transforms. *Pattern Recogn Lett* **29**(11), 1684-1693, 10.1016/j.patrec.2008.04.013.

Pacchierotti, F., Ranaldi, R., Eichenlaub-Ritter, U., Attia, S., and Adler, I. D. (2008). Evaluation of aneugenic effects of bisphenol A in somatic and germ cells of the mouse. *Mutat Res-Gen Tox En* **651**(1-2), 64-70, 10.1016/j.mrgentox.2007.10.009.

Parks Saldutti, L., Beyer, B. K., Breslin, W., Brown, T. R., Chapin, R. E., Campion, S., Enright, B., Faustman, E., Foster, P. M., Hartung, T., Kelce, W., Kim, J. H., Loboa, E. G., Piersma, A. H.,

Seyler, D., Turner, K. J., Yu, H., Yu, X., and Sasaki, J. C. (2013). In vitro testicular toxicity models: Opportunities for advancement via biomedical engineering techniques. *Altex* **30**(3), 353-77.

Patisaul, H. B., Mabrey, N., Adewale, H. B., and Sullivan, A. W. (2014). Soy but not bisphenol A (BPA) induces hallmarks of polycystic ovary syndrome (PCOS) and related metabolic co-morbidities in rats. *Reprod Toxicol* **49**, 209-218, 10.1016/j.reprotox.2014.09.003.

Paul Friedman, K., Watt, E. D., Hornung, M. W., Hedge, J. M., Judson, R. S., Crofton, K. M., Houck, K. A., and Simmons, S. O. (2016). Tiered High-Throughput Screening Approach to Identify Thyroperoxidase Inhibitors Within the ToxCast Phase I and II Chemical Libraries. *Toxicol Sci* **151**(1), 160-80, 10.1093/toxsci/kfw034.

Payne, A. H. (1990). Hormonal-Regulation of Cytochrome-P450 Enzymes, Cholesterol Side-Chain Cleavage and 17-Alpha-Hydroxylase C17-20 Lyase in Leydig-Cells. *Biol Reprod* **42**(3), 399-404, DOI 10.1095/biolreprod42.3.399.

Peng, H. C. (2008). Bioimage informatics: a new area of engineering biology. *Bioinformatics* **24**(17), 1827-1836, 10.1093/bioinformatics/btn346.

Peretz, J., Vrooman, L., Ricke, W. A., Hunt, P. A., Ehrlich, S., Hauser, R., Padmanabhan, V., Taylor, H. S., Swan, S. H., VandeVoort, C. A., and Flaws, J. A. (2014). Bisphenol A and Reproductive Health: Update of Experimental and Human Evidence, 2007-2013. *Environ Health Persp* **122**(8), 775-786, 10.1289/ehp.1307728.

Perez, P., Pulgar, R., Olea-Serrano, F., Villalobos, M., Rivas, A., Metzler, M., Pedraza, V., and Olea, N. (1998). The estrogenicity of bisphenol A-related diphenylalkanes with various substituents at the central carbon and the hydroxy groups. *Environ Health Persp* **106**(3), 167-174, DOI 10.1289/ehp.98106167.

Perkins, E. J., Antczak, P., Burgoon, L., Falciani, F., Garcia-Reyero, N., Gutsell, S., Hodges, G., Kienzler, A., Knapen, D., McBride, M., and Willett, C. (2015). Adverse Outcome Pathways for Regulatory Applications: Examination of Four Case Studies With Different Degrees of Completeness and Scientific Confidence. *Toxicol Sci* **148**(1), 14-25, 10.1093/toxsci/kfv181.

Perlman, Z. E., Slack, M. D., Feng, Y., Mitchison, T. J., Wu, L. F., and Altschuler, S. J. (2004). Multidimensional drug profiling by automated microscopy. *Science* **306**(5699), 1194-1198, DOI 10.1126/science.1100709.

Persson, M., and Hornberg, J. J. (2016). Advances in Predictive Toxicology for Discovery Safety through High Content Screening. *Chem Res Toxicol* **29**(12), 1998-2007, 10.1021/acs.chemrestox.6b00248.

Persson, M., Loye, A. F., Jacquet, M., Mow, N. S., Thougaard, A. V., Mow, T., and Hornberg, J. J. (2014). High-Content Analysis/Screening for Predictive Toxicology: Application to Hepatotoxicity and Genotoxicity. *Basic Clin Pharmacol* **115**(1), 18-23, 10.1111/bcpt.12200.

Persson, M., Loye, A. F., Mow, T., and Hornberg, J. J. (2013). A high content screening assay to predict human drug-induced liver injury during drug discovery. *J Pharmacol Tox Met* **68**(3), 302-313, 10.1016/j.vascn.2013.08.001.

Pfeifer, D., Chung, Y. M., and Hu, M. C. T. (2015). Effects of Low-Dose Bisphenol A on DNA Damage and Proliferation of Breast Cells: The Role of c-Myc. *Environ Health Persp* **123**(12), 1271-1279, 10.1289/ehp.1409199.

Phillips, D. H., and Arlt, V. M. (2009). Genotoxicity: damage to DNA and its consequences. *EXS* **99**, 87-110.

Pradip, A., Steel, D., Jacobsson, S., Holmgren, G., Ingelman-Sundberg, M., Sartipy, P., Bjorquist, P., Johansson, I., and Edsbagge, J. (2016). High Content Analysis of Human

Pluripotent Stem Cell Derived Hepatocytes Reveals Drug Induced Steatosis and Phospholipidosis. *Stem Cells Int* **2016**, 2475631, 10.1155/2016/2475631.

Qi, S. Q., Fu, W. J., Wang, C. M., Liu, C. J., Quan, C., Kourouma, A., Yan, M. S., Yu, T. T., Duan, P., and Yang, K. D. (2014). BPA-induced apoptosis of rat Sertoli cells through Fas/FasL and JNKs/p38 MAPK pathways. *Reprod Toxicol* **50**, 108-116, 10.1016/j.reprotox.2014.10.013.

Qian, W. Y., Wang, Y. X., Zhu, J. Y., Mao, C. F., Wang, Q., Huan, F., Cheng, J., Liu, Y. Q., Wang, J., and Xiao, H. (2015). The toxic effects of Bisphenol A on the mouse spermatocyte GC-2 cell line: the role of the Ca2+-calmodulin-Ca2+/calmodulin-dependent protein kinase II axis. *J Appl Toxicol* **35**(11), 1271-1277, 10.1002/jat.3188.

Qian, W. Y., Zhu, J. Y., Mao, C. F., Liu, J. L., Wang, Y. X., Wang, Q., Liu, Y. Q., Gao, R., Xiao, H., and Wang, J. (2014). Involvement of CaM-CaMKII-ERK in bisphenol A-induced Sertoli cell apoptosis. *Toxicology* **324**, 27-34, 10.1016/j.tox.2014.06.001.

Quan, C., Wang, C., Duan, P., Huang, W., Chen, W., Tang, S., and Yang, K. (2016a). Bisphenol a induces autophagy and apoptosis concurrently involving the Akt/mTOR pathway in testes of pubertal SD rats. *Environ Toxicol* doi: 10.1002/tox.22339, 10.1002/tox.22339.

Quan, C., Wang, C., Duan, P., Huang, W., and Yang, K. (2016b). Prenatal bisphenol a exposure leads to reproductive hazards on male offspring via the Akt/mTOR and mitochondrial apoptosis pathways. *Environ Toxicol* doi: 10.1002/tox.22300, 10.1002/tox.22300.

Radio, N. M., Breier, J. M., Shafer, T. J., and Mundy, W. R. (2008). Assessment of chemical effects on neurite outgrowth in PC12 cells using high content screening. *Toxicol Sci* **105**(1), 106-118, 10.1093/toxsci/kfn114.

Rahman, M. S., Kwon, W. S., Karmakar, P. C., Yoon, S. J., Ryu, B. Y., and Pang, M. G. (2016). Gestational Exposure to Bisphenol-A Affects the Function and Proteome Profile of F1 Spermatozoa in Adult Mice. *Environ Health Perspect* doi: 10.1289/EHP378, 10.1289/EHP378.

Rahman, M. S., Kwon, W. S., Lee, J. S., Yoon, S. J., Ryu, B. Y., and Pang, M. G. (2015). Bisphenol-A affects male fertility via fertility-related proteins in spermatozoa. *Sci Rep* **5**, 9169, 10.1038/srep09169.

Ramery, E., and O'Brien, P. J. (2014). Evaluation of the Cytotoxicity of Organic Dust Components on THP1 Monocytes-Derived Macrophages Using High Content Analysis. *Environmental Toxicology* **29**(3), 310-319.

Reif, D. M., Martin, M. T., Tan, S. W., Houck, K. A., Judson, R. S., Richard, A. M., Knudsen, T. B., Dix, D. J., and Kavlock, R. J. (2010). Endocrine Profiling and Prioritization of Environmental Chemicals Using ToxCast Data. *Environ Health Persp* **118**(12), 1714-1720, 10.1289/ehp.1002180.

Reis, M. M. S., Moreira, A. C., Sousa, M., Mathur, P. P., Oliveira, P. F., and Alves, M. G. (2015). Sertoli cell as a model in male reproductive toxicology: Advantages and disadvantages. *J Appl Toxicol* **35**(8), 870-883, 10.1002/jat.3122.

Repetto, G., del Peso, A., and Zurita, J. L. (2008). Neutral red uptake assay for the estimation of cell viability/cytotoxicity. *Nat Protoc* **3**(7), 1125-1131, 10.1038/nprot.2008.75.

Richter, C. A., Birnbaum, L. S., Farabollini, F., Newbold, R. R., Rubin, B. S., Talsness, C. E., Vandenbergh, J. G., Walser-Kuntz, D. R., and vom Saal, F. S. (2007). In vivo effects of bisphenol A in laboratory rodent studies. *Reprod Toxicol* **24**(2), 199-224, 10.1016/j.reprotox.2007.06.004.

Riu, A., Grimaldi, M., le Maire, A., Bey, G., Phillips, K., Boulahtouf, A., Perdu, E., Zalko, D., Bourguet, W., and Balaguer, P. (2011). Peroxisome Proliferator-Activated Receptor gamma Is a Target for Halogenated Analogs of Bisphenol A. *Environ Health Persp* **119**(9), 1227-1232, 10.1289/ehp.1003328.

Rochester, J. R. (2013). Bisphenol A and human health: A review of the literature. *Reprod Toxicol* **42**, 132-155, 10.1016/j.reprotox.2013.08.008.

Rochester, J. R., and Bolden, A. L. (2015). Bisphenol S and F: A Systematic Review and Comparison of the Hormonal Activity of Bisphenol A Substitutes. *Environ Health Persp* **123**(7), 643-650, 10.1289/ehp.1408989.

Roelofs, M. J. E., van den Berg, M., Bovee, T. F. H., Piersma, A. H., and van Duursen, M. B. M. (2015). Structural bisphenol analogues differentially target steroidogenesis in murine MA-10 Leydig cells as well as the glucocorticoid receptor. *Toxicology* **329**, 10-20, 10.1016/j.tox.2015.01.003.

Rogakou, E. P., Pilch, D. R., Orr, A. H., Ivanova, V. S., and Bonner, W. M. (1998). DNA double-stranded breaks induce histone H2AX phosphorylation on serine 139. *J Biol Chem* **273**(10), 5858-5868, DOI 10.1074/jbc.273.10.5858.

Roukos, V., Pegoraro, G., Voss, T. C., and Misteli, T. (2015). Cell cycle staging of individual cells by fluorescence microscopy. *Nat Protoc* **10**(2), 334-48, 10.1038/nprot.2015.016.

Ruwanpura, S. M., McLachlan, R. I., and Meachem, S. J. (2010). Hormonal regulation of male germ cell development. *J Endocrinol* **205**(2), 117-131, 10.1677/Joe-10-0025.

Ryan, K. R., Sirenko, O., Parham, F., Hsieh, J. H., Cromwell, E. F., Tice, R. R., and Behl, M. (2016). Neurite outgrowth in human induced pluripotent stem cell-derived neurons as a high-

throughput screen for developmental neurotoxicity or neurotoxicity. *Neurotoxicology* **53**, 271-281, 10.1016/j.neuro.2016.02.003.

Sadowski, R. N., Park, P., Neese, S. L., Ferguson, D. C., Schantz, S. L., and Juraska, J. M. (2014). Effects of perinatal bisphenol A exposure during early development on radial arm maze behavior in adult male and female rats. *Neurotoxicol Teratol* **42**, 17-24, 10.1016/Intt.2014.01.002.

Saegusa, Y., Fujimoto, H., Woo, G. H., Inoue, K., Takahashi, M., Mitsumori, K., Hirose, M., Nishikawa, A., and Shibutani, M. (2009). Developmental toxicity of brominated flame retardants, tetrabromobisphenol A and 1,2,5,6,9,10-hexabromocyclododecane, in rat offspring after maternal exposure from mid-gestation through lactation. *Reprod Toxicol* **28**(4), 456-467, 10.1016/j.reprotox.2009.06.011.

Saffarini, C. M., Heger, N. E., Yamasaki, H., Liu, T., Hall, S. J., and Boekelheide, K. (2012). Induction and persistence of abnormal testicular germ cells following gestational exposure to di-(n-butyl) phthalate in p53-null mice. *J Androl* **33**(3), 505-13, 10.2164/jandrol.111.013706.

Saito, J., Okamura, A., Takeuchi, K., Hanioka, K., Okada, A., and Ohata, T. (2016). High content analysis assay for prediction of human hepatotoxicity in HepaRG and HepG2 cells. *Toxicol in Vitro* **33**, 63-70, 10.1016/j.tiv.2016.02.019.

Sakaue, M., Ohsako, S., Ishimura, R., Kurosawa, S., Kurohmaru, M., Hayashi, Y., Aoki, Y., Yonemoto, J., and Tohyama, C. (2001). Bisphenol-A affects spermatogenesis in the adult rat even at a low dose. *J Occup Health* **43**(4), 185-190, DOI 10.1539/joh.43.185.

Salleh, N., Giribabu, N., Feng, A. O. M., and Myint, K. (2015). Bisphenol A, Dichlorodiphenyltrichloroethane (DDT) and Vinclozolin Affect ex-vivo Uterine Contraction in

Rats via Uterotonin (Prostaglandin F2 alpha, Acetylcholine and Oxytocin) Related Pathways. *Int J Med Sci* **12**(11), 914-925, 10.7150/ijms.11957.

Santamaria, C., Durando, M., de Toro, M. M., Luque, E. H., and Rodriguez, H. A. (2016). Ovarian dysfunctions in adult female rat offspring born to mothers perinatally exposed to low doses of bisphenol A. *J Steroid Biochem* **158**, 220-230, 10.1016/j.jsbmb.2015.11.016.

Schmitz, M. H., Held, M., Janssens, V., Hutchins, J. R., Hudecz, O., Ivanova, E., Goris, J., Trinkle-Mulcahy, L., Lamond, A. I., Poser, I., Hyman, A. A., Mechtler, K., Peters, J. M., and Gerlich, D. W. (2010). Live-cell imaging RNAi screen identifies PP2A-B55alpha and importin-beta1 as key mitotic exit regulators in human cells. *Nat Cell Biol* **12**(9), 886-93, 10.1038/ncb2092.

Schneider, C. A., Rasband, W. S., and Eliceiri, K. W. (2012). NIH Image to ImageJ: 25 years of image analysis. *Nat Methods* **9**(7), 671-675, 10.1038/nmeth.2089.

Schoonen, W. G. E. J., de Roos, J. A. D. M., Westerink, W. M. A., and Debiton, E. (2005). Cytotoxic effects of 110 reference compounds on HepG2 cells and for 60 compounds on HeLa, ECC-1 and CHO cells. II - Mechanistic assays on NAD(P)H, ATP and DNA contents. *Toxicol in Vitro* **19**(4), 491-503, 10.1016/j.tiv.2005.01.002.

Schurdak, M. E., Vernetti, L. A., Abel, S. J., and Thiffault, C. (2007). Adaptation of an in vitro phospholipidosis assay to an automated image analysis system. *Toxicol Mech Method* **17**(2), 77-86, 10.1080/15376510600860185.

Scinicariello, F., and Buser, M. C. (2016). Serum Testosterone Concentrations and Urinary Bisphenol A, Benzophenone-3, Triclosan, and Paraben Levels in Male and Female Children and Adolescents: NHANES 2011-2012. *Environ Health Perspect* **124**(12), 1898-1904, 10.1289/EHP150.

Setchell, B. P. (2008). Blood-Testis Barrier, Junctional and Transport Proteins and Spermatogenesis. *Molecular Mechanisms in Spermatogenesis* **636**, 212-233.

Shahane, S. A., Huang, R. L., Gerhold, D., Baxa, U., Austin, C. P., and Xia, M. H. (2014). Detection of Phospholipidosis Induction: A Cell-Based Assay in High-Throughput and High-Content Format. *J Biomol Screen* **19**(1), 66-76, 10.1177/1087057113502851.

Shen, Y., Ren, M. L., Feng, X., Cai, Y. L., Gao, Y. X., and Xu, Q. (2014). An evidence in vitro for the influence of bisphenol A on uterine leiomyoma. *Eur J Obstet Gyn R B* **178**, 80-83, 10.1016/j.ejogrb.2014.03.052.

Shi, J. C., Jiao, Z. H., Zheng, S., Li, M., Zhang, J., Feng, Y. X., Yin, J., and Shao, B. (2015). Long-term effects of Bisphenol AF (BPAF) on hormonal balance and genes of hypothalamus-pituitary-gonad axis and liver of zebrafish (Danio rerio), and the impact on offspring. *Chemosphere* **128**, 252-257, 10.1016/j.chemosphere.2015.01.060.

Shi, Z. X., Jiao, Y., Hu, Y., Sun, Z. W., Zhou, X. Q., Feng, J. F., Li, J. G., and Wu, Y. N. (2013). Levels of tetrabromobisphenol A, hexabromocyclododecanes and polybrominated diphenyl ethers in human milk from the general population in Beijing, China. *Sci Total Environ* **452**, 10-18, 10.1016/j.scitotenv.2013.02.038.

Shukla, S. J., Huang, R., Austin, C. P., and Xia, M. (2010). The future of toxicity testing: a focus on in vitro methods using a quantitative high-throughput screening platform. *Drug Discov Today* **15**(23-24), 997-1007, 10.1016/j.drudis.2010.07.007.

Sidhu, J. S., Ponce, R. A., Vredevoogd, M. A., Yu, X. Z., Gribble, E., Hong, S. W., Schneider, E., and Faustman, E. M. (2006). Cell cycle inhibition by sodium arsenite in primary embryonic rat midbrain neuroepithelial cells. *Toxicol Sci* **89**(2), 475-484, 10.1093/toxsci/kfj032.

248

Simonelli, A., Guadagni, R., De Franciscis, P., Colacurci, N., Pieri, M., Basilicata, P., Pedata, P., Lamberti, M., Sannolo, N., and Miraglia, N. (2017). Environmental and occupational exposure to bisphenol A and endometriosis: urinary and peritoneal fluid concentration levels. *Int Arch Occup Environ Health* **90**(1), 49-61, 10.1007/s00420-016-1171-1.

Singh, D. K., Ku, C. J., Wichaidit, C., Steininger, R. J., Wu, L. F., and Altschuler, S. J. (2010). Patterns of basal signaling heterogeneity can distinguish cellular populations with different drug sensitivities. *Mol Syst Biol* **6**, ARTN 369

10.1038/msb.2010.22.

Singh, S., Carpenter, A. E., and Genovesio, A. (2014a). Increasing the Content of High-Content Screening: An Overview. *J Biomol Screen* **19**(5), 640-50, 10.1177/1087057114528537.

Singh, S., Carpenter, A. E., and Genovesio, A. (2014b). Increasing the Content of High-Content Screening: An Overview. *Journal of Biomolecular Screening* **19**(5), 640-650, 10.1177/1087057114528537.

Sirenko, O., Mitlo, T., Hesley, J., Luke, S., Owens, W., and Cromwell, E. F. (2015). High-Content Assays for Characterizing the Viability and Morphology of 3D Cancer Spheroid Cultures. *Assay Drug Dev Techn* **13**(7), 402-414, 10.1089/adt.2015.655.

Skakkebaek, N. E., Rajpert-De Meyts, E., Louis, G. M. B., Toppari, J., Andersson, A. M., Eisenberg, M. L., Jensen, T. K., Jorgensen, N., Swan, S. H., Sapra, K. J., Ziebe, S., Priskorn, L., and Juul, A. (2016). Male Reproductive Disorders and Fertility Trends: Influences of Environment and Genetic Susceptibility. *Physiol Rev* **96**(1), 55-97, 10.1152/physrev.00017.2015.

Skledar, D. G., and Masic, L. P. (2016). Bisphenol A and its analogs: Do their metabolites have endocrine activity? *Environ Toxicol Phar* **47**, 182-199, 10.1016/j.etap.2016.09.014.

Skledar, D. G., Schmidt, J., Fic, A., Klopcic, I., Trontelj, J., Dolenc, M. S., Finel, M., and Masic, L. P. (2016). Influence of metabolism on endocrine activities of bisphenol S. *Chemosphere* **157**, 152-159, 10.1016/j.chemosphere.2016.05.027.

Sommer, C., and Gerlich, D. W. (2013). Machine learning in cell biology - teaching computers to recognize phenotypes. *Journal of Cell Science* **126**(24), 5529-5539, 10.1242/jcs.123604.

Stiegler, N. V., Krug, A. K., Matt, F., and Leist, M. (2011). Assessment of Chemical-Induced Impairment of Human Neurite Outgrowth by Multiparametric Live Cell Imaging in High-Density Cultures. *Toxicol Sci* **121**(1), 73-87, 10.1093/toxsci/kfr034.

Stossi, F., Bolt, M. J., Ashcroft, F. J., Lamerdin, J. E., Melnick, J. S., Powell, R. T., Dandekar, R. D., Mancini, M. G., Walker, C. L., Westwick, J. K., and Mancini, M. A. (2014). Defining Estrogenic Mechanisms of Bisphenol A Analogs through High Throughput Microscopy-Based Contextual Assays. *Chem Biol* **21**(6), 743-753, 10.1016/j.chembiol.2014.03.013.

Su, L., Agati, J. M., and Parsons, S. J. (2003). p190RhoGAP is cell cycle regulated and affects cytokinesis. *J Cell Biol* **163**(3), 571-582, 10.1083/jcb.200308007.

Sun, X., Kovacs, T., Hu, Y. J., and Yang, W. X. (2011). The role of actin and myosin during spermatogenesis. *Mol Biol Rep* **38**(6), 3993-4001, 10.1007/s11033-010-0517-0.

Sutherland., V., McIntyre., B., Pelch., K., Waidyanatha., S., Conley., J. M., Gray., L. E., and Foster, P. M. A Comparison of In Vivo Reproductive and Developmental Toxicity (DART) Endpoints for Bisphenol AF and Bisphenol A2017, Baltimore, Maryland.

Svingen, T., Lund Hansen, N., Taxvig, C., Vinggaard, A. M., Jensen, U., and Have Rasmussen, P. (2017). Enniatin B and beauvericin are common in Danish cereals and show high hepatotoxicity on a high-content imaging platform. *Environ Toxicol* **32**(5), 1658-1664, 10.1002/tox.22367.

Tada, Y., Fujitani, T., Yano, N., Takahashi, H., Yuzawa, K., Ando, H., Kubo, Y., Nagasawa, A., Ogata, A., and Kamimura, H. (2006). Effects of tetrabromobisphenol A, brominated flame retardant, in ICR mice after prenatal and postnatal exposure. *Food Chem Toxicol* **44**(8), 1408-1413, 10.1016/j.fct.2006.03.006.

Takao, T., Nanamiya, W., Nagano, I., Asaba, K., Kawabata, K., and Hashimoto, K. (1999). Exposure with the environmental estrogen bisphenol A disrupts the male reproductive tract in young mice. *Life Sci* **65**(22), 2351-2357, Doi 10.1016/S0024-3205(99)00502-0.

Tang, W. Y., Morey, L. M., Cheung, Y. Y., Birch, L., Prins, G. S., and Ho, S. M. (2012). Neonatal Exposure to Estradiol/Bisphenol A Alters Promoter Methylation and Expression of Nsbp1 and Hpcal1 Genes and Transcriptional Programs of Dnmt3a/b and Mbd2/4 in the RatProstate Gland Throughout Life. *Endocrinology* **153**(1), 42-55, 10.1210/en.2011-1308.

Tarca, A. L., Carey, V. J., Chen, X. W., Romero, R., and Draghici, S. (2007). Machine learning and its applications to biology. *Plos Comput Biol* **3**(6), 953-963, ARTN e116 10.1371/journal.pcbi.0030116.

Thompson, C. M., Fedorov, Y., Brown, D. D., Suh, M., Proctor, D. M., Kuriakose, L., Haws, L. C., and Harris, M. A. (2012). Assessment of Cr(VI)-Induced Cytotoxicity and Genotoxicity Using High Content Analysis. *Plos One* **7**(8), ARTN e42720 10.1371/journal.pone.0042720.

Tice, R. R., Austin, C. P., Kavlock, R. J., and Bucher, J. R. (2013). Improving the Human Hazard Characterization of Chemicals: A Tox21 Update. *Environ Health Persp* **121**(7), 756-765, 10.1289/ehp.1205784.

Tilmant, K., Gerets, H. H. J., De Ron, P., Cossu-Leguille, C., Vasseur, P., Dhalluin, S., and Atienzar, F. A. (2013). The automated micronucleus assay for early assessment of genotoxicity in drug discovery. *Mutat Res-Gen Tox En* **751**(1), 1-11, 10.1016/j.mrgentox.2012.10.011.

Tiwari, D., Kamble, J., Chilgunde, S., Patil, P., Maru, G., Kawle, D., Bhartiya, U., Joseph, L., and Vanage, G. (2012). Clastogenic and mutagenic effects of bisphenol A: An endocrine disruptor. *Mutat Res-Gen Tox En* **743**(1-2), 83-90, 10.1016/j.mrgentox.2011.12.023.

Tiwari, D., and Vanage, G. (2013). Mutagenic effect of Bisphenol A on adult rat male germ cells and their fertility. *Reprod Toxicol* **40**, 60-8, 10.1016/j.reprotox.2013.05.013.

Tokarz, J., Moller, G., de Angelis, M. H., and Adamski, J. (2013). Zebrafish and steroids: What do we know and what do we need to know? *J Steroid Biochem* **137**, 165-173, 10.1016/j.jsbmb.2013.01.003.

Tolosa, L., Gomez-Lechon, M. J., Perez-Cataldo, G., Castell, J. V., and Donato, M. T. (2013). HepG2 cells simultaneously expressing five P450 enzymes for the screening of hepatotoxicity: identification of bioactivable drugs and the potential mechanism of toxicity involved. *Arch Toxicol* **87**(6), 1115-1127, 10.1007/s00204-013-1012-x.

Tolosa, L., Pinto, S., Donato, M. T., Lahoz, A., Castell, J. V., O'Connor, J. E., and Gomez-Lechon, M. J. (2012). Development of a Multiparametric Cell-based Protocol to Screen and Classify the Hepatotoxicity Potential of Drugs. *Toxicol Sci* **127**(1), 187-198, 10.1093/toxsci/kfs083.

Trasler, J. M. (2009). Epigenetics in spermatogenesis. *Mol Cell Endocrinol* **306**(1-2), 33-36, 10.1016/j.mce.2008.12.018.

Uhlmann, V., Singh, S., and Carpenter, A. E. (2016). CP-CHARM: segmentation-free image classification made accessible. *Bmc Bioinformatics* **17**, ARTN 51

10.1186/s12859-016-0895-y.

Ullah, H., Jahan, S., Ul Ain, Q., Shaheen, G., and Ahsan, N. (2016). Effect of bisphenol S exposure on male reproductive system of rats: A histological and biochemical study. *Chemosphere* **152**, 383-391, 10.1016/j.chemosphere.2016.02.125.

Upson, K., Sathyanarayana, S., De Roos, A. J., Koch, H. M., Scholes, D., and Holt, V. L. (2014). A population-based case-control study of urinary bisphenol A concentrations and risk of endometriosis. *Hum Reprod* **29**(11), 2457-2464, 10.1093/humrep/deu227.

Usman, A., and Ahmad, M. (2016). From BPA to its analogues: Is it a safe journey? *Chemosphere* **158**, 131-42, 10.1016/j.chemosphere.2016.05.070.

Vagi, S. J., Azziz-Baumgartner, E., Sjodin, A., Calafat, A. M., Dumesic, D., Gonzalez, L., Kato, K., Silva, M. J., Ye, X. Y., and Azziz, R. (2014). Exploring the potential association between brominated diphenyl ethers, polychlorinated biphenyls, organochlorine pesticides, perfluorinated compounds, phthalates, and bisphenol a in polycystic ovary syndrome: a case-control study. *Bmc Endocr Disord* **14**, Artn 86 10.1186/1472-6823-14-86.

Vahedi, M., Saeedi, A., Poorbaghi, S. L., Sepehrimanesh, M., and Fattahi, M. (2016). Metabolic and endocrine effects of bisphenol A exposure in market seller women with polycystic ovary syndrome. *Environ Sci Pollut Res Int* **23**(23), 23546-23550, 10.1007/s11356-016-7573-5.

van de Water, F. M., Havinga, J., Ravesloot, W. T., Horbach, G. J. M. J., and Schoonen, W. G. E. J. (2011). High content screening analysis of phospholipidosis: Validation of a 96-well assay with CHO-K1 and HepG2 cells for the prediction of in vivo based phospholipidosis. *Toxicol in Vitro* **25**(8), 1870-1882, 10.1016/j.tiv.2011.05.026.

Van der Ven, L. T. M., de Kuil, T. V., Verhoef, A., Verwer, C. M., Lilienthal, H., Leonards, P. E. G., Schauer, U. M. D., Canton, R. F., Litens, S., De Jong, F. H., Visser, T. J., Dekant, W.,

Stern, N., Hakansson, H., Slob, W., Van den Berg, M., Vos, J. G., and Piersma, A. H. (2008). Endocrine effects of tetrabromobisphenol-A (TBBPA) in Wistar rats as tested in a one-generation reproduction study and a subacute toxicity study. *Toxicology* **245**(1-2), 76-89, 10.1016/j.tox.2007.12.009.

Vandenberg, L. N., Hauser, R., Marcus, M., Olea, N., and Welshons, W. V. (2007). Human exposure to bisphenol A (BPA). *Reprod Toxicol* **24**(2), 139-177, 10.1016/j.reprotox.2007.07.010.

Versaevel, M., Grevesse, T., and Gabriele, S. (2012). Spatial coordination between cell and nuclear shape within micropatterned endothelial cells. *Nat Commun* **3**, ARTN 67110.1038/ncomms1668.

Vidal, J. D., and Whitney, K. M. (2014). Morphologic manifestations of testicular and epididymal toxicity. *Spermatogenesis* **4**(2), e979099, 10.4161/21565562.2014.979099.

Vigezzi, L., Bosquiazzo, V. L., Kass, L., Ramos, J. G., Munoz-De-Toro, M., and Luque, E. H. (2015). Developmental exposure to bisphenol A alters the differentiation and functional response of the adult rat uterus to estrogen treatment. *Reprod Toxicol* **52**, 83-92, 10.1016/j.reprotox.2015.01.011.

Vilela, J., Hartmann, A., Silva, E. F., Cardoso, T., Corcini, C. D., Varela, A. S., Martinez, P. E., and Colares, E. P. (2014). Sperm impairments in adult vesper mice (Calomys laucha) caused by in utero exposure to bisphenol A. *Andrologia* **46**(9), 971-978, 10.1111/and.12182.

Vinggaard, A. M., Niemela, J., Wedebye, E. B., and Jensen, G. E. (2008). Screening of 397 chemicals and development of a quantitative structure-activity relationship model for androgen receptor antagonism. *Chem Res Toxicol* **21**(4), 813-823, 10.1021/tx7002382.

Vogl, A. W. (1989). Distribution and Function of Organized Concentrations of Actin-Filaments in Mammalian Spermatogenic Cells and Sertoli Cells. *Int Rev Cytol* **119**, 1-56.

vom Saal, F. S., Akingbemi, B. T., Belcher, S. M., Birnbaum, L. S., Crain, D. A., Eriksen, M., Farabollini, F., Guillette, L. J., Hauser, R., Heindel, J. J., Ho, S. M., Hunt, P. A., Iguchi, T., Jobling, S., Kanno, J., Keri, R. A., Knudsen, K. E., Laufer, H., LeBlanc, G. A., Marcus, M., McLachlan, J. A., Myers, J. P., Nadal, A., Newbold, R. R., Olea, N., Prins, G. S., Richter, C. A., Rubin, B. S., Sonnenschein, C., Soto, A. M., Talsness, C. E., Vandenbergh, J. G., Vandenberg, L. N., Walser-Kuntz, D. R., Watson, C. S., Welshons, W. V., Wetherill, Y., and Zoeller, R. T. (2007). Chapel Hill bisphenol A expert panel consensus statement: Integration of mechanisms, effects in animals and potential to impact human health at current levels of exposure. *Reprod Toxicol* **24**(2), 131-138, 10.1016/j.reprotox.2007.07.005.

Vrooman, L. A., Oatley, J. M., Griswold, J. E., Hassold, T. J., and Hunt, P. A. (2015). Estrogenic Exposure Alters the Spermatogonial Stem Cells in the Developing Testis, Permanently Reducing Crossover Levels in the Adult. *Plos Genet* **11**(1), ARTN e1004949 10.1371/journal.pgen.1004949.

Wan, X., Ru, Y., Chu, C., Ni, Z., Zhou, Y., Wang, S., Zhou, Z., and Zhang, Y. (2016). Bisphenol A accelerates capacitation-associated protein tyrosine phosphorylation of rat sperm by activating protein kinase A. *Acta Biochim Biophys Sin (Shanghai)* **48**(6), 573-80, 10.1093/abbs/gmw039.

Wang, C., Qi, S., Liu, C., Yang, A., Fu, W., Quan, C., Duan, P., Yu, T., and Yang, K. (2016a). Mitochondrial Dysfunction and Ca2+ Overload in Injured Sertoli Cells Exposed to Bisphenol A. *Environ Toxicol* doi: 10.1002/tox.22282, 10.1002/tox.22282.

Wang, C. M., Fu, W. J., Quan, C., Yan, M. S., Liu, C. J., Qi, S. Q., and Yang, K. D. (2015a). The role of Pten/Akt signaling pathway involved in BPA-induced apoptosis of rat sertoli cells. *Environmental Toxicology* **30**(7), 793-802, 10.1002/tox.21958.

Wang, H. F., Liu, M., Li, N., Luo, T., Zheng, L. P., and Zeng, X. H. (2016b). Bisphenol A Impairs Mature Sperm Functions by a CatSper-Relevant Mechanism. *Toxicol Sci* **152**(1), 145-54, 10.1093/toxsci/kfw070.

Wang, H. F., Liu, M., Li, N., Luo, T., Zheng, L. P., and Zeng, X. H. (2016c). Bisphenol A Impairs Mature Sperm Functions by a CatSper-Relevant Mechanism. *Toxicol. Sci.* **152**(1), 145-54, 10.1093/toxsci/kfw070.

Wang, K. H., Kao, A. P., Chang, C. C., Lin, T. C., and Kuo, T. C. (2015b). Bisphenol A-induced epithelial to mesenchymal transition is mediated by cyclooxygenase-2 up-regulation in human endometrial carcinoma cells. *Reprod Toxicol* **58**, 229-233, 10.1016/j.reprotox.2015.10.011.

Wang, L., Wang, M., Wang, S. Y., Qi, T. Y., Guo, L. J., Li, J. J., Qi, W. J., Ampah, K. K., Ba, X. Q., and Zeng, X. L. (2013). Actin Polymerization Negatively Regulates p53 Function by Impairing Its Nuclear Import in Response to DNA Damage. *Plos One* **8**(4), ARTN e60179 10.1371/journal.pone.0060179.

Wang, P., Luo, C. H., Li, Q. Y., Chen, S., and Hue, Y. (2014). Mitochondrion-mediated apoptosis is involved in reproductive damage caused by BPA in male rats. *Environ Toxicol Phar* **38**(3), 1025-1033, 10.1016/j.etap.2014.10.018.

Wang, T., Han, J., Duan, X., Xiong, B., Cui, X. S., Kim, N. H., Liu, H. L., and Sun, S. C. (2016d). The toxic effects and possible mechanisms of Bisphenol A on oocyte maturation of porcine in vitro. *Oncotarget* **7**(22), 32554-32565, 10.18632/oncotarget.8689.

Webster, M., Witkin, K. L., and Cohen-Fix, O. (2009). Sizing up the nucleus: nuclear shape, size and nuclear-envelope assembly. *Journal of Cell Science* **122**(Pt 10), 1477-86, 10.1242/jcs.037333.

Wegner, S., Hong, S., Yu, X., and Faustman, E. M. (2013). Preparation of rodent testis co-cultures. *Current Protocols in Toxicology* **Chapter 16**, Unit 16 10, 10.1002/0471140856.tx1610s55.

Wegner, S., Yu, X., Kim, S., Harris, S., Griffith, W. C., Hong, S., and Faustman, E. M. (2014). Effect of dipentyl phthalate in 3-dimensional in vitro testis co-culture is attenuated by cyclooxygenase-2 inhibition. *Journal of Toxicology and Environmental Health Sciences* **6(8)**, 161-169.

Westerink, W. M. A., Schirris, T. J. J., Horbach, G. J., and Schoonen, W. G. E. J. (2011). Development and validation of a high-content screening in vitro micronucleus assay in CHO-k1 and HepG2 cells. *Mutat Res-Gen Tox En* **724**(1-2), 7-21, 10.1016/j.mrgentox.2011.05.007.

Williams, J., and Foster, P. M. D. (1987). The Effect of 1,3-Dinitrobenzene and Mono-(2-Ethylhexyl)Phthalate on Lactate and Pyruvate Production by Rat Sertoli-Cell Cultures. *Arch Toxicol* doi, P6-P6.

Wisniewski, P., Romano, R. M., Kizys, M. M. L., Oliveira, K. C., Kasamatsu, T., Giannocco, G., Chiamolera, M. I., Dias-Da-Silva, M. R., and Romano, M. A. (2015). Adult exposure to bisphenol A (BPA) in Wistar rats reduces sperm quality with disruption of the hypothalamic-pituitary-testicular axis. *Toxicology* **329**, 1-9, 10.1016/j.tox.2015.01.002.

Wong, E. W. P., Mruk, D. D., and Cheng, C. Y. (2008). Biology and regulation of ectoplasmic specialization, an atypical adherens junction type, in the testis. *Bba-Biomembranes* **1778**(3), 692-708, 10.1016/j.bbamem.2007.11.006.

Wozniak, A. L., Bulayeva, N. N., and Watson, C. S. (2005). Xenoestrogens at picomolar to nanomolar concentrations trigger membrane estrogen receptor-alpha-mediated Ca2+ fluxes and

prolactin release in GH3/B6 pituitary tumor cells. *Environ Health Persp* **113**(4), 431-439, 10.1289/ehp.7505.

Wu, S., Wei, X. T., Jiang, J. J., Shang, L. Q., and Hao, W. D. (2012). Effects of bisphenol A on the proliferation and cell cycle of HBL-100 cells. *Food Chem Toxicol* **50**(9), 3100-3105, 10.1016/j.fct.2012.06.029.

Wu, X., Majumder, A., Webb, R., and Stice, S. L. (2016). High content imaging quantification of multiple in vitro human neurogenesis events after neurotoxin exposure. *Bmc Pharmacol Toxico* **17**, ARTN 62   10.1186/s40360-016-0107-4.

Wu, X., Yang, X., Majumder, A., Swetenburg, R., Goodfellow, F. T., Bartlett, M. G., and Stice, S. L. (2017). From the Cover: AstrocytesAre Protective Against Chlorpyrifos Developmental Neurotoxicity in Human Pluripotent Stem Cell-Derived Astrocyte-Neuron Cocultures. *Toxicol Sci* **157**(2), 410-420, 10.1093/toxsci/kfx056.

Xiao, X., Mruk, D. D., Tang, E. I., Wong, C. K., Lee, W. M., John, C. M., Turek, P. J., Silvestrini, B., and Cheng, C. Y. (2014). Environmental toxicants perturb human Sertoli cell adhesive function via changes in F-actin organization mediated by actin regulatory proteins. *Hum Reprod* **29**(6), 1279-91, 10.1093/humrep/deu011.

Xu, J. H. J., Henstock, P. V., Dunn, M. C., Smith, A. R., Chabot, J. R., and de Graaf, D. (2008). Cellular imaging predictions of clinical drug-induced liver injury. *Toxicol Sci* **105**(1), 97-105, 10.1093/toxsci/kfn109.

Xu, J. J., Diaz, D., and O'Brien, P. J. (2004). Applications of cytotoxicity assays and pre-lethal mechanistic assays for assessment of human hepatotoxicity potential. *Chem-Biol Interact* **150**(1), 115-128, 10.1016/j.cbi.2004.09.011.

Yamasaki, K., Noda, S., Imatanaka, N., and Yakabe, Y. (2004). Comparative study of the uterotrophic potency of 14 chemicals in a uterotrophic assay and their receptor-binding affinity. *Toxicol Lett* **146**(2), 111-120, 10.1016/j.toxlet.2003.07.003.

Yang, X. X., Liu, Y. C., Li, J., Chen, M. J., Peng, D., Liang, Y., Song, M. Y., Zhang, J., and Jiang, G. B. (2016). Exposure to Bisphenol AF disrupts sex hormone levels and vitellogenin expression in zebrafish. *Environmental Toxicology* **31**(3), 285-294, 10.1002/tox.22043.

Yang, Y. J., Guan, J., Yin, J., Shao, B., and Li, H. (2014). Urinary levels of bisphenol analogues in residents living near a manufacturing plant in south China. *Chemosphere* **112**, 481-486, 10.1016/j.chemosphere.2014.05.004.

Yang, Y. J., Yin, J., Yang, Y., Zhou, N. Y., Zhang, J., Shao, B., and Wu, Y. N. (2012). Determination of bisphenol AF (BPAF) in tissues, serum, urine and feces of orally dosed rats by ultra-high-pressure liquid chromatography-electrospray tandem mass spectrometry. *J Chromatogr B* **901**, 93-97, 10.1016/j.jchromb.2012.06.005.

Ye, N. N., Qin, J. H., Shi, W. W., Liu, X., and Lin, B. C. (2007). Cell-based high content screening using an integrated microfluidic device. *Lab Chip* **7**(12), 1696-1704, 10.1039/b711513j.

Ye, X., Wong, L. Y., Kramer, J., Zhou, X., Jia, T., and Calafat, A. M. (2015). Urinary Concentrations of Bisphenol A and Three Other Bisphenols in Convenience Samples of U.S. Adults during 2000-2014. *Environ Sci Technol* **49**(19), 11834-9, 10.1021/acs.est.5b02135.

Ye, Y., Weiwei, J., Na, L., Mei, M., Kaifeng, R., and Zijian, W. (2014). Application of the SOS/umu test and high-content in vitro micronucleus test to determine genotoxicity and cytotoxicity of nine benzothiazoles. *J Appl Toxicol* **34**(12), 1400-8, 10.1002/jat.2972.

259

Yin, L., Dai, Y., Cui, Z., Jiang, X., Liu, W., Han, F., Lin, A., Cao, J., and Liu, J. (2016). The regulation of cellular apoptosis by the ROS-triggered PERK/EIF2alpha/chop pathway plays a vital role in bisphenol A-induced male reproductive toxicity. *Toxicol Appl Pharmacol* **314**, 98-108, 10.1016/j.taap.2016.11.013.

Yin, L., Wei, H., Liang, S., and Yu, X. (2017). An animal-free in vitro three-dimensional testicular cell co-culture model for evaluating male reproductive toxicants. *Toxicol Sci* doi, 43-60.

Yoshihara, S., Mizutare, T., Makishima, M., Suzuki, N., Fujimoto, N., Igarashi, K., and Ohta, S. (2004). Potent estrogenic metabolites of bisphenol A and bisphenol B formed by rat liver S9 fraction: Their structures and estrogenic potency. *Toxicol Sci* **78**(1), 50-59, 10.1093/toxsci/kfh047.

Yu, X., Faustman, E. M., Hong, S., and Sidhu, J. S. (2003). Effects of methyl mercury and cadmium on stress signaling and ubiquitination pathways in a primary Sertoli cell-gonocyte co-culture system. *Toxicol Sci* **72**, 274-274.

Yu, X., Sidhu, J., Hong, J. S., and Faustman, E. M. (2005a). Effects of cadmium on ubiquitin-proteasome system and stress signaling in a primary sertoli cell-gonocyte co-culture system. *Journal of Andrology* doi, 65-65.

Yu, X. Z., Hong, S., Moreira, E. G., and Faustman, E. M. (2009). Improving in vitro Sertoli cell/gonocyte co-culture model for assessing male reproductive toxicity: Lessons learned from comparisons of cytotoxicity versus genomic responses to phthalates. *Toxicol Appl Pharm* **239**(3), 325-336, 10.1016/j.taap.2009.06.014.

Yu, X. Z., Hong, S. W., and Faustman, E. M. (2008). Cadmium-induced activation of stress signaling pathways, disruption of ubiquitin-dependent protein degradation and apoptosis in primary rat Sertoli cell-gonocyte cocultures. *Toxicol Sci* **104**(2), 385-396, 10.1093/toxsci/kfn087.

Yu, X. Z., Sidhu, J. S., Hong, S., and Faustman, E. M. (2005b). Essential role of extracellular matrix (ECM) overlay in establishing the functional integrity of primary neonatal rat sertoli cell/gonocyte co-cultures: An improved In vitro model for assessment of male reproductive toxicity. *Toxicol Sci* **84**(2), 378-393, 10.1093/toxsci/kfi085.

Zanella, F., Lorens, J. B., and Link, W. (2010). High content screening: seeing is believing. *Trends Biotechnol* **28**(5), 237-245, 10.1016/j.tibtech.2010.02.005.

Zang, Q. D., Rotroff, D. M., and Judson, R. S. (2013). Binary Classification of a Large Collection of Environmental Chemicals from Estrogen Receptor Assays by Quantitative Structure-Activity Relationship and Machine Learning Methods. *J Chem Inf Model* **53**(12), 3244-3261, 10.1021/ci400527b.

Zang, Z., Ji, S., Xia, T., and Huang, S. (2016). Effects of Bisphenol A on Testosterone Levels and Sexual Behaviors of Male Mice. *Advances in Sexual Medicine* **6**(04), 41.

Zatecka, E., Castillo, J., Elzeinova, F., Kubatova, A., Ded, L., Peknicova, J., and Oliva, R. (2014). The effect of tetrabromobisphenol A on protamine content and DNA integrity in mouse spermatozoa. *Andrology-Us* **2**(6), 910-917, 10.1111/j.2047-2927.2014.00257.x.

Zatecka, E., Ded, L., Elzeinova, F., Kubatova, A., Dorosh, A., Margaryan, H., Dostalova, P., and Peknicova, J. (2013). Effect of tetrabrombisphenol A on induction of apoptosis in the testes and changes in expression of selected testicular genes in CD1 mice. *Reprod Toxicol* **35**, 32-9, 10.1016/j.reprotox.2012.05.095.

Zhang, G., Ling, X., Liu, K., Wang, Z., Zou, P., Gao, J., Cao, J., and Ao, L. (2016). The p-eIF2alpha/ATF4 pathway links endoplasmic reticulum stress to autophagy following the production of reactive oxygen species in mouse spermatocyte-derived cells exposed to dibutyl phthalate. *Free Radic Res* **50**(7), 698-707, 10.3109/10715762.2016.1169403.

Zhang, X. W., Chang, H., Wiseman, S., He, Y. H., Higley, E., Jones, P., Wong, C. K. C., Al-Khedhairy, A., Giesy, J. P., and Hecker, M. (2011). Bisphenol A Disrupts Steroidogenesis in Human H295R Cells. *Toxicol Sci* **121**(2), 320-327, 10.1093/toxsci/kfr061.

Zhang, Z. Z., Gong, Y. H., Guo, Y., Hai, Y. N., Yang, H., Yang, S., Liu, Y., Ma, M., Liu, L. H., Li, Z., Gao, W. Q., and He, Z. P. (2013). Direct transdifferentiation of spermatogonial stem cells to morphological, phenotypic and functional hepatocyte-like cells via the ERK1/2 and Smad2/3 signaling pathways and the inactivation of cyclin A, cyclin B and cyclin E. *Cell Commun Signal* **11**, Artn 67 10.1186/1478-811x-11-67.

Zhao, X. X., Toyooka, T., Kubota, T., Yang, G., and Ibuki, Y. (2015). gamma-H2AX induced by linear alkylbenzene sulfonates is due to deoxyribonuclease-1 translocation to the nucleus via actin disruption. *Mutat Res-Fund Mol M* **777**, 33-42, 10.1016/j.mrfmmm.2015.04.006.

Zhivotosky, B., and Orrenius, S. (2001). Assessment of apoptosis and necrosis by DNA fragmentation and morphological criteria. *Current Protocols in Cell Biology* **Chapter 18**, Unit 18 3, 10.1002/0471143030.cb1803s12.

Zhong, Q., Busetto, A. G., Fededa, J. P., Buhmann, J. M., and Gerlich, D. W. (2012). Unsupervised modeling of cell morphology dynamics for time-lapse microscopy. *Nat Methods* **9**(7), 711-U267, 10.1038/Nmeth.2046.

Zhou, C. Q., Wang, W., Peretz, J., and Flaws, J. A. (2015). Bisphenol A exposure inhibits germ cell nest breakdown by reducing apoptosis in cultured neonatal mouse ovaries. *Reprod Toxicol* **57**, 87-99, 10.1016/j.reprotox.2015.05.012.

Zhou, W., Fang, F., Zhu, W., Chen, Z.-J., Du, Y., and Zhang, J. (2016). Bisphenol A and Ovarian Reserve among Infertile Women with Polycystic Ovarian Syndrome. *Int J Env Res Pub He* **14**(1), 18.

Zhuang, W. L., Wu, K. S., Wang, Y. K., Zhu, H. J., Deng, Z. Z., Peng, L., and Zhu, G. H. (2015). Association of Serum Bisphenol-A Concentration and Male Reproductive Function Among Exposed Workers. *Arch Environ Con Tox* **68**(1), 38-45, 10.1007/s00244-014-0078-7.

Zuchero, J. B., Belin, B., and Mullins, R. D. (2012). Actin binding to WH2 domains regulates nuclear import of the multifunctional actin regulator JMY. *Mol Biol Cell* **23**(5), 853-863, 10.1091/mbc.E11-12-0992.
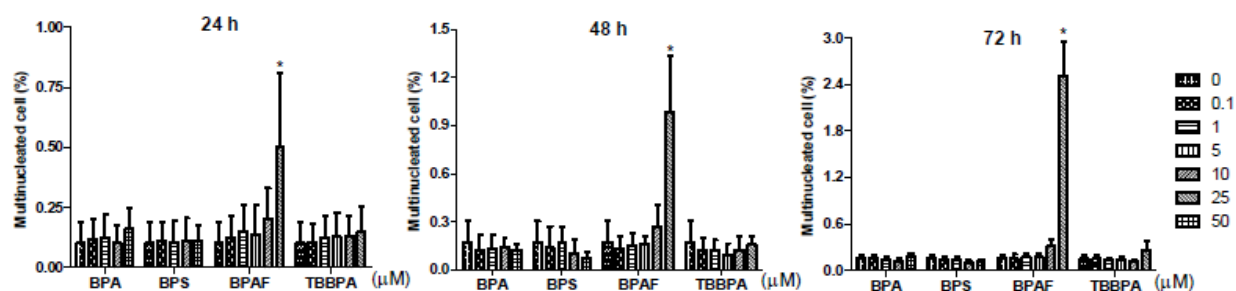
Figure S2.1. HCA of multinucleated cell number of spermatogonial cells treated with BPA, BPS, BPAF, and TBBPA. Cells were treated various concentrations of BPA and BPS (0.1, 1, 10, and 50 μM), and BPAF and TBBPA (0.1, 1, 5, 10, and 25 μM) for 24, 48, and 72 h. Cells treated with vehicle (0.05% DMSO) were used as vehicle controls (0). Multinucleated cells were identified as nuclei with area ≥ 500 μm^2 and P2A ≥ 1.35. The percentages of the multinucleated cells were presented as mean $\pm$ SD (n=9). Three replicates in three separate experiments were conducted. Statistical analysis was conducted by 1-way ANOVA followed by Tukey- Kramer multiple comparison (* P< 0.05).
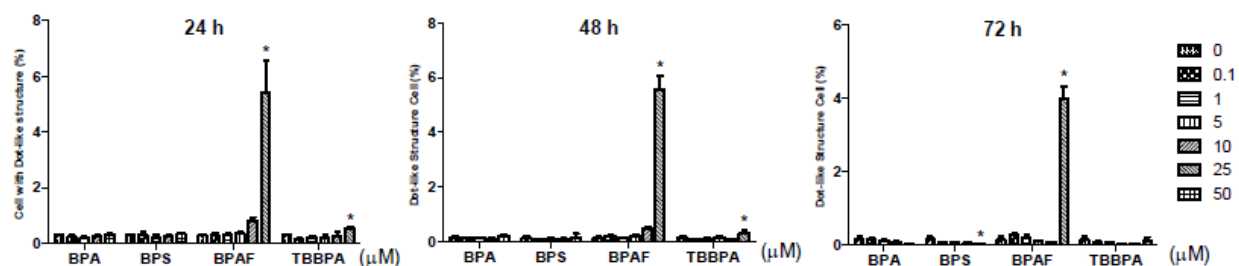
Figure S2.2. HCA of cells with dot-like structure of spermatogonial cells treated with BPA, BPS, BPAF, and TBBPA. Cells were treated with various concentrations of BPA and BPS (0.1, 1, 10, and 50 µM), and BPAF and TBBPA (0.1, 1, 5, 10, and 25 µM) for 24, 48, and 72 h. Cells treated with vehicle (0.05% DMSO) were used as vehicle controls (0). The dot-like structures were identified with objects area $\geq 159\mu m^2$, average intensity of F-actin ≥ 1028 pixels. The percentages of the dot-like structure were presented as mean $\pm$ SD (n=9). Three replicates in three separate experiments were included. Statistical analysis was conducted by 1-way ANOVA followed by Tukey-Kramer multiple comparison (* $P < 0.05$).
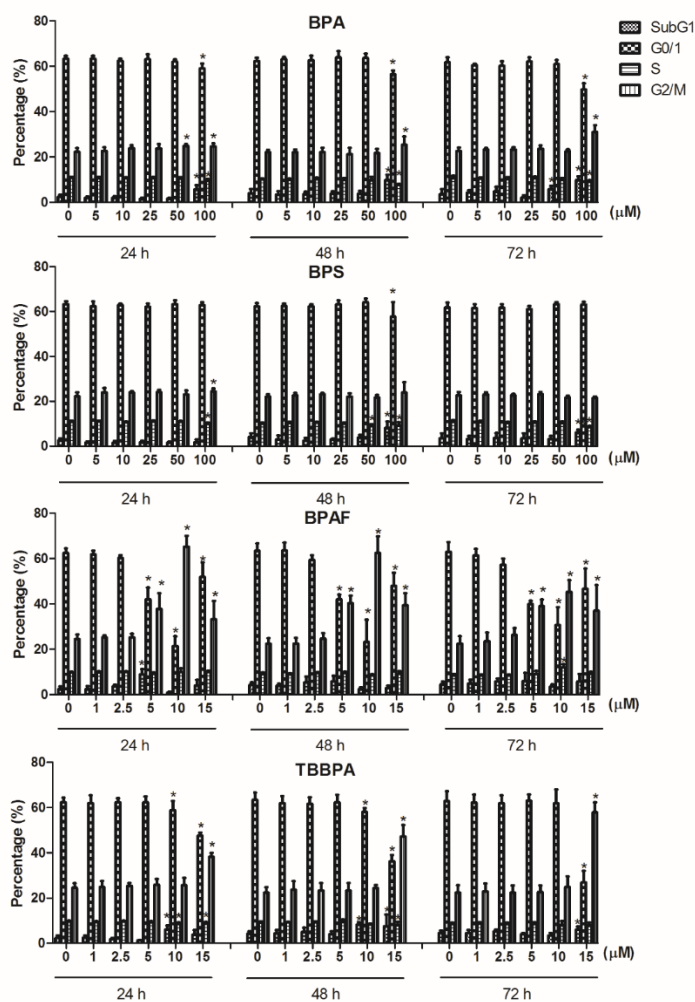
Figure S3.1. HCA of cell cycle of co-cultures treated with BPA, BPS, BPAF and TBBPA. Co-cultures were treated with various concentrations of BPA and BPS (5, 10, 25, 50, and 100 μM), and BPAF and TBBPA (1, 2.5, 5, 10, and 15 μM) for 24, 48, and 72 h. Cells treated with vehicle (0.05% DMSO) were used as vehicle controls (0 μM). Figure shows the quantification of the

percentage of each cell cycle stage, including sub-G1, G0/1, S and G2/M phase. Data are presented as mean ± SD, n=8. Four replicates in two independent experiments were included. Statistical analysis was conducted by 1-way ANOVA followed by Tukey-Kramer multiple comparison (*P<0.05).

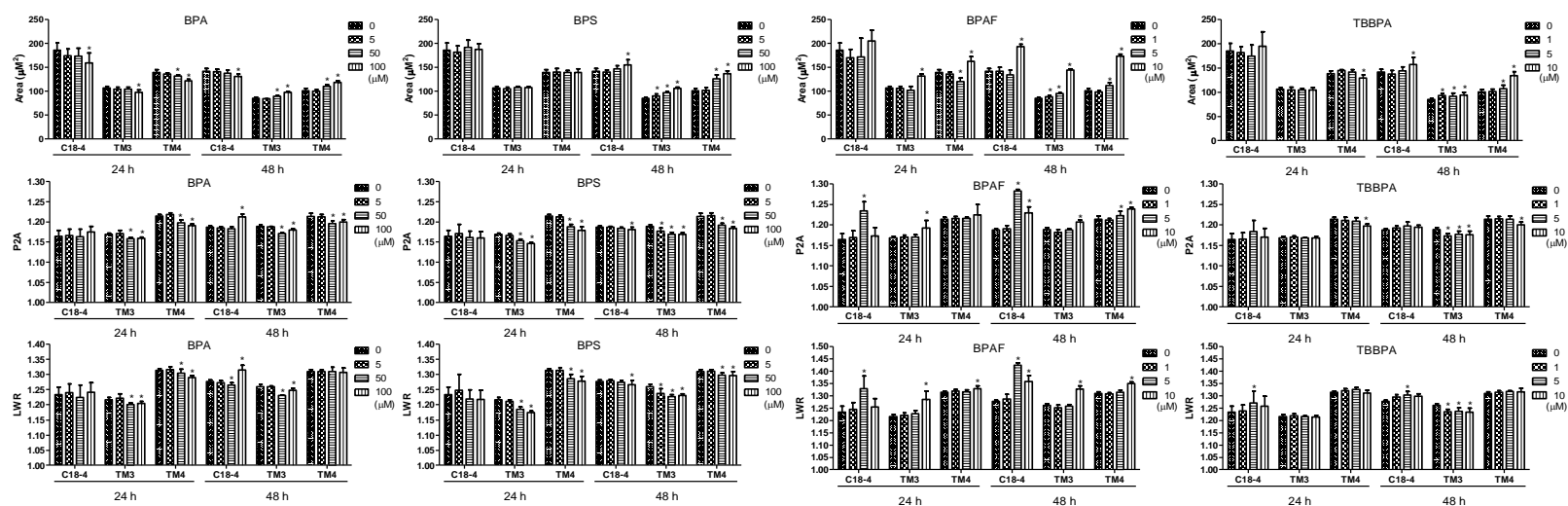## SUPPLEMENTARY DATA FOR CHAPTER 4

Figure S4.1.

HCA of the nuclear morphology of spermatogonial cells, Leydig cells, and Sertoli cells treated with BPA, BPS, BPAF, and TBBPA.

Cells were treated with various concentrations of BPA and BPS (5, 50, and 100 μM), and BPAF and TBBPA (1, 5, and 10 μM) for 24

and 48 h. Cells treated with 0.05% DMSO were used as vehicle controls (0 μM). The nuclei were stained with Hoechst 33342, and

images were automatically acquired with 40X objectives, and 49 fields per well. Figure shows the quantification of the absolute nuclear area (μm^2), LWR for nuclear roundness, and P2A for nuclear smoothness. Data are presented as mean ± SD, n=8. Four replicates in two independent experiments were included. Statistical analysis was conducted by 1-way ANOVA followed by Tukey-Kramer multiple comparison (*P<0.05).